Alma Mater Studiorum – Università di Bologna

Facoltà di Scienze Matematiche, Fisiche e Naturali

Scuola di Dottorato in Scienze Biologiche, Biomediche e Biotecnologiche

Dottorato in Biologia Cellulare, Molecolare ed Industriale/

Cellular, Molecular and Industrial Biology:

Progetto n.2: "Biologia Funzionale e Molecolare"

Ciclo XXIV

Settore concorsuale di afferenza: 05/E1

Settore scientifico-disciplinare: BIO/10

THE COUPLING BETWEEN ELECTRON TRANSFER AND PROTEIN/SOLVENT DYNAMICS IN PHOTOSYNTHETIC REACTION CENTERS: SPECTROSCOPIC STUDIES IN AMORPHOUS MATRICES

PhD student:

MARCO MALFERRARI

Advisor:

Chiar.mo Prof. GIOVANNI VENTUROLI

Co-advisor:

Dott. FRANCESCO FRANCIA

PhD Coordinator:

Chiar.mo Prof. VINCENZO SCARLATO

Final Exam Year 2012

Accademic Years 2009/2011

CONTENTS

1. INTRODUCTION

1.1 Protein dynamics and the energy landscape.

The study of the internal dynamics of proteins in relation to their structural and functional complexity represents nowadays a lively and promising field of research (Vinson, 2009; Henzler-Wildman, 2007). The interest in this topic is becoming more and more intense due to its implication in the understanding of many physiological and biochemical processes, as protein folding and unfolding (Onuchic, 1997), enzyme catalysis (Eisenmesser, 2002), and protein-protein interactions involved in the transmission of signals through intracellular and intercellular pathways (Smock, 2009). Furthermore, it is expected that a deep elucidation of protein dynamics will result in important pharmaceutical and biotechnological applications, as the development of new strategies for the design of drugs (Lee, 2009) and of artificial proteins (Koder, 2009).

Protein dynamics encompass a wide range of times, from femtoseconds to seconds, including in principle fast simple motions, as atom vibrations, as well as slow movements of large protein domains (Frauenfelder, 1998; Henzler-Wildman, 2007; Frauenfelder, 2009).

The concept of energy landscape of a protein, i.e. the potential energy of the system as function of all its atomic coordinates, offers a very useful representation of the structural and dynamical complexity of a protein (Frauenfelder, 1998; Frauenfelder, 2000). Since for a protein formed by N atoms, the energy landscape is defined in an hyperspace with 3N-6 dimensions, only a computer can appreciate its full complexity. Some insight can be gained however by considering one-dimensional cross sections through the energy landscape, as those reported in Figure 1.1. Fig.1.1A illustrates the energy landscape of ammonia and in particular the dependence of the potential energy of the molecule as a function of the distance between the nitrogen atom and the plane passing through its hydrogen atoms. Fig.1.1B presents a pictorial representation of a hypothetical one-dimensional cross section of the energy landscape of a protein. Both energy landscapes are characterized by minima (well defined conformational substates) separated by energy barriers. The most evident difference between these two examples consists in the huge number of minima and the variety of energy barriers which characterize the case of the protein, while for ammonia the small number of atoms gives rise to a much simpler energy landscape with just two minima

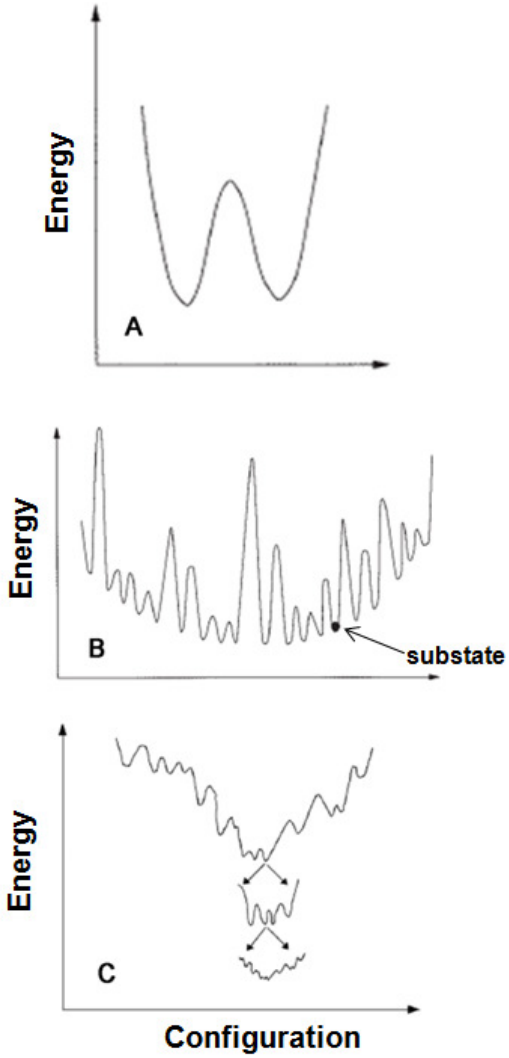

Figure 1.1
Pictorial representations of energy landscapes. A. The energy landscape of ammonia; the conformational coordinate refers to the distance between the nitrogen atom from the plane passing through the three hydrogen atoms. B. An extremely simplified one-dimensional cross section through the energy landscape of a protein. C. A schematic representation of the hierarchical organization of the protein energy landscape. Adapted from Frauenfelder, 1998 and Cordone, 2005.

separated by an energy barrier. Whereas for ammonia the energy landscape of Fig1.1A provides an acceptable representation of its dynamics, in the case of the protein the landscape of Fig.1.1B is oversimplistic, as the fractal organization of the energy landscape is not adequately represented. This concept is better illustrated in Fig.1.1C. Due to the extremely large number of atoms in a protein, the energy landscape has a hierarchic organization, where different tiers of substates can be individuated. Substates are grouped together in the same tier on the basis of the height of the energy barriers between them. With reference to Fig.1.1C, starting from the top profile, if one could

look at higher resolution into a conformational minimum, a new complex energy landscape would appear (a new tier) characterized by lower energy barriers, and so on going to the next tier. Since each tier includes a large number of minima, essentially isoenergetic, at the appropriate temperature the protein is supposed to fluctuate among the conformational substates of that tier over a characteristic time scale. In general small amplitude internal movements are fast, while large scale movements of protein domains, often requiring a sequence of collective structural rearrangements take place over much longer time scales. In this way, the fractal organization of the protein landscape gives rise to complex dynamics (from atoms vibration to protein unfolding) encompassing a vast time scale.

A large part of the experimental and theoretical studies aimed at understanding the constitutive properties of the protein energy landscape have focused on myoglobin (Frauenfelder, 2001), starting from the pioneering work of Austin and colleagues (Austin, 1975), who studied the rebinding kinetics of carbonmonoxyde to the heme group of carboxymyoglobin after photodissociation over a large temperature range (40-350K). From the multiphasic kinetics observed at cryogenic temperatures four rebinding processes were inferred, which, on the basis of the impressive structural information gained in the subsequent decades, could be interpreted in terms of the CO pathways inside the cavities which surround the heme group (see Frauenfelder, 2010). Most importantly, the seminal work of Austin and co-workers showed that rebinding at cryogenic temperature was strongly non-exponential in time. It was suggested that at cryogenic temperature the distributions of rate constants reflected an ensemble of structural conformations of the protein, and distribution of energy barriers between conformational substates were introduced (Austin, 1975). This static heterogeneity could not be observed at room temperature, since it was averaged on the time scale of the rebinding process by the fast fluctuations of the protein among conformational substates, giving rise to exponential kinetics.

Two hierarchical tiers of the myoglobin energy landscape have been clearly identified (Frauenfelder, 2010), which are formed by the so called taxonomical and statistical substates. This hierarchical organization (depicted in Fig. 1.2 A and B) is reflected in the infrared spectrum of carboxymyoglobin (Fig.1.2C): three sub-bands of the CO stretching vibration are resolved, corresponding to three different environments experienced by the CO molecule bound to the heme (Frauenfelder, 2001), i.e. it has been suggested by x-ray diffraction studies that the three taxonomic substates

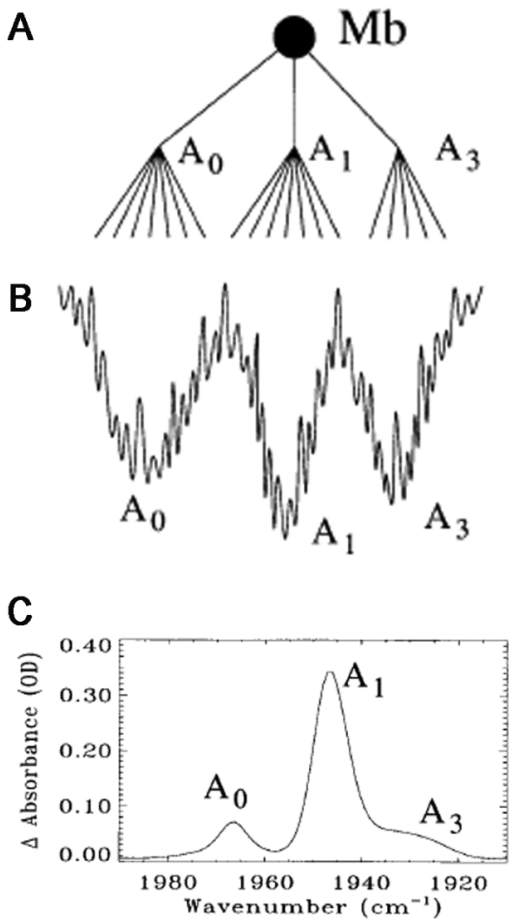

Figure 1.2
Hierarchy of the myoglobin energy landscape for the rebinding of CO to the heme. A. Tree graph of the tassonomic conformational substates and low level statistical substates. B. Pictorial representation of the energy landscape of the tassonomic substates A_0, A_1 and A_3; the roughness of the energy potential curves corresponds to the organization of the low level statistical substates in each taxonomic level. C. Infrared absorption spectrum of carboxymyoglobin in the CO stretching region. The three taxonomic substates, corresponding to the three sub-bands peaking at 1967, 1947 and 1929 cm^{-1}, are indicated as A_0, A_1 and A_3. Adapted from Frauenfelder, 2001.

correspond to distinct conformations of myoglobin in the surroundings of the carbonmonoxyde molecule (Vojtechovsky, 1999). The lower tier statistical substates, schematically represented by the roughness of the taxonomic wells in Fig.1.2B, are thought to arise from structural fluctuations of the three taxonomic substates, and cause the broadening of the three sub-bands in the CO stretching spectrum (Fig.1.2C). Experimental evidence for the presence of additional tiers in the hierarchy has been obtained (Thorn-Leeson, 1995; Young, 1991) and time-resolved x-ray diffraction (Schotte, 2004) and scattering (Cho, 2010) studies are defining in some detail the structural basis of the hierarchical organization of myoglobin conformational substates.

1.2 The slaving of protein dynamics to solvent fluctuations.

The physics of glass forming liquids has provided deep insights into several aspects of protein dynamics. Indeed, many properties of proteins and glasses appear to be similar. An important example is given by the so called *dynamical transition* (Frauenfelder, 2009; Doster, 2010). When a protein/solvent system is slowly warmed starting from cryogenic temperatures, the mean-square displacements of its atoms, which increase linearly with absolute temperature (T) at low T, undergo a much steeper, non linear increase above a temperature (indicated by T_d in Fig.1.3A) around 200 K. This abrupt increase in protein dynamics (the d*ynamical transition*) was characterized initially by neutron scattering on myoglobin (Doster, 1989), and then investigated by a number of different experimental approaches also in other protein systems (Doster, 2010). A key point to interpret the dynamical transition in terms of protein/solvent dynamical coupling is that T_d strongly depends on the hydration level of the system (Fig.1.3B-C) (Ferrand, 1993; Tsai, 2000; for a review see Fenimore, 2004) and is affected by the chemical nature of co-solvents (the latter item will be further discussed in chapter 1.3 in relation with the dynamics of proteins incorporated into dehydrated glassy matrices). The dependence of T_d upon the hydration level seems to be crucial, since in extremely dried samples (see for example the data indicated as *dry* in Fig 1.3B) the transition is not observed even at room T.

An important common feature of protein and glasses appears to be the occurrence of two types of equilibrium fluctuations, known as α and β fluctuations (Lunkenheimer, 2000; Doster, 2010). In glasses α and β relaxations have been characterized mainly by dielectric spectroscopy on the basis of the temperature dependence of the relaxation rate coefficient: while β processes follow an Arrhenius behavior, in the case of α relaxations the temperature dependence is adequately described by the Vogel-Tammann-Fulcher (VTF) equation. In glasses, α relaxations are interpreted as arising from the cooperative movement of many particles, whereas β relaxations are thought to be related to "rattling" movement of individual particles in the transient cage formed by their neighbours.

The α and β processes have been observed in proteins by dielectric spectroscopy (Frauenfelder, 2009), as well as by specific heat spectroscopy (Doster, 2010). The temperature dependence of α and β dielectric relaxations, measured in myoglobin in 50:50 (wt/wt) water-glycerol matrices, is shown in Figure 1.4A. The α relaxations (obeying the VTF equation) stop immediately below the dynamical transition

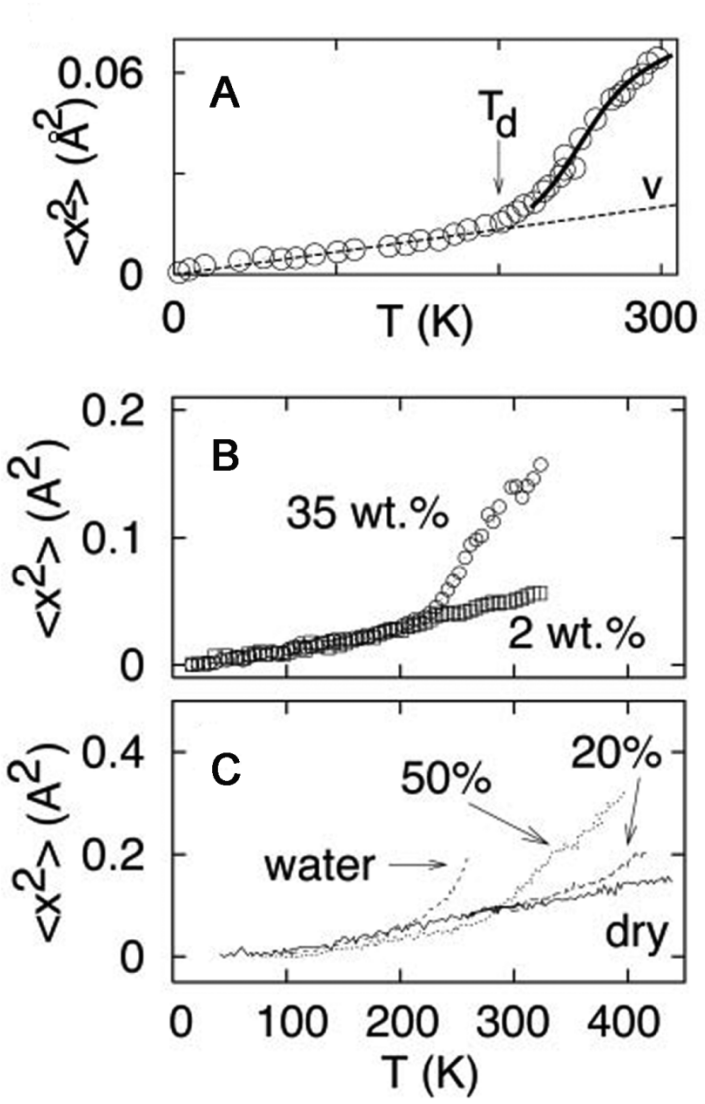

Figure 1.3
The *dynamical transition* observed in different proteins at various hydration levels. Mean square displacements, $\langle x^2 \rangle$, have been measured as a function of temperature by using different experimental techniques. A. $\langle x^2 \rangle$ of ^{57}Fe in myoglobin crystals measured by Mossbauer spectroscopy. The dashed line represents the vibrational contribution to $\langle x^2 \rangle$(T), extrapolated also for T higher than 200 K. For more details see Parak, 1982. B. $\langle x^2 \rangle$ of the hydrogen atoms in bacteriorhodopsin, measured by neutron scattering at 2% w/w (open square) and 35% w/w hydration (circles) (from Ferrand, 1993). C. $\langle x^2 \rangle$ of the hydrogen atoms of lysozime, measured by neutron scattering in different solvents. *Water*: lysozime 70% and water 30%; *50%* : lysozime 50% and glycerol 50%; *20%* : lysozime 20% and glycerol 80%; *dry*: dry lysozime. For more details see Tsai, 2000. Adapted from Fenimore, 2004.

temperature. On the contrary, the β relaxations are present also at very low temperatures. Their temperature dependence follows the Arrhenius law, also in solid matrices characterized by very low contents of residual water (Fig.1.4B) (Fraunfelder, 2009).

All the observations described above have been rationalized by proposing that α and β fluctuations in proteins originate from their coupling with solvent dynamics (Fraunfelder, 2009); in particular, α processes have been associated with the dynamics of the bulk solvent and β processes with the dynamics of the hydration shell, formed by one to two layers of water molecules interacting with the surface of the protein. Indeed, many experimental and theoretical studies (Pal, 2002; Ebbinghaus, 2007; Grossman, 2011) indicate distinct dynamical properties for these two classes of water molecules. In this unified model of protein dynamics (Fraunfelder, 2009) three types of motions are identified on the basis of their slaving to the solvent dynamics (Fenimore, 2004): solvent-coupled (α-slaved) processes (Class I); hydration-shell coupled (β-slaved) processes (Class II); and inner molecular processes (Class III), such as molecular vibrations in the force-field potential of molecular atom-atom interactions, that are higher in energy and non-slaved to solvent fluctuations. Class I, solvent-slaved motions, follow the dielectric (α-) fluctuations in the bulk solvent; they involve large-scale conformational changes, such as those controlling the entrance and exit of ligands in myoglobin or of diprotonated quinol (Q_BH_2) in the photosynthetic bacterial reaction center of *Rb. sphaeroides* (RC) (see par. 1.3 and Savitsky, 2010). Since these motions are controlled by the bulk-solvent viscosity, η(T), they are considered to be absent in rigid environments ($\eta \rightarrow \infty$). Class II motions are slaved to fast (β-) fluctuations in the hydration shell; this statement is well supported by the results reported in Fig.1.4B, showing that the temperature dependence of the β-relaxations in myoglobin is markedly affected by the hydration state of the sample at low residual water contents, when the protein hydration shell is progressively depleted (Frauenfelder, 2009). On these basis, class II motions are expected to be absent in fully dehydrated proteins. Such β-fluctuations are supposed to involve side chains of the protein, and to govern processes such as the movement of ligands between different cavities inside myoglobin. In the case of myoglobin, the distinction between Class I and II processes (α- and β-fluctuations) has been put in relation with two hierarchically organized "tiers" of the energy landscape, CS^2 (the lowest) and CS^1 (the next higher one (Frauenfelder, 2009). Remarkably, in the frame of this unified model, the interpretation of the dynamic transition (Fig.1.3) becomes particularly simple: the increase of mean-square displacements above T_d is due to the "activation" of β fluctuation in the hydration shell.

We notice that such a close relationship between the dynamics of the protein and of its surroundings (Frauenfelder, 2009; Doster, 2010; Grossman, 2011) is likely to be

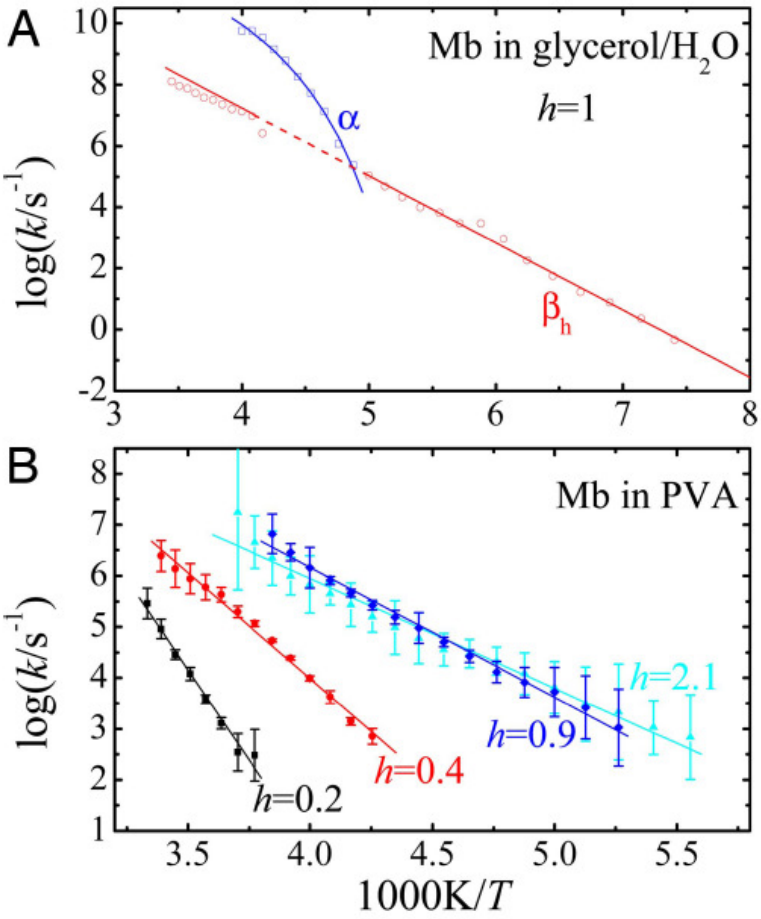

Figure 1.4
Relaxation processes in myoglobin measured by dielectric relaxation spectroscopy. A. Arrhenius plot of the α and β processes in 50:50 (w/w) water : glycerol samples, with a water/protein weight ratio equal to 1. The dependence for the α processes have been fitted to a Vogel-Tammann-Fulcher relation, while β relaxation follows approximately an Arrhenius law. For further details on the fitting models refer to Frauenfelder, 2009. B. Arrhenius plot of β processes for myoglobin embedded in polivinilalcool matrices, at the weight water/protein ratio *h* indicated in the figure. Adapted from Frauenfelder, 2009.

very important for the understanding proteins function *in vivo*, where, due to molecular crowding, proteins operate under conditions which are far from the idealized ones used in "traditional" biochemical enzymatic or functional assays (Zhou, 2008). In these respect we believe that the studies presented in the present thesis, mainly performed *at room temperature* in strongly dehydrated protein-matrix systems, can contribute to clarify function/dynamics relationships under conditions of physiological relevance.

1.3 The photosynthetic reaction center of *Rb. sphaeroides*: structure and photochemistry.

The photosynthetic reaction center (RC) of anoxygenic purple bacteria is one of the best-characterized membrane proteins and has become a reference model in studying the primary processes of photosynthesis. The RC is the key protein in the photosynthetic machinery which upon light excitation initiates a sequence of electron transfer processes coupled to the pumping of protons across the energy transducing membrane. The resulting electrochemical potential difference of protons drives the synthesis of ATP via a chemiosmotic circuit, which enables the transformation of electromagnetic energy into chemical energy (Cramer, 1990).

The reaction center of *Rhodopseudomonas viridis* has been the first membrane protein for which the crystallographic structure has been solved (at 3 Å) (Deisenhofer, 1985). Soon after the crystallographic structure of the RC purified from *Rhodobacter (Rb.) sphaeroides* R26 (a carotenoid-less strain) was also determined at 2.8 Å resolution (Allen, 1986). The structure is now available at the maximal resolution of 1.8 Å for the RC purified from the wild type strain 2.4.1 of *Rb. sphaeroides* (Koepke, 2007). The comparison of the wt 2.4.1 and the R26 structures showed no relevant difference between the two proteins, except for the presence in the R26 RC of a molecule of detergent (LDAO) in the binding site of the carotenoid (a spheroidene or a spheroidenone in the 2.4.1 strain). RCs purified from both strains have been used in the present thesis.

Figure 1.5 shows views of the RC structure derived from the crystallographic coordinates. The protein complex is formed by three subunits, named L, M and H (*Low*, *Medium* and *High*) from their apparent molecular weight derived from SDS-PAGE analysis. It was predicted that two of the three subunits (L and M) were strongly associated with the membrane and that the H subunit was only loosely associated with the phospholipids bilayer, as it could be easily detached from the membrane by gentle detergent treatments. The crystallographic structure confirmed this prediction. As shown in Fig. 1.5A,B, the L and M subunits have both five transmembrane α-helices, that in the LM complex are arranged according to a C2 pseudo-symmetry with the axis passing through the non-heme iron atom and the P special pair. The H subunit is composed of an α-helix inserted into the phospholipid bilayer, in close contact with the LM complex, and of a globular domain which includes a β-strand surrounded by 2

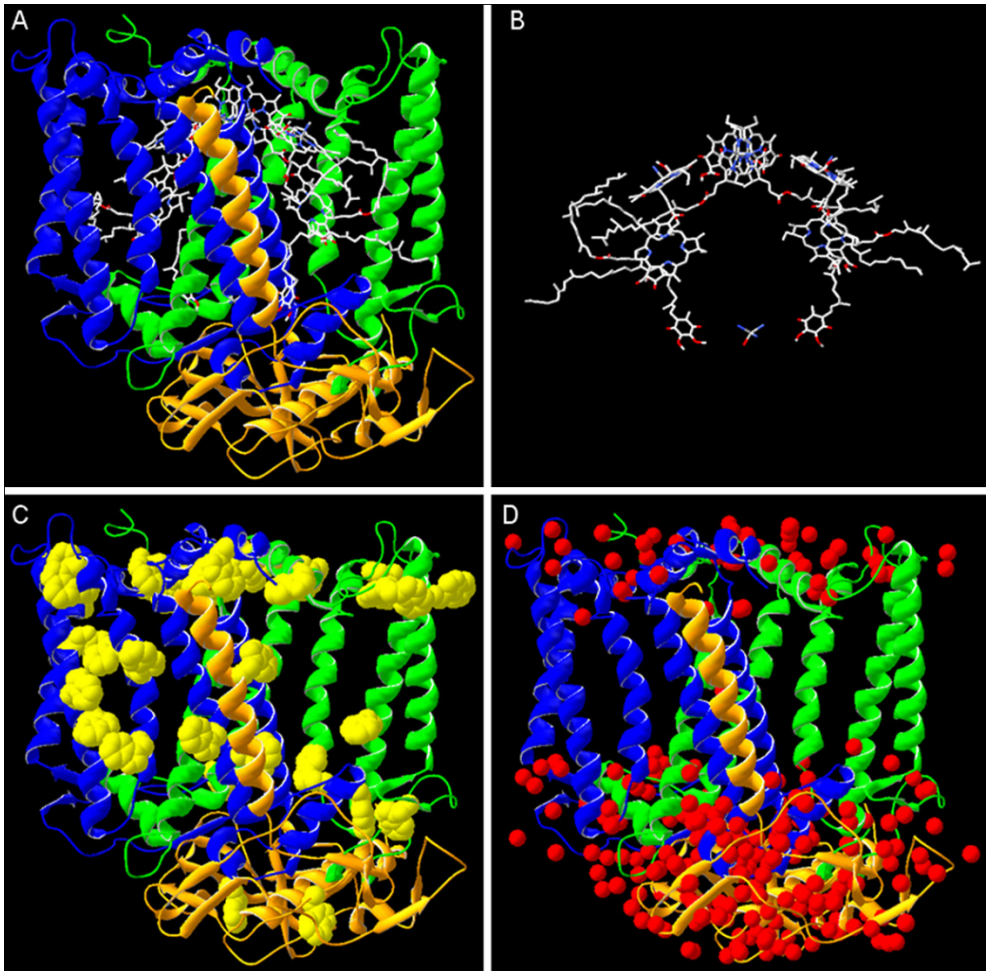

Figure 1.5
The crystallographic structure of *Rb. sphaeroides* RC. A. The L, M and H subunits are represented in green, blue and orange respectively; the cofactors of the RC are represented in wireframe with CPK colours. B. The structure of the cofactors. Branch A is represented on the left side of the Fe^{2+} atom. For each branch, from the bottom to the top, a ubiquinone-10, a bacteriopheophytin, and a monomeric bacteriochlorophyll are present. On the top, the bacteriochlorophyll molecules forming the P special pair are showed, with their parallel tetrapyrrole planes. C. Tryptophan residues are shown in a space-filling representation (yellow). On the periplasmic side (top) tryptophan residues are organized in a ring, which is thought to contribute to the positioning of the protein complex within the phospholipid bilayer. D. The resolved water molecules are shown as red spheres. All images have been done with the Swiss PDB-Viewer software (Guex, 1997), using the PDB coordinates 1RG5 (A, B and C; Roszak, 2004) and 2J8C (D; Koepke, 2007).

α–helices and some loops. This subunit protrudes on the citoplasmic side of the membrane.

As shown in Fig.1.5C, on the periplasmic side of the membrane a ring of tryptophan residues is present, which, due to the hydrophobic interactions of the indolic groups with the phospholipids, is supposed to regulate the position of the protein complex in the membrane, with respect to the normal to the membrane plane. Figure 1.5D shows as red spheres the many water molecules (430) resolved at 1.8 Å in the crystallographic structure of the wt RC, located both on the external surfaces and inside the complex (Koepke, 2007). A very large number of water molecules (1300), many of which also in the interior of the protein and often organized in water channels, has been found recently in the high resolution (1.9 Å) crystallographic structure of photosystem II from the cyanobacterium *Thermosynechococcus vulcanus* (Umena, 2011). These observations are particularly relevant for the studies reported in the present thesis, which deals with many aspects of the dynamical coupling between the protein and its hydration shell (see in particular Chapter 6).

The LM complex binds the RC cofactors, which also obey a C2 pseudo-symmetry (see Fig.1.5B). The cofactors are: 4 bacteriochlorophyll *a* molecules (two forming the P special pair (BChlP) and two known as accessory monomeric bacteriochlorophylls (BChlB)), 2 bacteriopheophytin (BPheo), 2 ubiquinone-10 (UQ_{10}) molecules and one non-heme iron atom Fe^{2+} (see also Fig.1.8). The cofactors are arranged in two symmetrical branches, called A and B; branch A is mainly surrounded by aminoacidic residues of the L subunit, while the cofactors of branch B are mainly associated to aminoacidic residues of the M subunit.

The transfer of the electron donated by the P special pair following the absorption of a photon of appropriate wavelength takes place only through branch A, while the cofactors of branch B are supposed to be involved in the dissipation of non productive excited states of the P pair under stress conditions. In the wt 2.4.1 RC structure in fact the BChlB of branch B ($BChlB_B$) is located in the vicinity of the isoprene tail of spheroidenone, which runs parallel to the $BChlB_B$ porphyrin ring. It is well known that carotenoids are able to dissipate bacteriochlorophyll triplet states and this is one of the functional roles attributed to the spheroidenone molecule in the native RC.

The sequence of events which results in the physiological incorporation of the carotenoid molecule into the protein structure is not fully unravelled. However it has been demonstrated (Roszak, 2004) that, as illustrated in Fig.1.6A, a phenylalanine

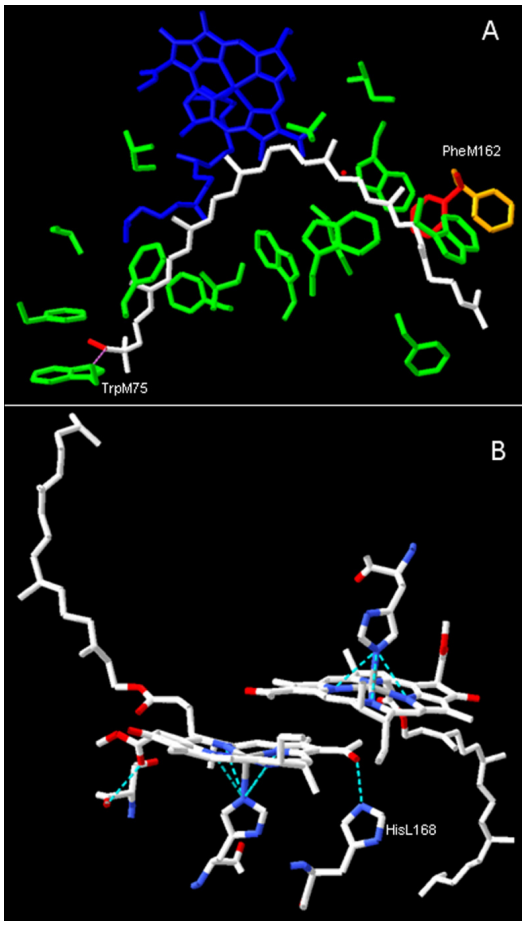

Figure 1.6
The binding sites of spheroidenone and of the bacteriochlorophylls of the P special pair in the RC of *Rb. sphaeroides*. A. Spheroidenone binding site. In green the lateral groups of hydrophobic amino acidic residues, in blue the monomeric BChl of branch B and in CPK the spheroidenone. The conformations adopted by the phenylalanine residue M162 in the presence and in the absence of the carotenoid have been represented in orange and red respectively. TrpM75 (on the left) forms a hydrogen bond with the spheroidenone. B. The coordination geometry of the P bacteriochlorophyll molecules. Images were constructed with Swiss PDB-Viewer (Guex, 1997) from the PDB files 2J8C (Koepke, 2007), 1RG5 (Roszak, 2004) (panel A), and 2J8C (Koepke, 2007) (panel B).

residues acts as a gatekeeper, determining the entrance of the pigment only from one side of the binding site; a tyrosine residue ensures the correct positioning of the cofactor, through the formation of an hydrogen bond between the OH group of the spheroidenone and the nitrogen atom of the tryptophan indolic ring. A structural role of the carotenoid is suggested by other studies, indicating a larger rigidity of the wt 2.4.1 as compared to the R26 RC (Gall, 2001; Gall, 2004).

Also the other cofactors are bound to the protein through hydrogen bonds or hydrophobic interactions with the lateral groups of aminoacidic residues belonging to

the transmembrane helices of the L and M subunits. The case of the P special pair binding site is of particular interest since it has been shown that the extension of the hydrogen bond network which involves these two bacteriochlorophyll molecules has functional consequences on the electron transfer, by affecting the standard midpoint reduction potential ($E°'$) of the electron donor P (Lin, 1994). More specifically, as illustrated in Figure 1.6B, in the wt RC the BChlP, in addition to the coordination of the two magnesium atoms by two histidines, establishes an hydrogen bond with HisL168 (the bond involves the oxygen atom of the acetyl group of one of the two bacteriochlorophylls and one nitrogen atom of the imidazolic group of the histidine). In this native situation the $E°'$ value of the (P^+/P) redox couple is approximately 505 mV. Lin and coworkers (Lin, 1994), through site-specific mutagenesis, obtained RCs in which 1, 2 or 3 hydrogen bonds are formed between different protein residues and BChlP. These authors obtained a series of 11 mutated RCs with in which $E°'$ varies in the range between 410 and 765 mV. As a general rule it has been observed that $E°'$ increases with the number of hydrogen bonds involving BChlP, by 60-125 mV for each new hydrogen bond added.

The bacteriochlorin RC cofactors, being characterized by extended π systems, give rise to a RC absorption spectrum rich of bands in the spectral interval from the ultraviolet to the near infrared (Figure 1.7A). The main absorption bands are attributed to electronic transitions of specific individual cofactors inside the reaction center, as detailed in the caption of Figure 1.7.

Photoinduced electron transfer takes place according to the scheme of Figure 1.8. Following the absorption of a photon of $\lambda \approx 860$ nm by the BChlP (or the transfer of excitation energy from another photoexcited pigment in the RC or in the antenna system), the special pair enters the first excited singlet state, BChlP*, which donates an electron to the quinone bound at the Q_A site, *via* the intermediate bacteriopheophytin of branch A. This photochemical event, being the P special pair approximately 20 angstrom away from the quinone Q_A, produces a charge separated state in the protein complex. The formation of the primary charge separated state $P^+Q_A^-$ is characterized by a time constant $\tau \approx 200$ ps. The electron is then delivered from Q_A^- to the quinone bound at the Q_B site, which is reduced to the semiquinone form, Q_B^-. This process, occurring over the time scale of 10-100 μs, is conformationally gated, i.e. rate limited by a conformational change of the RC (Graige, 1998). Under physiological conditions, the photoxidized primary donor, P^+ is rapidly reduced by a soluble cytochrome c

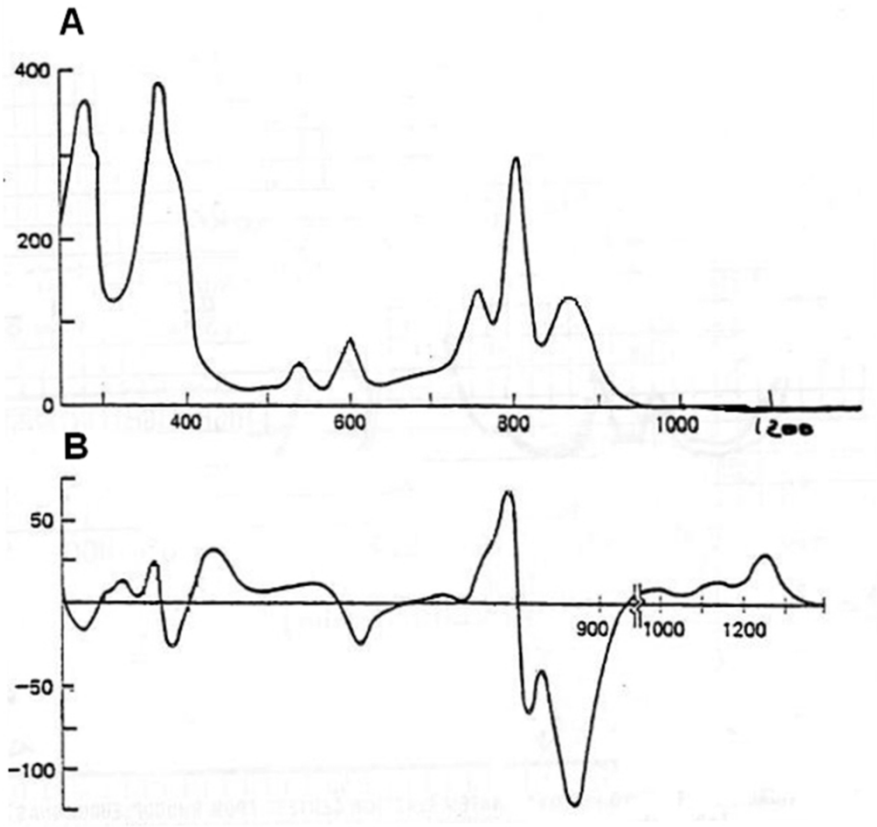

Figure 1.7
The absorption spectrum of dark-adapted RC from *Rb. sphaeroides* R26 (A) and the light-minus-dark difference spectrum (B) between 250 and 1300 nm. In A, the bands around 560 and 757 nm are attributed to the Q_X and Q_Y transitions of the bacteriopheophytin molecules; the bands at 800 nm and 860 nm result from the Q_Y transitions of the monomeric and dimeric (P) bacteriochlorophyll molecules, respectively. All bacteriochlorophyll molecules contribute to the Q_X band at 600 nm. Adapted from Bagley, 1990.

(cytochrome c_2). The ri-reduction of P^+ makes possible a subsequent photoexcitation of BChlP and a new charge separation event within the RC. The second photochemical event produces the double reduction of Q_B which, following the uptake of two protons from the cytoplasm is released from its binding pocket into the phospholipid bilayer as dihydroquinone or quinol (QH_2). A two-electron gate operates therefore at the level of the secondary acceptor Q_B . The reactions described above represent the first step in the cyclic electron transfer chain which *in vivo* generates the electrochemical potential difference of protons across the intracytoplasmic membrane driving ATP synthesis.

For each of the forward, charge separating processes considered a finite probability exists that the inverse reaction takes place, resulting in a charge recombination process, in which the electron on the acceptor recombines with the hole on the donor cofactor. In the absence of electron donors to the photoxidized P^+,

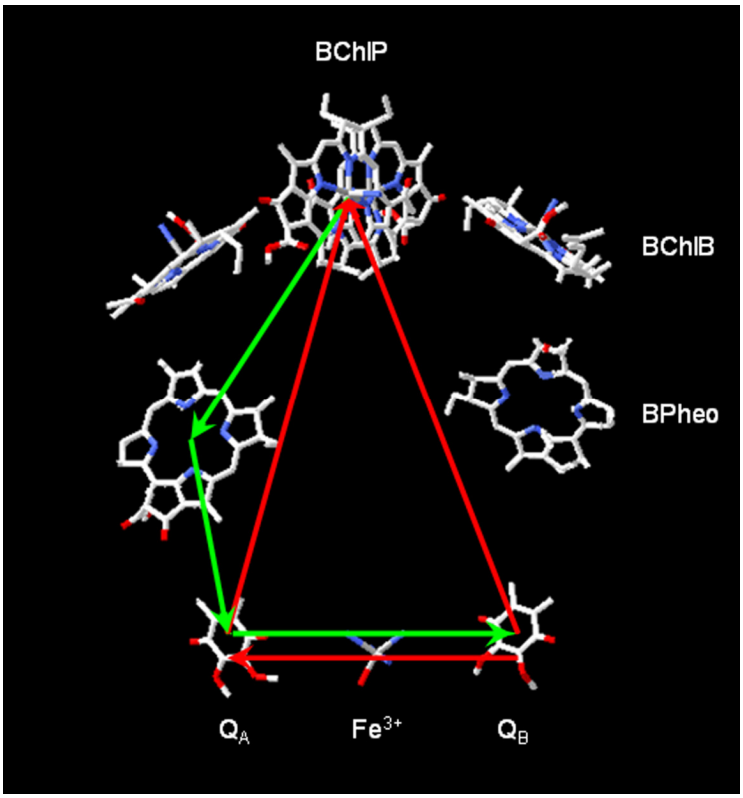

Figure 1.8
Light-induced electron transfer processes within the *Rb. sphaeroides* RC. The lateral chains of cofactor have been omitted. The electron transfer reactions which produce the separated states are shown with green arrows; charge recombination processes from Q_A and from Q_B are indicated by red arrows.

recombination of the light-generated $P^+Q_B^-$ state occurs according to the following kinetic scheme:

$$PQ_AQ_B \xrightarrow[k_{AP}]{} P^+Q_A^-Q_B \underset{k_{AB}}{\overset{k_{BA}}{\rightleftharpoons}} P^+Q_AQ_B^-$$

$$P^+Q_AQ_B^- \xrightarrow{k_{BP}} PQ_AQ_B$$

where k_{AP}, k_{AB} and k_{BA} are first-order rate constants. The state $P^+Q_A^-Q_B$ can either recombine yielding the ground state PQ_AQ_B with a rate constant $k_{AP} \cong 10\ s^{-1}$ or, in the presence of ubiquinone bound at the Q_B site, yield $P^+Q_AQ_B^-$. Under physiological conditions, the state $P^+Q_AQ_B^-$ is stabilized with respect to $P^+Q_A^-Q_B$ by approximately 70 meV and, since $(k_{AB}+k_{BA}) \cong 10^4\ s^{-1} >> k_{AP}$, electron transfer to Q_B occurs with an extremely high quantum efficiency. The state $P^+Q_AQ_B^-$ recombines slowly (lifetime ≅

1s) essentially *via* the $P^+Q_A^-Q_B$ state, with the direct route (k_{BP}) being negligible at room temperature (Kleinfeld, 1984; Labahn, 1995). By contrast, the fast recombination of $P^+Q_A^-Q_B$ (lifetime ≅ 0.1s) is observed when electron transfer to Q_B is blocked by a competitive inhibitor as o-phenantroline.

The kinetics of the electron transfer processes outlined above can be studied by time-resolved optical spectroscopy, since the light-minus-dark difference spectrum of the RC (see Fig.1.7B) has a number of relatively intense and well characterized bands resulting from the oxidation of the primary donor, from the reduction of the Q_A and Q_B acceptors, as well as from electrochromic effects (for further details see par.3.3).

1.4 The conformational dynamics of the bacterial photosynthetic reaction center.

The bacterial RC is considered to be an excellent model system for investigating the relationship between protein internal motions and long range electron transfer. A number of investigations, exploiting independent spectroscopic, electrometric, and biochemical approaches (Kleinfeld, 1984; Kriegl, 2004) indicate coherently that following the light-induced primary charge separation, the RC protein-solvent system responds to the generated electric field by relaxing from a *dark-adapted* to a *light-adapted* conformation which stabilizes the charge separated $P^+Q_A^-$ state relative to the PQ_A ground state. Fundamental information on the interplay between this RC conformational dynamics and electron transfer has been provided by low temperature studies of $P^+Q_A^-$ recombination kinetics (Kleinfeld, 1984; Ortega, 1996; McMahon, 1998; Kriegl, 2004). In a pioneering study, Kleinfeld and coworkers (Kleinfeld, 1984) showed that the recombination kinetics is accelerated by a factor of five, with respect to room temperature, when RCs are frozen to 77 K *in the dark*; at variance the above process is sizably slowed down when cooling takes place *in the light* (see Fig. 1.9). This behavior was interpreted as reflecting the trapping at low temperature of the *dark-adapted* or the *light-adapted* conformation. In addition, the strongly non-exponential kinetics measured both in the *dark-* and *light-adapted* states at cryogenic temperature (Fig. 1.9) were interpreted as reflecting an ensemble of frozen conformational substates giving rise to a continuous distribution of electron transfer rates. Such a behavior is not observed at room temperature due to the rapid substates interconversion over the time scale of the electron transfer reaction. The rapid fluctuations among conformational substates bring about result in averaging over the rate constant distribution, leading at room temperature to exponential recombination kinetics. Kleinfeld and colleagues

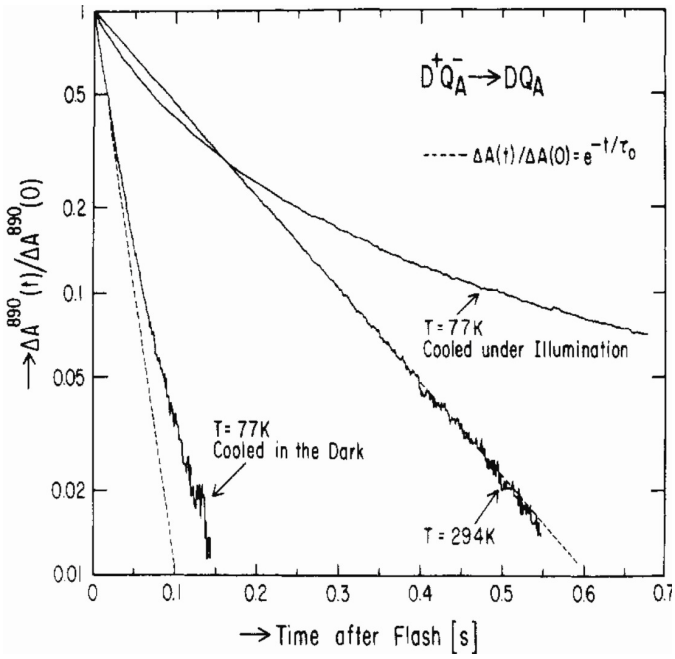

Figure 1.9
Charge recombination kinetics recorded in R26 RCs at room temperature (T=294K) and at cryogenic temperature (T=77K) for RCs cooled in the dark and in the light. From Kleinfeld, 1984.

(Kleinfeld, 1984) proposed that the *dark-adapted* and the *light-adapted* conformations differed essentially in the distance between between P^+ and Q_A^- and that the distribution of rate constants reflected essentially a distribution of distances between the cofactors. This interpretation has been recently disfavoured on the basis of high-field EPR measurements performed on RC crystals grown in the light or in the dark (Flores, 2010). No change in the distance and relative orientations between P and Q_A have been observed between RC in the neutral or charge separated state.

Kleinfeld and colleagues (Kleinfeld, 1984) also showed that RCs frozen in the dark were incompetent for the final electron transfer step ($P^+Q_A^-Q_B \rightarrow P^+Q_AQ_B^-$). On the other hand, RCs frozen under illumination retained their ability to extend the charge separation to the final electron acceptor, Q_B. This dependence on the illumination history was fully reversible upon thawing. These results indicate that the protein changes its structure in response to photoinduced charge separation (conformational relaxation) and suggest that some of these conformational changes are a prerequisite for the $P^+Q_A^-Q_B \rightarrow P^+Q_AQ_B^-$ electron transfer (conformational gating). The existence of a conformational gate, which rate limits the electron transfer from the primary to the

secondary quinine has been subsequently confirmed by independent, room temperature studies (Graige et al. (1998).

In the crystal structure of the RC cooled to cryogenic temperatures under illumination, i.e. trapped in an active state, Q_B was found 2.7 Å closer to Q_A than in the protein frozen in the dark and flipped by 180^o around the isoprenoid chain (Stowell, 1997). This movement of Q_B from an inactive-distal to an active-proximal site was originally proposed as the major structural change involved in the conformational gating step. However the correlation between the large shift in Q_B configuration and the rate limiting conformational change has been questioned on the basis of subsequent work performed in native and mutated RCs, which suggests more subtle structural rearrangements, possibly involving protein groups or hydrogen-bonding networks, as responsible of the gate (Kuglstatter, 2001; Xu, 2002a; Xu, 2002b; Breton, 2004).

Besides the Q_B movement reported by Stowell and colleagues (Stowell, 1997) confirmed by other laboratories (Fritzsch, 2002; Walden, 2002; Rahaman, 2004), other structural changes revealed by X-ray diffraction studies have been associated to charge separation, including a concerted movement of the H subunit after prolonged illumination (Katona, 2005) and, more recently, a light-induced change involving the side chain of a tyrosine residue close to P, caught by time-resolved Laue diffraction in the RC from the related species *Blastochloris viridis* (Wöhri, 2010). Furthermore, spectroscopic studies of charge recombination reactions (form the states $P^+Q_A^-$ and $P^+Q_B^-$) following a prolonged photoexcitation of the RC indicate that additional conformational changes take place in the light over the time scale of minutes, which lead to a dramatic stabilization of the charge separated states (Gouscha, 1997; Gouscha, 2000; Andréasson, 2003; Gouscha, 2003; Manzo, 2011). These dynamics have been proposed to play an important role in regulating the RC photochemistry *in vivo*, where the RC is exposed to light for long periods.

In the following we will focus again on the conformational dynamics which governs $P^+Q_A^-$ recombination. The kinetic analysis of this electron transfer process has been in fact used in the present thesis as the reference probe to investigate the associated RC relaxations and fluctuations in the different environmental conditions examined.

After the pivotal observations of Kleinfeld and coworkers (Kleinfeld, 1984), the kinetics of $P^+Q_A^-$ recombination have been systematically examined as a function of temperature (5-300K), illumination protocol and warming rate (McMahon, 1998). In this study a quantitative analysis of the coupling between electron transfer and protein

motions was developed, based on a quantum-mechanical electron transfer model (Fermi's golden rule and the spin-boson model). The static heterogeneity of the protein ensemble, conformational relaxations, and fluctuations between conformational substates were all cast into a single parameter, the energy gap between the charge separated ($P^+Q_A^-$) and the neutral (PQ_A) states, which was mapped on a single conformational coordinate along which the RC protein performs slow, diffusive motions (see Fig.1.10). The model accounts quantitatively for the behavior observed over the whole accessible temperature range in native (McMahon, 1998) and genetically modified RCs (Kriegl, 2004), in a water-glycerol solvent and in RCs trapped in a sol-gel matrix (Kriegl, 2003). According to this dynamic model (McMahon, 1998), at physiological temperatures the RC protein, following light-induced transition to the $P^+Q_A^-$ state, relaxes rapidly from the *dark-adapted* to the *light-adapted* conformation, solvating the altered charge distribution. This relaxation is associated with a decrease in the energy gap between $P^+Q_A^-$ and the PQ_A ground state, which is reflected in a decrease of the electron transfer rate, i.e. in the stabilization of the charged separated state (Fig.1.10). At room temperatures, moreover, the RC protein rapidly samples the conformational substate ensemble, so that averaging of the corresponding rate distribution occurs over the time scale of charge recombination. This gives rise to an almost exponential kinetics of $P^+Q_A^-$ recombination (life time, $\tau \approx 10^{-1}$ s). At variance, freezing RCs in the dark at temperatures between 250 and 150K hampers progressively the relaxation from the *dark-adapted* to the stabilized, *light adapted* conformation, as well as the interconversion between conformational substates: this hindrance of the conformational dynamics results in a progressive increase of the average rate constant for $P^+Q_A^-$ recombination and in a progressively broader distribution of rate constants (McMahon, 1998). In summary, it appears that the recombination kinetics of the primary charge separated state is a sensitive probe of the associated internal RC dynamics.

The structural basis of the relaxation from the dark- to the light-adapted conformation has not yet been clarified, and different mechanisms of stabilization of the primary charge separated state have been proposed. From FTIR studies (Nabedryk, 1990b) it was suggested that highly localized conformational changes of the protein matrix near the Q_A site might play a key role in assisting the stabilization of the primary charge-separated state; alternatively it has been proposed that the protonation of amino-acid residues located at a large distance from Q_A (> 16 Å) can participate in the stabilization of the Q_A^- anion radical (Kalman, 1994). This appears reasonable since the

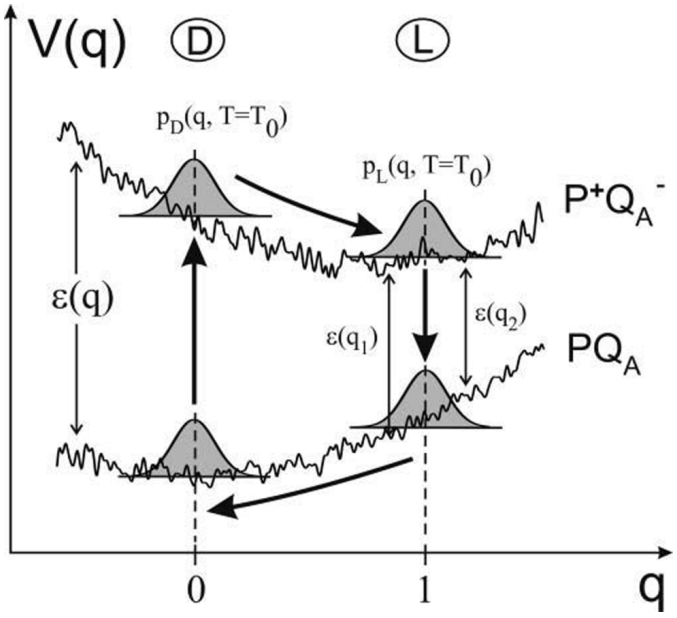

Figure 1.10
Schematic representation of the rugged energy surfaces of the primary charge separated state ($P^+Q_A^-$) and the neutral state (PQ_A). The energy gap ε separating the $P^+Q_A^-$ and the PQ_A state varies as a function of the conformational coordinate, *q*. D and L indicate the *dark-adapted* and the *light-adapted* conformations of the RC. Vertical arrows represent electron transfer processes, while the arrows along the energy surfaces indicate conformational relaxations of the RC structure. The shadowed distributions refer to the structural heterogeneity of the RC. From Kriegl, 2004.

the formation of one-electron states of the quinones in the primary photosynthetic electron transfer chain, Q_A and Q_B, is accompanied by protonation reactions, but the H^+ binding targets are protein residues rather than the quinone cofactors themselves (Maroti, 1997). A time-resolved optical spectroscopy study performed on wild-type RCs and four site-specific mutants with widely modified free-energy gaps for $P^+Q_A^-$ recombination has led to the suggestion to associate conformational relaxation with subtle rearrangements of the cofactors within their cavities (Kriegl, 2004). Finally, the involvement of water molecules, weakly bonded to the RC and perturbed by light-induced Q_A reduction (see below), has been recently invoked as playing a major role in the relaxation process which stabilizes the primary charge separation (Iwata, 2009).

Although low temperature studies represent the classical approach to study protein dynamics, in the last years, however, it has been shown that complementary information can be obtained following an alternative method, which consists in embedding the protein into amorphous matrices and in probing dynamical parameters of the protein *at room temperature* as a function of the hydration level of the matrix (see par. 1.6 and

Cordone, 2005). In particular, both in the case of a soluble (myoglobin) and of a membrane (RC) protein, the incorporation into dehydrated matrices formed by the disaccharide trehalose proved to be especially effective in reducing protein dynamics to levels comparable to the ones attained at cryogenic temperature. The use of glassy matrices, and the choice of trehalose among other saccharides, were suggested by the observation that vitrification in the presence of disaccharides appears to be the key strategy adopted in nature to preserve life under conditions of extreme drought and high temperature. This biological phenomenon, known as *anhydrobiosis*, is accompanied by a temporary, reversible arrest of metabolism, brought about by an extremely effective block in the dynamics of biomolecules. In the following paragraph we introduce the anhydrobiosis and its relation with glass-forming saccharides.

1.5 Anhydrobiosis and glass-forming disaccharides.

It is well known that some organisms are able to survive in *anhydrobiosis*, i.e. under conditions of high temperature and almost in the absence of water. As a convention, the state of anhydrobiosis starts at a content of residual water lower than 0.3% (grams of water per grams of dry weight of the cell or of the organism). The group of organisms capable of anhydrobiosis comprises: unicellular eukaryotes, as yeast; some fungal spores; some invertebrates, as the crustacean *Artemia salina*, and various species of nematodes; the mould *Dictyostelium*; some tardigrades; various plants (Crowe, 1998), including ferns, mosses and angiosperms, but not gymnosperms. In the case of angiosperms the ability to survive in the absence of water is extremely important in the seeds and in the pollen, but in some cases also in the sporophyte. The resistance to this specific kind of stress, also in relation to the possible biotechnological applications, is intensively studied in vegetal organisms. Two types of resistance are usually distinguished (Hoeckstra, 2001): when water availability is lower than usual, the stress is classified as *drought*, while when the residual water is not even sufficient to solvate protein surface and cover phospholipid bilayers surface, the organism is said to be tolerant to *desiccation* in an anhydrobiosis condition.

Anhydrobiotic organisms in general adopt two active strategies to withstand water depletion: they produce compatible solutes, e.g. proline, mannitol and in particular di- or oligo-saccharides, and/or proteins, more or less specific for the kind of stress they are experiencing. In plants the two strategies are usually concomitant and the proteins produced belong mainly to the LEA family (*Late Embryogenesis Abundant proteins*) or

to the dehydrin family. In yeast, at variance, the HSP12 protein, belonging to the Heat-Shock protein family, is produced in association with mannitol; its function is to stabilize the plasmatic cellular membrane under water stress conditions (Sales, 2000).

The production of disaccharides during water stress conditions, in particular of α,α-trehalose (currently called trehalose), and of maltose, is a conserved, widespread method to face water depletion, and it is used also by multicellular organisms: under water stress conditions, *Artemia salina*, or the desert plant *Selaginella*, produce trehalose up to 20% of their dry weight (Crowe, 1998). Also a more common plant, as *Phaseolus vulgaris*, following water depletion accumulates trehalose, thanks to the work of its symbiont *Rhizobium* (Farias-Rodriguez, 1998).

The elucidation of the molecular basis of the bioprotective role exerted by disaccharides has catalyzed a very large number of chemico-physical studies. Many of them have attempted to clarify the molecular mechanism leading to preserve the structure of phospholipid bilayers. As a consequence of desiccation, in fact, these cellular components can undergo wasteful structural alterations. Destabilization occurs not only when the water content is decreased, but also when the system is rehydrated. Upon desiccation phospholipid bilayers, undergo a liquid-crystalline to gel transition, due to the depletion of water molecules interacting with the phospholipid head groups. During this phase transition, delamination of the bilayer is common and it strongly affects the functionality of cellular membranes. Similar processes occur upon freezing when water molecules sequestered in crystals become unable to interact with the polar head groups of phospholipids. When these stress conditions stop, rehydration generally produces the fusion between phospholipid bilayers and increases membrane permeability. As far as proteins are concerned, desiccation affects their hydration shell, which plays a fundamental role in protein folding (Tanford, 1978). Furthermore, molecules which under normal conditions only weakly interact with the protein, due to their increased activity bind to the protein and cause the dislocation of one or more structural elements; these events can trigger the irreversible unfolding of the protein.

Several, often complementary, hypotheses have been proposed to explain the ability of saccharides to protect and preserve biostructures such as membranes and proteins. The proposed models also attempted to explain the peculiarity of trehalose, i.e. its superior bioprotective efficacy in comparison with other saccharides.

The first is the *water replacement hypothesis* which proposes that the sugar forms, upon water removal, hydrogen bonds directly with the biostructure, thus replacing the

hydrogen bonds normally formed in solution with water molecules (Carpenter, 1989). This hypothesis is supposed to be at the basis of membrane bioprotection by trehalose (Sum, 2003; Pereira, 2004; Pereira, 2006). It has been suggested that the peculiar efficacy of α,α-trehalose for membrane preservation in comparison to other disaccharides involves its α,α–(1,1) glycosidic linkage. The axial, axial linkage allows this molecule to adopt a clam shell structure that probably facilitates interactions between the sugar and the headgroup region by creating the appropriate hydrogen-bonding geometry to adjacent lipids (Albertorio, 2007).

The second hypothesis, i.e. the *water entrapment hypothesis* assumes that trehalose, during desiccation, rather than directly binding to biomolecules, confines and entraps the residual water molecules at the biostructure-matrix interface by glass formation, thus preserving the native salvation (Belton, 1994).

A third hypothesis, the *high viscosity hypothesis*, considers that the discriminating factor in cellular structure conservation is the ability of the sugar to form glassy matrices (characterized by an extreme high viscosity) at room temperature (Sampedro, 2004). Since trehalose vitrifies also at conditions which are sub-optimal for the other sugars, this would explain its peculiar bioprotective efficacy. The bioprotective effect of the host glassy matrix is thought to cause, at low water content, motional inhibition and hindering of the dynamic processes that lead to loss of native structure and denaturation.

Cesáro and co-workers (Sussich, 2001) have suggested that the peculiarity of trehalose arises from its polymorphism, i.e. from its capability to interconvert between the structurally similar anhydrous form and dehydrate form. This would favour in nature smooth, reversible dehydration/rehydration processes.

Recently, Cordone and colleagues (Francia, 2008) have proposed a fourth hypothesis, the *anchorage hypothesis,* which incorporates some aspects of the not mutually exclusive models outlined above, being in particular related to the *water entrapment hypothesis.* The model, based on a number of experimental observations and molecular dynamics simulations, proposes in fact that the inhibition of protein dynamics at the basis of the bioprotective properties of trehalose is due to the formation of a network of hydrogen bonds which, besides connecting sugar molecule to each other in the matrix, involves, at the sugar-matrix interface, water molecules of the hydration shell, simultaneously bonded to surface groups of the protein and to trehalose molecules of the matrix. This network “anchors” the protein surface to the matrix, thus coupling the internal protein dynamics to that of the matrix. In the framework of this model, the

peculiar efficacy of trehalose as a bioprotectant is due due to its propensity to form *intermolecular* hydrogen bonds. In spite of its structural similarity with trehalose, sucrose has a higher propensity to form *intramolecular* H bonds. Consistently, it has been shown that sucrose is almost ineffective in inhibiting the dynamics of RCs, even at extremely low contents of residual water of the embedding matrix (Francia, 2008; see also the next paragraph).

1.6 Electron transfer in RCs embedded in α,α-trehalose glassy matrices.

The kinetics of $P^+Q_A^-$ recombination have been extensively studied at room temperature in RCs embedded in dehydrated matrices formed by α,α-trehalose (for a review see Cordone, 2005) or sucrose (Francia, 2008). Figure 1.11A shows examples of recombination kinetics measured following a laser pulse in solution and in an amorphous α,α-trehalose matrix characterized by two different hydration levels. Incorporation of the RC in the glassy matrix and dehydration result in a remarkable acceleration of the decay. Additionally, the kinetics, which is essentially exponential in solution, become markedly non exponential in the dehydrated matrix. These effects are fully reversible upon rehydration.

The accelerated and distributed kinetics measured at room temperature in extensively dehydrated α,α-trehalose glasses are comparable to those observed in RC water-glycerol samples cooled in the dark at cryogenic temperatures (see par.1.4). It was therefore inferred that in sufficiently dehydrated matrices the RC conformational dynamics is hindered to an extent comparable to that observed in water-glycerol systems at cryogenic temperatures (Palazzo, 2002). More specifically it was concluded that at sufficiently low hydration of the α,α-trehalose matrix both the RC relaxation from the dark-adapted to the light-adapted conformation and the interconversion among lower tier conformational substates are suppressed on the time scale of charge recombination.

As previously reported (Palazzo, 2002; Francia, 2004a; Francia, 2004b; Francia, 2008), description of the survival probability *N(t)* of the $P^+Q_A^-$ state after the photoexcitation pulse requires a continuous distribution *p(k)* of rate constants *k*, i.e.:

$$N(t) = \frac{P^+Q_A^-(t)}{P^+Q_A^-(0)} = \int_0^\infty p(k)e^{-kt}dk \qquad \text{(eq. 1.1)}$$

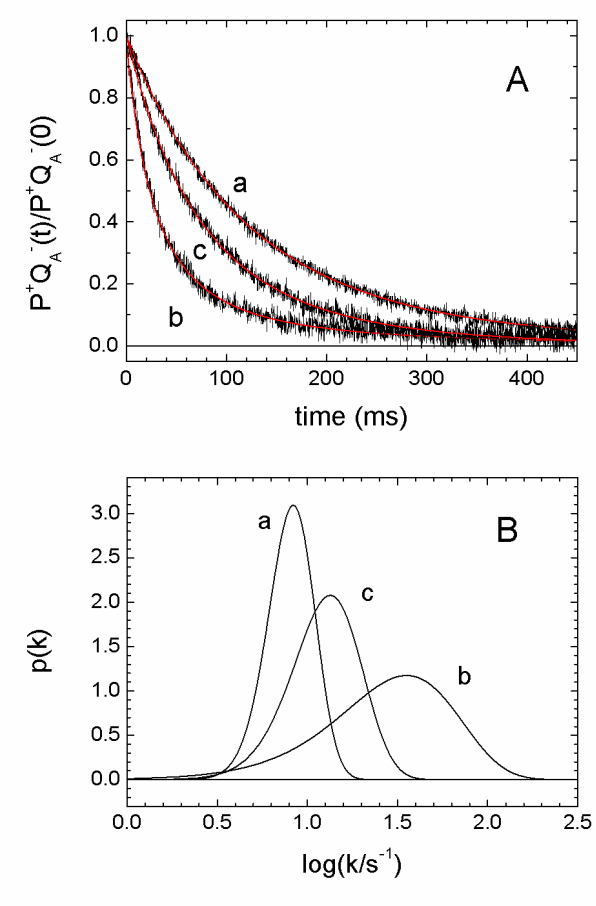

Figure 1.11
Kinetic analysis of $P^+Q_A^-$ charge recombination following laser excitation of RCs embedded in α,α-trehalose glassy matrices. Panel A shows recombination kinetics measured in solution (trace a) and in a sugar glassy matrix at two different hydration levels, corresponding to 4700 H_2O molecules per RC (trace b) and to 7800 H_2O molecules per RC (trace c). Continuous red lines are best fits to eq.1.9, yielding the following values of the kinetic parameters: (a) <k> = 8.3 s^{-1}, σ = 2.5 s^{-1}; (b) <k> = 35.5 s^{-1}, σ = 26.5 s^{-1}; (c) <k> = 13.4 s^{-1}, σ = 5.8 s^{-1}. Panel B shows the corresponding distributions of rate constants (Gamma distributions). From Francia, 2004b.

where t=0 is the time at which the laser pulse is fired. Following the approach first adopted by Feher and coworkers (Kleinfeld, 1984) to analyze $P^+Q_A^-$ recombination kinetics in RCs frozen at cryogenic temperature, the decay of the $P^+Q_A^-$ state can be fitted to a power law of the form

$$N(t) = (1 + k_0 t)^{-n} \qquad \text{(eq.1.2)}.$$

with k_0 and n as free parameters.

This parameterization in the time domain has the advantage that the corresponding distribution function *p(k)*, i.e. the inverse Laplace transform of *N(t)* (see eq.1.1), can be obtained analytically (Abramowitz, 1965), that is:

$$p(k) = \frac{k^{n-1}}{k_0^n} \frac{\exp(-k/k_0)}{\Gamma(n)} \qquad \text{(eq.1.3)}$$

where $\Gamma(n)$ is the gamma function and k_0 and n are related to the average rate constant, $\langle k \rangle$, and to the variance, σ^2, of the distribution by:

$$\langle k \rangle = nk_0 \qquad \sigma^2 = nk_0^2 \qquad \text{(eq.1.4).}$$

It was found that under all the conditions considered (i.e. both in solution RC and in RC-trehalose matrices at different hydration levels) the approach described above gave an adequate description of $P^+Q_A^-$ recombination kinetics.

The rate distributions calculated using eq.1.3 from the kinetic parameters best fitting the kinetic traces of Fig.1.11A are shown in Figure 1.11B. It can be seen that upon incorporation of the RC into the matrix and dehydration the distribution moves to higher <k> values (acceleration of the kinetics) and undergoes a dramatic and progressive broadening. In extensively dehydrated trehalose matrices, a quasi-static structural heterogeneity of the RC is revealed by the large broadening of the distribution of electron transfer rates which results from the trapping of conformational substates. At variance, in relatively wet glasses interconversion between substates and protein relaxation, although slowed down as compared to solution, take place over the time-scale of charge recombination. This leads to partial averaging of the static conformational heterogeneity of RCs (narrowing of p(k)) and partial stabilization of the charge separated state (decrease of <k>) (see the values of the kinetic parameters in the caption of Fig.1.11).

Fig.1.12 shows the dependence of the average rate constant, <k>, and of the rate distribution width, σ, upon the content of residual water of the matrix ((H_20/trehalose) molar ratio) obtained from measurements similar to those shown in Fig.1.11. When the H_20/trehalose ratio is decreased below approximately 0.7 both <k> and σ increase steeply. As already mentioned, we remark that the maximal values of <k>, measured at room temperature in extremely dehydrated matrices, are comparable to those measured

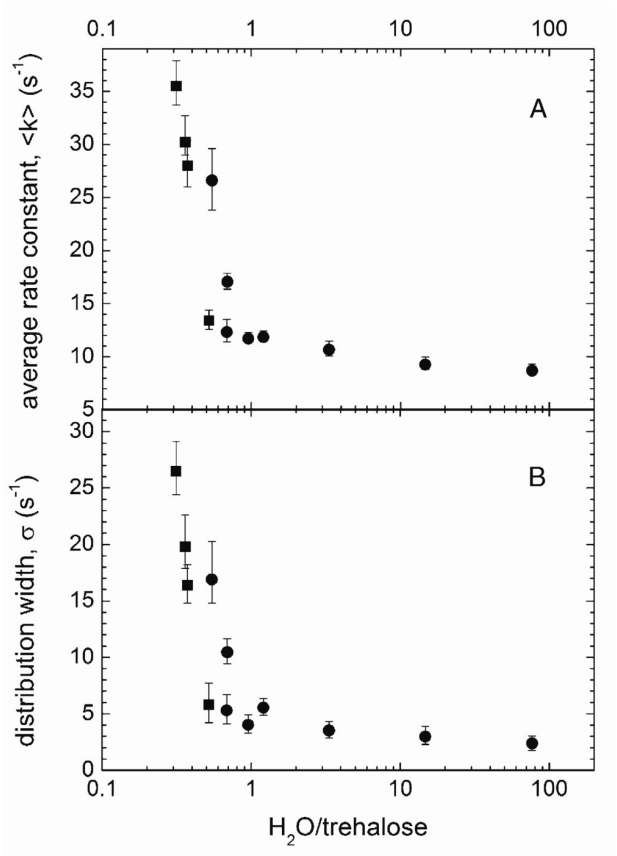

Figure 1.12
Dependences of the average rate constants (A) and distribution width (B) from the H_20/disaccharide molar ratio for RC embedded in α,α-trehalose matrices. The α,α-trehalose/RC molar ratio is equal to 10^4. From Cordone, 2005.

in water-glycerol samples at temperature lower than 40K (McMahon, 1998). Furthermore, the width of the rate distribution in the driest matrices is even larger than that observed at 10K in water-glycerol. It appears in conclusion that in dehydrated trehalose matrices the RC relaxation from the dark- to the light-adapted conformation (see Fig.1.10) and the RC thermal fluctuation among lower tier conformational substates are essentially blocked over the time scale (0.1 s) of the charge recombination process. These results are consistent with the *anchorage model* outlined above (see par. 1.5), i.e. with the notion that a water mediated H bond network "anchors" the protein surface to the matrix, thus tightly coupling the internal dynamics of the RC to that of the embedding glass.

The *anchorage model* has been further supported by studies in which the kinetics of $P^+Q_A^-$ recombination have been studied as a function of the photoexcitation time, also following prolonged illumination periods (up to 200 s) (Francia et al, 2004b). The

underlying idea was that, even with a protein dynamics strongly inhibited on the tens-of-ms time scale, when the RC experience the charge separated state for a sufficiently long spell of time, the protein-water-trehalose structures postulated by the *anchorage model* could undergo structural rearrangements stabilizing $P^+Q_A^-$. The results of these measurements (shown Figure 1.13) have revealed that, upon increasing the duration of the photoexcitation from about 10 ms to a few seconds, the charge recombination process become progressively slower (Fig.1.13A) and less distributed (Fig.1.13B). Control measurements performed in RC solutions show that the effect is observed only in the glassy matrix. In line with the *anchorage model* it was proposed that, when the electric field perturbation generated by primary charge separation is maintained for a sufficiently long time, the continuous attempts of the protein to undergo conformational changes toward the more stable *light-adapted* state, cause a partial collapse of the hydrogen bond network connecting the protein surface to the matrix. This, in turn, results in partial unlocking of the protein surface and increases the protein motional freedom. During continuous illumination, the RC protein is gaining therefore a limited conformational flexibility which allows both partial relaxation (decrease of <k>) and substate averaging (decrease of σ).

Matrices formed by α,α-trehalose exhibit a peculiar efficacy in hindering the RC protein dynamics. As an example, when the RC was embedded in polyvinyl alcohol matrices (PVA), the effects on $P^+Q_A^-$ charge recombination were extremely weak even at PVA hydration levels lower than those obtainable in trehalose matrices (Francia, 2004a). The peculiarity of trehalose became particularly evident when the charge recombination kinetics were compared in dehydrated matrices formed by α,α-trehalose or by sucrose (Francia, 2008). Fig.1.14 compares the dependence of the average rate constant <k> and of the rate distribution width σ upon the (H_2O/RC) molar ratio in trehalose and sucrose matrices. As already observed, in the case of trehalose both $<k>$ and σ undergo a sudden, dramatic increase, when the residual water content of the matrix is decreased below a threshold of ~8 x 10^3 H_2O molecules per RC. On the contrary, in the sucrose matrices, $<k>$ and σ values remains essentially unchanged upon decreasing the water content over this range. It is noteworthy that, even in extremely dehydrated, hard sucrose glasses $P^+Q_A^-$ recombination kinetics are scarcely affected as compared to solution and strongly resemble those measured in weakly interacting PVA matrices (Francia, 2004b). This behavior suggests that in sucrose matrices, upon dehydration, the sucrose molecules, which have a high propensity to

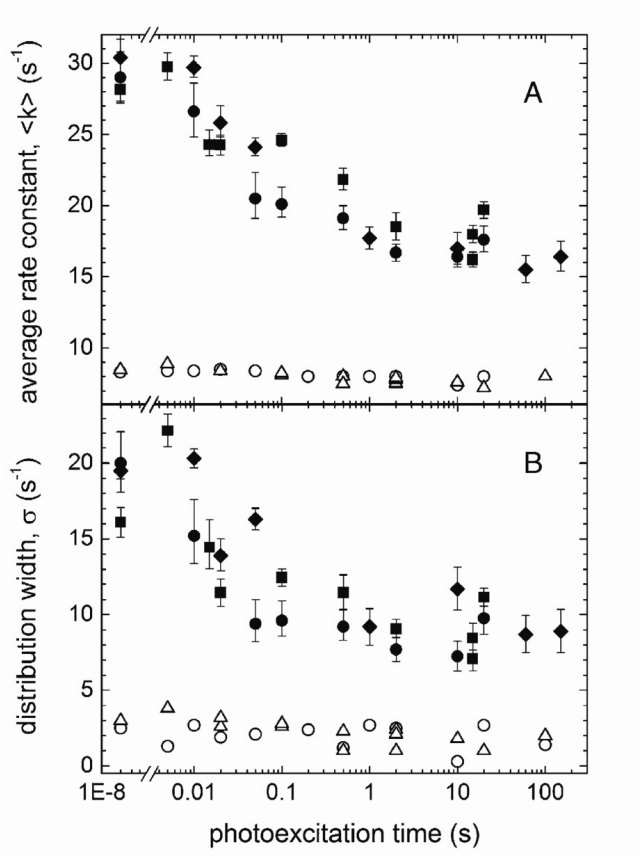

Figure 1.13
Prolonged illumination experiments in RCs embedded in α,α-trehalose matrices. The filled symbols refer to extremely dehydrated matrices (H_2O/trehalose ≈ 0.5); circles, squares and diamonds refer to different sets of independent measurements performed at slightly different contents of residual water (from 5900 to 5400 water molecules per RC). The empty symbols correspond to measurements in solution RCs (in the presence of 0.4 M trehalose). Panels A and B show the dependences of <k> and σ upon the duration of the illumination period. The measurements in solution are control data and show that in these conditions, as expected, the duration of the photoexcitation does not affect the charge recombination kinetics. From Francia, 2004b.

form intramolecular H bonds, compete successfully with the RC protein for hydrogen bond formation. As a consequence, the resulting structural and dynamic protein-matrix coupling is very weak, even at extreme dehydration: the motional freedom of the RC surface is essentially unrestricted, in spite of the rigidity of the sucrose embedding matrix and the RC protein undergoes a fast relaxation to the *light-adapted* conformation, as well as a rapid interconversion among low tier conformational substates. On these basis it can be also expected that the bioprotective action of sucrose is weaker than that of trehalose. The study of the thermal stability of RC embedded in these two sugar glassy matrix fully confirmed this conclusion (Francia, 2008).

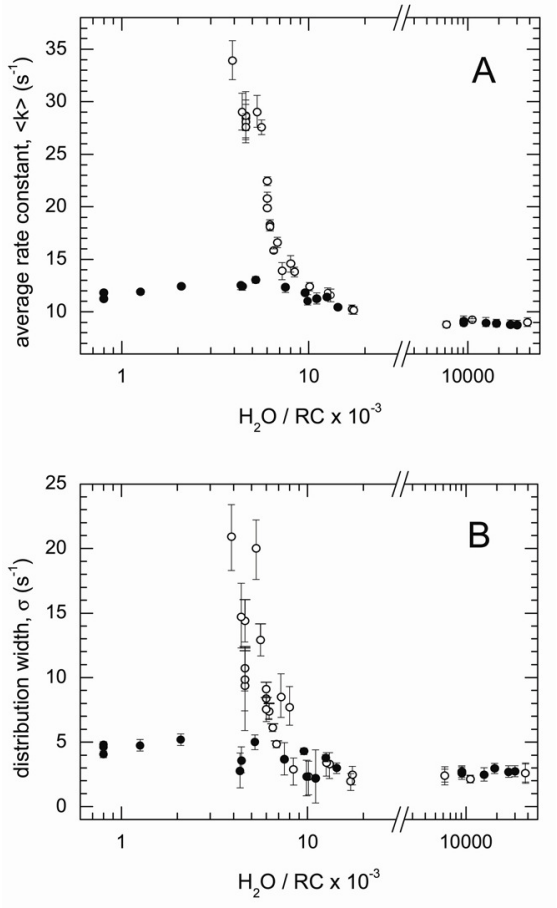

Figure 1.14
Analysis of $P^+Q_A^-$ charge recombination kinetics for RCs embedded in α,α-trehalose (empty circles) and sucrose (filled circles) matrices. Panels A and B show the dependence of the average rate constant, <k>, and of the distribution width, σ, upon the H_2O/RC molar ratio, respectively. From Francia, 2008.

As a whole, the results summarized in this section, are in line with the proposal that the structural/dynamical coupling in water-protein-sugar matrices is mainly regulated by hydrogen-bond networks involving residual water molecules, and anchoring the protein surface to the matrix. The underlying protein-sugar-water interactions can be highly specific, as shown by the radically different behavior of glassy matrices formed by structurally related disaccharides.

2. AIM OF THE RESEARCH

Inasmuch as myoglobin can be regarded as an established paradigm to study function-dynamics relationships in soluble proteins, the bacterial photosynthetic reaction center has become a prototype when approaching similar problems in integral membrane proteins which catalyze electron transfer, one of the simplest, and largely widespread bio-catalytic events. As outlined in the Introduction, the internal conformational dynamics of the RC protein play a central role in stabilizing the primary charge separated state ($P^+Q_A^-$) induced by photoexcitation. The RC protein behaves as an inhomogeneous dielectric medium, which relaxes over different time scales in response to the electric field generated across the protein complex by its primary photochemical activity. These conformational relaxations, which reduce the probability of wasteful charge recombination events, are of great importance in regulating the photochemical activity of the RC, optimizing the quantum yield of photosynthesis. The structural basis and the temporal sequence of these conformational events are at present lively debated. A closely related, unraveled problem concerns the dynamical coupling between the RC and its environment. Although in soluble proteins the slaving of internal dynamical processes to thermal fluctuations of the solvent has been deeply studied, both on the experimental and theoretical ground, (see par.1.1), much less is known about solvent/protein interactions and their effects on internal dynamics, in the case of large integral membrane complexes as the RC.

The main purpose of the present thesis has been to contribute to elucidate these interconnected questions. The thermal fluctuations of the RC and its dielectric conformational relaxation following photoexcitation have been probed by analyzing the recombination kinetics of the primary charge-separated ($P^+Q_A^-$) state, using time resolved optical and EPR spectroscopies. The RC dynamics coupled to this electron transfer process has been modulated *at room temperature* by incorporating the RC into amorphous matrices and by varying the hydration state of the system. Specifically, the incorporation of the RC into extensively dehydrated trehalose matrices inhibits *at room temperature* the RC dynamics to an extent comparable to that attained at cryogenic temperatures in water-glycerol system. This matrix approach represents a valuable tool in the study of function/dynamics relationships in proteins, providing, at the same time,

unique information on the mechanisms of protein/solvent interaction and on the role of the hydration shell dynamics in driving and controlling internal protein motions.

The work presented has addresses in parallel the problem of clarifying, at the molecular level, the tight dynamical coupling between the protein and the matrix, arising in trehalose glasses at low hydration levels. We aimed, in particular, at testing a molecular model (the *anchorage hypothesis*) previously developed to explain the extraordinary and peculiar ability of dehydrated trehalose matrices to protect biostructures against thermal denaturation. This property is receiving an increasing attention, in view of the growing employment of trehalose in food, pharmaceutical and biotechnological sciences to optimize long-term storage of biological samples. The kinetics of thermal denaturation, analyzed in RCs incorporated into different amorphous matrices, have provided concomitantly useful information on the large scale RC dynamics involved in the loss of its native structure.

The results obtained are presented and discussed in 5 chapters, dealing with different aspects of the RC/matrix dynamical coupling and with the conformational stabilization of the RC charge-separated state. In Chapter 4 the effects of the internal flexibility of the RC structure on the protein/matrix dynamical coupling are investigated by combining kinetic measurements of charge recombination and Brownian dynamics simulations performed on native and mutated RCs. In Chapter 5 high-field EPR spectroscopy, both in cw and pulsed modes, has been used to examine the structural and dynamical properties of the RC cofactors involved in primary charge separation when the protein is embedded into polymeric and glassy trehalose matrices. In Chapter 6, water sorption has been studied by FTIR spectroscopy in RC-detergent films dehydrated under controlled relative humidity in the absence of trehalose. The spectral analysis of the water combination and association bands, carried out in parallel with the kinetic analysis of $P^+Q_A^-$ recombination, has provided convincing evidence that the thermal fluctuation and conformational relaxations which stabilize the charge-separated state are driven and controlled by the dynamics of the RC hydration shell. This result is fully consistent with the proposed *anchorage model* of trehalose matrices. The results of Chapters 7 and 8 have better defined the role of the sugar in forming the network of hydrogen bonds which, according to the *anchorage model*, modulates the RC internal dynamics. It has been shown, in particular, that the dynamical properties of the trehalose-water-RC structures formed upon dehydration of the matrix are markedly affected by the duration of photoexcitation as well as by the sugar/protein molar ratio.

Furthermore, a minimum ratio, corresponding to a monolayer of trehalose coating the RC complex, appears to be necessary to completely block the large scale RC dynamics leading to thermal denaturation. Finally, in Chapter 9, we acquired light-minus-dark difference FTIR spectra in hydrated and dehydrated RC films, in an attempt to determine the chemical nature and the possible location of the groups involved in the long-time (10 s) stabilization of the primary charge-separated state of the RC. Possible candidates are water molecules weakly hydrogen bonded to the RC and aminoacidic residues in the vicinity of the primary donor (P) and acceptor (Q_A) binding pockets.

3. MATERIALS AND METHODS

3.1 Reaction center purification and preparation of samples.

3.1.1 Reaction center purification.

Purified RC preparations have been obtained from the carotenoid-containing *Rb. sphaeroides* wild type 2.4.1 strain and from the carotenoid-less strain R26, essentially as described by Baciou (Baciou, 1995) and Gray (Gray, 1990), respectively.

Bacterial cells from R26 and wild type 2.4.1 strains were grown respectively on RCV and Sistrom mediums (Sistrom, 1960); chromatophores of both strains were prepared from bacterial cells as described by Baccarini-Melandri (Baccarini-Melandri, 1971). The purification procedures for the wt and the R26 RCs, as described in the references cited above, differ significantly, although in both cases the detergent N,N-dimethyldodecylamine-N-oxide (LDAO) is used to solubilise the RC complex.

In the wt 2.4.1 purification procedure, starting from 100 mL of chromatophores in 100 mM phosphate buffer, pH 7.5 at an optical density OD_{800} = 50, a first extraction is performed at 26°C with 0.35% (volume/volume) LDAO; the suspension is stirred in the dark for 15' and then ultracentrifuged for 1h30' at 4°C and 40000 rpm (50.2Ti Beckman rotor). The supernatant is supplemented with ammonium sulphate 22% (weight/volume) in the dark at 4°C, stirred for 10' and centrifuged at 27000g for 10' at 4°C. A floating pellet is obtained which is collected, resuspended in ≈ 25 mL of 10 mM TRIS HCl, pH 8.0, 0.08% LDAO, and dialyzed overnight at 4°C against 10 mM TRIS HCl, pH 8.0, 0.08% LDAO, to eliminate ammonium sulphate. After dialysis, the preparation is loaded on a DEAE column (DE52, Whatman) and extensively washed with buffer at increasing ionic strength (80 mM and 135 mM NaCl). Finally, the RC is eluted from the DEAE column with 280 mM NaCl and the preparation is dialyzed overnight at 4°C against 10 mM TRIS HCl, pH 8.0, 0.025% LDAO.

At variance, in the case of R26, starting from 100 mL of chromatophores in 20 mM TRIS HCl, pH 8.0 at an optical density OD_{800} = 50, two LDAO extractions, are performed. The first extraction is carried out at room temperature with 0.25% (volume/volume) LDAO, after the addition to the chromatophore suspension of 125 mM NaCl, 1 mM Na-ascorbate and 0.5 mM PMSF; following LDAO addition, the suspension is stirred in the dark for 45' and ultracentrifuged for 1h30' at 4°C and 40000 rpm (50.2Ti Beckman rotor). The pellet is harvested and, after adding NaCl, Na-

ascorbate and PMSF at the same concentration of the previous extraction, extracted with 0.35% (volume/volume) LDAO. The preparation is stirred on ice for 30' in the dark and ultracentrifuged for 1h30' at 4°C and 40000 rpm (50.2Ti Beckman rotor). The supernatant is collected and diluted 1:2 with buffer, to decrease NaCl concentration. The preparation is then loaded on a DEAE column (DE52, Whatman) and washed at increasing ionic strength (80 mM, 110 mM and 135 mM NaCl). The RC is eluted from the DEAE column with 280 mM NaCl and the preparation is dialyzed overnight at 4°C against 10 mM TRIS HCl, pH 8.0, 0.025% LDAO.

Generally, following the described purification procedure, the secondary quinone acceptor, Q_B, is washed out in about half of the RC population, both in wt 2.4.1 and R26 RCs. To reconstitute the quinone at the Q_B site, the RC preparation was loaded on a smaller DEAE column (volume ≈ 10 mL) and extensively washed with ≈ 250-300 mL of a 20 μM UQ_{10} solution in 10 mM TRIS HCl, pH 8.0, 0.08%, LDAO. The RC is eluted from the DEAE column with 280 mM NaCl and dialyzed overnight at 4°C against 10 mM TRIS HCl, pH 8.0, 0.025% LDAO. The occupancy of the Q_B site is estimated from the relative amplitude of the slow kinetic phase (see par.1.3) of charge recombination following a laser pulse. This reconstitution method yields an occupancy of the Q_B site of 95-98% for R26 RCs and 89-91% for wt 2.4.1 RCs.

When needed, to replace the detergent LDAO with n-octyl β-D-glucopyranoside (OG) the LDAO suspension of purified RCs, eluted from the DEAE column (DE52, Whatman), was dialyzed twice for 10 hours against a one hundred times larger volume of 10 mM Tris buffer, pH 8.0 in the presence of 0.1 % OG rather than 0.025 % LDAO. LDAO and OG were from Sigma-Aldrich and Anatrace (Maumee, OH, USA), respectively.

3.1.2 Samples for optical and difference FTIR measurements.

RC-detergent films for optical and FT-NIR measurements (see chapter 6) were prepared by depositing a drop (0.168 mL) of the dialyzed RC-detergent solution at 60 μM RC concentration, in the presence of 10 mM o-phenanthroline and 0.025 % LDAO or 0.1 % OG, at the center of a 50 mm diameter CaF_2 window. The sample was subsequently dried in a desiccator for about 4 hours under N_2 flow at room temperature and equilibrated at a given relative humidity as described in par.3.2. Essentially the same procedure was used for the preparation of samples examined by light-induced

FTIR difference spectroscopy (see chapter 9), except that the volume of the RC solution drop was decreased to 40-60 μL.

RC-trehalose glassy samples for optical and FT-NIR spectroscopy have been prepared according to the following procedure. A drop (160 μL) of 60 μM RC in 10 mM TRIS HCl, pH 8.0, 0.025 %; LDAO was mixed with 40 μL or 80 μL of a 1.2 M α,α-trehalose solution in 10 mM TRIS HCl, pH 8.0, 0.025% LDAO in order to obtain a disaccharide/RC molar of 5000:1 or 10000:1, respectively. The mixed solution drop is deposited on a 50 mm diameter CaF_2 (CRYSTAN, Poole, UK) or optical glass window. The vitrification method, which consists essentially in flowing dried nitrogen on the liquid drop, was somewhat different for the matrices characterized by a sugar/RC molar ratio equal to 5000 or 10000. An undesirable phenomenon, which can occur when drying a drop of a suspension containing solute particles, is the migration of the solute toward the perimeter of the drop during evaporation of the solvent. The solute, initially dispersed in the liquid drop, becomes concentrated into a ring along the perimeter of the dried sample. Such ring deposits, common wherever drops containing dispersed solids (e.g. coffee) evaporate on a surface, can occur also in the case of RC suspensions. This characteristic pattern of the deposition has been ascribed to a form of capillary flow in which pinning of the contact line of the drying drop ensures that liquid evaporating from the edge is replenished by liquid from the interior. The resulting outward flow can carry in principle all the dispersed material to the edge (Deegan, 1997). In the case of RC containing trehalose solutions this behaviour can easily result in strongly inhomogeneous dried glassy matrices, which render problematic optical and IR measurements, also hampering a physically meaningful definition and measurement of the water per RC molar ratio. The outward capillary flow which can cause the formation of a dense RC ring at the perimeter of the dried drop can be prevented or limited by increasing the viscosity of the solution or by creating a gradient in the evaporation flow, i.e. by inducing a faster evaporation at the center of the drop. For a disaccharide/protein molar ratio of 10000, reasonably homogeneous wet RC-trehalose glasses can be obtained by flowing at room temperature dried nitrogen in a desiccator which contains the deposited sample drop for approximately 5 hours and by placing a small fan over the drop at a distance of approximately 10 cm. The viscosity of the drop in the presence of the relatively high concentration of trehalose employed in this case, and the gentle wind produced by the fan counteracts the migration of the RC toward the perimeter during the time interval necessary to induce the glass transition. When the transition has occurred,

RC migration inside the matrix is blocked. In the case of the samples with a lower trehalose/RC molar ratio ($5 \cdot 10^3$), characterized by a lower viscosity, a different strategy is employed. The sample is vitrified by fluxing the dried nitrogen directly over a localized area in the middle of the drop through a thin Pasteur capillary. By this way a gradient for water evaporation is created which apparently contrasts the capillary flow. The further dehydration of the solid samples and the control of their hydration level by an isopiestic method are described in par.3.2.

3.1.3 Samples for EPR measurements.

In order to examine EPR signals from the ubiquinone UQ_{10} radical anions, the high-spin non-heme Fe^{2+} (S = 2) of the RC has to be removed and replaced by diamagnetic Zn^{2+}, thus avoiding fast spin relaxation of the UQ_{10} anions. The procedure used for the replacement of Fe^{2+} by Zn^{2+}, modified from Utschig and colleagues (Utschig, 1997), is described in the following. A volume of 5 mL of a R26 RC preparation with optical density at 803 nm OD_{803} = 20 in 10 mM TRIS HCl, pH 8.0, 0.025% LDAO and 10 μM EDTA (obtained as described in the previous paragraph) is incubated on ice in the presence of 5 mM o-phenanthroline and ≈ 50 μM UQ_{10} for 5 minutes. After 30 minutes of additional incubation on ice in the presence of 1.5 M lithium thyocyanate (LiSCN), 8 mM mercaptoethanol and 1 mM zinc sulfate ($ZnSO_4$) are added to the solution which is incubated for 30' always at ice temperature. The removal of the H subunit by LiSCN allows the replacement of Fe by Zn. Following this treatment, the preparation is extensively dialyzed at 4°C against 1 L of 10 mM TRIS HCl, pH 8.0, 0.045% LDAO and 5 grams of CHELEX to remove completely the excess zinc.

This procedure resulted in a partial replacement of Fe^{2+} by Zn^{2+}: The ratio of the $Q_A^{\bullet-}$-to-$P_{865}^{\bullet+}$ spectral intensities in the Q-band EPR spectra (see par.5.1.1) showed that Fe^{2+} was retained in about half of the RC population. Evaluation of the Fe^{2+} and Zn^{2+} content by Inductively Coupled Plasma Atomic Emission Spectroscopy (ICPAES) before and after the replacement showed additionally that the ≈50% decrease of the Fe^{2+}/RC ratio was compensated by an approximately corresponding increase of the Zn^{2+}/RC ratio. The absence of a significant fraction of Fe-depleted RCs, lacking bound Zn^{2+}, was confirmed by the comparable extent of photoxidized $P_{865}^{\bullet+}$ induced by a saturating laser flash in the native and Zn^{2+}-replaced RC preparation. On the contrary, a considerably reduced efficiency of light-induced charge separation is expected in Fe-

depleted RCs which have no metal ion occupying the Fe site. In our preparation, the fraction of photoactive RC, after the replacement, was larger than 90%. This was estimated from the absorbance change induced by a train of six laser pulses at 422 nm, assuming a differential extinction coefficient $\Delta\varepsilon_{422} = 17.5 \quad mM^{-1}cm^{-1}$.

The Zn^{2+}-RC preparation (at a concentration of about 50 μM) was supplemented with stigmatellin, one of the most potent inhibitors of the $Q_A^{\bullet-}$-to-Q_B electron transfer, at a stigmatellin-to-RC molar ratio of 2. The suspension was subsequently concentrated by ultrafiltration using a 100 kDa cut-off cartridge (Amicon) up to a RC concentration of 335 μM. An aliquot, frozen in liquid nitrogen after addition of glycerol at a final concentration of 20% v/v, was stored at -80 °C for EPR and optical measurements of RC/water samples.

The RC/trehalose glassy sample for EPR measurements was prepared according to the following procedure: A volume of 50 μL of the concentrated (335 μM) RC was mixed with 100 μL of 1.67 M trehalose to obtain a sugar-to-RC molar ratio of 10^4. Trehalose (> 99% purity) was purchased from Hayashibara Shoij (Okayama, Japan). The RC/trehalose solution was layered on an optical window and dried in a desiccator under N_2 flow at room temperature. The glassy sample obtained in about four hours of flux was further dehydrated by alternating incubation under N_2 atmosphere at room temperature for 18 hours and direct N_2 flux for six hours; this drying cycle was repeated three times.

The RC/PVA sample for EPR measurements was prepared by mixing 75 μL of the concentrated RC (335 μM) with an equal volume of 10% w/v PVA (Fluka, $M_w \approx 130000$). To form the film, the same drying procedure used for the RC/trehalose sample was employed. Since optical measurements were not possible in these samples, because their absorbance was too high, RC/trehalose and RC/PVA samples, with a three- and four-times lower RC concentration, respectively, were prepared in parallel. These samples were characterized by the same trehalose-to-RC and PVA-to-RC molar ratios as those prepared for EPR measurements. Also the same drying procedure was applied for the two matrices. RC/trehalose glassy matrices were stored at room temperature, while RC/PVA films were kept at 4° C.

3.2 Control of the hydration state of amorphous matrices.

Different hydration levels of the RC-detergent films were obtained by equilibrating the samples with hydrating saturated solutions providing defined values of relative humidity, *r*. To this end the window on which the RC film was formed was inserted into a specifically designed sample holder, equipped with a second CaF_2 window, to form a gastight cylindrical cavity (volume ≅7.7 mL), which contained at the bottom about 1.5 mL of the hydrating solution. A picture of the sample holder, showing the salt solution at the bottom of the cavity and a RC-LDAO film formed on the inner side of one of the optical windows is shown in Figure 3.1.

The following saturated solutions were employed to obtain the desired relative humidity (indicated in brackets) at 297 K: KNO_3 (94%), KCl (84%), NaCl (75%), NH_4NO_3 (63%), $Mg(NO_3)_2$ (53%), K_2CO_3 (43%), $MgCl_2$ (33%), CH_3COOK (23%), LiCl (11%), $KOH{\cdot}2H_2O$ (9%), $NaOH{\cdot}H_2O$ (6%), P_2O_5 (3%). The indicated values of relative humidity at 297 K have been taken from Greenspan, 1977. Spectroscopic measurements (see par. 3.3 and 3.4) were performed directly on the film exposed to the saturated atmosphere inside the holder. This allowed to monitor directly the time course of water sorption/desorption during equilibration of the RC film by following the evolution of the NIR water combination band at about 1940 nm (see par 6.1.1). When the relative humidity inside the holder was varied over the explored range ($3\% \leq r \leq 94$ %), a steady hydration level was reached in a few hours. After replacement of the hydrating solution in the holder, RC-detergent films were always allowed to equilibrate for a minimum of 15 hours.

In several sets of measurements (see par. 7.1.1-7.1.3 and chapter 8) the same isopiestic method was also applied to control the hydration level of RC-trehalose glassy matrices. In this case, however, due to the large amount of sugar present in the matrix and to the high affinity for water of trehalose, the attainment of thermodynamic equilibrium at given value of relative humidity was much slower, as compared to RC-detergent films. In fact, significant changes in the hydration level of RC-trehalose matrices occurred on the time scale of days, rather than a few hours as in RC-detergent films. Furthermore, even over this long time scale, a true equilibrium could be obtained only for matrices characterized by $5 \cdot 10^3$ trehalose molecules per RC, and not for a (trehalose/RC) molar ratio equal to 10^4 (see par 7.1 and 7.2 of the Results). Nevertheless, the isopiestic method proved to be very useful, allowing a fine tuning of the content of residual water.

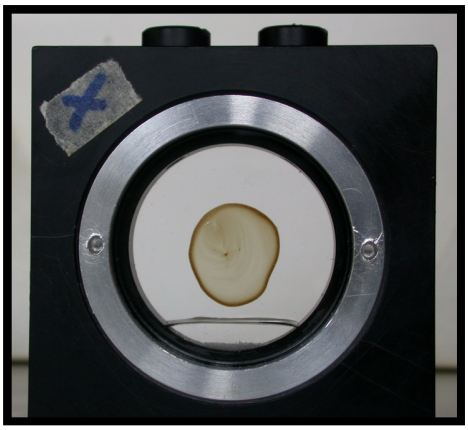

Figure 3.1
Picture of a RC-detergent film deposited on a CaF_2 window and incubated in the presence of a saturated salt solution visible at the bottom of the gastight holder.

In other sets of measurements, the RC-trehalose matrices were dehydrated by incubating them under nitrogen atmosphere. As a general rule, following the formation under dry N_2 flow of the glassy matrix in about 4 h (see par. 3.1), the content of residual water (typically ≈1.2 H_2O molecules per trehalose molecule) was further reduced by alternating incubation under N_2 atmosphere at 30°C for about 12 hours and under vacuum for approximately the same time. The maximum dehydration was attained after several days of incubation, i.e. in a time comparable to that needed to reach an equivalent dehydration by the isopiestic method. During spectroscopic measurements, to avoid water exchange between the sample and the environment, the optical window on which the RC-trehalose glassy matrix was formed was inserted into same type of gastight sample holders used to control the hydration state through the isopiestic method, filled with dry N_2.

During the long incubation times necessary to vary the hydration level of the system, the RC-trehalose matrices retained a good transparency, except for a few samples in which under rather hydrated conditions small areas of micro-crystallization appeared. Upon extensive dehydration clefts became often visible at the surface of the matrices. At the same time the matrices became more fragile and the samples had to be handled with care to avoid fractures in the glass and its detachment from the optical window. Pictures of a typical RC-trehalose glass taken during the dehydration period are shown in Figure 3.2.

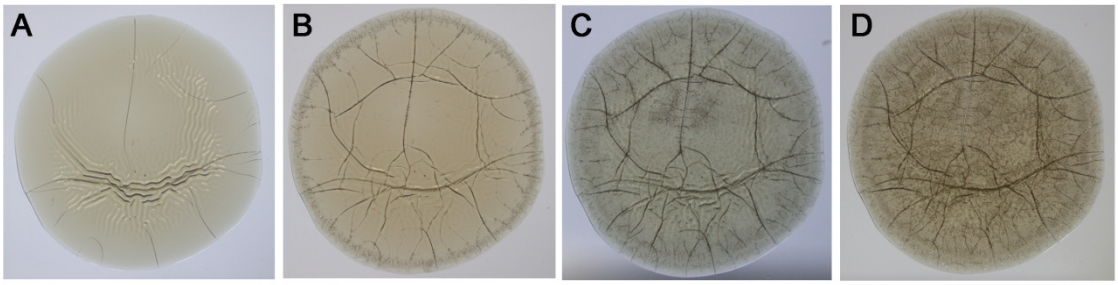

Figure 3.2
Photographs of a typical RC-trehalose glass taken during dehydration. The content of residual water in the matrix decreases from left to right. Values of the (water/sugar) molar ratio are the following: 1.36 (A), 1.04 (B), 0.81 (C), 0.52 (D).

3.3 Time-resolved optical absorption measurements.

The kinetics of charge recombination of the primary charge separated state $P^+Q_A^-$, induced by a laser pulse or by continuous illumination, have been measured by time-resolved absorption optical spectroscopy using a spectrophotometer of local design.

A scheme of the instrument is shown in Figure 3.3. Optical components are aligned on a Oriel optical bench. The measuring beam (yellow line) is provided by an illuminator (1) equipped with a 100 W quartz tungsten halogen lamp.

The wavelength is selected by a double monochromator (2) and the monochromatic beam is collimated by two focusing lenses (4). When measurements are performed on solid amorphous matrices, the cuvette holder routinely used for measurements in RC solutions (5), is replaced by a dual-axis x-z micropositioner fixed on a carrier of the optical bench. The gastight sample holder containing the amorphous matrix on one of its optical windows is fixed to the micropositioner, with its optical windows forming an angle of 45° with both the measuring beam and the excitation light, in order to minimize reflections of the actinic light on the photomultiplier (see Figure 3.4).

To avoid actinic effects on the sample due to the measuring light, the monitoring beam is gated until approximately 1 s before photoexcitation by an electromechanical shutter (3), placed between the monochromator and the focusing lenses, activated by a delay line (12). The photomultiplier (6) (Philips XP2013B) is protected from scattered excitation light by a 0.01% blocking, 10 nm bandwidth interference filter, centered at

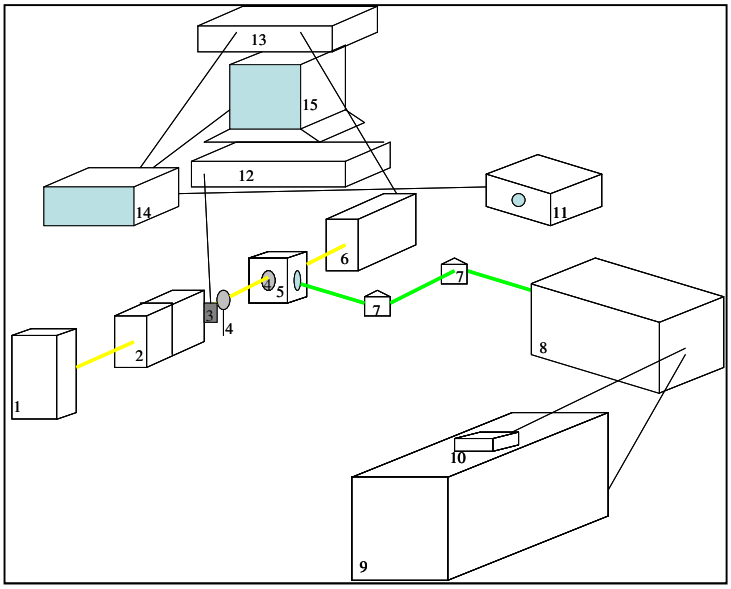

Figure 3.3
Schematic representation of the laser kinetic spectrophotometer. Each component, identified by a numerical label, is described in the text.

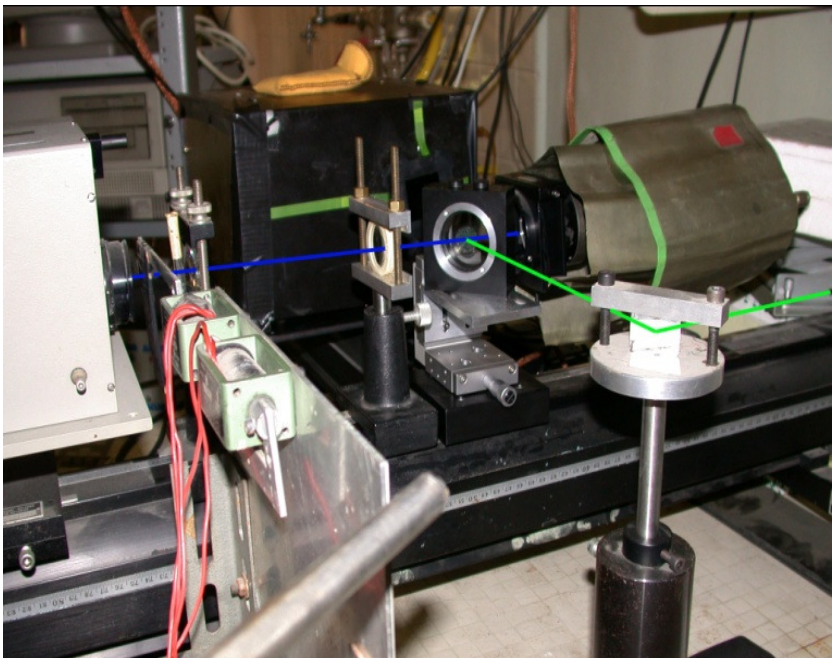

Figure 3.4
View of a detail of the optical spectrometer which shows at the center the sample holder containing an amorphous matrix. The blue line indicates the direction of the measuring beam coming from the monochromator (on the left) and hitting the photomultiplier (on the right). The green line represents the pathway of the laser excitation beam.

420 or at 450 nm. When recombination kinetics exhibit fast decay phases in the 10^{-5} s time scale, to avoid transient artifacts due to the scattered laser light, the photomultiplier is additionally protected by a holographic notch filter centered at 532 nm plus a Corning 4-96 glass filter.

Rapid digitization and averaging of the amplified (13) photomultiplier signal is done by a Le Croy 9410 digital oscilloscope (14) controlled by an Olivetti M290 personal computer (15). Signal acquisition by the oscilloscope can be triggered by a photodiode (11) sensing the laser pulse. From 4 to 64 kinetic traces have been averaged depending on the required time resolution and signal-to-noise ratio. During averaging the sample has been allowed to dark adapt for at least 1 min between successive photoexcitations.

Excitation, at 90° with respect to the measuring beam, is provided by a frequency doubled Nd:YAG laser (Handy 710, Quanta System, Milano, Italy) delivering 150 mJ pulses of 7 ns width (8), operated by a power supply (9) and triggered by a pulse generator (10). The laser beam (green line in Fig.3.3) hits the sample after reflection by two prisms (7). In some measurements the Nd-YAG laser was used to pump a dye-laser (RDP-1; Radiant Dyes GmbH, Wermelskirchen, Germany). Styryl 9 was used as a dye (λ_{max} at 810 nm). In both cases the saturation of a single photoexcitation was around 85%.

Continuous illumination was provided by a 200 W quartz tungsten halogen lamp collimated by an optical condenser and filtered by 8 cm of thermostated water and by a colored glass long-pass filter with a cut-on wavelength of 780 nm. In continuous illumination experiments we used a Uniblitz electro-programmable shutter system, characterized by a 3 ms closure time (Vincent Associates, Rochester, NY).

The recombination kinetics of $P^+Q_A^-$ has been recorded at 422 nm and at 450 nm (Sloten, 1972). The relative contribution of P^+ and Q_A^- to the absorption change at 422 nm and at 450 nm can be evaluated from the differential extinction coefficients for P^+/P and Q_A^-/Q_A at the two wavelengths. By using the spectral data of Sloten and colleagues (Sloten, 1972) and extinction coefficients $\varepsilon_{605}(P^+/P)$=19.5 mM^{-1} cm^{-1} and $\varepsilon_{450}(Q_A^-/Q_A)$ = 8.5 mM^{-1} cm^{-1} (Wraight, 1975; Bowyer, 1981), we estimated $\varepsilon_{450}(P^+/P)$=13.1 mM^{-1} cm^{-1}, $\varepsilon_{422}(P^+/P)$=28.8 mM^{-1} cm^{-1}, and $\varepsilon_{422}(Q_A^-/Q_A)$= 4.9 mM^{-1} cm^{-1}. These values imply a relative contribution of Q_A^- to the flash-induced absorbance change measured at 422 nm and at 450 nm of 14.5 % and 39.4 %, respectively.

3.4 Numerical analysis of kinetic signals, best fitting procedures and Brownian dynamics simulations.

Fitting of recombination kinetics to eqs.1.2, 6.4 and 6.5 was performed by least-squares minimization routines, based on a modified Marquardt algorithm (Bevington, 1969). Confidence intervals of the fitting parameters (average rate constant, <*k*>, and width, σ, of the distribution function) were evaluated numerically through an exhaustive search method (Beechem, 1992; Holzwarth, 1996). A series of nonlinear χ^2 minimizations was performed by varying stepwise the value of each *i*th fitting parameter, allowing the remaining fitting parameters to adjust. The obtained minimized χ^2 values were plotted versus the value of the *i*th parameter, obtaining an error graph for each *i*th fitting parameter. The confidence interval was calculated by using an *F*-statistic to evaluate the probability of a given fractional increase in χ^2 according to

$$\chi^2/\chi^2_{min} = 1 + [m/(n-m)]F(m, n-m, 1-p) \quad \text{(eq.3.1)}$$

where *m* is the number of parameters, *n* is the number of data points, and *F* is the upper *(1-p)* quantile for Fisher's *F* distribution with *m* and *(m-n)* degrees of freedom. Confidence intervals are generally given within two standard deviations (*p*=0.95).

Decomposition of absorption bands into Gaussian components (see par.6.1.2, 7.1.3, 7.1.4), as well as fitting of hydration data to sorption isotherms (see par.6.1.1), was performed by non-linear least-squares minimization using Origin (Microcal Software, Northampton, MA, USA). Confidence intervals of the fitting parameters were evaluated numerically through the exhaustive search method, described in detail above, using routines written in LabTalk language (Origin), or software written in C language, based on grid search algorithms (Bevington, 1969).

Brownian dynamics simulations, performed to compare the flexibility of the 2.4.1 RC and of the R26 mutant, have been carried out essentially as described in Sacquin-Mora, 2007a. The simulations adopted a coarse-grained protein model (Zacharias, 2003), in which each amino acid is represented by one pseudoatom located at the Cα position, and small side chains (with the exception of Gly) have a second pseudoatom at the geometric center of the heavy atoms of the side chain, while larger side chains (Arg, Gln, Glu, His, Lys, Met, Trp, Tyr) have a pseudoatom at the center of the Cβ-Cγ bond and a third pseudoatom at the geometrical center of the heavy atoms of the side chain atoms beyond Cγ. Interactions between the pseudoatoms are treated according to the

standard elastic network model (Tozzini, 2005), i.e. all pseudoatoms lying closer than 9 Å are joined with quadratic springs having the same force constant of 0.6 kcal mol^{-1} $Å^{-2}$. Springs are assumed to be relaxed in the reference conformation of the protein, derived from the crystallographic data. Brownian dynamics simulations use an implicit solvent description via the diffusion and random displacement terms in the equation of motion (Ermak, 1978). Other details of the simulation procedure are given in Sacquin-Mora, 2006.

From the positional fluctuations resulting from Brownian dynamics simulations, carried out for 50,000 steps at a temperature of 300K, effective force constants for displacing each particle *i* are calculated as

$$k_i = \frac{3k_BT}{\langle (d_i - \langle d_i \rangle^2) \rangle} \qquad \text{(eq.3.2)}$$

where brackets ⟨ ⟩ indicate an average taken over the whole simulation, k_B is the Boltzmann constant, and d_i is the average distance of particle *i* from the other particles *j* in the protein, excluding the pseudoatoms which belong to the same residue *m* to which particle *i* belongs. Also the distances between the Cα pseudoatom of residue *m* and the Cα pseudoatoms of the adjacent residues *m+1* and *m-1* are not included in the average. The force constant associated with each residue *m* is taken to be the average of the force constants calculated according to eq.3.2 for each of the pseudoatoms *i* forming this residue. Within this framework, the mechanical properties of the protein are described at the residue level by its "rigidity profile", i.e. by the ordered sequence of the force constants calculated for each residue.

3.5 Redox titrations of the P^+/P couple in RC detergent suspensions.

The P^+/P redox midpoint potentials of RCs purified from the 2.4.1 and R26 strains were determined by chemical oxidation-reduction titrations, essentially as described in Hochkoeppler, 1995. At a given ambient redox potential (E_h), the degree of reduction of the primary electron donor was measured by monitoring spectrophotometrically the maximal extent of P photoxidation induced in the RC suspension by a train of 6 flashes fired 100 ms apart. The extent of P photoxidation was measured from the absorbance change induced at 542 nm (ΔA_{542}). Excitation was provided by a Xenon flash lamp (3.25 J discharge energy, 4 μs pulse duration at half-maximal intensity) screened by a

Kodak Wratten 88A filter. E_h was measured with a platinum electrode and a calomel reference electrode, calibrated using equimolar ferri/ferrocyanide mixtures (O'Reilly, 1973). The potential was adjusted by the addition of small volumes of concentrated potassium ferricyanide or Na-ascorbate solutions. Titrations were performed at RC concentrations ranging between 0.5 and 2.0 μM in 20 mM Tris, pH 8.0, 60 mM KCl, in the absence and in the presence of the redox mediators 2,3,5,6-tetramethyl-p-phenylene diamine (DAD) and p-benzoquinone (pBQ) at 20 μM concentrations. To compare with previously published results (Williams, 1992), titrations of the wt RCs were also performed in the presence of 0.1% Triton X-100 and 1 mM EDTA. Equilibration between the redox center P and the platinum electrode was assessed by verifying reversibility during an oxidative and a successive reductive titration.

The midpoint potential (E_m) was obtained by fitting the titrations to the one electron Nernst equation:

$$\Delta A_{542}(E_h) = \Delta A_{542}^{max} \Big/ \left\{1 + exp\left[\frac{F(E_h - E_m)}{RT}\right]\right\} \quad \text{(eq.3.3)}$$

where E_h is the ambient redox potential relative to the hydrogen electrode, R and F are the gas and Faraday constant respectively, and T is the absolute temperature. The free parameters were the midpoint potential, E_m and ΔA_{542}^{max}, defined as the expected absorbance change induced by the train of flashes in a fully reduced sample.

3.6 FTIR spectroscopy and isotopic exchange of water.

FTIR absorption measurements in RC-detergent films and RC-trehalose matrices were performed at 297 K using a Jasco Fourier transform 6100 spectrometer, equipped with a DLATGS detector. Spectra in the mid IR range (7000-1000 cm^{-1}) were acquired using a standard high-intensity ceramic source. Measurements were extended to the NIR region (15000-2200 cm^{-1}) using a halogen lamp source, replacing the Ge/KBr with a Si/CaF_2 beam splitter, and the KRS-5 with a CaF_2 exit interferometer window. Occasionally FTIR spectra were also recorded with a Bruker Tensor 27 spectrometer. The spectra were recorded with the resolution of 4 cm^{-1}, adding 10^2 and 10^3 scans per spectrum in samples equilibrated at $r > 11\%$ and $r \leq 11\%$, respectively.

Light-minus-dark difference spectra were recorded following essentially the procedure described by Breton, 1991a. Interferograms in the 5000-1000 cm^{-1} range

were acquired at 281 K before and during continuous illumination (lasting 20 s) using a MCT detector. During averaging each light-minus-dark cycle was separated by a dark time sufficient to allow a complete recovery of the RC neutral state after the light-induced charge separation, as judged from the kinetics of $P^+Q_A^-$ recombination monitored by time-resolved visible absorption spectroscopy following a 20 s period of continuous photoexcitation (see par.9.1.5). The duration of dark adaptation between averaging cycles was set to 80 s and 140 s for the RC films equilibrated at r =11% and r=74%, respectively.

Continuous illumination was provided by a 250 W (24 V) quartz tungsten halogen lamp collimated by an optical condenser and filtered through a water layer 8 cm thick and two coloured glass filters, resulting in a transmitted band centred at 760 nm with 0.01 transmittance for $\lambda < 700$ nm and $\lambda > 850$ nm.

$P^+Q_A^-$ light-minus-dark ($P^+Q_A^-/PQ_A$) difference spectra were obtained by averaging interferograms taken in many measurement cycles on different (from 2 up to 14) RC-LDAO films equilibrated at the same values of relative humidity. RC-detergent films (see par.3.1.2) were prepared on CaF_2 windows (25 mm diameter). A small gastight compartment of volume ≈ 1 mL, was obtained by opposing a second CaF_2 window to the one carrying the RC-detergent film in a clipping sample holder, using a rubber O-ring sprinkled with vacuum grease, interposed between the two windows, as a spacer.

The relative humidity r within the compartment containing the sample was controlled by a few microliter drops of saturated sodium chloride or lithium chloride solutions, to achieve values of relative humidity at 281 K of 76% and 11% respectively (Malferrari, 2011; Greenspan, 1977).

The exchange of H_2O with D_2O or H_2O_{18} was performed by a new isopiestic method (Malferrari, 2012). RC-detergent films equilibrated at r=76% with D_2O or H_2O^{18} were obtained following a sequence of dehydration/re-hydration equilibria. Essentially the film was first dehydrated by equilibrating it, within a gastight chamber of volume≈ 40 mL, with about 3 mL of a saturated lithium chloride solution in H_2O for 3 hours. The film was then rehydrated in a D_2O or H_2O^{18} atmosphere by replacing in the same chamber the H_2O lithium chloride solution with a saturated sodium chloride solution in D_2O or H_2O^{18}. The efficiency of the isotope substitution procedure has been evaluated in the range between 90% and 100% from the residual differential bands

attributed to H_2O, detectable in $P^+Q_A^-/PQ_A$ spectra of RC-LDAO films re-hydrated at *r*=76% with D_2O and H_2O^{18} (see par.9.1.2).

In the case of D_2O substitution, an extent of isotopic replacement larger than 95% can be independently estimated from the spectra acquired between 5500 and 1400 cm^{-1} in RC-detergent films equilibrated in the presence of H_2O at *r*=76%, dehydrated by incubation at *r*=11% and rehydrated at *r*=76% in the presence of D_2O (see Figure 3.5). In Fig.3.5A, the amide A (at ~3295 cm^{-1}), the amide I (at ~1655 cm^{-1}), and the amide II (at ~1550 cm^{-1}) bands are easily identified, in agreement with spectra obtained in air dried RCs reconstituted in phospolipid vesicles (Nabedryk, 1982). The peaks around 2900 cm^{-1} are attributed to the various CH_2 stretching modes (Nabedryk, 1982). The amide A band overlaps largely with the OH stretching band of water. As a consequence the large band at ~3300 cm^{-1} is strongly reduced when the sample is dehydrated by equilibration at *r*=11% as compared to *r*=76%. The dehydration of the sample can be better evaluated from the $(\nu_2+\nu_3)$ combination band of water, centred at 5150 cm^{-1}, which is shown enlarged in Fig.3.5B. The area below this band has been shown to be proportional to the water content, independently of the H bonding organization (see par.6.1.1). The peak at 4850 cm^{-1}, on the lower wavenumber side of the water combination band, is attributed to a combination of the NH stretching frequency at 3280 cm^{-1} and the peptide frequency at 1550 cm^{-1} (see par. 6.1.1), and is clearly resolved at *r*=11%. When the water combination band is corrected for this contribution by subtracting a background, it can be estimated that at *r*=11% less than 20% of the water content of the sample detected at *r*=76% is retained. The association band of water visible at ~2100 cm^{-1} in the spectrum at *r*=76% is also strongly reduced at *r*=11% (Fig.3.5A).

When the dehydrated sample (*r*=11%) is rehydrated in the presence of NaCl in D_2O (*r*=76%) the spectrum exhibits strong alterations, diagnostic of an efficient deuteration. In Fig.3.5A, all the spectra have been normalized to the amplitude of the amide I band, which is less affected by D_2O replacement as compared to the amide II band. Although the region of the amide I includes some contribution from the water bending mode, normalization to the amplitude of the amide I band allows a better comparison between the spectra recorded in the presence of H_2O and D_2O at *r*=76%. Fig.3.5A shows that upon rehydration with D_2O the band centred at 3300 cm^{-1} is almost halved in amplitude, consistently with a reduction of the water OH stretching contribution and the partial deuteration of the NH group of the amide A band. As

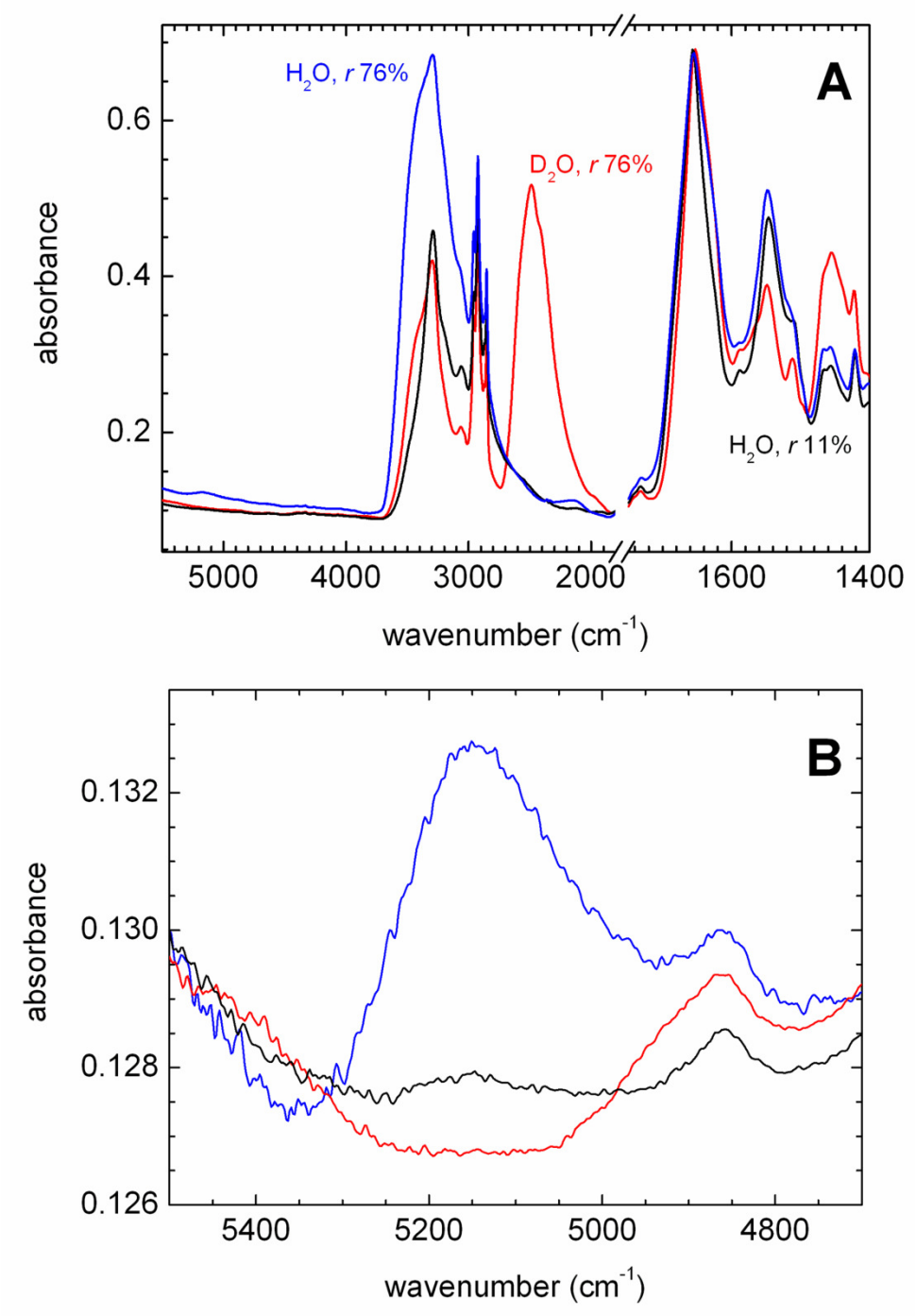

Figure 3.5
A. FTIR spectra recorded in a RC film equilibrated at r =76% (blue), dehydrated at r=11% (black) and rehydrated at r =76% in the presence of D_2O (red). B. Enlargement of the 5500-4700 cm^{-1} spectral region, showing the ($\nu_2+\nu_3$) combination band of water at 5150 cm^{-1}.

expected, upon rehydration with D_2O, the OH stretching band of water is blue-shifted by about 800 cm^{-1} (Max, 2002), resulting in a strong absorption band centred at 2500 cm^{-1}. In the hydrated samples at r=76%, both in H_2O and in D_2O, the amide A band exhibits a shoulder on the high wavenumber side. This shoulder, which essentially disappears in the dehydrated sample at r=11%, is attributed to the water OH stretching mode, and to OH and NH groups of the protein. We propose that the disappearance of the shoulder in the dehydrated sample reflects not only water depletion, but also a shift to lower wavenumbers of the protein OH and NH groups, presumably due to a strengthening of the H-bonds. This interpretation explains why the shoulder becomes again detectable upon rehydration with D_2O, although much reduced in amplitude and width. Since in D_2O the extent of deuteration is very high and H_2O is essentially absent (see below), the contribution of protein OH and NH groups is likely to be responsible for the band shoulder in the deuterated sample.

It is known that N-deuteration converts largely the amide II mode to a CN stretching vibration at 1490-1460 cm^{-1}, named amide II' band (Barth, 2007). In line with this change, we observe a weakening of the band at 1550 cm^{-1} (amide II) and a large increase of the absorbance between 1420 and 1500 cm^{-1}, giving rise to a peak at 1460 cm^{-1}, which can be attributed to the appearance of the amide II' band. Interestingly a peak at 1550 cm^{-1} also appears, which corresponds to the wavenumber expected for the water association band upon D_2O replacement (Max, 2002).

The extent of D_2O replacement can be evaluated from Fig.3.5B. Following rehydration with D_2O, the spectrum between 5500 and 4700 cm^{-1} still exhibits the NH band at 4850 cm^{-1}, while the ($\nu_2+\nu_3$) combination band of water essentially disappears. We infer that the efficiency of D_2O replacement achieved upon rehydration in the presence of D_2O is larger than 95%. Since rehydration with D_2O occurs in samples which still retain some residual H_2O (see the spectrum at r=11% in Fig.3.5B), it appears that equilibration with D_2O vapour not only leads to rehydration with deuterated water, but also results in the exchange of the residual H_2O with D_2O.

The isopiestic method for isotopic replacement described above offers significant advantages over the currently used methods based on dialysis: (i) the efficiency of the isotopic replacement is much higher; (ii) the amount of D_2O needed is extremely low; (iii) dehydration and D_2O rehydration require a short time (less than 6 hours as compared to more than 12 for dialysis); (iv) the hydration state of the sample can be concomitantly controlled.

3.7 EPR spectroscopy.

For EPR measurements the dehydrated, fragile RC/trehalose glasses described above were crumbled into small flakes which, by applying reduced pressure, could be quickly inserted into the cylindrical quartz capillaries (ID = 0.6 mm) for the 95-GHz EPR cavity. The small strips from dehydrated RC/PVA film (1 mm length, 0.4 mm height) were fitted into the EPR capillary. The capillary was positioned into the EPR cavity with the strip surface perpendicular to the light beam direction to ensure the maximum excitation of the sample.

High-field EPR and ESE measurements were performed on a laboratory-built W-band (95 GHz/3.4 T) spectrometer that had been optimized for a variety of cw and pulse experiments, as described previously (Möbius, 2009).

The spectrometer was equipped with a TE_{011} optical transmission microwave (mw) cavity with an unloaded quality factor $Q_U = 5000$ (empty) for optimum detection sensitivity. The samples were contained in thin-walled quartz capillaries. For optical sample irradiation the light was guided to the center of the cavity through a quartz fiber of 0.8 mm diameter (see Figure 3.6). The electron transfer was initiated by singlet excitation of the primary donor at 532 nm using a frequency-doubled Nd:YAG laser assembled from various commercial components (5 ns pulse length, 1-10 Hz repetition rate, 0.5 mJ/pulse on the sample surface) or at 690 nm using a cw diode laser (25 mW output, 10 mW on the sample surface).

The ESE measurements were performed using the standard mw pulse sequence for primary spin-echo generation: $(t_p)_{x,-x}$-τ-$(2t_p)$-τ-echo. The pulse length t_p of the $\pi/2$ mw pulses was generally set to 30 ns. To acquire field-swept ESE detected spectra the pulse separation time τ was fixed to 150 ns. The 2-pulse echo decay traces were recorded by incrementing τ from a starting value $\tau_0 = 50$ ns. The time-resolved cw W-band transient EPR (TREPR; Kim, 1979) measurements of short-lived paramagnetic intermediates were performed without field modulation using the direct-detection technique with a time resolution of 10 ns. The $P_{865}^{\bullet+}Q_A^{\bullet-}$ charge-recombination kinetics data were obtained for radical pairs with thermally equilibrated spin polarization by recording their transient EPR absorption after a laser flash, using 30 kHz field modulation and lock-in detection with 1 ms time resolution. Temperature control was achieved by a gas-flow cryostat housing the cavity probehead. The accumulation time for an EPR spectrum was typically 300 s depending on the sample temperature and solvent matrix.

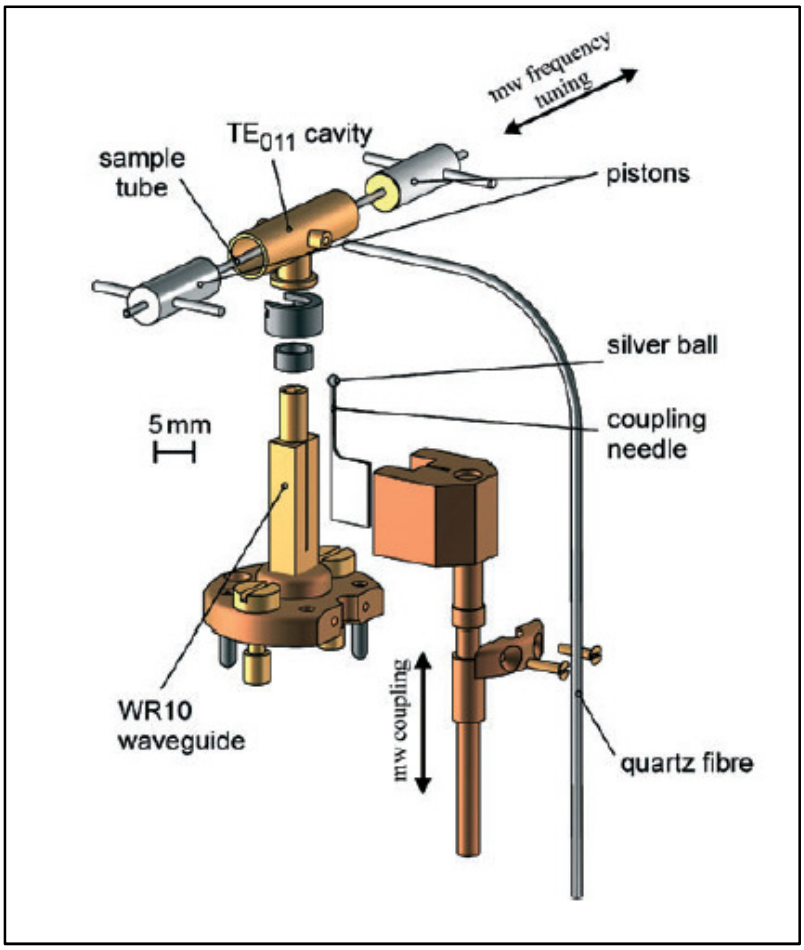

Figure 3.6
Exploded view of the 95 GHz EPR probehead with TE_{011} cavity.

All experimental spectra analysis and simulation procedures were performed on the basis of the EasySpin toolbox (Stoll, 2006; Stoll, 2007) for the Matlab program package.

4. THE PROTEIN/MATRIX DYNAMICAL COUPLING IN TREHALOSE GLASSES: INSIGHTS FROM THE KINETIC ANALYSIS OF $P^+Q_A^-$ RECOMBINATION IN WILD TYPE AND CAROTENOID-LESS RCs

As outlined previously (see par.1.5 and 1.6), according to the *anchorage hypothesis* the peculiar ability of α,α-trehalose matrices in hindering protein dynamics is bought back to the formation, during dehydration, of an extended hydrogen bond network which involves the protein surface and the surrounding glassy matrix (Francia, 2008). This network, in the case of α,α–trehalose as compared to other sugars, is characterized by a higher fraction of residual water molecules simultaneously hydrogen bonded with protein surface residues and sugar molecules. In this model the effects of the dynamical constraints applied by the sugar matrix at the protein surface will propagate to the interior of the protein, affecting the internal dynamics of the protein. In the case of the RC, in particular, these mechanical constraints will inhibit the protein dynamics involved in the stabilization of the primary charge separated state.

On this basis the anchorage hypothesis predicts that the inhibition of specific internal protein dynamics is related to the overall, and possibly local, mechanical properties of the protein: a larger overall structural rigidity of the protein should lead in principle to a better coupling between the dynamics of the matrix-locked protein surface and the dynamics of the protein inner regions. A more flexible protein structure, on the contrary, should allow a significant residual dynamics, even upon extreme hardening of the constrains applied by the surrounding matrix to the protein surface.

Previous high-pressure studies, performed comparatively in the sphaeroidene containing RC purified from *Rb. sphaeroides* wt 2.4.1 and in the carotenoid-less RC obtained from strain R26 (Gall, 2001; Gall, 2004) have shown that the presence of the carotenoid results in a more compact structure, putting in evidence a larger compressibility of the carotenoid-less protein. In view of the above arguments, we expect a different inhibition of the internal protein dynamics for these two RC structures, when they are embedded in progressively dehydrated α,α-trehalose amorphous glassy matrices. If the more flexibile structure (R26) leads to a significantly looser coupling between the matrix-locked RC surface and the inner RC dynamics which controls the stability of $P^+Q_A^-$, we also expect a weaker response of $P^+Q_A^-$ recombination kinetics to dehydration (hardening) of the embedding trehalose matrix.

In this chapter a kinetic analysis of $P^+Q_A^-$ recombination is presented for both wt and R26 RCs embedded at room temperature in α,α-trehalose glassy matrices, characterized by a sugar/protein molar ratio equal to 10^4. These kinetics are compared with those measured at room temperature in solution and in RC films dehydrated in the absence of sugar under dry N_2 flow. Finally, to rationalize the differences observed between the carotenoid-containing and the carotenoid-less RCs, the mechanical properties of the two RCs have been modeled by means of Brownian dynamics simulations, performed in collaboration with Dr. Sophie Sacquin-Mora of the Laboratoire de Biochimie Théorique (Institut de Biologie Physico-Chimique, Paris, France) (Francia et al., 2009).

4.1 Results.

4.1.1 Kinetics of $P^+Q_A^-$ recombination in RC-trehalose glasses and dried RC films.

The room temperature kinetics of $P^+Q_A^-$ recombination following a laser pulse have been compared in RC purified from the carotenoid-containing wt strain and from the carotenoid-less mutant R26 under different environmental conditions, which are known to affect markedly the RC dynamics coupled to the reaction (Palazzo, 2002; Francia, 2008; Francia, 2004b). Fig.4.1 shows kinetics recorded in solution, in a RC film extensively dehydrated employing a dry nitrogen flux (panel A) and in a RC-trehalose glassy matrix characterized by an extremely low content of residual water (panel B). As previously observed in R26 reaction centers, under all the conditions tested kinetics are accurately described by a power law (eq.1.2, see par.1.6); accordingly, the kinetic process can be fully described by a Gamma distribution of rate constants (eq.1.3, see par.1.6). In solution, the kinetics recorded in the wt and in the R26 RCs essentially coincides, marginally deviating from an exponential decay, as shown by the narrow rate distributions (Fig.4.1A'). The values obtained for the average rate constant, $\langle k \rangle$, and for the rate distribution width, σ, are close to 11 s^{-1} and 2 s^{-1}, respectively, for both strains, in agreement with previous data obtained in the R26 mutant (Palazzo, 2002; Francia, 2008; Francia, 2004b). When the RC suspensions are dehydrated by N_2 flux to the maximum extent attainable by this method, RC films are produced with weakly accelerated recombination kinetics for both carotenoid-containing and carotenoid-less RCs (Fig.4.1A), reaching $\langle k \rangle$ values close to 20 s^{-1}. The rate distributions (Fig.4.1A') become correspondingly broader, with σ values in the range of 10 s^{-1}. In the dehydrated RC-films, however, the kinetics of $P^+Q_A^-$

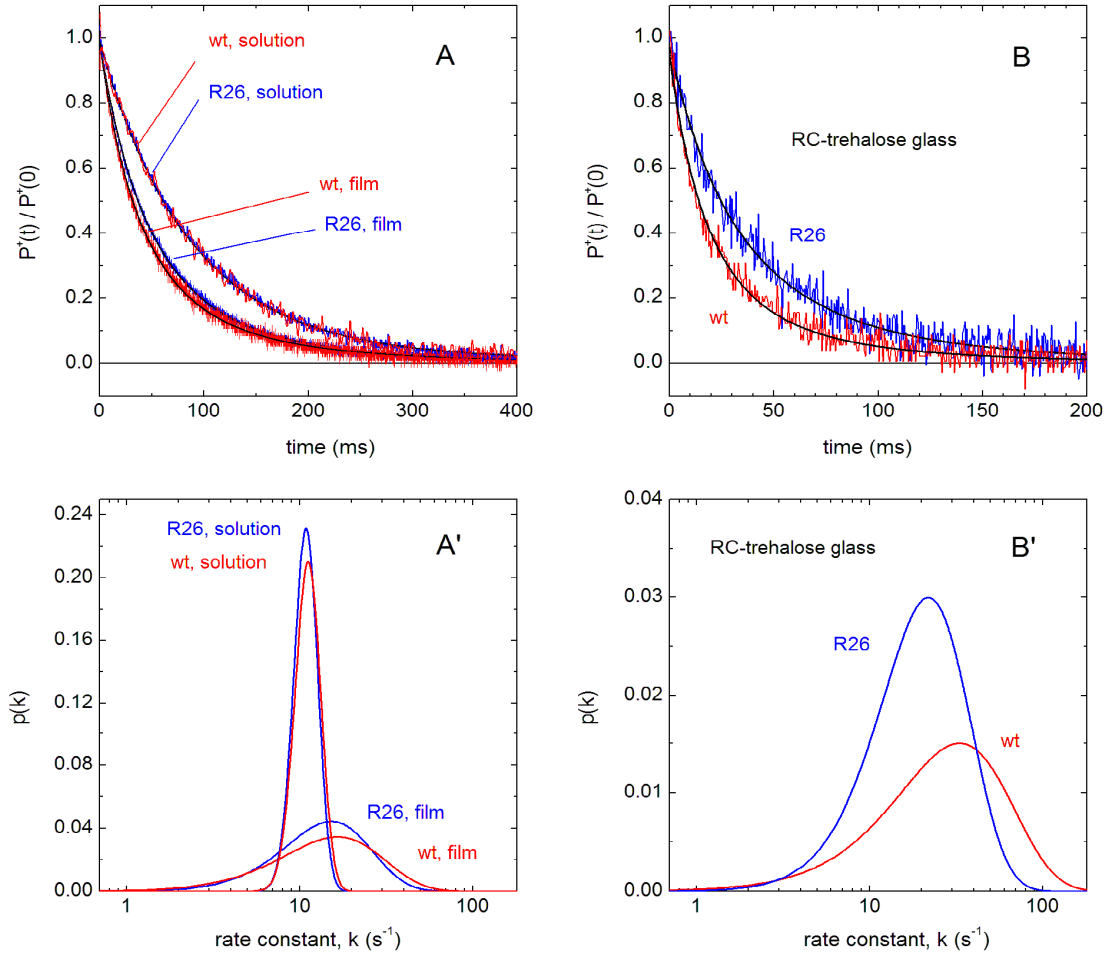

Figure 4.1
Kinetic analysis of $P^+Q_A^-$ recombination following flash excitation of RC purified from the wt 2.4.1 and the R26 mutant of *Rhodobacter sphaeroides* measured under different environmental conditions. The decays of the absorbance change induced at 422 nm by a laser pulse have been measured at T=21°C in detergent RC solution (panel A), in dehydrated RC films (panel A), and in extensively dried trehalose-RC glassy matrices (panel B). Traces recorded in the wt and in the R26 RC are shown in red and blue respectively. Kinetics have been normalized to the maximal change immediately after photoexcitation (t=0). Best fits to eq.1.2 are shown as black continuous lines. The corresponding rate distributions (see eq.1.3) are shown in the lower panels (A' and B'). The values obtained for the average rate constant $\langle k \rangle$ and the distributions width σ (see eqs.1.2, 1.3 and 1.4) are reported in the following, with the extremes of the calculated confidence intervals within two standard deviations indicated in brackets. Panel A: wt, solution $\langle k \rangle$= 11.5 (11.3, 11.8) s^{-1}, σ= 1.9 (0.0, 3.4) s^{-1}; R26, solution $\langle k \rangle$= 11.1 (11.0, 11.3) s^{-1}, σ= 1.1 (0.0, 1.9) s^{-1}; wt, film $\langle k \rangle$= 24.0 (23.9, 24.6) s^{-1}, σ= 13.4 (11.3, 16.3) s^{-1}; R26, film $\langle k \rangle$= 20.3 (20.2, 20.5) s^{-1}, σ= 10.2 (10.0, 10.3) s^{-1}. Panel B: wt RC-trehalose glass $\langle k \rangle$= 52.3 (47.4, 57.6) s^{-1}, σ= 32.0 (26.2, 37.4) s^{-1}; R26 RC-trehalose glass $\langle k \rangle$= 29.7 (27.0, 32.7) s^{-1}, σ= 15.2 (12.0, 18.7) s^{-1}. The dehydrated trehalose matrices embedding the wt and the R26 RCs contained 5.2 x 10^3 H_2O/RC. In the RC films the residual water was below the detection limit of NIR spectroscopy (see chapter 3 for further details).

recombination appears slightly but systematically and reproducibly faster and more distributed in the wt than in the R26 reaction centers. In a trehalose glassy sample, characterized by ~5 x 10^3 residual water molecules per RC, the kinetics measured in the carotenoid-less reaction center are further accelerated, as compared to the dried RC-film, reaching a $<k>$ value ~30 s^{-1} and a σ value ~15 s^{-1} (Fig.4.1B, B'; note the different time scale in Fig.4.1B and 4.1A). In RCs from the carotenoid-containing wt, incorporated into a trehalose glass of comparable content of residual water, these effects are remarkably larger, giving rise to an approximately two-fold accelerated and distributed decay: $P^+Q_A^-$ recombination kinetics are in fact characterized by $<k>$=52 s^{-1} and σ=32 s^{-1} (Fig.4.1B').

The behavior observed in the trehalose matrix led us to study systematically the response of the kinetics to a variation in the content of residual water of the embedding sugar glass. The dependence of the average rate constant $<k>$, and of the distribution width σ, upon the H_2O/RC molar ratio is shown in Fig.4.2A and B respectively for trehalose glasses in which wt or R26 RCs had been incorporated. For both strains, upon decreasing the water content below about 15 x 10^3 water molecules per RC, the average rate constant and the distribution width undergo a steep increase. The kinetic parameters measured in the R26 and in the wt RC do not differ significantly at H_2O/RC values larger than about 10^4. However, at lower contents of the residual water the dependences observed for the two RCs diverge progressively. A remarkably steeper increase of both $<k>$ and σ is observed in the wt RC. At the maximal dehydration attained, corresponding to about 5000 H_2O/RC (i.e. 0.5 water per trehalose molecule), the average rate constant and the distribution width obtained in the wt RC are about two-times larger than the corresponding values in the R26 mutant. The effects observed in the dehydrated systems are fully reversible upon redissolving the RC-sugar matrix (see Fig.4.2, open triangles) and the RC film, as already reported for the R26 RC (Palazzo, 2002; Francia, 2004b).

To confirm that in solution samples $P^+Q_A^-$ kinetics are essentially coincident in RCs from both strains and that the observed differences emerge as a consequence of the progressive hardening of the surrounding glassy matrix during dehydration, we examined the temperature dependence of the kinetics in solution between -6 and +30°C. As shown in Fig.4.3, very close $<k>$ values were obtained for the wt and R26 RC over this temperature range. The values of the average rate constant exhibit a slight inverse temperature dependence, in agreement with previous results obtained in R26 RCs

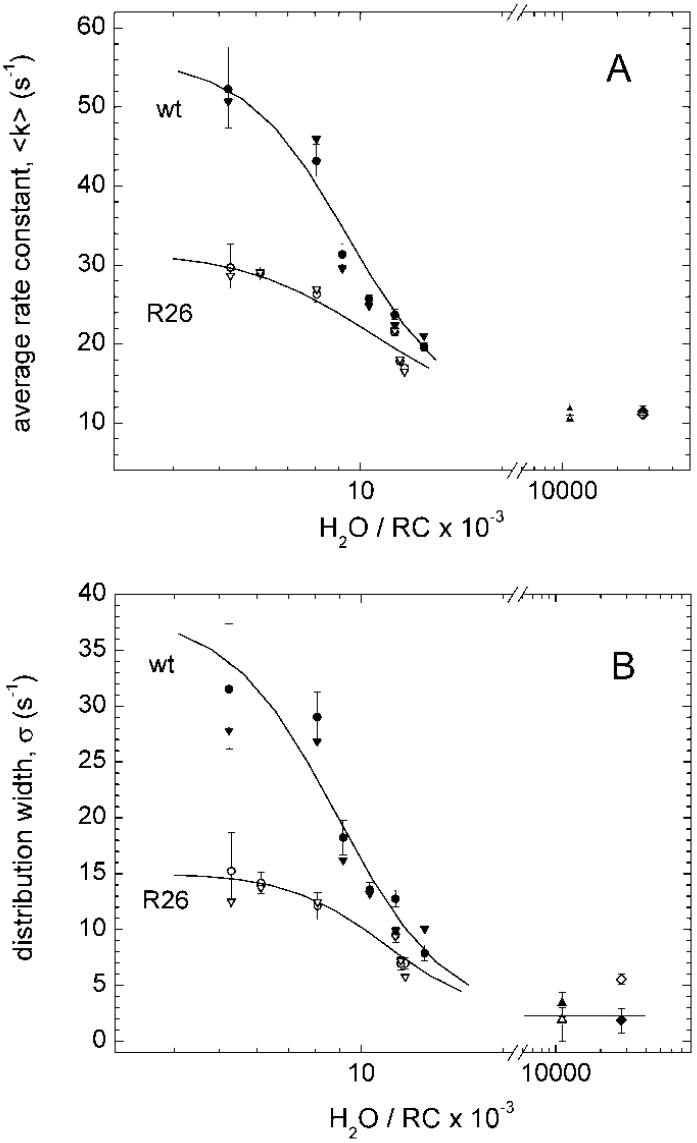

Figure 4.2
Dependence of the kinetics of $P^+Q_A^-$ recombination upon the content of residual water (H_2O/RC molar ratio) in trehalose-water glassy matrices incorporating the wt (filled circles) and the R26 (open circles) RCs. Measurements performed in solution in the absence of trehalose, and after redissolving the trehalose glasses are also shown with filled (wt) and open (R26) diamonds and triangles, respectively. Kinetic analysis was performed as illustrated in Figure 4.1 (see par.3.4 and par.1.4, eq.1.2). Values of the average rate constant $\langle k \rangle$ and of the distribution width σ are presented in panel A and B respectively. Vertical bars indicate confidence intervals within two standard deviations (see par.3.4). The values at the right of the break in the abscissa scale have been obtained in solution, the ones on the left in glassy matrices. Values of $\langle k \rangle$ and σ evaluated by fitting the same experimental traces to a third order cumulant expansion, i.e.: $N(t) = exp(-\langle k \rangle t + \mu_2 t^2/2! - \mu_3 t^3/3!)$, where $N(t)$ is the survival probability of the $P^+Q_A^-$ state after the photoexcitation pulse, $\mu_2 \equiv \sigma^2$ is the variance and the third moment μ_3 provides a measure of the skewness or asymmetry of the monomodal rate distribution. The values of $\langle k \rangle$ and σ^2 for the best fits with the cumulant expansion are shown for comparison with filled (wt) and open (R26) inverted triangles. Sigmoidal curves are drawn through the experimental points just to guide the eye.

Table 4.1
The midpoint potential of the P^+/P couple measured under different conditions in detergent suspensions of RC from the wt 2.4.1 strain and from the R26 mutant.

Strain	Additions	Redox midpoint potential, E_m (mV)
wt 2.4.1	20 µM DAD, 20 µM pBQ	503 ± 5
wt 2.4.1	0.1% Triton X-100, 1 mM EDTA	503 ± 5
R26	-	508 ± 5
R26	20 µM DAD, 20 µM pBQ	506 ± 5

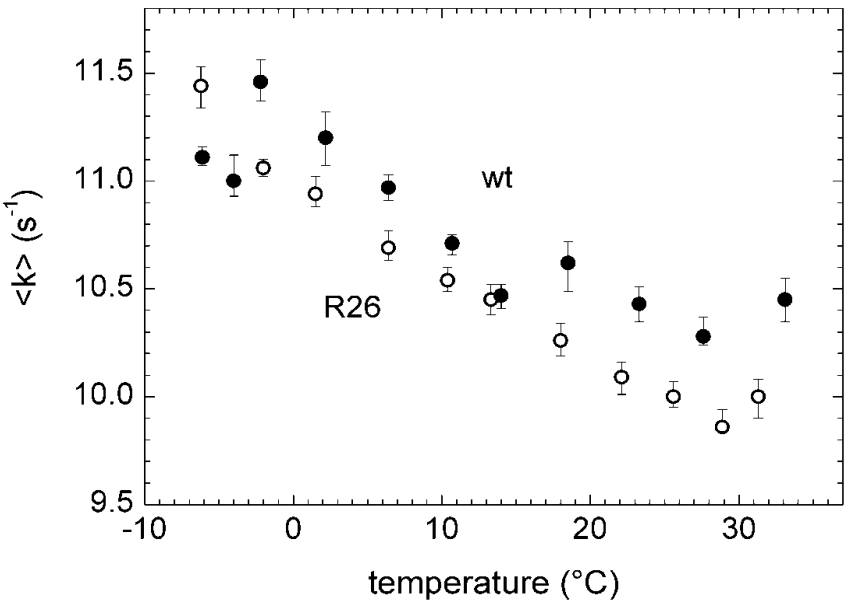

Figure 4.3
Temperature dependence of the average rate constant for $P^+Q_A^-$ recombination measured in detergent solutions of wt (closed circles) and R26 (open circles) RCs in the presence of 58% (v/v) glycerol. Vertical bars give the calculated confidence intervals within two standard deviations.

(Palazzo 2008). Over this temperature range, kinetics are almost exponential, and the width of the calculated rate distribution (not shown) appears to be temperature independent and coincident for the two RC strains within the experimental uncertainty ($\sigma \cong 2\ s^{-1}$). These observations suggest that, in solution, both wt and R26 RC proteins undergo a fast relaxation from the *dark-adapted* to the *light-adapted* conformation, which results in a comparable stabilization of the $P^+Q_A^-$ state i.e. in a comparable free energy difference between the charge separated $P^+Q_A^-$ and the ground PQ_A states. This is in line with the results of redox titrations of the P^+/P couple reported in Table 4.1, which yielded essentially the same redox midpoint potential (E_m=505±5 mV) in the wt and R26 RCs, in excellent agreement with values previously determined in the wt RC (Williams, 1992; Lin, 1994).

The data obtained in the dried RC-films and in the trehalose matrices indicate that when the RC dynamics is progressively hindered (as inferred from the accelerated and increasingly distributed kinetics of $P^+Q_A^-$ recombination), the kinetics of the wt and R26 RCs differ progressively. Already in the RC-films (see Fig.4.1A, A'), the $<k>$ and the σ values in the wt RC exceed by 16% and 25% respectively the corresponding parameters measured in the R26 mutant. In extensively dehydrated RC-trehalose glasses this difference increases to 80% for $<k>$ and 110% for the distribution width. The behavior observed in dry films and trehalose matrices suggests therefore that, when severe environmental constraints affect the RC dynamics, both the relaxation to the stabilized, *light-adapted* $P^+Q_A^-$ state and the thermal fluctuations between conformational substates are hampered to a markedly different extent in the wt and R26 RCs.

4.1.2 Brownian dynamics simulations on the wt and R26 RC protein.

In order to investigate the structural/dynamical origin of the different recombination kinetics observed in the mutant RC when incorporated into dry trehalose matrices, we performed a theoretical analysis of the internal mechanics of the wt and R26 RC proteins. Brownian dynamics simulations on coarse-grained representations of bacterial RC proteins have been able to account for an increased flexibility of RC mutants, experimentally demonstrated by elastic and quasi-elastic neutron scattering data (Sacquin-Mora, 2007a). The aim of this simulative approach (Sacquin-Mora, 2006; Lavery, 2007) is to give a description of the mechanical properties of the protein at the level of each single residue. The strategy employed is to carry out Brownian dynamics

simulations on a simplified structural model of the protein. This representation is achieved starting from the protein crystallographic structure and by representing each residue by pseudoatoms: one pseudoatom is located at the crystallographic coordinate of the Cα carbon atom and one or two pseudoatoms are assigned to the side chain, following established rules previously proven to give the best compromise between simplification of the side chains chemical structures and representation of the heterogeneity among aminoacidic side chains masses (a detailed description of the protocol adopted for translating the all atom crystallographic information into the reduced pseudoatom representation is given in par.3.4 of Materials and methods). The interactions between each pseudoatom are then treated in the frame of the standard elastic network model (see par.3.4 of Materials and methods). For each subunit of the protein "rigidity profiles" are then obtained performing Brownian dynamics simulations on the coarse-grained model at 300K; in these profiles for each pseudoatoms effective force constants, k_i , for displacing each particle *i* are calculated as described in par.3.4 of Materials and methods. Within this framework, the mechanical properties of the protein are described at the residue level by its "rigidity profile", i.e. by the ordered sequence of the force constants calculated for each residue.

The results obtained from the crystallographic structures of wt (pdb 2j8c) and R26 (pdb 1rg5) RCs are shown in Fig.4.4A, B. The upper lines in panel A and B are the rigidity profiles for the L and M subunit respectively of the wt RC; the lower lines represent the difference for any residue between the force constant calculated for the R26 mutant and that of the wt RC. The H subunit is much more flexible than the L and M subunits, with force constants which do not exceed 50 kcal mol^{-1} $Å^{-2}$, and do not change significantly when comparing the wt RC and the R26 mutant (not shown). The profiles of the wt RC L and M subunits are very similar to the ones already published for the same RC (Sacquin-Mora, 2007a), starting from a different crystallographic structure (pdb 1k6l). As already noticed, regions close to the non-heme iron atom (L180-L195, L225-L240, M210-M230, and M260-M275) exhibit the largest rigidity. The lower curves indicate quite clearly that the R26 reaction center is considerably more flexible than the wt RC. More specifically, the largest decrease in the calculated force constants occurs for residues in the more rigid region of the protein (notably for residues M216, M217, M219 and M222), located on the quinone acceptor side of the RC. In the same region, other residues undergo a significant decrease in the force

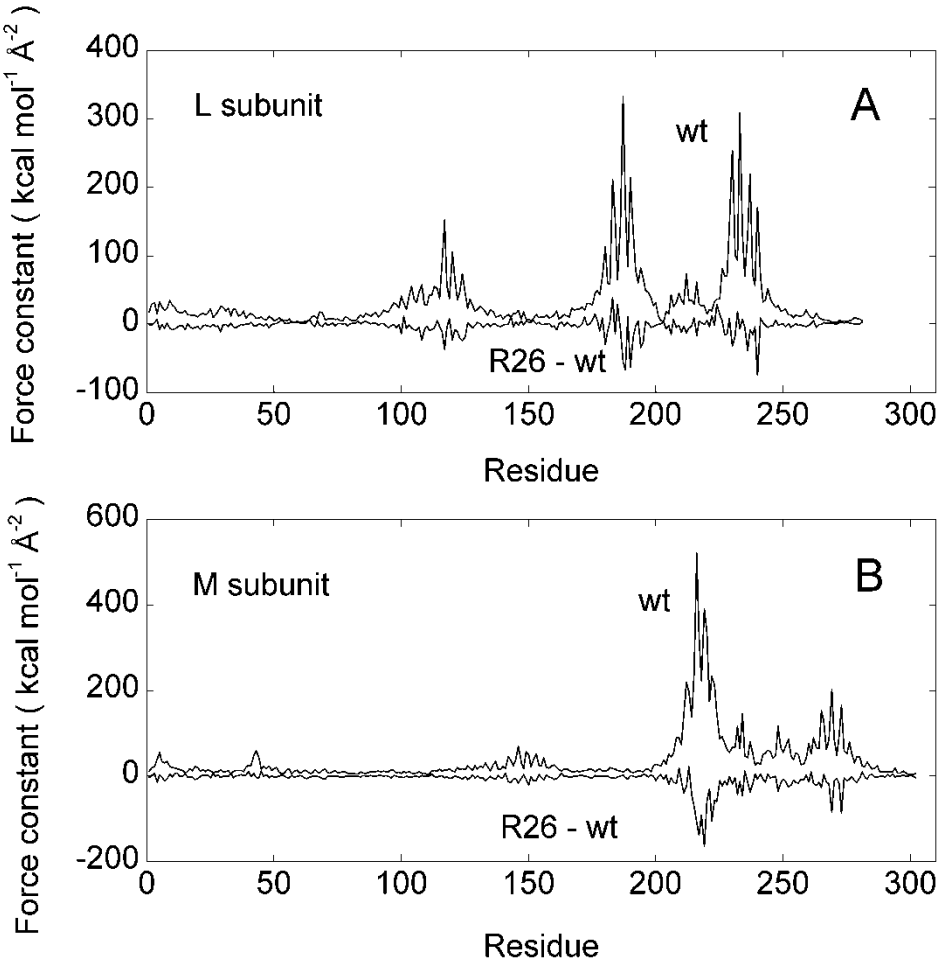

Figure 4.4
Comparison between the local rigidity of the wt and of the R26 reaction centers as evaluated from the results of Brownian dynamics simulations. Effective force constant profiles are shown for the residues belonging to the L (panel A) and to the M (panel B) subunit of the RC. In each panel, the upper curves refer to the profile calculated for the wt RC, while the lower curves represent the difference between the effective force constant calculated in the R26 RC and in the wt RC.

constant (L187, L188, L190, L240, M211, M214, M215, M218, M220, M221, M223, M224, M232, M234, M269, and M273).

As it will be discussed deeply in the next section, the higher local rigidity of the wt RC revealed by Brownian dynamics simulations is fully consistent with the larger inhibition of wt RC dynamics indicated by the kinetic analysis of $P^+Q_A^-$ recombination in dried RC-trehalose glasses (Fig.4.2).

4.2 Discussion.

The kinetic analysis of $P^+Q_A^-$ decay shows that in extensively dehydrated RC-trehalose glasses, characterized by a comparable content of residual water, recombination occurs two times faster in the wt RC than in the carotenoid-less R26 mutant. Moreover, in the wt RC the rate distribution is more than two-times broader. The former observation indicates that over the time scale of charge recombination, the flash-induced $P^+Q_A^-$ state is less stabilized in the wt than in the R26 RCs. The broader rate distribution in the wt RC also indicates that in trehalose glasses the wt RC is trapped over a larger ensemble of substates as compared to the R26 RC.

Taken together, the two observations strongly suggest that the protein dynamics probed by $P^+Q_A^-$ recombination kinetics is more severely hindered in the carotenoid-containing wt RC. Specifically, this means that, in the wt RC, trehalose coating causes a more efficient trapping of the unrelaxed, *dark adapted* $P^+Q_A^-$ conformation and of the static structural heterogeneity of the protein. In the R26 mutant, at variance, a residual internal dynamics would be present even in the driest trehalose matrices, which would partially stabilize the $P^+Q_A^-$ recombination kinetics and lead to a partial averaging over the conformational substates that determine the rate distribution.

Inhibition of protein dynamics in room temperature dehydrated trehalose glasses implies that the energy barriers between protein conformational substates are dramatically increased, i.e. that the entire enegy landscape of the embedded protein is dramatically perturbed. In principle, following extensive drying of the trehalose-RC glasses, the energy landscapes could differ significantly for the carotenoid-containing (wt) and the carotenoid-less (R26) RC structures, leading eventually to a different energy gap between the *dark-adapted* $P^+Q_A^-$ and the PQ_A ground state. In the frame of the model adopted (see par.1.4 of the Introduction), a larger energy gap in the wt as compared to the R26 RC would give rise to a faster charge recombination in the wt RC. It is therefore possible that a larger energy gap between the *dark-adapted* $P^+Q_A^-$ and the PQ_A ground state in the solid glass contributes substantially to accelerate charge recombination in the wt RC. In other words, alterations of the protein energy landscapes and of the internal protein dynamics are constitutively interconnected. Whether the different effects observed in the kinetics of charge recombination for the wt and R26 RC arise mainly from a structural/energetic difference (due to different energy landscapes of the proteins in the dried trehalose glass) or can be predominantly brought back to different dynamics (again due to the different energy landscapes in the extensively

dehydrated glass) cannot be inferred unequivocally from our data. We note, however, that the large broadening of the rate distribution function in the wt, as compared to the R26 RC, indicates, in the former RC type, a stronger inhibition of the internal protein dynamics which determines the interconversion between conformational substates. This observation strongly favor a predominantly dynamic origin of the different recombination kinetics observed in the solid trehalose glasses, since there is no *a priori* reason for assuming a different static heterogeneity in the two RC types.

In moderately dehydrated trehalose glasses and in RC-film extensively dried in the absence of sugar the differences observed in the recombination kinetics between the wt and R26 RCs are less pronounced. This is consistent with the notion that, when the dynamics of the RC protein is less inhibited, relaxation to the *light-adapted* state and interconversion between substates can occur over a time scale comparable with that of charge recombination both in the wt and in the R26 RCs. No significant differences in the kinetics can be detected between the two RCs in solution. Under these conditions, narrow rate distributions are found (almost-exponential kinetics), indicating that interconversion between conformational substates takes place rapidly over the time of recombination in both RCs. The very close values of $<k>$ show moreover that in solution samples the free-energy difference between the relaxed *light-adapted* $P^+Q_A^-$ state and PQ_A is the same in the wt and in the R26 mutant. This is consistent with the coincident values we found for the redox midpoint potential of the primary donor P^+/P couple in the two RCs.

According to the *anchorage model* of trehalose-protein interaction, dehydration of the trehalose-RC matrix results in the formation of an hydrogen-bond network, which connects surface groups of the protein, via molecules of residual water, to the trehalose matrix (Cordone, 2005; Giuffrida, 2006; Francia, 2008). In strongly dehydrated glasses, this network reduces dramatically the motional freedom of the protein surface. The internal mechanical properties of the protein are expected to determine the range and extent of propagation of the mechanical constraints introduced by the sugar matrix at the protein surface. The *anchorage* model, therefore, implies that the stronger structural/dynamical protein-matrix coupling revealed in the wt RC-trehalose glasses by the kinetics of charge recombination reflects a larger rigidity of the wt RC protein as compared to the R26 mutant. This conclusion is fully consistent with the results of Brownian dynamics simulations carried out in the present study.

Brownian dynamics simulations performed on reduced protein representations have proven to be a useful tool to analyze protein mechanical properties on a residue-by-residue basis (Lavery, 2007). This approach has been previously applied to a variety of proteins, including hemoproteins (Sacquin-Mora, 2006) and the photosynthetic reaction center (Sacquin-Mora, 2007a). The force constant profiles calculated for the wt RC from the pdb structure 2j8c (Fig.4.4) agree well with the rigidity profiles previously obtained from a different crystallographic structure (pdb file 1k6l) of the same RC protein, showing in particular a rigid core located in the vicinity of the non-heme iron atom. When the force constant profile is calculated for the R26 mutant it appears that this protein is more flexible than the wt, and that the largest variations of the force constants occur within the most rigid core of the RC. The force constant profiles shown in Fig.4.4 have been calculated in the absence of cofactors, i.e. the carotenoid molecule was not taken into account in the structure of the wt RC. The inclusion of the prosthetic groups did not change significantly the results of the simulation, in agreement with what found previously for the other proteins studied (Sacquin-Mora, 2006; Sacquin-Mora, 2007b). This means that softening of the R26 RC evidenced by the simulations is an intrinsic mechanical property of the apoprotein architecture. The different "rigidity" derives uniquely from the differences, revealed by the crystallographic data, in the conformation of the two proteins in response to the presence/absence of the carotenoid molecule. Following structural alignment of the two RCs, the overall Cα rmsd between the wt and the R26 L and M subunit structures, calculated over the residues included in the Brownian dynamics simulations, results in a value of 0.75 Å. The larger compactness of the wt compared to the R26 structure appears directly in the spring networks built from the crystallographic data: the reduced model obtained from the wt crystallographic structure (2j8c) is made of 1822 pseudoatoms and 29152 springs, while the one constructed from the R26 structure (1rg5) comprises 1826 pseudoatoms and 27505 springs. In accordance with the lower number of springs in the R26 representation, analysis of the RC cavities based on the two RC structures reveals a significantly larger internal void volume of the R26 structure as compared to the wt. The less dense structure of the R26 mutant is in line with comparative high pressure studies which suggest a larger compressibility of the carotenoid-less mutant (Gall, 2001; Gall, 2004).

The location of the residues which in the R26 protein undergo a more pronounced softening are shown by van der Waals envelopes in Fig.4.5. The largest changes in force

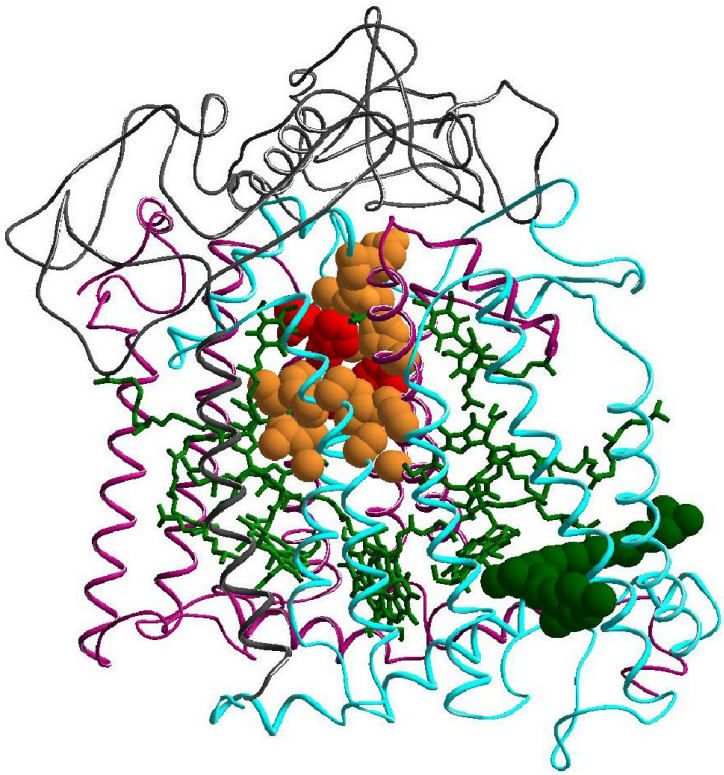

Figure 4.5
Localization of the residues which undergo significant changes in rigidity when passing from the wt to the R26 RC. A ribbon representation of the L (pink), M (cyan) and H (grey) subunits of the wt RC (pdb structure 2j8c) is shown, with the cofactors in green. Van der Waals envelopes represent the carotenoid molecule (green), which is absent in the R26 RC, and the residues which undergo significant changes of the effective force constant in the R26 as compared to the wt RC. Residues characterized by the largest variations of the force constant (between -100 and -165 kcal mole^{-1} Å^{-2}) are shown in red. Those which exhibit a variation between -40 and -100 kcal mole^{-1} Å^{-2} are colored in orange.

constant (between -100 and -165 kcal mole^{-1} Å^{-2}) occur for residues (PheM216, AlaM217, HisM219 , ThrM222), shown in red in Fig.4.5, which belong to the M subunit, to which the carotenoid molecule is bound in the wt structure. These residues form a cluster with 12 additional residues of the M subunit and with 4 residues of the L subunit (orange colored in Fig.4.5), for which the force constant undergoes smaller variations (between -40 and -100 kcal mole^{-1} Å^{-2}). Three of the residues which exhibit a significant variation in the force constant (HisM219, GluM234 and HisL190) act as ligands of the iron atom.

The residues which become more flexible in the R26 RC are at a considerable distance from the position occupied by the carotenoid molecule in the wt structure (the

minimal edge-atom to edge-atom distance between the carotenoid and the closer residue of the cluster (AlaL188) is 19 Å). It appears therefore that the subtle structural rearrangements induced by removal of the carotenoid cause long-range variations in the mechanical properties of the RC protein. A similar long-range softening effect has been found by Brownian dynamics simulation when comparing the rigidity profiles calculated for the wt RC with those of a non-functional mutant carrying the mutations GluL212/AspL213→Ala/Ala (Sacquin-Mora, 2007a). Also in this case the mutations mainly affect residues which belong to the most rigid region of the RC around the iron atom, and which are relatively distant from the site of the point mutations.

In conclusion, from the results of the Brownian dynamics simulations it appears that softening of a cluster of residues in the R26 RC protein looses the dynamical coupling between the trehalose-water matrix and the RC site(s) involved in relaxation of $P^+Q_A^-$ from the *dark adapted* to the *light-adapted* conformation. Interestingly, the high resolution structure of the wt RC (Koepke, 2007) reveals that most of the residues undergoing a rigidity change in the R26 mutant are part of an hydrogen bond network which also involves a large number of bound water molecules and a few additional residues close to the surface of the protein. It seems reasonable therefore to propose that, through this hydrogen bond network, the force constants of a few key residues affect the mechanical coupling between the protein surface and the residue(s) involved in the stabilization of the charge separated state.

The largest differences in force constants between the wt and the R26 are found for residues which cluster around the quinone acceptor complex. This suggests that residues localized on the quinone acceptor side of the RC, possibly in the proximity of the binding pocket of Q_A, play a role in the conformational relaxation which stabilizes the $P^+Q_A^-$ state. FTIR studies on the *Rb. sphaeroides* RC have shown that formation of $P^+Q_A^-$ is associated with a light-induced differential band at 1650 cm^{-1}, most likely reflecting some change in a peptide C=O vibration belonging to the Q_A pocket (Nabedryk, 1990a). The authors propose that the involved residue is an alanine (Ala M260), conserved in *Rhodopseudomonas viridis*. The peptide nitrogen of this residue is within hydrogen bonding distance from one of the C=O groups of Q_A. As noticed by the authors, the conformational change could alternatively involve ThrM222, which is also at hydrogen bond distance from the other C=O group of Q_A in *Rb. sphaeroides*. Notably, Brownian dynamics simulations predict a large decrease (- 105 kcal $mole^{-1}$ $Å^{-2}$) for this residue in the R26 mutant as compared to the wt.

5. PROTEIN/SOLVENT DYNAMICS AND THE STABILIZATION OF THE LIGHT-INDUCED $P^+Q_A^-$ STATE: STUDIES BY HIGH-FIELD EPR SPECTROSCOPY

The present chapter presents a collaborative study of laser-flash and high-field EPR spectroscopies on RCs from *Rb. sphaeroides* R26, embedded in different matrices, specifically in PVA films and trehalose glasses. High-field EPR measurements (at 95 GHz/3.4 T) have been performed in collaboration with Prof. Klaus Möbius and Dr. Anton Savitsky at the Institut für Experimentalphysik, Freie Universität, Berlin (see Savitsky, 2010).

High-field EPR methods, both in cw and pulse modes, offer powerful tools for a deep structural and dynamical characterization of radicals, radical pairs and their immediate neighbourhood (for an overview see Möbius, 2009). This has been demonstrated for many protein systems, and notably for light-induced electron transfer intermediates of bacterial photosynthetic RCs (see Möbius, 2009).

As outlined in the previous chapter, kinetic analysis of $P^+Q_A^-$ recombination by optical absorption spectroscopy indicates that the RC conformational dynamics at room temperature are severely restricted in dehydrated trehalose glasses. It has been shown that a similar inhibition, although to a lesser extent, also occurs in PVA matrices under extreme dehydration (Francia, 2004a), indicating that at room temperature the dynamics of the protein were regulated by the dynamics of the external matrix (Cordone, 2005). We thought to exploit the possibilities offered by high-field EPR to gain detailed structural and dynamical information on the P^+ and Q_A^- sites with the aim to contribute to clarify the molecular basis of the RC relaxation involved in the stabilization of the primary charge separated state and to get insight into the mechanism of inhibition of this protein dynamics exerted by dehydrated α,α-trehalose glassy matrices. Specifically, photo-generated P^+ and Q_A^- radical ions as well as $P^+Q_A^-$ radical pairs were studied to probe, at low and room temperature, potential changes of the coupling between conformational protein dynamics and electron transfer rates in these matrices, and to compare the results with those deduced from laser-flash spectroscopy. We aimed to find out, on the molecular level, whether any local changes in structure and dynamics of the electron transfer cofactor sites occur when changing the matrix from water to dry PVA and trehalose or, alternatively, whether the inhibition of the RC relaxation

following light excitation is more delocalized over the protein structure, possibly involving a number of residues and/or bound water molecules. In this sense, the concomitant study of matrix effects by optical and EPR spectroscopies has yielded information on the mechanisms by which dielectric relaxation of the RC/solvent system stabilizes the primary charges separated state of the RC.

To investigate the role of the matrix properties, both in terms of composition and dynamics, in the coupling between the fluctuations of the Q_A binding site, the solvent matrix and the electron transfer characteristics in the $P^+Q_A^-$ recombination process, we performed W-band EPR measurements on Zn-substituted RCs from *Rb. sphaeroides* R26 in water/glycerol, PVA, and trehalose matrices at 290 K and 150 K. Since the sample requirements for optical and EPR measurements are quite different, e.g. in terms of concentration and paramagnetic perturbations and/or impurities, in a first step the various RC/matrix samples have been characterized according to their EPR behaviour. Equivalent samples, in terms of relative matrix-protein composition, were subsequently analyzed by laser optical spectroscopy, and used for estimating the hydration level by visible-NIR spectroscopy.

5.1 Results.

5.1.1 W-band cw EPR at 290 K.

Figure 5.1a shows the cw EPR spectrum of Zn-substituted RCs in water solution at room temperature during continuous illumination (690 nm) and after illumination. Under illumination the EPR spectra of the $Q_A^{\bullet-}$ and $P_{865}^{\bullet+}$ radical ions appear. After switching off the diode laser, only very small photo-accumulated signals of $Q_A^{\bullet-}$ and $P_{865}^{\bullet+}$ remain (< 5%). This shows that the sample is almost 100% cyclic. In Figure 5.1b, the difference spectrum (in blue) is overlaid with the corresponding simulation (in red). The ratio of the $Q_A^{\bullet-}$-to-$P_{865}^{\bullet+}$ spectral intensities allows one to check the Zn-substitution grade to be about 50% (see Möbius 2009, section 5.2). The g-values of both $Q_A^{\bullet-}$ and $P_{865}^{\bullet+}$, resulting from the spectra simulations, are given in the figure caption.

In Figure 5.2 the results of a similar W-band cw EPR experiment performed on the solid RC/PVA sample at room temperature are shown together with the overlaid spectrum simulation. Both spectra, with the laser ON and OFF, are dominated by a

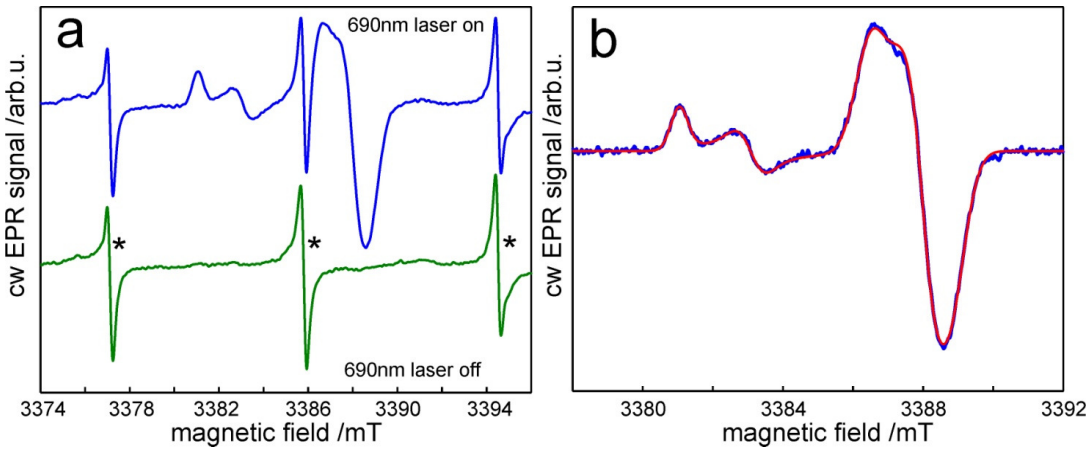

Figure 5.1
(a) W-band cw EPR spectra of dark-adapted Zn-RCs from *Rb. sphaeroides* in water at room temperature under continuous laser-diode illumination at 690 nm (ON: blue trace) and after the laser is switched off (OFF: green trace) recorded using field modulation at 8.2 kHz with amplitude 50 µT. (b) difference spectrum (ON-OFF) overlaid with the spectrum simulation giving: $g(Q_A^-)$=[2.00647 2.00525 2.00223]; $g(P^+)$=[2.00325 2.00240 2.00189]. The EPR intensity ratio of Q_A^- to P^+ is 0.52, revealing a Zn-substitution grade of 52%. (*) marks the line positions of the field calibration standard (Mn^{2+}).

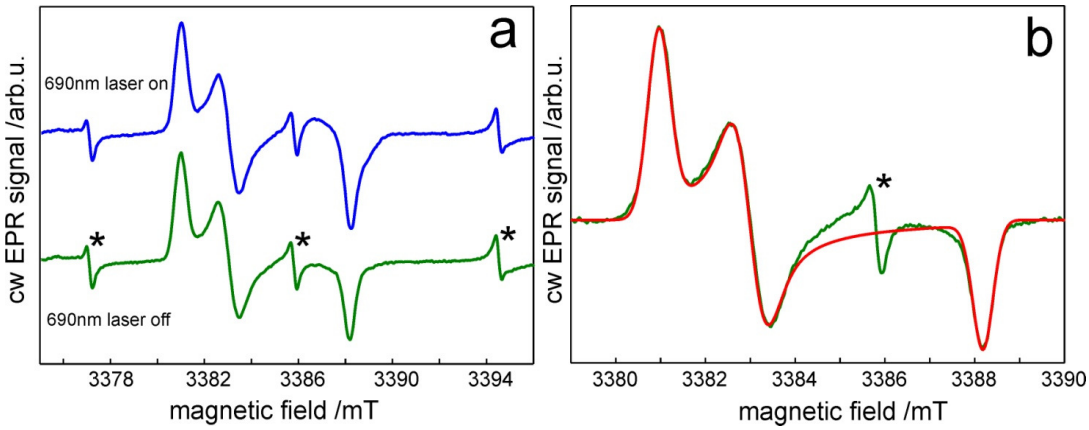

Figure 5.2
(a) W-band cw EPR spectra of dark-adapted Zn-RCs in PVA at room temperature under prolonged continuous illumination at 690 nm and after the diode laser is switched off. (b) Laser OFF spectrum (green) overlaid with its simulation (red) resulting in: $g(Q_A^{\bullet-})$=[2.00652 2.00531 2.00224]. (*) marks the Mn^{2+} line positions of the field calibration standard.

signal which is attributed to the $Q_A^{\bullet-}$ radical ion (see Möbius 2009, section 5.2) The extracted g-values agree perfectly with results of numerous previous EPR investigations of $Q_A^{\bullet-}$ at low temperatures (Burghaus, 1993; Isaacson, 1995; Tang, 1999). As compared to the RC/water sample, however, the g_{xx} and g_{yy} values are slightly larger. This is probably due to partial averaging of the g-tensor in liquid water because of still rapid overall motion of the RC in aqueous solution at room temperature. Such a motion is severely restricted in solid PVA and trehalose matrices even at room temperature. The EPR measurements on the RC/trehalose sample yielded the same results as on the RC/PVA sample.

When recording the echo-detected EPR spectra of dark-adapted RCs in PVA and trehalose matrices at room temperature in a fresh sample (spectra not shown) a small steady-state EPR signal was observed prior to actinic illumination. According to its g-factor values, it presumably stems from a quinone-type anion radical rather than from a neutral (protonated) semiquinone radical (Hales, 1981; Feher, 1985) and is probably due to a photo-accumulation process which at room temperature is initiated by residual light in the laboratory during sample handling. In the following, we call this radical, whose exact identity cannot be determined by EPR alone but would require additional ENDOR experiments (Lubitz, 1985; Feher, 1985) the "Q_A-type radical". Switching on the 690 nm diode laser results in a growing of both $Q_A^{\bullet-}$ and $P_{865}^{\bullet+}$ EPR signals. After turning off the laser, a strong and stable Q_A-type radical signal remains. There is no concentration dependence of the photo-accumulation process. Next, the RC/PVA and RC/trehalose samples containing steady-state Q_A-type radicals were dissolved in water (about 50:50). The dissolved samples were cooled down to 150 K and inspected by W-band EPR. Prior to illumination, no Q_A-type radical signal was detected. The water-solution behaviour was fully restored. Up to now, the identity of the photo-accumulated Q_A-type radical remains uncertain. The photo-accumulation of such a Q_A-type radical in dehydrated trehalose matrices at room temperature is consistent with the previous observation (Palazzo, 2002) that, in similarly dried trehalose glasses, a repetitive laser-flash excitation resulted in the decrease of the extent of optically detected $P_{865}^{\bullet+}$, photoxidized by the laser pulse. In fact the formation of the primary charge-separated state $P_{865}^{\bullet+}Q_A^{\bullet-}$ will be prevented in the RC sub-population where photo-accumulation of a Q_A-type radical anion has occurred, leading to a decrease of the total $P_{865}^{\bullet+}$ signal, as is observed at μs resolution after the laser pulse (see Discussion). Consistent with the EPR results,

also this optically detected effect reverted fully upon re-dissolving the solid RC-trehalose matrix (Palazzo, 2002).

5.1.2 W-band pulse EPR at 150 K.

Figure 5.3 shows the echo-detected EPR spectra of dark-adapted RCs in the three matrices, water, PVA, and trehalose, at 150 K (frozen in the dark). In water solution the behaviour of the sample is perfect in the sense that there are no EPR signals prior to 690 nm illumination and no signals after switching off the diode laser (Figure 5.3, panel *a*). In the RC/trehalose and RC/PVA samples (panel *b* and *c*, respectively), a small Q_A-type anion-radical signal is again observed prior to illumination, similar to what was observed at room temperature. Under 690 nm irradiation the EPR spectra from all three samples are exactly the same. After switching off the laser, a small accumulated signal is observed in PVA and trehalose (compare the red and blue traces in Figure 5.3, panels *b* and *c*). To compare these results with the room temperature spectra shown in Figure 5.1 and 5.2, we show in Figure 5.3, panel *d*, the ESE spectra of the transiently formed radical pairs (light ON minus light OFF) and of the radicals photo-accumulated upon illumination (light OFF minus dark spectrum, recorded prior to illumination) in first derivative representation for the case of the RC/PVA sample. Simulation of the spectrum due to transiently formed radical pairs yields parameters in close agreement with those obtained from the cw spectrum measured in water at room temperature (see Figure 5.1, panel b). The signal of the radicals photo-accumulated upon illumination (red trace in Figure 5.3, panel *d*) , in contrast to room temperature illumination, is due to non-recombining $P_{865}^{\bullet+}Q_A^{\bullet-}$ pairs, as can be inferred from the relative spectral intensities, and is not due to photo-accumulation of a Q_A-type radical. Thus, at 150 K photo-accumulation of such a Q_A-type radical does not take place, and the RC behaviour is the same in all three matrices. By comparing the intensities of the $Q_A^{\bullet-}$ signal in the spectra of Figure 5.3, panel c, it can be evaluated that in the PVA sample about 15% of the RC population is not photo-active, 80% is cyclically photoactive, and only 5% is non-cyclically photo-active, due to non-recombining $P_{865}^{\bullet+}Q_A^{\bullet-}$ pairs.

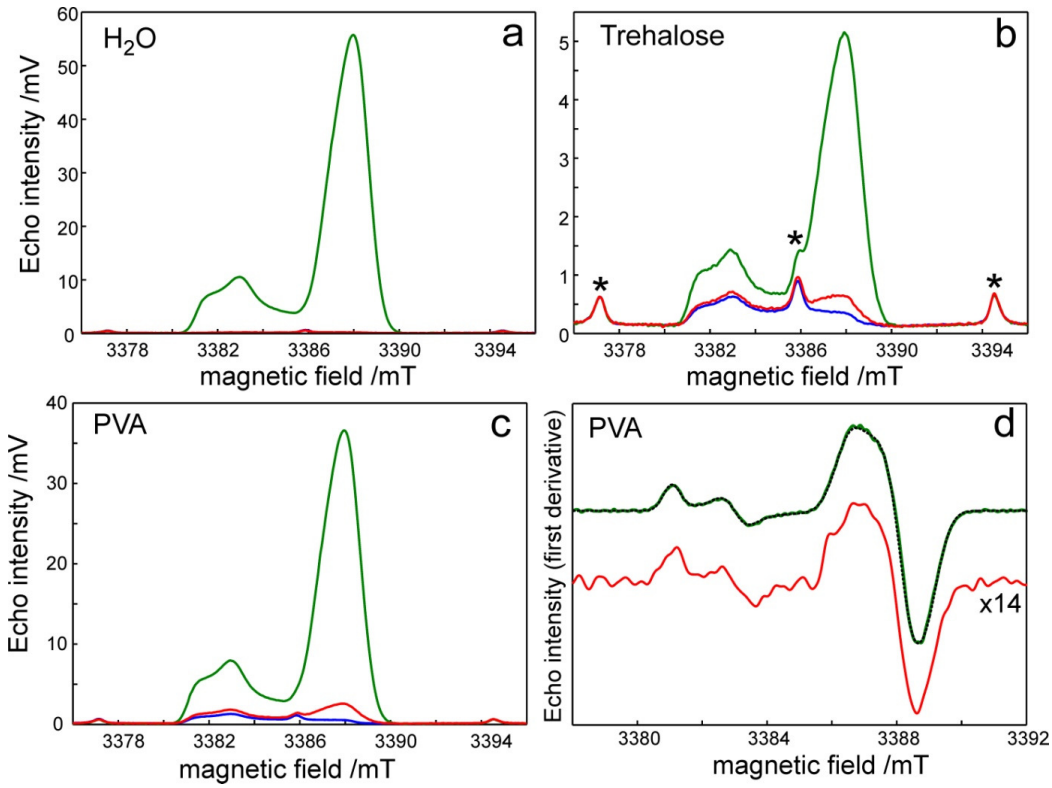

Figure 5.3
W-band 2-pulse ESE-detected EPR spectra of dark-adapted Zn-RCs in (a) water, (b) trehalose and (c) PVA at 150 K prior to illumination at 690 nm (blue trace), under continuous illumination at 690 nm (green trace), and after the 690 nm diode laser is switched off (red trace). (d) Comparison of the light induced spectral changes observed in PVA. The green line shows the ESE-detected EPR spectrum (in first derivative representation) due to transiently formed radical pairs (light ON minus light OFF traces in panel c) overlaid with its simulation (dotted line) corresponding to a spectral intensity ratio $Q_A^{\bullet-}$ to $P_{865}^{\bullet+}$ of 0.48 and to the parameters reported previously by Savitsky and colleagues (Savitsky, 2007). The red line corresponds to the EPR spectrum due to stationary formed pairs (light OFF minus dark spectra in panel c) magnified by a factor 14). (*) marks the Mn^{2+} line positions of the field calibration standard.

5.1.3 $P_{865}^{\bullet+}Q_A^{\bullet-}$ recombination kinetics from transient EPR and optical flash absorption spectroscopy.

Figures 5.4a and 5.5 show selected EPR decay traces, due to charge recombination of the $Q_A^{\bullet-}$ and $P_{865}^{\bullet+}$ radical ions, at 290 K and 150 K, respectively. They have been measured by transient direct-detection EPR absorption from dark-adapted Zn-RCs in water/glycerol mixture, PVA and trehalose matrices following excitation by a 532 nm laser flash of 5 ns duration, firing at 1.25 Hz repetition rate. Under all the conditions tested the time profiles could be adequately fitted to a power law (see eq.1.2 in chapter

Table 5.1
Kinetic parameters of $P_{865}^{\bullet+}Q_A^{\bullet-}$ recombination determined at 290 K from the EPR and optical absorption decays (see text for details). Confidence intervals are given within 2 standard deviations.

RC matrix	τ /ms	<k> /s^{-1}	σ /s^{-1}
From EPR-detected kinetics			
H_2O-glycerol	114 ± 4	8.8 ± 0.3	0
PVA	59 ± 3	16.8 ± 0.7	8.0 ± 0.8
Trehalose	48 ± 2	21 ± 1	12 ± 3
From optically-detected kinetics			
H_2O/glycerol	104 ± 4	9.6 ± 0.3	1.1 ± 1.0
PVA	58 ± 2	17.0 ± 0.2	8.1 ± 0.3
Trehalose	46 ± 2	21.5 ± 0.6	9.5 ± 0.7

Table 5.2
Kinetic parameters of $P_{865}^{\bullet+}Q_A^{\bullet-}$ recombination kinetics determined at 150 K from the decay of EPR absorption.

RC matrix	τ /ms	<k> /s^{-1}	σ /s^{-1}
H_2O-glycerol	35 ± 2	29 ± 2	12 ± 2
PVA	20 ± 2	50 ± 4	24 ± 5
Trehalose	22 ± 4	45 ± 8	29 ± 4
For comparison data given for deuterated RCs measured by EPR (Flores, 2008)			
H_2O (dark)	22 ± 2	46 ± 4	23 ± 3
H_2O (light)	52 ± 4	19 ± 2	17 ± 2
Data given by Kleinfeld et al. (Kleinfeld, 1984)			
H_2O (dark)	22	45.4	18.4
H_2O (light)	65	15.4	14.3

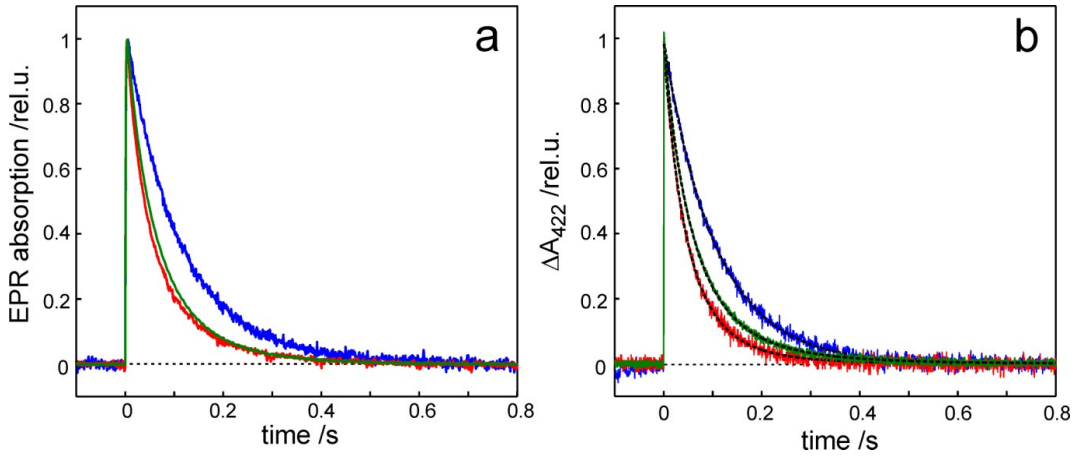

Figure 5.4

Kinetics of $P_{865}^{\bullet+}Q_A^{\bullet-}$ recombination measured at 290 K following a 532 nm laser pulse by transient EPR absorption (a) and by optical absorption spectroscopy (b) at 422 nm in dark-adapted Zn-RCs. Measurements have been performed in water-glycerol RC solutions (blue traces), in dehydrated RC-PVA films (green traces), and in dehydrated trehalose glasses (red traces). Fitting the signals to a power law, dashed lines in (b), yielded the values of the average rate constant, <k>, and of the rate distribution width, σ, given in Table 5.1.

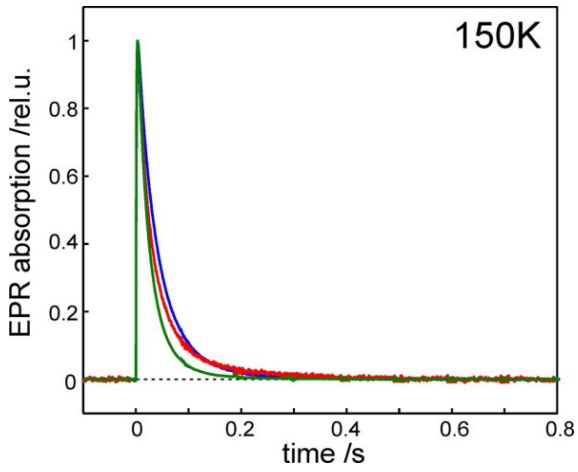

Figure 5.5

EPR-detected kinetics of $P_{865}^{\bullet+}Q_A^{\bullet-}$ recombination following a laser pulse in dark-adapted Zn-RC measured at 150 K in water-glycerol (blue trace), in PVA (green trace) and in trehalose (red trace). Traces have been fitted to a power law obtaining the values of the average rate constant, <k>, and of the rate distribution width, σ, given in Table 5.2.

1.6 in the Introduction; Kleinfeld, 1984; Steinbach, 1992): the results of the fit are summarized in Table 5.1 for 290 K and in Table 5.2 for 150 K. For comparison, Table 5.2 reports also previous data obtained by W-band EPR for deuterated Zn-RCs (Flores, 2008) and by optical absorption spectroscopy in water glycerol suspensions of RCs without Fe→Zn substitution (Kleinfeld, 1984).

At 290 K the kinetics of $P_{865}^{\bullet+}Q_A^{\bullet-}$ recombination after a laser pulse were also measured in a parallel experiment by optical absorption spectroscopy (see Figure 5.4, panel b). These measurements could not be performed directly on the same samples examined by EPR, due to their high optical absorbance. They were carried out in samples that were prepared following the same procedures and using the same Zn-substituted RC preparation, but at a lower RC concentration, as described under Materials and Methods (par.3.1.3). To make the two sets of samples comparable as much as possible, the PVA-to-RC and trehalose-to-RC molar ratios were kept constant for both the optical and EPR measurements (i.e., ≈ 57 and 10^4, respectively). Fitting the kinetics to the power law gave the kinetic parameters summarized in Table 5.1. Both the values of the average rate constant, <k> , and of the rate distribution width, σ, are in excellent agreement with those determined by EPR (see Table 5.1). The kinetics measured in the RC/PVA samples are considerably accelerated and distributed in rate as compared to those measured in liquid water/glycerol solutions. These effects are slightly more pronounced in the RC/trehalose samples.

Due to their relatively low absorption in the visible and NIR spectral regions, the solid samples used for flash absorption spectroscopy allowed a determination of the amount of residual water in the dehydrated matrices by NIR spectroscopy (see Materials and Methods, par.3.2). Interestingly, the RC/Trehalose glass was characterized by approximately (11800 ± 100) water molecules per RC, while the RC/PVA film yielded a H_2O-to-RC molar ratio of about 1100 ± 100. It appears therefore, in agreement with previous measurements (Palazzo, 2002; Francia, 2004a; Francia, 2009), that incorporation of the RC into a dehydrated PVA matrix results in kinetic parameters of $P_{865}^{\bullet+}Q_A^{\bullet-}$ recombination similar to those observable in dehydrated trehalose matrices, but the content of residual water is about one order of magnitude lower in the case of the PVA matrix. In view of the close agreement between the recombination kinetics measured by EPR and optical spectroscopy, these estimates of the hydration levels can be reasonably extrapolated to the samples examined by EPR. We have shown, indeed, that the values of <k> and σ are univocally related, and quite sensitive to the water

content of the embedding matrices (Palazzo, 2002; Francia, 2004a; Francia, 2009). The fact that an acceleration of the recombination kinetics almost comparable to that seen in trehalose is observed in PVA only under much more dried conditions suggests that the protein-matrix interaction, which governs the dynamic coupling, is different in the two systems: it is considerably weaker in the PVA as compared to the trehalose matrix (see Discussion).

5.1.4 Direct-detection transient W-band EPR of $P_{865}^{\bullet+}Q_A^{\bullet-}$ radical pairs.

Figures 5.6 and 5.7 depict the W-band transient EPR (TREPR; Kim, 1979) signals from the spin-correlated radical pair $P_{865}^{\bullet+}Q_A^{\bullet-}$ measured at 290 K and 150 K respectively, shortly after the laser flash. Apparently, the signals of the radical pairs in the different matrices of the Zn-RCs look very similar. This suggests that distance and orientation of $Q_A^{\bullet-}$ and $P_{865}^{\bullet+}$ relative to each other do not change significantly upon solvation in the different host matrices embedding the RC. This conclusion follows from established theory of spin-correlated radical pairs: according to the "Correlated Coupled Radical Pairs" (CCRP) model (Stehlik, 1989; Hore, 1989) the spin-polarized EPR spectrum of two weakly coupled electron spins in a biradical system consists, for each orientation of the dipolar axis with respect to the external magnetic field, of two "antiphase doublets" of equal intensity, i.e., in each doublet of the 4-line spectrum one line is in emission (E), the other in absorption (A). In frozen-solution samples, the transient EPR spectrum reflects the powder average over all possible orientations of the dipolar axis, and the observed lineshape is governed by the magnitude and sign of the dipolar coupling of the two electron spins. This, in turn, is determined by distance and relative orientation of the radical-pair partners. Hence, lineshape analysis of the spin-polarized EPR spectrum gives direct information on the structure of the radical-pair complex formed in its specific matrix.

5.1.5 Relaxation dynamics of $Q_A^{\bullet-}$ due to molecular librations in the binding site.

Finally, to clarify whether the dynamic behaviour of the primary electron acceptor $Q_A^{\bullet-}$ in its binding pocket changes upon changing the matrix in which the RC is embedded, we used two-dimensional ESE detected high-field EPR at 95 GHz to measure the T_2 relaxation times of $Q_A^{\bullet-}$ and their anisotropies in the different RC/matrix

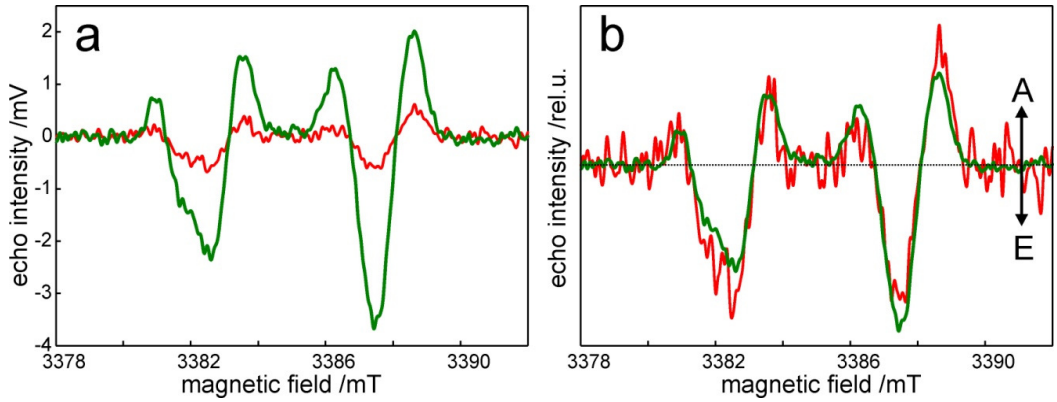

Figure 5.6
The transient W-band EPR signals of the spin-correlated $P_{865}^{\bullet+}Q_A^{\bullet-}$ radical pair in dark-adapted Zn-RCs obtained 400 ns after a 532 nm laser flash in PVA (green) and trehalose (red) samples at 290 K. (a) In absolute signal units. (b) With matched $P_{865}^{\bullet+}$ spectral part. The $Q_A^{\bullet-}$ part of the spectrum is at the low-field side (higher g-values than the $P_{865}^{\bullet+}$ part). A stands for absorptive, E for emissive type of spin polarization.

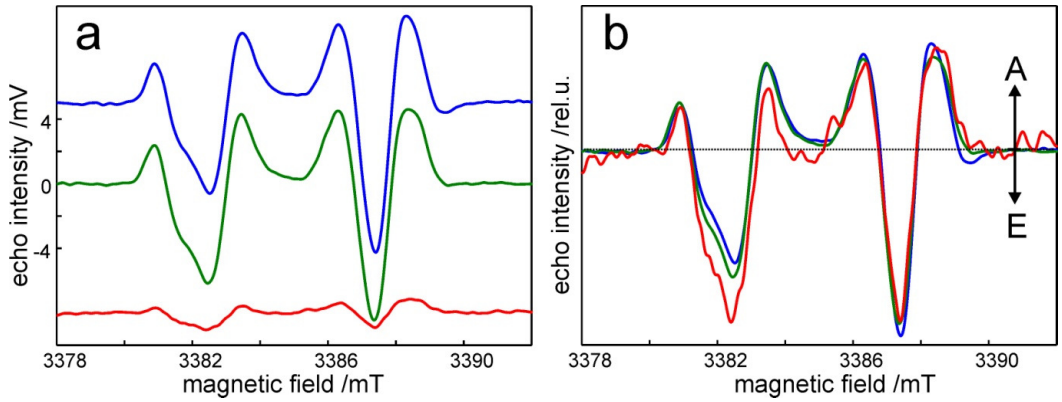

Figure 5.7
The transient W-band EPR signals of the spin-correlated $P_{865}^{\bullet+}Q_A^{\bullet-}$ radical pair in dark-adapted Zn-RCs obtained 400 ns after a 532 nm laser flash in PVA (green), trehalose (red) and water (blue) samples at 150 K. (a) In absolute signal units. (b) With matched $P_{865}^{\bullet+}$ spectral part. The $Q_A^{\bullet-}$ part of the spectrum is at the low-field side (higher g-values than the $P_{865}^{\bullet+}$ part). A stands for absorptive, E for emissive type of spin polarization.

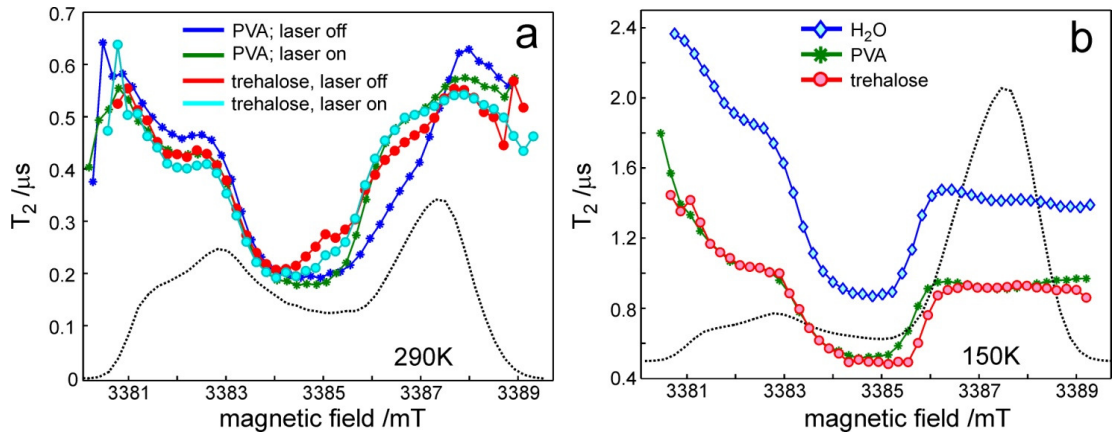

Figure 5.8
Field dependence of the anisotropic T_2 spin-spin relaxation times at 290 K (a) and 150 K (b). The black dotted traces represent the ESE-detected $P_{865}^{\bullet+}Q_A^{\bullet-}$ radical-pair EPR spectrum at the inter-pulse separation time $\tau = 0$. The $Q_A^{\bullet-}$ part of the spectrum is at the low-field side (higher g-values than the $P_{865}^{\bullet+}$ part). For more details, see section materials and methods.

systems. In the present case, T_2 is governed by librational fluctuations of $Q_A^{\bullet-}$ in the H-bonding network of its binding site in dark-adapted Zn-RCs dissolved either in water, PVA or trehalose. The anisotropic contributions to T_2 have minima (longest T_2) along the canonical orientations of the g-tensor, because in their neighbourhood fluctuations of g-values translate only weakly to fluctuations of the Larmor frequencies. Thus, the determination of T_2 as a function of the resonance position in the high-field EPR spectrum provides information about the directions and amplitudes of molecular motions and their correlation times. This is indicative as to whether the quinone is hydrogen bonded in its protein binding site or not, and in which direction the dominant hydrogen-bonding amino-acid partner is located. This holds as long as the temperature is sufficiently low ($T \approx 150$ K) for a uniaxial motion about a dominating H-bond. When going to higher temperatures, the orientation dependence of the relaxation times of $Q_A^{\bullet-}$ changes. The differences in T_2 values between canonical and intermediate orientations increase, while the T_2 values at the canonical orientations become equal. This shows that at temperatures higher than ≈150 K, the motional modes loose their directional preference, probably because of thermally activated additional fluctuations between conformational substates of the protein (Parak, 1980), superimposing the fluctuations of the quinones around their H-bond axis.

Figure 5.8 shows the field dependence of T_2 relaxation profiles, as evaluated from the mono-exponential decays of 2-pulse echo intensities. At 290 K the T_2 profiles were obtained for the two cases, 690 nm diode laser either ON or OFF, to compare the relaxation dynamics of photo-accumulated and "cyclic", i.e., transient radicals. Within experimental error the relaxation dynamics of $Q_A^{\bullet-}$ in PVA and trehalose matrices agree both in absolute values and anisotropies (Figure 5.8a). Thus, with respect to the $Q_A^{\bullet-}$ dynamics, there is no difference in the H-bonding network of the binding site between PVA and trehalose matrices at room temperature. The ESE experiments at 150 K give a similar picture for PVA and trehalose, as shown in Figure 5.8b. In water, the relaxation dynamics of $Q_A^{\bullet-}$ is about a factor of 2 slower, but the anisotropy picture stays the same as compared to the PVA and trehalose samples. The increased T_2 values measured in water as compared to RCs embedded in the dehydrated PVA and trehalose matrices are most likely due the much higher RC concentration in the latter samples. Indeed measurements in water, performed at two RC concentrations, differing by a factor of 2.3, yielded sizeably smaller T_2 values in the more concentrated sample (not shown). A more pronounced effect is expected in the PVA and trehalose matrices, where, due to extensive dehydration, a RC concentration is attained, which is at least one order of magnitude larger than in the water solution. Such a concentration effect on T_2 values is well documented in the literature (Eaton, 2000). The important point is, however, that, independently from the absolute T_2 values which differ in water, the T_2 anisotropy is essentially the same in water, PVA and trehalose. We conclude that the motional dynamics of $Q_A^{\bullet-}$ in its binding site remain the same in all three solvent matrices.

5.2 Discussion.

The results of the W-band EPR study, both by cw and pulse techniques, and of the laser- flash absorption experiments on dark-adapted Zn-RCs, dissolved in water, PVA or trehalose matrices, can be summarized as follows:

1. The behaviour of the Zn-RC preparations in water solution is as expected: a) the degree of Fe→Zn substitution in the RC is about 50%, b) the $P_{865}^{\bullet+}Q_A^{\bullet-}$ charge-recombination kinetics at 290 K and 150 K are in agreement with the literature (Kleinfeld, 1984; Flores, 2008), c) the cyclicity of the RC/water sample is > 95%

both at 290 K and 150 K. Apparently, the RC-preparation procedures for the EPR measurements have left the structure and dynamics of the protein intact.

2. Illumination of the RC/PVA and RC/trehalose samples at 290 K results in a strong steady-state signal of a Q_A-type radical anion (at present our EPR experiments cannot reveal the exact structure of the photo-accumulated radical species, but additional ENDOR experiments are planned for future structure information). After about 1 hour of illumination only about 20% of RCs are still intact, i.e., show cyclic ET behaviour. The process of the Q_A-type radical photo-accumulation is independent of RC concentration, i.e., is not due to a photo-heating of the sample. After adding water (≈ 50%), the steady-state signal of the Q_A-type radical disappears and normal behaviour like in RC/water solutions is restored. The photo-accumulation of a Q_A-type radical anion is reflected in the comparable decrease of the optically detected $P_{865}^{\bullet+}$ signal recorded in room-temperature trehalose glasses following repetitive laser excitation.
3. At 150 K, the behaviour of all three RC/matrix samples is similar. The Q_A-type radical photo-accumulation process (in RC/PVA and RC/trehalose samples) does not take place. The $P_{865}^{\bullet+}Q_A^{\bullet-}$ charge-recombination kinetics are similar for all three matrices.
4. At 290 K, the $P_{865}^{\bullet+}Q_A^{\bullet-}$ recombination kinetics probed by EPR and optical absorption are in excellent agreement. They differ significantly in the RC/trehalose and RC/PVA matrices, as compared to the water/glycerol RC solution, which is in line with previous optical measurements (Palazzo, 2002; Francia, 2004a; Francia, 2009).
5. Both at 290 K and 150 K, there is no significant difference in the electron spin T_2 relaxation dynamics due to librational fluctuations of $Q_A^{\bullet-}$ in all three RC/matrix samples (except for a factor of about 2 in the T_2 time for the RC/water sample at 150 K) .
6. The shape of the spin-correlated $P_{865}^{\bullet+}Q_A^{\bullet-}$ radical-pair spectrum is similar in all three samples at 150 K and 290 K.

Thus, from the high-field EPR and laser-flash absorption measurements it has to be concluded that the motional dynamics of $Q_A^{\bullet-}$ in its binding site remain the same in the three solvent matrices, suggesting that the observed matrix dependence of the $P_{865}^{\bullet+}Q_A^{\bullet-}$ recombination kinetics in dark-adapted RCs at room temperature (RC/water *versus* RC/PVA and RC/trehalose, see Figure 5.4) is not due to changes in the local

environment of the $Q_A^{\bullet-}$ cofactor in its binding site, but it rather originates in the high rigidity of the dry trehalose glassy matrix firmly coating the surface of the RC already at room-temperature.

As outlined in the Introduction, a rich body of independent experimental evidences indicates that in room-temperature solutions the RC protein rapidly fluctuates among an extremely large number of conformational substates (Frauenfelder, 2009). This is essential for biological function since such an high structured energy landscape with its multi-frequency fluctuations among the substates provides the reservoir of entropy that dictates to which extent a given quantity of thermal energy is available for doing biologically useful work. Following the light-induced primary charge separation, the RC relaxes from a *dark-adapted* to a *light-adapted* state, thereby stabilizing the $P_{865}^{\bullet+}Q_A^{\bullet-}$ state. Despite the fact that a central goal in photosynthesis research over the last decades has been to relate structure, dynamics and function, the structural and dynamical basis of the relaxation by which the RC responds to the light-induced generation of the electric field around $P_{865}^{\bullet+}$ and $Q_A^{\bullet-}$ remains elusive at present (see chapter 1.4 in the Introduction).

With the aim to contribute to clarify the confusing scenario of proposed strategies for stabilizing the charge-separated primary radical pair $P_{865}^{\bullet+}Q_A^{\bullet-}$, we have compared the behavior of RCs embedded in water solution and incorporated into dehydrated matrices; the latter were shown to hinder the RC relaxation following $P_{865}^{\bullet+}Q_A^{\bullet-}$ formation and to trap the RC distributed over a large ensemble of conformational substates (see chapter 4 of the present thesis and (Palazzo, 2002; Francia, 2004a; Francia, 2009)). In fact, the embedding of the RC in a dehydrated trehalose glassy matrix or in a strongly dried PVA film gives rise, at room temperature, to significantly accelerated $P_{865}^{\bullet+}Q_A^{\bullet-}$ recombination kinetics, as compared to water-glycerol solutions. Such matrix effects have been consistently probed in parallel by laser optical absorption spectroscopy and by direct-detection EPR microwave absorption (see Fig.5.4); it is satisfying that similar kinetics were obtained for such vastly different spectroscopic methods (see Table 5.1). Both measurements show additionally that, while in aqueous solutions the $P_{865}^{\bullet+}Q_A^{\bullet-}$ decay is essentially exponential with a unique rate constant, a distribution of rate constants is needed to fit the recombination kinetics in the dehydrated trehalose and PVA matrices. This indicates that, over the time scale of $P_{865}^{\bullet+}Q_A^{\bullet-}$ recombination, in the latter matrices trapping of conformational substates occurs already at room temperature. We observed

slightly faster and rate-distributed kinetics in the RC/trehalose sample, as compared to the RC/PVA one, in spite of the much lower content (by one order of magnitude) of residual water in the PVA matrix. The values measured for the kinetic parameters and for the residual water content in the two matrices fit well the previously observed relationship between the kinetics of charge recombination and the hydration level (Palazzo, 2002; Francia, 2004a; Francia, 2009).

Interestingly, analysis of the charge-recombination kinetics, probed by EPR at 150 K, shows that the average rate constant and the width of the rate distribution are further increased in the same trehalose and PVA matrices at cryogenic temperatures (see Table 5.2). These values are significantly larger than those obtained for the water-glycerol system at the same temperature which, in turn, are in good agreement with the values measured by optical laser spectroscopy at cryogenic temperatures (McMahon, 1998). It appears, therefore, that the observed inhibition of relaxation from the *dark-adapted* to the *light-adapted* state in the trehalose and PVA matrices, although quite significant, was not complete at room temperature. Apparently, some conformational dynamics, coupled to the ET process, survived at room temperature in the examined samples, most likely due to their residual water content. Indeed, we have shown that a more extensive dehydration of RC/trehalose matrices leads at room temperature to larger <k> and σ values, which are comparable to those measured in glycerol-water systems at cryogenic temperatures (see chapter 4 of the present thesis and ref. (Palazzo, 2002; Francia, 2009)).

As another important result we want to point out that W-band EPR experiments performed on both RC/PVA and RC/trehalose samples at room temperature have revealed the photo-accumulation of a stable Q_A-type radical (probably a quinone anion radical, see above). A simple explanation for the photo-accumulation of a Q_A-type radical is that, in the subpopulation of RCs in which photo-accumulation takes place, reduction of the flash-oxidized $P_{865}^{\bullet+}$ by an exogenous electron donor occurs faster than recombination between $P_{865}^{\bullet+}$ and $Q_A^{\bullet-}$. Such an adventitious electron donor is expected to be eventually present in the liquid sample at very low concentrations, being therefore unable to reduce, through a collisional process, $P_{865}^{\bullet+}$ at a rate which efficiently competes with $P_{865}^{\bullet+}Q_A^{\bullet-}$ recombination. Correspondingly, no photo-accumulation of a Q_A-type radical is detected in water RC solutions. In the solid PVA and trehalose matrices, due to the extensive dehydration, the concentration of the putative electron donor to $P_{865}^{\bullet+}$

would be greatly increased, possibly leading to a close complex between the exogenous electron donor and the RC, and making possible a fast electron donation to $P_{865}^{\bullet+}$. If this is the case, we have to assume that the electron transfer is thermally activated, since no photo-accumulation of a Q_A-type radical has been observed in the RC/PVA and RC/trehalose samples at 150 K.

The photo-accumulation of a Q_A-type radical revealed by W-band EPR is consistent with previous observations by flash absorption spectroscopy: in progressively dried RC/trehalose glasses, repetitive photo-excitation led, in fact, to a decreased amplitude of the flash-induced optically detected $P_{865}^{\bullet+}$ signal (Palazzo, 2002). This decrease had been attributed to a fraction of RCs in which $P_{865}^{\bullet+}Q_A^{\bullet-}$ was not formed, and charge recombination occurred on a sub-nanoseconds time scale from the photo-reduced bacteriopheophytin. Since this decay was much faster than the time resolution of the optical measurements, it resulted in a decrease of the signal of the photo-oxidized $P_{865}^{\bullet+}$. The present EPR experiments are fully consistent with this observation by optical spectroscopy, because photo-accumulation of a radical in a subpopulation of RCs will clearly prevent the formation of the primary charge-separated state $P_{865}^{\bullet+}Q_A^{\bullet-}$ leading in that subpopulation to photo-reduced bacteriopheophytin. Upon dissolving the glassy sample, the EPR-detected photo-accumulated Q_A-type radical was no more observed in the dark. Consistently, the dissolution of dehydrated RC/trehalose glasses fully restored the original extent of $P_{865}^{\bullet+}$ photo-oxidized by a laser flash, as detected by optical spectroscopy (Palazzo, 2002).

Rather unexpectedly, the W-band EPR and ESE experiments on the photo-generated $P_{865}^{\bullet+}$ and $Q_A^{\bullet-}$ radical ions as well as on $P_{865}^{\bullet+}Q_A^{\bullet-}$ radical pairs when performed on the same glycerol-water, trehalose and PVA samples, that are characterized by different recombination kinetics at room temperature (see Table 5.1), did not show any significant matrix-induced effects, neither on the spectra nor on the echo decays. The transient W-band EPR signals of the spin-correlated $P_{865}^{\bullet+}Q_A^{\bullet-}$ radical pair, measured at 290 K in the dehydrated PVA and trehalose matrices, and at 150 K in the glycerol-water system, did not exhibit significant differences when normalized in amplitude. This suggests that incorporation of RCs into the dehydrated trehalose and PVA matrices does not change significantly the distance and the relative orientation of the $P_{865}^{\bullet+}$ and $Q_A^{\bullet-}$ cofactors as compared to RCs in water-glycerol, i.e., the glassy matrices do not cause

any structural distortions of the cofactor binding sites of the RC. Therefore, the effects observed on the kinetics of electron transfer cannot be simply traced back to matrix-induced structural changes, but rather have to be related to the dynamics and/or the energetics of the protein/solvent system, with its characteristic fluctuations between conformational substates of the energy landscape, as was originally proposed by Palazzo et al. (Palazzo, 2002) and Francia et al. (Francia, 2004b).

From these observations we also infer that the RC relaxation from the *dark-adapted* to the *light-adapted* state occurring under physiological conditions (McMahon, 1998; Kleinfeld, 1984) is quite unlikely to involve any change in the geometry of the cofactors. Moreover, the ESE experiments show that the field dependence of the anisotropic T_2 spin-spin relaxation times is essentially coincident in the trehalose and PVA matrices at 290 K, and quite similar in these two matrices and in the glycerol-water system at 150 K. This indicates that the relaxation dynamics of $Q_A^{\bullet-}$ (dominated, under high-field conditions, by its g-tensor anisotropy) are essentially the same in the three solvent matrices, implying, in turn, that also the hydrogen-bond network in the Q_A binding pocket is unaffected by the different matrices. Therefore, this hydrogen-bond network does not appear to be involved in the conformational response of the RC to the light-induced electric field generated by the formation of the charge-separated radical pair $P_{865}^{\bullet+}Q_A^{\bullet-}$.

Taken together, the results imply that the relative geometries of the primary donor and acceptor, as well as the local environment of Q_A in its binding pocket, do not differ significantly in the *light-adapted* state, which is observed at room temperature in solution RCs, with respect to the *dark-adapted* state, which is trapped both in the dehydrated trehalose and PVA matrices at room temperature and in water-glycerol mixtures at cryogenic temperature. This conclusion has been further supported by a recent high-field EPR study, in which the dark- and light-adapted conformations have been trapped at cryogenic temperatures (Flores, 2010)**.** These findings suggest that the structural and dynamical basis of the RC relaxation processes following charge separation resides rather in changes throughout the protein-solvent system that do not involve the geometry or local environment of the cofactors. Thus it appears possible that the stabilizing relaxation process consists mainly in a reorientation of amino-acid side chains in response to the light-induced electric field around $P_{865}^{\bullet+}$ and $Q_A^{\bullet-}$. However, if this is the case, these side chains are unlikely to be involved in the

formation of the Q_A binding pocket. Otherwise one would expect that, at variance with what was observed by the high-field ESE experiment on the T_2 anisotropy, the $Q_A^{\bullet-}$ environment and dynamics would be significantly altered by incorporation of the RC into solid matrices, which substantially inhibit the relaxation processes, as is shown by the kinetics of charge recombination.

As an alternative explanation, besides solvation effects due to residues of the RC protein, a major energetic contribution to stabilizing the primary charge-separated state is also expected from internal water molecules interacting with the RC cofactors. In a recent work, Iwata et al. (Iwata, 2009) have observed light-induced FTIR spectral changes, associated with the photo-reduction of Q_A, in the O-H stretching region (3700-3500 cm^{-1}), which is characteristic of weakly hydrogen-bonded water molecules. The authors have proposed that the orientation of these "free" water molecules plays a major role in stabilizing the $P_{865}^{\bullet+}Q_A^{\bullet-}$ state by dielectric screening of the light-induced electric dipole of the charge-separated radical pair. As compared to previous crystallographic RC structures, for example that of Ermler et al. with 2.65 Å resolution (Ermler, 1994), crystal structures with significantly better resolution have become available by now, allowing more and more unbound water molecules in the protein to be identified. Recently, Koepke et al. have reported a *Rb. sphaeroides* RC structure with a resolution of 1.87 Å, which is the best resolution obtained so far (Koepke, 2007) and, indeed, the number of modeled water molecules that was included in the structure could be extended from 160 (Ermler, 1994) to 430: many newly assigned unbound water molecules are clustered at the cytoplasmic surface of the RC (where the quinone acceptor are located), and several unbound water molecules are buried in its membrane-spanning region. Hence, unbound water molecules are expected to be able to reorient in the electric field of the cofactor ions following charge separation, thereby giving rise to a significant "dynamic screening".

The notion that a water-mediated dynamic screening of the light-generated $P_{865}^{\bullet+}Q_A^{\bullet-}$ can largely contribute to the relaxation from the *dark-adapted* to the *light-adapted* RC conformation is in line with the *anchorage model* (Francia, 2008; see also chapter 1.5 of the Introduction) that was proposed to explain the tight dynamic coupling which characterizes glassy trehalose-water protein matrices. According to this hypothesis, in trehalose-water systems of low water content, the residual water preferentially surrounds the protein: upon drying, an increasing fraction of this hydration shell becomes involved into an H-bond network which bridges protein groups and sugar

molecules, thus anchoring the protein surface to the surrounding trehalose matrix. Such a locking of the protein surface (and of the protein hydration shell) to the dynamics of the solid matrix is expected to hinder protein fluctuations and conformational changes that are related to amino-acid side-chain reorganization as well as to the reorientation of water molecules interacting with the RC, thus contributing to the stabilization of the charge-separated $P_{865}^{\bullet+}Q_A^{\bullet-}$ state. This scenario is consistent with the present EPR results, because such a matrix-protein interaction does neither necessarily involve any alteration of the distance and relative orientation of the cofactors, nor necessarily any dynamic-coupling change on the local scale of the Q_A binding pocket. Changes in these parameters are, therefore, not necessarily involved in the stabilization mechanism of charge separation by protein/solvent relaxation.

The control exerted on the RC dynamics and electron transfer kinetics by the fluctuations of the cofactor environment can be further clarified in the framework of a "unified model of protein dynamics" developed by Frauenfelder and colleagues (Frauenfelder, 2009), which summarizes decades of experimental and theoretical investigations focused on myoglobin (Mb). As discussed in detail in the Introduction (see chapter 1.2), three types of protein motions are essentially identified as relevant for biological function (Fenimore, 2004; see also chapter 1.2 of the Introduction): solvent-coupled (α-slaved) processes (Class I); hydration-shell coupled (β-slaved) processes (Class II); and inner-molecular processes (Class III), such as molecular vibrations in the force-field potential of inner-molecular atom-atom interactions, that are higher in energy and non-slaved to solvent fluctuations. Except for the latter processes, which do not appear to be controlled by external thermal fluctuations, the dominant internal protein motions and concomitant protein functions are driven by the dynamics of the solvent.

In an attempt to apply this concept to the RC dynamics coupled to light-induced electron transfer we propose to ascribe the structural relaxation from the *dark-adapted* to the *light-adapted* state to Class II processes, slaved to the β-fluctuations of the hydration shell. According to the *anchorage model* outlined above, in a sufficiently dehydrated RC/trehalose-water matrix, we expect that the H-bond network involving the hydration shell substantially reduces its motional degrees of freedom, i.e., restricts the β-fluctuations, thus hindering the β-slaved relaxation from the *dark-adapted* to the *light- adapted* state. In line with the concept of a β-slaved relaxation, also an extensive drying of the RC in the absence of trehalose sugar, which leads to a substantial

depletion of the hydration shell, is able to inhibit the conformational change from the *dark-adapted* to the *light-adapted* state at room temperature, as probed by the strongly accelerated and distributed kinetics of $P_{865}^{\bullet+}Q_A^{\bullet-}$ recombination in *superdry* RC films following a laser pulse (see chapter 6 and Malferrari, 2011).

A reduction of the β-fluctuations in solid matrices is expected to depend on the specific molecular interactions between the matrix and the hydration shell of the protein (e.g., the ability to form H-bond networks). In the case of PVA matrices this interaction appears to be weaker than in trehalose, resulting in a weaker protein-matrix dynamic coupling (Giachini, 2007). Accordingly, in agreement with previous observations (Francia, 2004a), in the RC/PVA sample an almost comparable acceleration of the charge-recombination kinetics has been observed at hydration levels one order of magnitude lower than those prevailing in the RC/trehalose sample. Because of the low content of residual water, it is likely that the observed inhibition of the transition from the *dark-* to the *light-adapted* conformation is due, in this case, not only to a reduction of the RC hydration-shell dynamics (β-fluctuations) as caused by interaction with the PVA matrix, but also to a depletion of the protein hydration layer where the β-fluctuations occur. A different mechanism of matrix-protein coupling in the RC/PVA and RC/trehalose sample is further supported by the observation that in the dehydrated trehalose matrix the RC can withstand temperatures as high as 50 °C for several weeks without undergoing any denaturation (a prominent example of *anhydrobiosis*), while in PVA a significant fraction of the RC population undergoes under the same conditions thermal denaturation during the period of a few days (data not shown).

Interestingly, the librational fluctuations of $Q_A^{\bullet-}$ in the H-bond network of its binding site turned out to be non-slaved to the matrix environment, since the observed anisotropy of the transversal spin-relaxation time T_2 is essentially independent of the chosen matrix, even in the extreme case of dehydrated trehalose glass. Although, in general, librational fluctuations of the whole cofactor might be expected to belong to the energetic tier of Class II processes (β-fluctuations), they turned out to be not controlled externally by the solid protein-coating trehalose matrix but rather internally by temperature-dependent amplitudes of fluctuation affecting the hierarchy of H-bond strengths between the quinone and local amino-acid residues (Schnegg, 2002). In the frame of the "unified model of protein dynamics" proposed by Frauenfelder and co-workers (Frauenfelder, 2009; Fenimore, 2004) we tend, therefore, to ascribe the RC cofactor dynamics, as revealed by the present high-field EPR measurements at 290 K

and 150 K, to Class III processes. The cofactor dynamics, non-slaved to the micro-environment, appear to be coupled to the process of light-induced charge separation, which proceeds even in the dehydrated RC and in solid matrices at room and cryogenic temperatures.

6. ELECTRON TRANSFER AND PROTEIN-SOLVENT DYNAMICS IN RC FILMS AT DIFFERENT HYDRATION LEVELS

As discussed in the previous chapter, one of the main conclusions of the high-field EPR studies performed on RC-trehalose glasses been the assignment of the protein relaxation events which stabilize the $P^+Q_A^-$ state to Class II motions, i.e. to the internal protein dynamics slaved to β fluctuations of the water molecules belonging to the protein hydration shell (Fenimore, 2004; Frauenfelder, 2009; see also par.1.2).

If this attribution is correct we expect that depletion of the hydration shell of the protein even in the absence of any embedding matrix is able *per se* to inhibit the RC dynamics, leading, at sufficiently low water contents, to a strong retardation of the RC internal motions coupled to $P^+Q_A^-$ recombination. The main aim of the experimental studies presented in the present chapter (the results have been published in Malferrari, 2011) has been to test this expectation by analyzing the kinetics of $P^+Q_A^-$ recombination in RC-detergent films over a large range of controlled hydration levels. Fourier transform infrared (FTIR) spectral analysis of the combination (5155 cm^{-1}) and of the association (2130 cm^{-1}) bands of water allowed to estimate the water content of the films even at very low hydration, to construct water sorption isotherms, and to correlate the effects observed on the electron transfer kinetics with the structural/dynamical properties of the residual hydration shell of the complex. The results, obtained in the presence of two different detergents, indicate that dehydration of the complex retards the RC thermal fluctuations and relaxations probed by the kinetics of $P^+Q_A^-$ recombination, mimicking at room temperature effects observed at cryogenic temperatures in the hydrated system. Furthermore, data at extremely low hydration suggest that a limited number of tightly bound water molecules are essential to stabilize the primary, light-induced charge separated state on the time scale of 10^{-2} s.

6.1 Results.

6.1.1 Hydration isotherms.

The (ν_2+ ν_3) combination band of water around 1940 nm is particularly suited to evaluate the water content of the RC-detergent films. This NIR band originates from the combination of bending (ν_2 or δ-OH at 1638 cm^{-1}) and asymmetric stretching (ν_3 or ν-OH at 3000-3700 cm^{-1}) vibrations (Max, 2002). The area under this band can be taken

to be proportional to the water concentration, being unaffected, at variance with other water IR bands, by co-solvents (Bonner, 1974b; Dickens, 1999), by the physical state of the water sample (solid or liquid) (Fornés, 1978), and therefore by the extent of hydrogen bonding. A proportionality constant (absorptivity) a_w = 101.9 M^{-1} cm^{-1} nm inferred from water absorption in reverse micelles (Giustini, 1996) was used. Since the average thickness of the RC-detergent film, i.e. the effective optical path, is not easily measured to a sufficient accuracy, we used as an internal standard the area of the amide II band of the RC (centered around 1550 cm^{-1}). Under the assumption that the proportionality constant (absorptivity) a_{II} between the concentration of the RC and the area of this band does not depend on the hydration level of the RC-detergent film, the (H_2O/RC) molar ratio can be calculated as:

$$\left(\frac{H_2O}{RC}\right) = \frac{A_w a_{II}}{A_{II} a_w} \qquad \text{(eq.6.1)}$$

where A_w and A_{II} represent the area of the water combination band and of the amide II band respectively. The value of a_{II} was determined from the RC absorption at 802 nm (i.e. at the peak of the Q_y band of the monomeric RC bacteriochlorophyll) using an extinction (Straley, 1973) ε_{802}=288 mM^{-1} cm^{-1}. Spectra were collected over the 15000-1000 cm^{-1} range in 5 freshly prepared RC-detergent films equilibrated at different relative humidity (43% ≤ r ≤ 94%), and a_{II} evaluated as $(\varepsilon_{802} A_{II})/A_{802}$, being A_{802} the absorbance of the sample at 802 nm. By this approach we obtained a_{II}=(32.7 ± 2.8) $\cdot 10^6$ M^{-1} cm^{-1} nm and a_{II}=(56.6 ± 4.3) $\cdot 10^6$ M^{-1} cm^{-1} nm in the case of RC-OG and RC-LDAO films, respectively. The value in the presence of OG is in excellent agreement with an estimate based on spectra recorded in dried RC reconstituted into phospholipid vesicles after replacement of LDAO with OG (Nabedryk, 1982). The larger value obtained for a_{II} in RC-LDAO films can be explained by considering that the detergent LDAO contributes significantly to the IR absorption in the amide II region (Giguère, 1961). The a_{II} value determined in RC-LDAO films cannot therefore be considered a true value for the RC amide II absorptivity. This does not preclude, however, its correct use in eq.6.1, since the LDAO to RC molar ratio in the samples is fixed, being essentially determined by the number of LDAO molecules organized as a detergent belt around the hydrophobic region of the RC (see par. 6.2.1).

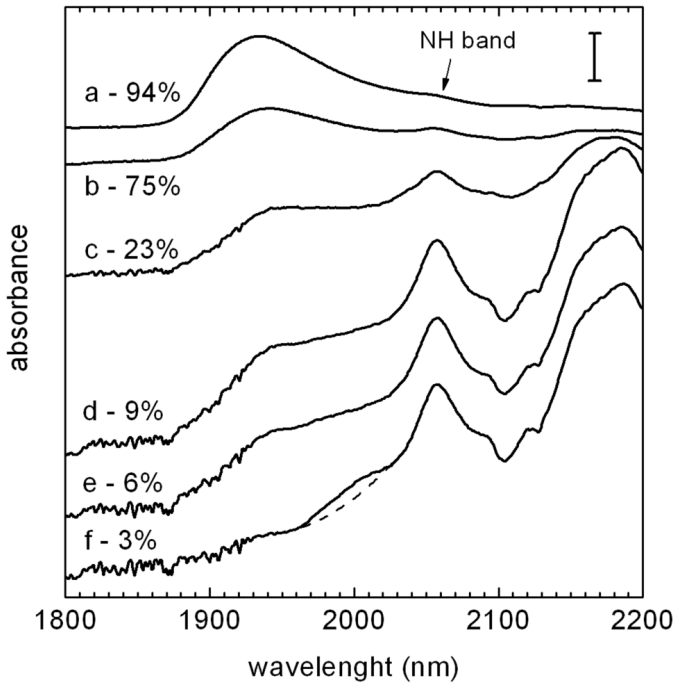

Figure 6.1
NIR spectra of RC-LDAO films at different hydration levels in the wavelength range of the ($\nu_2+\nu_3$) combination band of water. The relative humidity of the atmosphere at which the samples were exposed is indicated in the labels. The vertical bar corresponds to 40 mA for spectrum *a*, 16 mA for spectrum *b*, 5 mA for spectrum *c*, and 2 mA for spectra *d-f*. The dashed line shows the background of spectrum *f* in the water absorption region, evaluated as described in the text. Spectra have been normalized on the basis of the area of the amide II band.

Fig.6.1 shows FTIR spectra in the region of the water combination band, measured in RC-LDAO films equilibrated at different values *r* of relative humidity, as described in par.3.2. The band is progressively reduced in amplitude when *r* decreases from 94 to 3 %. Upon dehydration the band shifts to higher wavelengths and becomes narrower. The band at 2058 nm (4859 cm^{-1}), assigned to a combination (Hecht, 1956) of the NH stretching frequency at 3280 cm^{-1} and the peptide frequency at 1550 cm^{-1}, partially overlaps with the water combination band. Under extensive dehydration, the NH band is clearly resolved, as already observed in gelatin and soluble proteins (Vandermeulen, 1980). In order to correct for contributions arising from the NH band, a background spectrum has been estimated using a quadratic form to connect the regions proximal to the water band in the spectrum at *r*=3% (curve *f* of Fig.6.1). The background spectrum (simulating the one of a fully dehydrated sample) has been subtracted from all the other spectra, after normalization based on the area of the corresponding amide II bands.

The (H_2O/RC) molar ratios evaluated as described above (see eq.6.1) in RC-detergent films equilibrated at different relative humidity were used to construct water sorption isotherms. The films formed under nitrogen flow (see par.3.1.2) were characterized by (H_2O/RC) molar ratios between 1000 and 2000. Each film was first equilibrated at a relative humidity between 3% and 85%. In order to construct the isotherm, data were subsequently collected for each film at increasing relative humidity. The (H_2O/RC) molar ratios determined at a given relative humidity in different films and sorption sequences were quite reproducible, and did not show any dependence upon the value of the relative humidity at which the films were initially equilibrated. No hysteresis effect was therefore observed, since each film was subjected to a desorption/sorption sequence over a different range of relative humidity. After a 3 days exposure of the RC films at room temperature, the RC bacteriochlorin pigments started to lose the native coordination, as judged from the alterations in their Q_y bands (Hughes, 2006), particularly when the RC-detergent system was highly hydrated. Since the films were equilibrated at any value of *r* for at least 15 hours, this limited the number of *r* values which could be explored in a single film: each sorption sequence included a maximum of 4 values of relative humidity. The hydration isotherms obtained by this procedure in a series of RC-LDAO and RC-OG films are shown in Figure 6.2. The hydration of the RC-detergent complex is given as the measured (H_2O/RC) molar ratio or as water-to-RC mass ratio, *h*, assuming a molecular weight of 100 KDa for the RC. The dependence of the hydration upon *r* exhibits the typical sigmoidal character observed for water sorption by a number of globular and fibrillar proteins (Careri, 1979; Lüscher-Mattli, 1982). Over the whole *r* range the RC-LDAO complex is systematically more hydrated than the RC-OG complex, indicating that the hydration properties of the two detergents differ significantly and that the RC detergent belt contributes substantially to water sorption.

To analyze the sorption data we choose the Hailwood and Horrobin model (Hailwood, 1946), which assumes that water sorption is governed by two sets of equilibria: (*a*) the formation of hydrates between water and definite sites of the absorbing complex, and (*b*) the formation of an ideal solid solution of water in the complex. Accordingly, adsorption data have been fitted to the Hailwood and Horrobin equation (Hailwood, 1946):

Table 6.1
Parameters of the Hailwood and Horrobin equation (eq.6.2) best fitting the hydration isotherms in RC-LDAO and RC-OG films. Water-to-reaction center molar ratios (H_2O/RC) have been converted into water-to-protein mass ratios by assuming a RC molecular mass of 100 KDa. Values in brackets indicate the calculated confidence intervals within one standard deviation.

	h_0 (g water/g protein)	h_0 (H_2O/RC) molar ratio	K_1	K_2
RC-LDAO	0.27 (0.25-0.29)	1500 (1390-1610)	10.5 (4.8-23.0)	1.02 (1.01-1.02)
RC-OG	0.18 (0.17-0.21)	1000 (944-1170)	2.0 (1.0-3.3)	0.94 (0.93-0.95)

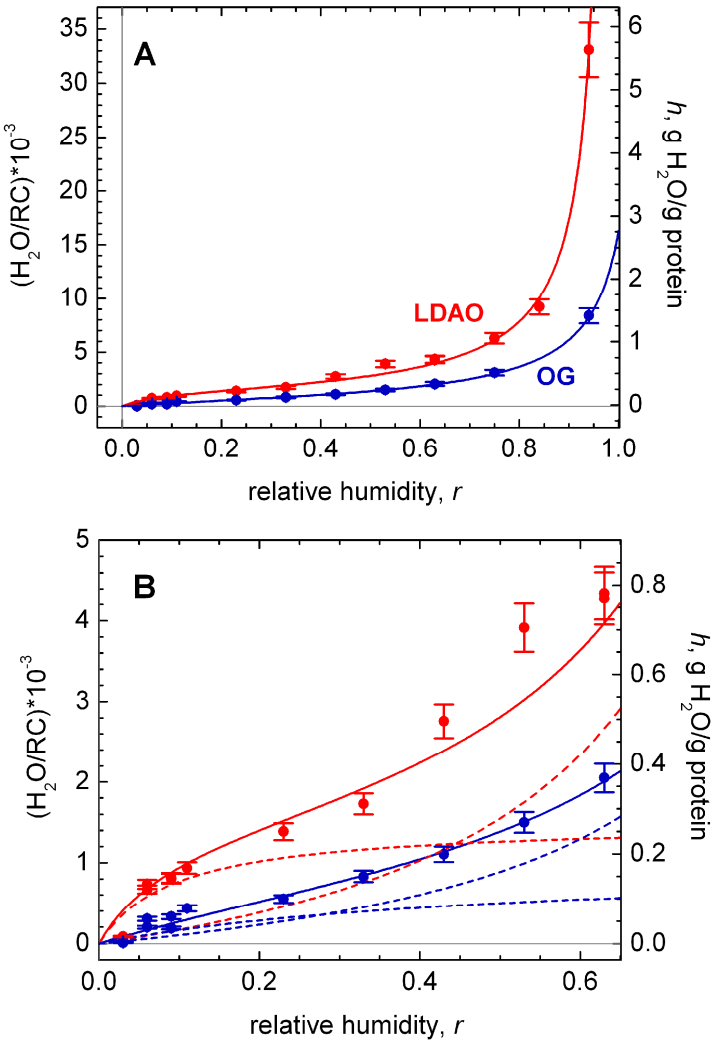

Figure 6.2
Hydration isotherms at 297 K determined in RC-LDAO and RC-OG films. Continuous lines represent best fit to eq.6.2. The corresponding parameters are given in Table 6.1. Panel B shows an enlargement of the data in panel A over the low relative humidity range. The dashed curves describe the contributions to water uptake of the two processes considered in eq.6.2, i.e. adsorption at strong binding sites and water condensation prevailing at high r values.

$$h = h_0 \left(\frac{K_1 r}{1+K_1 r} + \frac{K_2 r}{1-K_2 r} \right) \quad \text{(eq.6.2)}$$

where h represents the equilibrium water content of the film, h_0 and K_1 are constants, proportional to the number and activity of the hydration sites, respectively (process *a*); K_2 is related to the water activity of the solid solution formed by water condensing at the surface of the complex (process *b*). Best fitting to eq.6.2 (continuous lines in Fig.6.2) yields the h_o, K_1 and K_2 values reported in Table 6.1, and allows to resolve the contributions to the film hydration of water adsorbed at (strong) binding sites (process *a*) and at (weak) condensation sites (process *b*). These contributions are shown as dashed curves in Fig.6.2B. The h_0 value is significantly larger in RC-LDAO as compared to RC-OG films, indicating in the latter system a smaller number of strong binding sites. The activity of the strong binding sites (K_1) is about 5 times larger in the presence of LDAO. The different K_1 and h_0 values appear to be mainly responsible for the systematically larger total hydration observed in the RC-LDAO as compared to RC-OG films. Similar best fitting values have been in fact obtained in the presence of LDAO and OG for the water activity K_2 of the solid solution. This finding is consistent with the notion that K_2 governs the progressive binding of water molecules at condensation sites to form a multilayer structure: most of this water population, therefore, does not interact directly with the detergent micelle which surrounds the RC.

6.1.2 Spectral analysis of the water combination and association bands.

The shape and location of the water combination band appear to be governed mostly by hydrogen bonding organization (Dickens, 1999; Bonner, 1974). This band can therefore provide information when attempting to qualify and quantify the intermolecular hydrogen bonds of water adsorbed to the RC-detergent complex. Upon decreasing *r*, particularly for r <20%, the band as a whole shifted to lower wavenumbers and narrowed markedly (Fig. 6.3). In RC-LDAO films the band peak shifted from 5160 cm^{-1} at r=84% to 5000 cm^{-1} at 3%, and the band width at the half-intensity decreased correspondingly from 245 cm^{-1} to 100 cm^{-1}. Similar effects were observed in the RC-OG films.

In an attempt to resolve the contribution of water populations differing in structure and/or dynamics we performed a numerical decomposition of the band into three Gaussian sub-bands. Such a decomposition has been previously employed to

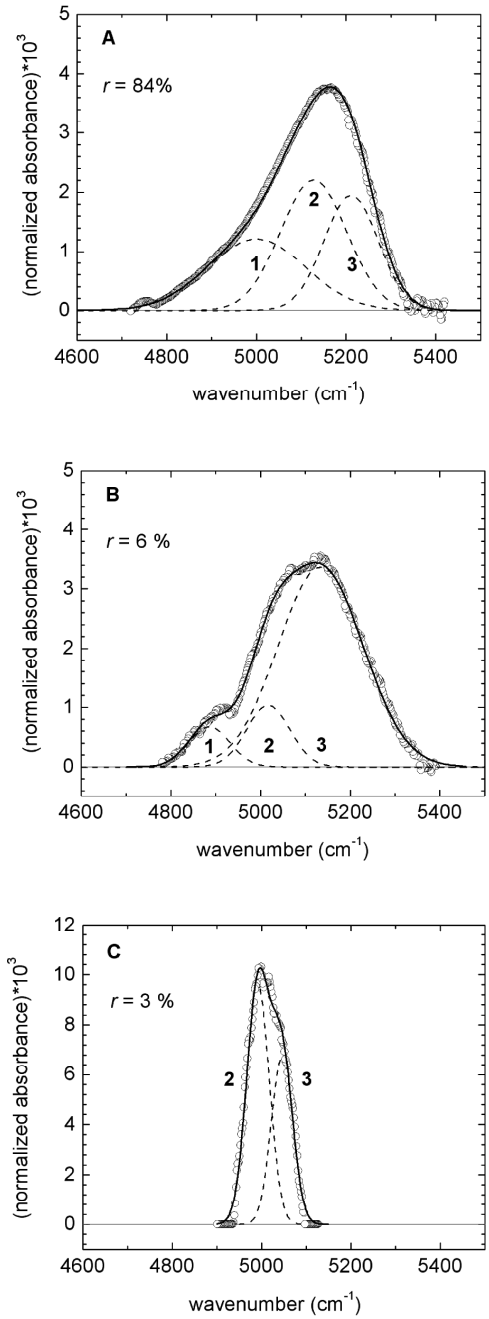

Figure 6.3
Resolution into three Gaussian components (dashed lines) of the combination band of water, corrected for the NH contribution (see Fig.6.1), in RC-LDAO films equilibrated at three different values of relative humidity: 84 % (A), 6 % (B), 3 % (C). Values of the fractional area, peak wavenumber and width of the Gaussian components are reported in Fig.6.4.

analyze the combination band of water in solution as a function of temperature (Fornés, 1978; Czarnik-Matusewicz, 2006; Malsam, 2009), in mixed solvent systems (Bonner, 1974b; Bonner, 1974a), and when adsorbed to solid surfaces (Takeuchi, 1960). The same Gaussian decomposition has been successfully applied to analyze the temperature

dependence of the OH stretching band in pure water (Brubach, 2005) and the effect of the water-to-detergent ratio on the OH stretching band in reverse micellar aggregates (Onori, 1993). In all these systems, the resolved bands are attributed to water sub-populations differing in the H bonding organization. The lowest frequency Gaussian is assigned to molecules having a high H bond coordination number, as this component sits close to the band observed in ice. Conversely, the highest frequency Gaussian is ascribed to water molecules poorly connected to their environment, according to the idea that the less H bonds are established, the stiffer the oscillator.

After normalization of the bands to a unitary area, the absorbance *A* as a function of the wavenumber $\tilde{\upsilon}$ was fitted to:

$$A(\tilde{\nu}) = \frac{1}{\sqrt{2\pi}} \sum_{i=1}^{3} \frac{A_i}{\sigma_i} exp\left[-\frac{(\tilde{\nu}-\tilde{\nu}_i)^2}{2\,\sigma_i^2}\right] \qquad \text{(eq.6.3)}$$

with A_i, $\tilde{\nu}_i$, and σ_i as adjustable parameters. Examples of the obtained decomposition in RC-LDAO films are shown in Fig.6.3 for three values of *r*. Gaussian sub-bands are labeled as band 1-3 in order of increasing peak wavenumber. The dependences upon *r* of the best fitting parameters, i.e. the fractional area (A_i), the position ($\tilde{\nu}_i$) and width (σ_i) of the sub-bands, are presented in Fig. 6.4 A,B, C and Fig. 6.4 A',B', C' for RC-LDAO and RC-OG films respectively. In the presence of the detergent LDAO (Fig.6.4 A-C), under the most hydrating condition (*r*=94%), the peak positions ($\tilde{\nu}_1$=4990 cm^{-1}, $\tilde{\nu}_2$=5125 cm^{-1}, $\tilde{\nu}_3$=5220 cm^{-1}) and the widths (σ_1=140 cm^{-1}, σ_2=80 cm^{-1}, σ_3=55 cm^{-1}) of the three sub-bands essentially coincide with those found in pure water at a comparable temperature (Fornés, 1978; Czarnik-Matusewicz, 2006; Malsam, 2009). The bandwidths follow the order: $\sigma_1 > \sigma_2 > \sigma_3$. This is consistent with the attribution of the lowest frequency band to water molecules for which the H bonding connection is maximized, since hydrogen bonding is known to increase the breath of the band, in parallel with a decrease of the frequency (Kawai, 1985). In fully hydrated films, it appears therefore that the resolved sub-populations exhibit the spectral properties of pure water components, suggesting that most of the adsorbed water molecules are H bonded as bulk water and do not interact with the protein-detergent complex.

At values of the relative humidity between 94% and about 40% the sub-bands did not undergo significant changes, except for a slight shift to lower wavenumbers of bands 2 and 3, and a decrease of the width of band 1. At lower *r* values, however,

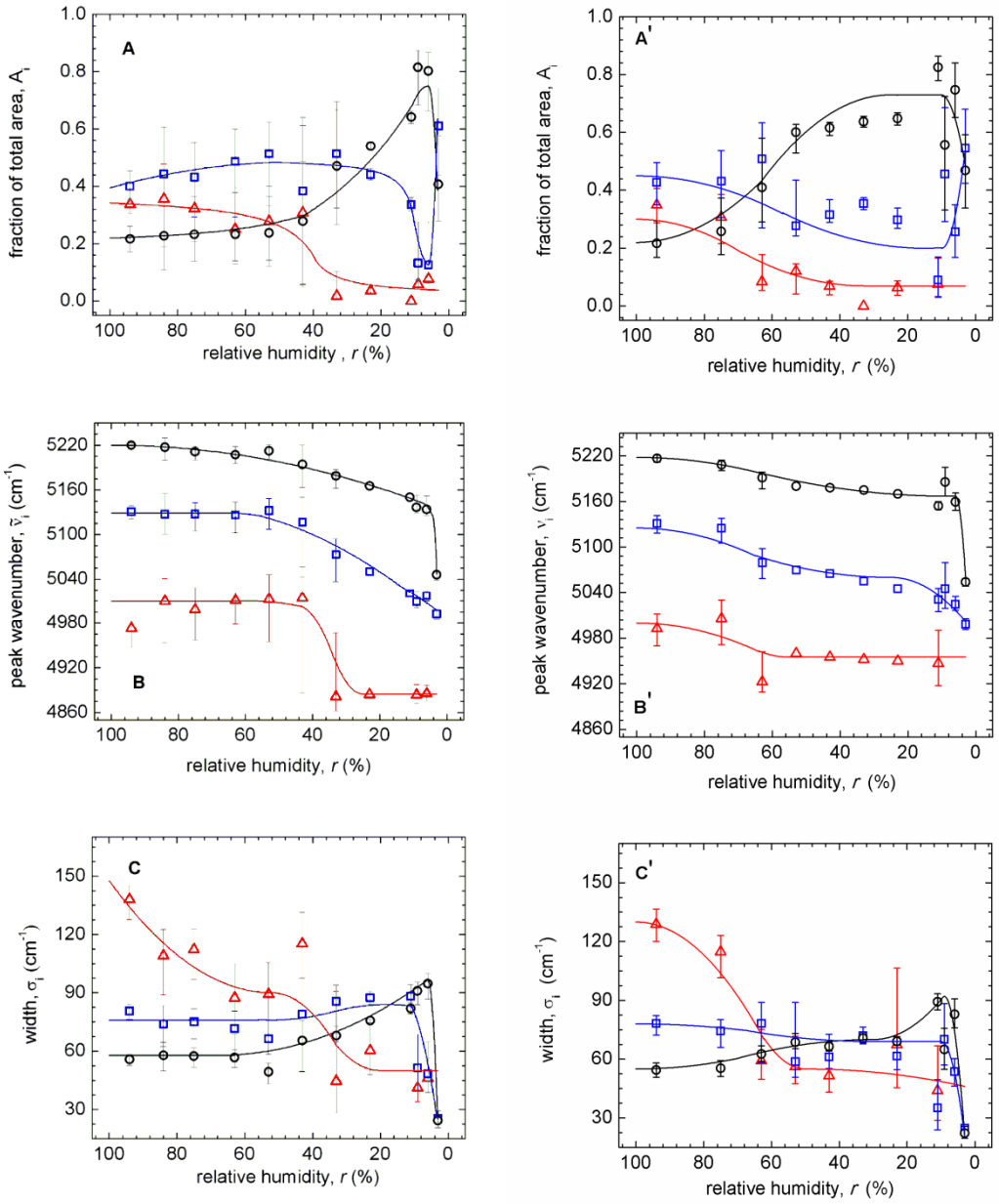

Figure 6.4
Fractional area (A, A'), peak wavenumber (B, B'), and width (C, C') of the three Gaussian components of the water combination band in RC-LDAO (A, B, C) and RC-OG (A', B', C') films, as a function of the relative humidity *r*. Bands are numbered according to the increasing value of their peak wavenumber as band 1 (red triangles), band 2 (blue squares), band 3 (black circles). Vertical bars correspond to the confidence interval within 2 standard deviations of the parameters of the Gaussian components. Continuous lines are drawn through the experimental points just to guide the eye.

dehydration of the film resulted in marked alterations, particularly prominent at r <10%. The contribution of band 1 essentially vanished at r <40%. The disappearance of band 1 was accompanied by a progressive increase of the fractional area of band 3, from about 0.25 at r=40% to about 0.80 at r=9%; this increase occurred also at the expenses of band 2. Further, extensive dehydration (from r=6% to r=3%) induced a sudden reduction of the contribution of band 3, compensated by the increase of band 2 fractional area. In parallel with these drastic changes, the peaks of band 2 and 3 shifted to lower frequencies by about 150 cm^{-1}. Dehydration at r < 10% also induced a strong narrowing of band 2 and 3.

In RC-OG films the spectral analysis evidenced essentially a similar dependence upon r of the fractional area, of the position and of the width of the three Gaussian sub-bands, as shown in Fig. 6.4 A'-C'. In particular, in the hydrated RC-OG films (r=94%) the peak positions and widths coincided within the experimental error with those determined in the hydrated RC-LDAO films. Also in the presence of OG, the fractional area of band 1, close to 0.3 at r=94%, decreased upon dehydration and reduced to zero at r<40%. This decrease occurred mainly at the expenses of band 3, the contribution of which was maximum at r=11%. The sudden increase of the fractional area of band 2, paralleled by a decrease of that of band 3, was also observed in RC-OG films at r<9%. The shift to lower frequency of band 2 and 3 were the same in RC-LDAO and RC-OG films. In the latter system these two bands underwent a larger narrowing ($\sigma_2 \cong \sigma_3 \cong 20$ cm^{-1} at r=3%).

The disappearance of the lowest frequency band 1 upon decreasing the hydration of the film below r = 40% appears to correlate with the strong decrease observed at this relative humidity in the amount of weakly adsorbed water, as resolved by fitting the hydration isotherms to the Hailwood and Horrobin equation. As shown in Fig. 6.2B, in fact, the contribution of this subpopulation of adsorbed water molecules, presumably condensed in multilayer structures, is strongly reduced upon decreasing the relative humidity from 94% to about 40%. Specifically, at r < 45% in RC-LDAO films, and r < 30% in RC-OG films, the contribution of the water adsorbed at strong binding sites starts to prevail over the weakly bound sub-population. Consistently, band 1 is attributed to water molecules organized in structures highly connected through H bonding, which are characteristic of pure water (Fornés, 1978; Czarnik-Matusewicz, 2006; Malsam, 2009). The increase in the relative contribution of band 3 which accompanies the disappearance of band 1 and the decrease of band 2 (see above) is

paralleled by a downward shift of their peak wavenumber at *r* values decreasing from ~40% to ~10%. This response, indicative of a strengthening of the H bonds involving these two water populations, suggests that water molecules adsorbed at stronger binding sites of the protein-detergent complex are progressively depleted upon drying. When the films are drastically dried, at 10% > *r* > 3%, the steep variations observed in the relative area of band 2 and 3, the additional downward shift of the peak wavenumber, and the strong narrowing of both sub-bands indicate that drastic changes occur in the structure/dynamics of the residual water when the inner hydration shell is removed.

Additional information to characterize the interaction between water and the RC-detergent complex is provided by a second IR band of water, the so called association band around 2130 cm^{-1}, ascribed to a combination of the bending mode of water with intermolecular vibrational modes (Eisenberg, 1960). The association band, which is absent in water vapors and is not structured in pure liquid water, becomes sizably structured when water interacts with phospholipids and acylglycerols in liquid-crystalline phases (Nilsson, 1991) and in powders of disaccharides (Giuffrida, 2003), suggesting that the coupling of the bending modes of water molecules with intermolecular modes involves also non-water H bonding groups (Giuffrida, 2006). This makes the band potentially useful when analyzing the structural organization of water adsorbed to RC-detergent films, since, at sufficiently low hydration levels, it can reflect the multiplicity of the environments experienced by the water molecules.

Fig. 6.5A and B show the association band of water measured in RC-LDAO and RC-OG films at selected values of the relative humidity; bands were normalized to a unitary area in order to better examine the evolution of the band in terms of width and structuredness. In the presence of both detergents the band underwent a progressive, strong narrowing but remained scarcely structured when dehydrating the film down to a relative humidity of about 10%. At lower *r* values no further narrowing occurred in the bands, which however became strongly structured. A pronounced shoulder appeared around 2080 cm^{-1} in the RC-LDAO film. In the RC-OG film a shoulder at approximately this wavenumber was already evident at *r*=23%. At $r \leq 9\%$ structuring of the band resulted in two well resolved peaks at 2070 and 2120 cm^{-1}. In the light of the arguments summarized above, this behavior suggests that, when the RC-detergent films are equilibrated at *r* <10%, the residual water interacts prevalently with surface groups of the protein and of the detergent micelle surrounding the hydrophobic portion of the RC. Consistently, the profile of the association band was very similar in highly

Table 6.2
Ratio $r_A=A_A/A_C$ between the area underlying the association (A_A) and the combination (A_B) band of water as a function of the relative humidity r determined in RC-LDAO and RC-OG films.

r (%)	94	84	75	63	53	43	33	23	11	9	6	3
r_A (RC-LDAO)	1.20	0.88	0.78	0.86	0.74	0.64	0.84	0.88	0.77	1.37	1.80	36.4
r_A (RC-OG)	1.43	0.98	1.30	0.80	0.80	0.84	0.81	0.85	1.01	2.02	1.69	50.1

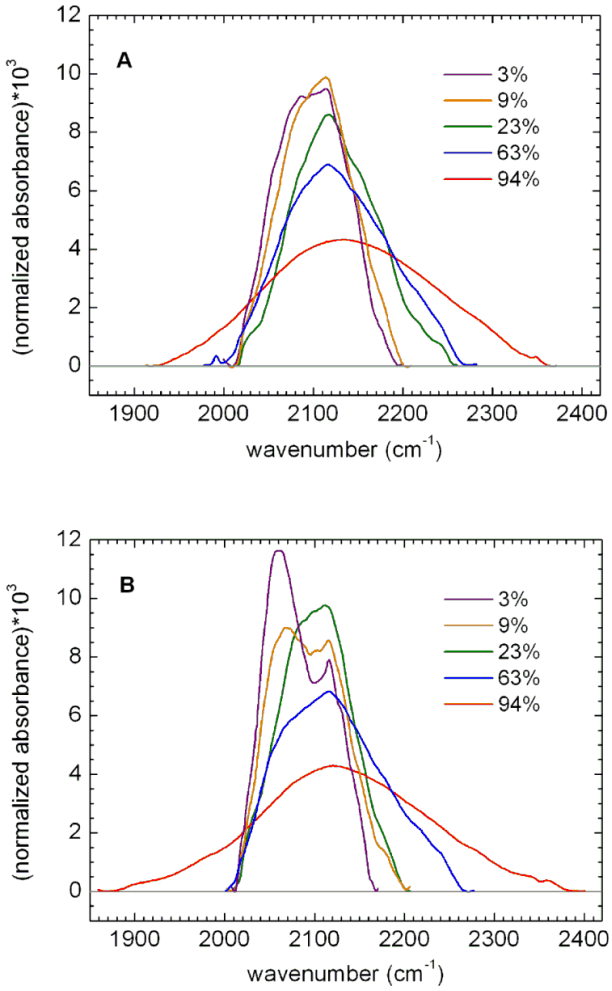

Figure 6.5
Evolution of the association band of water as a function of the relative humidity r in RC-LDAO (panel A) and RC-OG (panel B) films. The r values are indicated in the labels.

hydrated RC-LDAO and RC-OG films (where water-water intermolecular modes mainly contribute to the association band) while, on the contrary, it differed significantly in extensively dried films (where the fraction of weakly adsorbed water molecules, mostly interacting with other water molecules, is expected to be greatly reduced).

The area of the intramolecular ($\nu_2+\nu_3$) combination band of water is proportional to the total water content of the sample, being essentially independent of the extent of interaction of water with neighboring molecules (see above). At variance, the area of the association band, due to its intermolecular origin, strongly depends on the specific interaction of the water molecules with the environment, showing large differences between liquid water and ice (Zelent, 2004). This sensitivity was clearly shown by studies in which the ratio r_A between the area of the association (A_A) and of the combination (A_C) bands was determined in pure water, in water-sugar powders, and in protein-water-sugar glassy systems under different hydration conditions and in the presence of different saccharides (Giuffrida, 2006). When comparing pure water with trehalose dihydrate powders r_A was found to incresase from 1.8 to 73. The value of r_A increased by at least one order-of-magnitude upon extensive dehydration of sugar-water-protein amorphous systems. Furthermore, the r_A value measured in the driest matrices depended significantly on the structure of the saccharide molecule. From these studies it was argued that the ratio r_A estimates roughly the extent of the interaction of water molecules with non-water H bond forming groups, with large r_A values indicating large fractions of water molecules H bonded with non-water groups (Giuffrida, 2006). The r_A values calculated from the area A_A and A_C measured in RC-LDAO and RC-OG films at different values of relative humidity are reported in Table 6.2. At $11\% < r < 94\%$, the r_A ratio does not show systematic changes, fluctuating around an average value close to 0.9. At lower contents of residual water the r_A value increases, jumping to 36 and 50 in the driest (r=3%) RC-LDAO and RC-OG films, respectively. This behavior is in line with the one observed in protein-water-sugar glassy systems (Giuffrida, 2006), and suggests that under the driest conditions the large majority of the adsorbed water molecules interacts directly with non-water H bonding groups of the RC-detergent complex.

6.1.3 Recombination kinetics of the primary charge separated state $P^+Q_A^-$.

As outlined in the previous paragraphs, the thermodynamic and spectral analyses of water sorption by RC-detergent films concur to identify two main hydration regimes. When the relative humidity is decreased from 94% to about 30% the amount of adsorbed water undergoes a large change, from $35 \cdot 10^3$ to $1.6 \cdot 10^3$ H_2O molecules per RC in RC-LDAO films, and from $8 \cdot 10^3$ to $6 \cdot 10^2$ H_2O molecules per RC in RC-OG films (Fig.6.2). At $r > 30\%$, the combination band of water exhibits spectral features similar to those of bulk water (Fig.6.4), indicating that such a change of the relative humidity affects essentially the number of water molecules weakly bound at condensation sites (Fig.6.2). However, the progressive narrowing of the intermolecular association band observable over this hydration range (Fig.6.5) suggests that depletion of the outer hydration shell already affects the structural organization and dynamics of the residual water. Such changes are reflected also in the intra-molecular water combination band (Fig.6.4) only when (at $10\% < r < 30\%$) the amount of bound water is further reduced to ~10^3 and ~400 H_2O molecules per RC in RC-LDAO and RC-OG films, respectively. Hydration isotherms show indeed that under these conditions the contribution of water adsorbed to strong binding sites of the complex becomes relevant, and overcomes the one of the weakly bound water molecules. Finally, dramatic changes are observed both in the combination and in the association band when the second hydration regime is entered, at $r < 10\%$, i.e. when the most tightly bound water molecules, presumably forming the inner hydration shell, are removed progressively.

In order to examine how the extent of hydration and the structure/dynamics of the hydration shell affect intraprotein electron transfer we have analyzed the kinetics of flash-induced $P^+Q_A^-$ recombination in RC-detergent films as a function of their water content. Kinetic measurements were performed in parallel with the spectral analysis described above, over the same samples.

As summarized in the Introduction the recombination kinetics of the light-induced $P^+Q_A^-$ state can be considered a sensitive probe of : (a) the RC relaxation from the *dark-adapted* to the *light-adapted* conformation in response to the electric field generated by the light-induced charge separation; (b) the RC thermal fluctuations among a large ensemble of conformational substates (see par.1.4 in the Introduction). The analysis of $P^+Q_A^-$ recombination in RC-detergent films characterized by a different, controlled hydration, is therefore expected to provide information on the conformational

dynamics of the RC and on its coupling with the structure and dynamics of the RC-detergent hydration shell.

Fig.6.6A shows the kinetics of $P^+Q_A^-$ recombination, measured by recording the absorbance change at 422 nm after a laser pulse, in RC-LDAO films equilibrated at relative humidity between 63 % and 9 %. Dehydration of the RC-detergent complex results in a progressive acceleration of the kinetics, which become also more and more distributed. A similar behavior was observed in RC-OG films (see below). To account for the non-exponential, distributed character of the kinetics, $P^+Q_A^-$ charge recombination kinetics have been fitted to a single power law (see eq.1.2 and the Introduction, section 1.6).

Fitting to eq.1.2 yielded a reasonable description of the kinetics measured in RC-films equilibrated at relative humidity *r* as low as 23 % (see Fig. 6.6, panel A and B). In hydrated films, characterized by ~4300 H_2O molecules per RC (*r*=63%), <k>=15.3±0.2 s^{-1}. Upon dehydration <k> increases and reaches a value of 27.8±0.6 s^{-1} when the hydration layer is decreased to ~1400 H_2O molecules per RC (*r*=23%). As shown in Fig.6.6C, the acceleration of the kinetics is paralleled by a progressive broadening of the rate distribution, calculated according to eq.1.3 (see the Introduction par.1.6). To allow a more direct comparison with the rate distributions obtained at low temperatures (McMahon, 1998) or in dehydrated matrices (Palazzo, 2002; Francia, 2009), rate distributions *f(k)* defined on a logarithmic *k* scale (*f(k)dlog(k)=p(k)dk*) are shown. From the described kinetic effects (Fig.6.6) we infer that dehydration of the film progressively hampers the RC relaxation from the *dark-adapted* to the *light-adapted* conformation, and concomitantly inhibits the RC thermal fluctuations. Both dynamics are affected by a reduction of the weakly bound hydration layer, since a decrease of *r* from 63% to 23% mainly affects this sub-population of the adsorbed water, without depleting the tightly bound water layer (Fig.6.2).

When the hydration of the RC-LDAO film is further reduced (at *r* <23%) the recombination kinetics is further accelerated (Fig6.6A). Under such dehydrated conditions eq.1.2 becomes unable to fit adequately the kinetics: as shown in Fig.6.6B, in fact, while in hydrated samples the residues of the fit to eq.1.2 are randomly distributed, for traces acquired at *r* <23% the residues exhibit a systematic increase at short times after the laser, suggesting the presence of an additional, faster kinetic component which cannot be accounted for by eq.1.2. This unsatisfactory residue pattern, which already appears in the trace at *r* =23%, becomes more and more evident upon

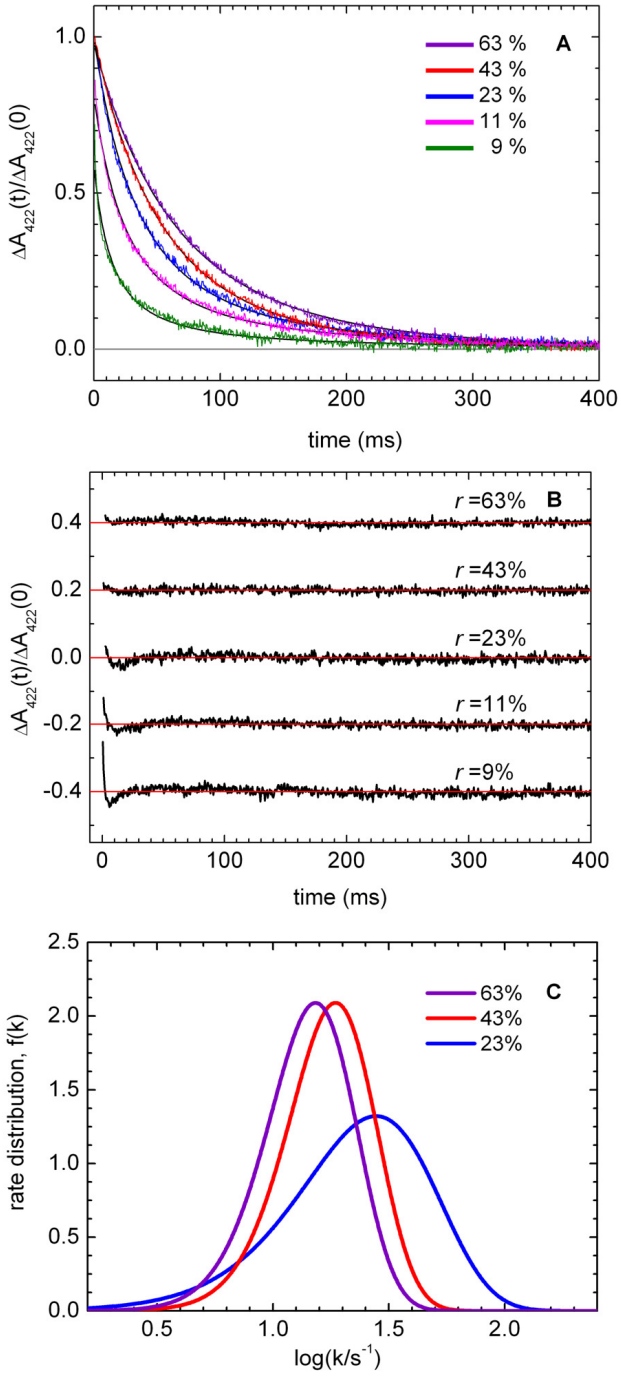

Figure 6.6
Kinetic analysis of $P^+Q_A^-$ recombination following laser flash excitation of RC-LDAO films equilibrated at the indicated relative humidity *r*. A. Normalized decay of the $P^+Q_A^-$ state. Best fit to eq.1.2 are shown as black continuous lines. The values of the average rate constant <k> and distribution width σ are reported in the following only for the kinetic traces measured at $r \geq 23\%$., i.e. for the kinetics which are satisfactorily fit to a power law (see panel B). The extremes of the calculated confidence intervals within two standard deviations are indicated in brackets. Fit to eq.1.2 yielded: <k> = 15.3 (15.1, 15.5) s^{-1}, σ = 6.6 (6.3, 6.9) s^{-1} at *r*=63%; <k> = 18.6 (18.4, 18.9) s^{-1}, σ = 8.1 (7.7, 8.4) s^{-1} at *r*=43%; <k> = 27.8 (27.2, 28.5) s^{-1}, σ = 18.6 (17.9, 19.4) s^{-1} at *r* =23%. Although for the sake of visual clarity only the first 400 ms of $P^+Q_A^-$ decay are shown, the time scale of kinetic recording (time resolution 0.5 ms) extended out to 1 s after the laser pulse and the whole information was used when fitting kinetics to eq.1.2. B. Residues of the fit to eq.1.2. Traces have been arbitrarily shifted along the vertical scale. C. The rate distributions *f(k)* corresponding to the fit to a power law of the kinetics at *r* =63%, 43% and 23%. The distributions, calculated according to eq.1.3 are defined on a logarithmic scale.

dehydration, when *r* is decreased from 11% to 9% (Fig.6.6B). In order to better analyze the short time behavior we have increased the time resolution of the kinetic measurements to 10 μs over the 0-100 ms time range. Fig. 6.7 shows an example of the kinetics measured at higher time resolution under extremely dehydrated conditions (*r*=3%) as compared to the kinetics measured in the hydrated film (*r*=63%). The log-log plot of panel A makes evident that, at variance with the trace at *r*=63%, under the most dehydrated conditions the decay is drastically distributed in rate, occurring over more than four orders of magnitude. Fig. 6.7A and B suggest that the faster kinetic component present at *r*=3% is also markedly distributed in rate. We have found that kinetic traces acquired at *r* <23% fit well the sum of two power laws, i.e.:

$$N(t) = \left(1 - A_f\right)(1 + k_0\, t)^{-n} + A_f\left(1 + k_{0f} t\right)^{-n_f} \quad \text{(eq.6.4)}$$

where A_f is the relative amplitude and k_{0f} and n_f are the kinetic parameters of the fast phase. The best fit to a single power law (eq.1.2) of the kinetics at *r*=63% and to the sum of two power laws (eq.6.4) for the kinetics measured at *r*=3% are shown as red lines in Fig.6.7A over the whole time window examined, and, in Fig.6.7B, over a time scale which better resolves the fast phase at *r*=3%. The inability of a single power law (eq.1.2) to fit the kinetics in strongly dehydrated RC-detergent films, already suggested by the residue distribution of the traces acquired at the lower time resolution (Fig.6.6B), is seen more clearly at the higher time resolution. As illustrated in the upper panel of Fig.6.7A, the residues of the fit to a single power law (eq.1.2) are uniformly distributed in the hydrated sample (*r*=63%), but increase systematically in the most dehydrated RC-detergent film (*r*=3%) at short times (green dots). In the upper panel of Fig.6.7A, the residues of this unacceptable fit are compared with those of the fit to the sum of two power laws (eq.6.4), which at variance appear randomly distributed also in the short time-range (see red dots, *r*=3%). Similar patterns of residues were obtained when comparing the best fit to eq.1.2 and eq.6.4 in all the kinetic traces measured at the higher time resolution for *r*<23% both in the presence of the detergent LDAO and OG. Consistently, the fit to the sum of two power laws (eq.6.4) yielded *reduced* chi-square values systematically lower than the fit to a single power law (eq.1.2) at *r* <23%.

As a possible alternative to eq.6.4, and to further test the presence of a second kinetic component under strongly dehydrated conditions, we have fitted the kinetics

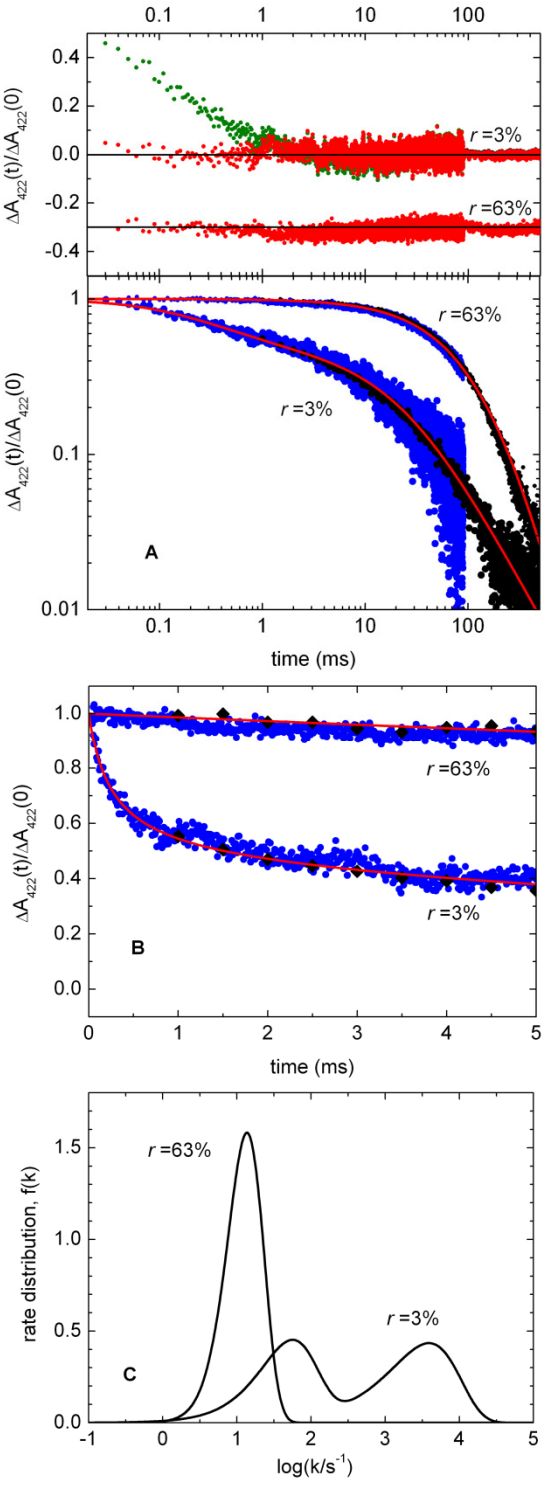

Figure 6.7
Kinetic analysis of $P^+Q_A^-$ decay in RC-LDAO films equilibrated at relative humidity *r*=63% and *r* =3%. The data have been acquired on each sample in two sets with time resolutions of 10 µs per point (blue trace) and 0.5 ms per point (black trace). Data recorded over both time windows were used when fitting the kinetics. A. Log-log plot of the normalized kinetics. The best fit to a single power law (eq.1.2) at *r* =63% and to the sum of two power laws (eq.6.4) at *r* =3% are shown as continuous red lines. The upper panel shows the corresponding residues (red dots), and the residues of the fit to a single power law for the kinetic trace at *r* =3% (green dots). B. Expanded view of the first 5 ms of the decays. C. The rate distribution functions *f(k)*, defined on a logarithmic scale, calculated according to eq.1.3 (at *r* = 63%) and to eq. 6.6 (at *r* = 3%) from the best fitting parameters.

also to a stretched exponential, i.e. to the Kohlrausch-Williams-Watts (KWW) decay function

$$N(t) = exp\left[-(t/\tau)^{\beta}\right] \qquad \text{(eq.6.5)}$$

with τ and β as free parameters. The best fits, and the corresponding residues, obtained in RC-LDAO films equilibrated at *r*=3% and *r*=9% using eq.6.4 and the KWW function are compared in Figure 6.8. The KWW function, although providing a fit better than eq.1.2 in strongly dehydrated RC-detergent films, yielded reduced chi-square values slightly but systematically larger than the sum of two power laws (eq.6.4). Most importantly, the residues of the best fit to the KWW function exhibited a significant and systematic increase in the (0-1 ms) time range (see Fig.6.8), indicating that the KWW function was not able to satisfactorily account for the short-time behavior of the kinetics. This finding further supports the notion that an additional, distributed kinetic component appears in the $P^+Q_A^-$ decay upon extensive dehydration.

The use of eq.6.4 to describe the kinetics leads to a bimodal rate distribution function *p(k)* given by the weighted sum of two Gamma distributions:

$$p(k) = \left(1 - A_f\right)\frac{k^{n-1}exp(-k/k_0)}{k_0^n\Gamma(n)} + A_f\ \frac{k^{n_f-1}exp\left(-k/k_{0f}\right)}{k_{0f}^{\ n_f}\Gamma(n_f)} \qquad \text{(eq.6.6)}$$

The average rate constant $\langle k_f \rangle$ and the distribution width σ_f of the fast kinetic component are obtained from the fitting parameters k_{0f} and n_f through eq.1.4.). The unimodal (eq.1.3) and bimodal (eq.6.6) rate distribution functions which describe the kinetics at *r*=63% and *r*=3%, respectively, are represented in Fig.6.7C.

The values of $\langle k \rangle$ and σ obtained for the slow kinetic component are plotted in Fig.6.9 as a function of the relative humidity *r* at which the film were equilibrated. The kinetic parameters of the fast component are reported in Table 6.3. The kinetic parameters of the fast phase exhibited a limited variability (cf e.g. Table 6.3). Both in RC-LDAO and RC-OG films the fast kinetic phase appears abruptly when the films are equilibrated at *r* < 23 %: its relative amplitude exceeds 50 % of the total at *r*=9%, and remains unaffected within the experimental error when the residual water of the films is further reduced. Also the average rate constant $\langle k_f \rangle$ and distribution width σ_f of

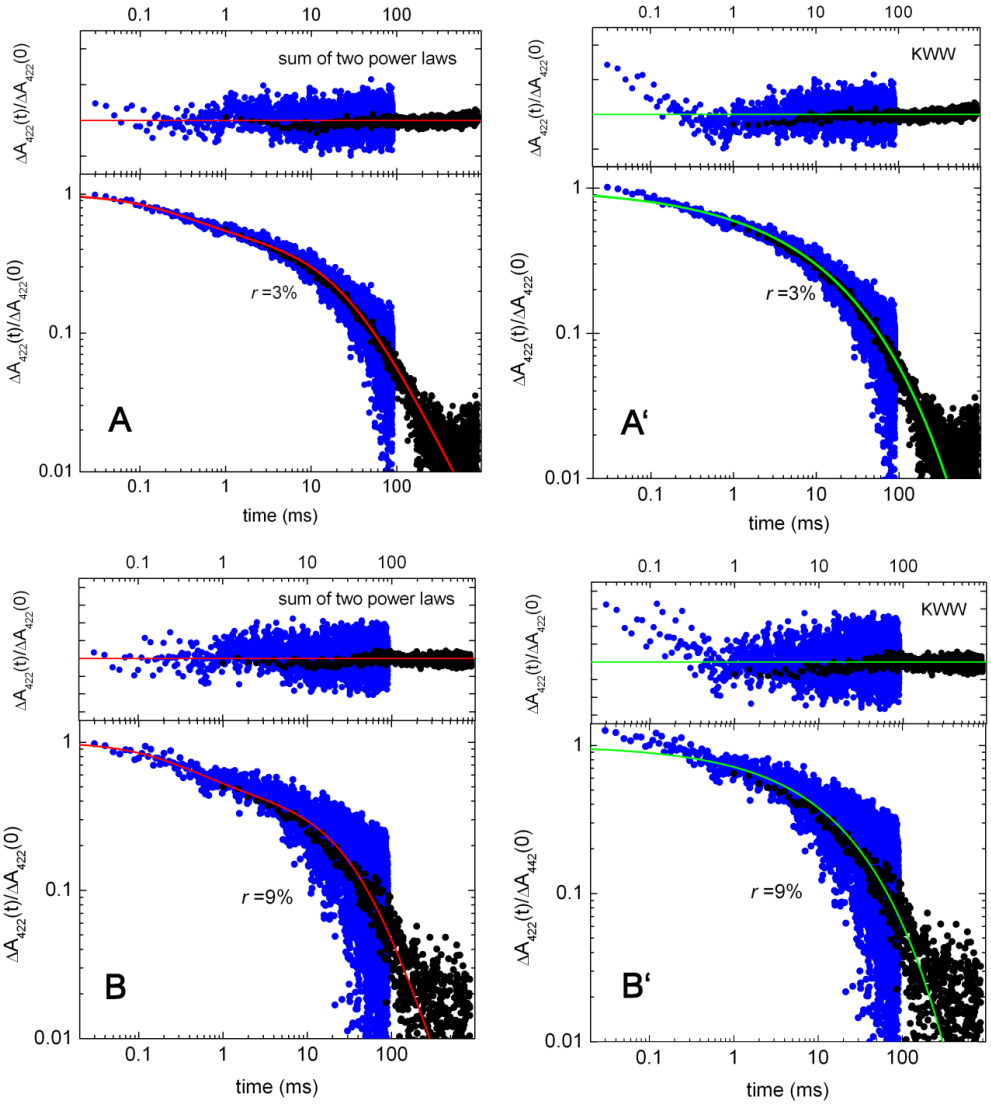

Figure 6.8
Log-log plots of $P^+Q_A^-$ kinetics measured in RC-LDAO films equilibrated at r =9% and r =3%, fitted to the sum of two power laws (A, B) or to the KWW function (A', B'). Best fits are shown as continuous lines (red: sum of two power laws; green: KWW function); the corresponding values of the reduced chi-square, χ^2_ν , are: χ^2_ν =1.108 (A), χ^2_ν =1.165 (A'), χ^2_ν =1.035 (B) and χ^2_ν =1.056 (B'). In the upper part of each panel the residues of the best fit are shown; the kinetics parameters obtained by fitting to the sum of two power laws are reported in Table 6.3; fitting to the KWW function yielded: $\tau = 5.90 \cdot 10^{-3}$ s^{-1}, $\beta = 0.368$ for the trace acquired at r =3% (panel A'); $\tau = 5.46 \cdot 10^{-3}$ s^{-1}, $\beta = 0.376$ for the trace acquired at r =9% (panel B').

Table 6.3
Kinetic parameters of the fast phase of $P^+Q_A^-$ recombination detected upon extreme dehydration of RC-LDAO and RC-OG films. The extremes of the calculated confidence intervals within two standard deviations are indicated in brackets.

relative humidity, *r* (%)	H_2O/RC molar ratio	relative amplitude, A_f (%)	average rate constant, $<k_f>$ (s^{-1})	distribution width, σ_f (s^{-1})
RC-LDAO				
11	935	38.9 (33.0, 45.8)	1569 (568, 3964)	1505 (398, 5458)
9	815	61.0 (54.1,69.2)	3421 (2537, 4622)	3660 (2152, 8332)
6	670	60.2 (55.3, 65.8)	3668 (2547, 6004)	4136 (2729, 7370)
3	85	56.4 (50.5, 63.3)	3884 (2882 , 5658)	4211 (2754, 8164)
RC-OG				
11	435	47.1 (42.4, 52.4)	1678 (1412, 2021)	1805 (1501, 2203)
9	330	61.4 (55.8, 68.2)	1780 (1540, 2083)	1908 (1625, 2238)
6	305	55.9 (51.9, 60.5)	1913 (1614, 2312)	2114 (1816, 2552)
3	30	42.0 (37.5, 46.5)	1705 (1447, 2032)	2223 (1893, 2648)

the fast component stay essentially constant at $3\% \leq r \leq 9\%$, around $3.5 \cdot 10^3$ s^{-1} and $1.8 \cdot 10^3$ s^{-1} in RC-LDAO and RC-OG films, respectively.

Quite remarkably, although the water content of the RC-LDAO and RC-OG films differ markedly at each value of *r* (see Fig.6.2), Fig.6.9 shows a unique dependence of <k> and of σ upon the relative humidity, irrespective of the chemical nature of the detergent. The simplest interpretation of this behavior appears to be that the hydration of the detergent belt has a negligible impact on the RC dynamics probed by the kinetics of charge recombination (see Discussion, par.6.2.2). The increase of <k> and of σ occurs steeply below a threshold value of relative humidity, $r \sim 0.4$ This value of *r* corresponds to a molar ratio (H_2O/RC) ~2000 and ~1000 in the presence of LDAO and OG, respectively. When the fast kinetic component becomes detectable, at r ~ 0.1, corresponding to (H_2O/RC)≅900 in RC-LDAO and (H_2O/RC)≅400 in RC-OG films, both <k> and σ have already increased by almost three times, and appear to be close to their maximal values reached at the minimum value of the relative humidity. The continuity found in the values of <k> and σ over the whole range of relative humidity, even when a second, additional kinetic phase, characterized by $<k_f>$ and σ_f, has to be included in the fit, supports the physical adequacy of the fitting model adopted in the kinetic analysis. Interestingly, the fast kinetic component of P^+ decay is observed rather abruptly when all the weakly bound water molecules have been essentially withdrawn,

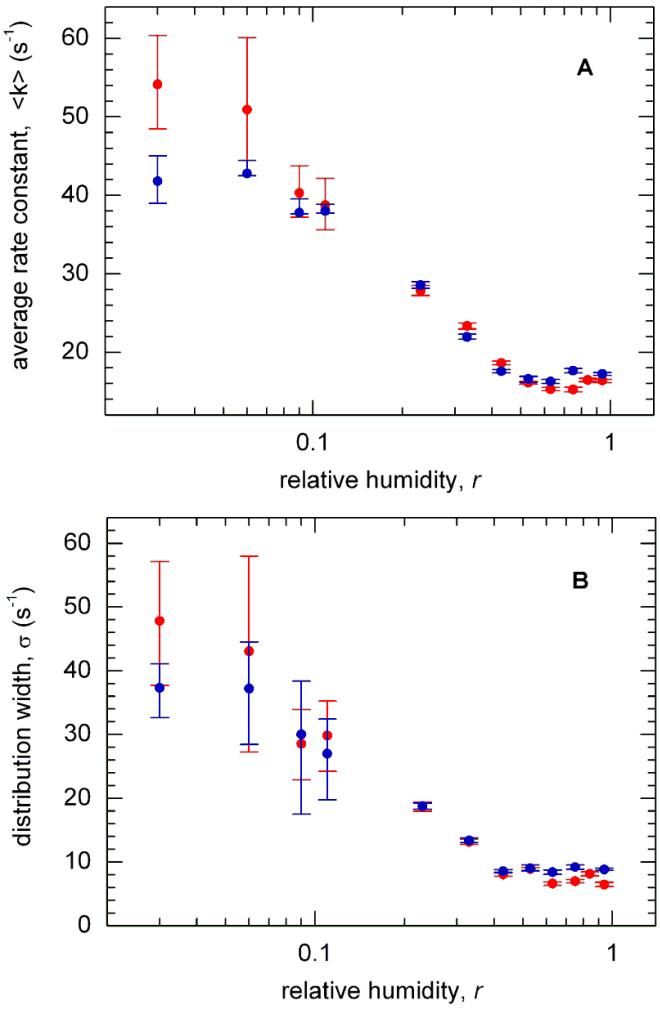

Figure 6.9
Dependence of the kinetics of $P^+Q_A^-$ recombination upon the relative humidity, *r*, in RC-LDAO (red circles) and RC-OG (blue circles) films. Panels A and B show the values of the average rate constant <k> and of the rate distribution width σ, respectively. Kinetic analysis was performed as described in the text, and illustrated in Fig.6.6 and 6.7. When the $P^+Q_A^-$ decay includes two kinetic phases, i.e. in films equilibrated at *r* <23%, the plotted <k> and σ values refer to the slow phase. The corresponding kinetic parameters of the fast phase are reported in Table 6.3. Vertical bars indicate confidence intervals within two standard deviations.

and a significant fraction of the inner, most tightly bound hydration shell has been also removed, as judged from the water sorption isotherms (cf. Fig. 6.2B).

The fast phase of the decay measured at 422 nm occurs on the hundreds-of-micros time scale (Fig.6.7 and Table 6.3). To attribute safely this kinetic component to $P^+Q_A^-$ recombination, excluding side electron donation which could concur to re-reduce P^+ and re-oxidize Q_A^-, we have measured in parallel the decay of the laser induced absorbance change at 450 nm, i.e. at the peak of the differential semiquinone/quinone spectrum. As detailed in par.3.3, at 422 nm the relative contribution of P^+ to the flash

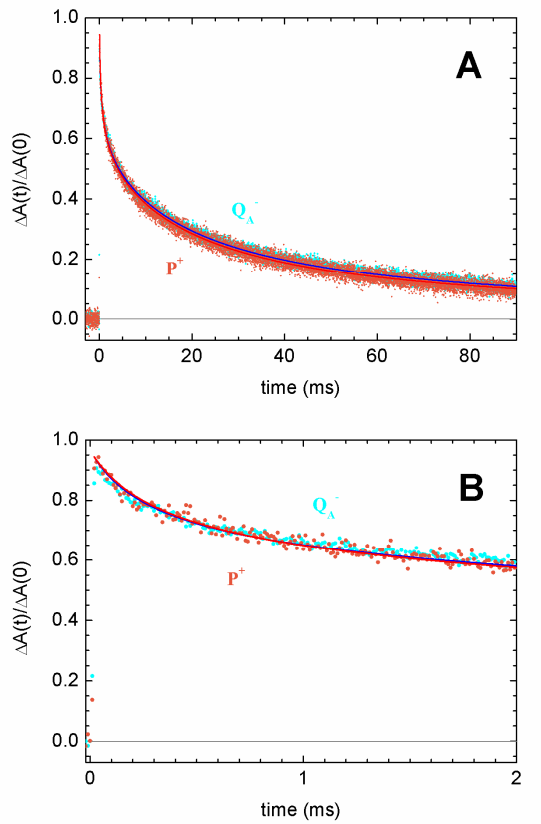

Figure 6.10
$P^+Q_A^-$ recombination kinetics measured on RC-LDAO films at r =3% following absorption changes at 422 nm and at 450 nm, reported respectively with orange and cyan filled symbols (for more details on the relative contributions of P^+ and Q_A^- at the two wavelength see par.3.3 and par.6.2.2). With continuous lines the best fit to the sum of two power laws are reported for each trace and the values of the kinetics parameters are the following: fast phase amplitude = 0.54, $\langle k \rangle_F$ = 2230 s^{-1}, σ_F = 3175 s^{-1}, $\langle k \rangle_S$ = 42.93 s^{-1}, σ_S = 39.64 s^{-1} for the kinetics measured at 422 nm (orange); fast phase amplitude = 0.49, $\langle k \rangle_F$ = 2579 s^{-1}, σ_F = 3433 s^{-1}, $\langle k \rangle_S$ = 42.33 s^{-1}, σ_S = 39.92 s^{-1} for the kinetics measured at 450 nm (cyan).

induced absorbance change largely dominates. At 450 nm the contribution of Q^- becomes more significant (~40%). If events different from $P^+Q_A^-$ recombination contribute to the decay of the photogenerated radical pair we expect that the kinetics of P^+ and Q_A^- recovery after photoexcitation will in general differ, resulting in a different kinetics of the absorbance change measured at 422 nm and at 450 nm. The time course of signals recorded in parallel at 422 nm and at 450 nm was always found to coincide, as shown in Figure 6.10, even in RC-detergent films equilibrated at r =3%. This observation strongly supports the attribution to $P^+Q_A^-$ recombination of both kinetic phases measured under the most dehydrating conditions. Thus under extreme dehydration two RC populations can be identified, in which the stability of the primary charge separated state differs by almost two orders of magnitude.

6.2 Discussion.

6.2.1 The hydration shell of the RC-detergent complex: thermodynamic properties and structural organization.

Water sorption by RC-detergent complexes can be studied profitably by coupling the use of thin films of the protein-detergent complex with the isopiestic method to control hydration. The combination band of water at 5155 cm^{-1} is well suited to study water binding to protein complexes: its position and width yield information on the H bonding organization of water molecules, while the area below the band measures the amount of bound water, being independent of the H bonding organization (Bonner, 1974b; Dickens, 1999; Fornés, 1978). The sensitivity of the FTIR spectroscopic determination of water makes possible the study of water sorption/desorption on small amounts of RC-detergent complexes (about 1 mg) which equilibrate rapidly (typically in a few hours) at a relative humidity between 94% and 3%.

Hysteresis phenomena have been reported in several investigations involving desorption/sorption cycles on soluble proteins (see, e.g. Lüscher-Mattli, 1982). Scanning experiments on α-chymotripsin and tropocollagen have shown however that hysteresis effects occur only as a consequence of an almost complete water removal (Lüscher-Mattli, 1982). Our data (par.6.1.1) do not reveal any hysteresis effect. We could for instance verify that the water content of a film equilibrated at r=63% was independent of its dehydration/rehydration history, i.e the same for the following desorption/sorption sequences: (i) solution → (r=63%); (ii) solution → (r=11%) → (r=63%); (iii) solution → (r=3%) → (r=6%) → (r=9%) → (r=63%). We consider this as a reasonable test that the obtained data represent true equilibrium states, accessible to thermodynamic interpretation.

The sorption isotherms obtained in RC-LDAO and RC-OG films (Fig.6.2) exhibit the typical sigmoidal type II character (Brunauer, 1938) observed for a large number of polypeptides. To describe such a behaviour different theoretical models, roughly falling in two classes (surface and solution models), have been adopted (for a review see Kuntz, 1974). Our data fit well the Hailwood and Horrobin equation (eq. 6.2), based on a solution model, which provides a convenient way to separate the "monolayer" (tightly bound water) and "multilayer" (weakly bound water) contributions to a given isotherm. The equation includes only three adjustable parameters, related to the number (h_0) and activity (K_1) of "tight" binding sites ("monolayer" component) and to the activity (K_2) of water condensing in "multilayer" structures. We have also fitted

our experimental isotherms to the D'Arcy and Watt equation (D'Arcy, 1970), which accounts for an additional set of weak binding sites. Although an equally good fit was obtained (not shown), confidence analysis resulted in unacceptably large uncertainties of the parameters, indicating that no information was gained, and that the Hailwood and Horrobin equation yielded a possibly rough, but physically more sound interpretation of the data.

At any value of relative humidity, the H_2O/RC molar ratio is approximately two-times larger in RC-LDAO as compared to RC-OG complexes, indicating that the binding of water to the detergent belt which surrounds the hydrophobic region of the RC contributes substantially to the overall water sorption process. The best fitting parameters (Table 6.1) show that the activity K_2 of water in the solid solution is comparable for RC-LDAO and RC-OG complexes, as expected for water molecules which form the outermost hydration shells. The larger hydration systematically observed in RC-LDAO as compared to RC-OG is traced back to the larger number h_0 of binding sites and to the ~5 times larger activity K_1 of water forming the inner hydration layer. Since both the exposed hydrophilic portion of the RC protein and the surface of the detergent belt are expected to bind water molecules, we discuss in the following a simple geometrical model of the RC-detergent complex, which allows a rough estimate of the water binding surfaces in the case of LDAO and OG solubilized RCs.

The number of LDAO molecules associated with the RC from *Rb. sphaeroides* (wild type Y) has been determined by chromatography using ^{14}C-labelled detergent. Values of (206 ± 12) (Rivas, 1980) and 289 (Møller, 1993) have been reported. By monitoring the resolubilization of detergent-free RC preparations from *Rb. sphaeroides* R26 values of (150±20) and (370±100) were obtained at pH 8.0 for LDAO and OG, respectively (Gast, 1996). Using (LDAO/RC)=150 or 289 and (OG/RC)=370±100, it can be easily evaluated that in the solutions used to prepare our RC-detergent films (0.025% LDAO or 0.1% OG) the molar ratio ("free"/total) detergent is about 11% or 6 % (LDAO) and (13±3) % (OG); we assume therefore that in our samples essentially all the detergent is associated with the RC protein. The low-resolution structure of the RC-detergent complexes obtained by neutron diffraction in crystals of *Rps. viridis* showed that LDAO is concentrated in rings, forming a micelle around the transmembrane helices of the RC (Roth, 1989). The extension of this approach to localize the detergent OG in crystals of *Rb. sphaeroides* strain Y (Roth, 1991) indicated a quasi identity of shape and position of the OG and LDAO rings around the transmembrane helices. In

both cases the thickness of the detergent phase perpendicular to the membrane plane was nearly 30 Å, suggesting that the detergent belt can be regarded as a half-torus of minor radius close to 15 Å. It has to be noted, however, that crystallization in the presence of LDAO can be accomplished only in conjunction with additional amphiphiles, such as 1,2,3-heptanetriol, which was present in the *Rps. viridis* crystals used to obtain the low-resolution structure of RC-LDAO complexes (Roth, 1989). The micellar radius of LDAO in solution is significantly decreased upon addition of heptanetriol (Timmins, 1991). A SANS determination of micelle structure (Thiyagarajan, 1994) has shown that the addition of heptanetriol perturbs substantially not only the dimension but also the shape of pure LDAO micelles in solution. Thiyagarajan and Tiede (Thiyagarajan, 1994) found that the LDAO micelle can be assimilated to an ellipsoid with semiaxes of 30.6 and 19.4 Å, and the OG micelle to a sphere of radius 22.9 Å. Addition of heptanetriol to pure LDAO micelles resulted in smaller, spherical micelles, with radii in the range 17-21 Å, in agreement with ref. 79. In view of these results we believe that under the condition of our samples, the shape and dimension of the detergent belt can be reasonably described using the parameters determined by Thiyagarajan and Tiede (Thiyagarajan, 1994) for LDAO and OG micelles. Figure 6.11 shows the geometrical model we adopted. In a crude approximation subunits L and M of the RC have been represented as forming a cylinder of height h=50 Å and radius R=25 Å; the H subunit is approximated to a hemisphere of radius *R*, which caps the LM cylinder (Yeates, 1987). The LDAO belt (Fig.6.11A) is modeled as an oblate ellipsoidal ring, generated by rotation of half an ellipse of semiaxes *a*=19.4 Å and *b*=30.6 Å (Thiyagarajan, 1994) removed by the distance *R* from the axis (of rotation) of the LM cylinder. We note that the choice of an oblate ellipsoidal ring implies a thickness of the detergent phase perpendicular to the membrane plane equal to 2*a*=38.8 Å, in good agreement with a calculated thickness of the hydrophobic portion of the RC LM subunit of 42 Å (Yeates, 1987). The OG belt (Fig.6.11B) is represented as a half torus of minor radius *r*=22.9 Å, corresponding to the radius of the spherical OG micelle (Thiyagarajan, 1994), and major radius *R*. The surface area A_{HT} of the half torus is given by (Wolfram, 1999):

$$A_{HT} = 2\pi^2 rR + 4\pi r^2 \qquad \text{(eq.6.7)}$$

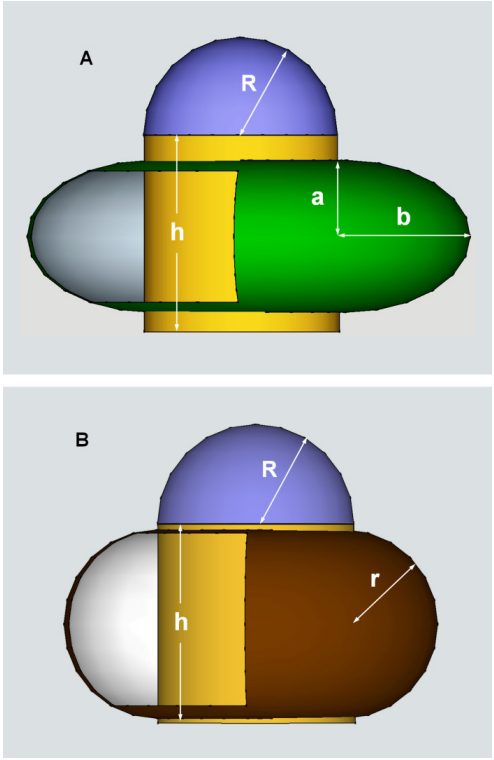

Figure 6.11
Geometrical model of the RC-LDAO (A) and RC-OG (B) complexes (see par.4.1 for details).

The surface area A_{OE} of the oblate ellipsoidal ring can be calculated as (see Appendix, section 6.3, in this chapter):

$$A_{OE} = \frac{2\pi b}{a}\int_{-a}^{+a}\left[a^2 - \frac{x^2}{a^2}(a^2 - b^2)\right]^{1/2} dx + 2\pi R\int_{-a}^{+a}\left[1 + \frac{b^2x^2}{a^2(a^2 - x^2)}\right]^{1/2} dx \qquad \text{(eq. 6.8)}$$

by numerical integration. Starting from the geometrical model of Fig.6.11, and using eqs.6.7 and 6.8, it can be estimated that the area of the LDAO detergent belt is equal to $21.5 \cdot 10^3$ Å^2, while that of the OG ring is $17.9 \cdot 10^3$ Å^2. Unfortunately the large uncertainty in the number of detergent molecules per RC complex (see above) does not allow a strict test of consistency of the geometrical model with the surface area of the detergent head groups. However, the calculated area of the detergent LDAO and OG rings, when divided by the number *n* of detergent per RC complex experimentally

estimated, yields an area per LDAO molecule equal to 74 $Å^2$ (for n=289) or 143 $Å^2$ (for n=150), and an area per OG head group equal to (48 ± 13) $Å^2$ (n=370±100). These values are reasonably consistent with literature data: a value of 44 $Å^2$ has been determined for the area of the head group of OG using independent experimental approaches (Nilsson, 1991; Rojas, 2005); for the LDAO head group areas around 60 $Å^2$ and 70 $Å^2$ have been determined by SANS, respectively excluding or including hydration water. A recent molecular dynamics simulation of LDAO micelles (Lorenz, 2011) has provided a value of 94.8 $Å^2$ which compares favorably with the range derived from the area of the LDAO ring in our model.

In the geometrical model of Fig. 6.11, the area of the exposed protein surface, not screened by the detergent ring, is equal to $7.65 \cdot 10^3$ $Å^2$ (RC-LDAO) and $6.55 \cdot 10^3$ $Å^2$ (RC-OG), implying that the contribution of the protein surface interacting directly with water is ~ 27% of the total surface area of the RC-detergent complex, for both detergents. The total surface area is larger in RC-LDAO ($29.2 \cdot 10^3$ $Å^2$) as compared to RC-OG complexes ($24.4 \cdot 10^3$ $Å^2$). From these values and from the number h_0 of water binding sites derived from sorption isotherms (Table 6.1) we can estimate the average area per binding site, A_b equal to 19.5 $Å^2$ and 24.4 $Å^2$ for the RC-LDAO and RC-OG complex respectively. A_b can be usefully compared with the average area per binding site estimated in soluble proteins. To this end, among the large number of available data, we have selected those obtained in proteins for which Hailwood and Horrobin analyses of hydration isotherms and high resolution crystallographic structures are available. The protein surface area accessible to water has been evaluated from the structural data (pdb files are listed in Table 6.4) using the "rolling ball" algorithm implemented in the Swiss PDB Viewer molecular graphics software with a radius equal to 1.4 Å. From the values of h_0 (g water/g protein) (Lüscher-Mattli, 1982) and from the evaluated surface are of the protein, the area per water binding site has been calculated. The results, summarized in Table 6.4, indicate that the area per water binding site does not change too much over a set of structurally different proteins which span a large range of molecular masses, yielding an average area per binding site, A_{bp}=(102 ± 21) $Å^2$. This value is about 4-5 times larger than the average area per binding site A_b estimated over the whole RC-detergent complex. It appears therefore that the surface density of water molecules tightly bound to the detergent ring of the RC is much higher than the average density of water tightly bound to the protein surface. If we assume that the A_{bp} value evaluated from the data of Table 6.4 holds also for the exposed surface of

Table 6.4
Thermodynamic and structural parameters used to evaluate the average area A_{bp} per tightly bound water molecule in soluble proteins. The values of h_0, obtained by fitting the experimental sorption isotherms to the Hailwood and Horrobin equation, are from Lüscher-Mattli, 1982.

protein	molecular weight (KDa)	pdb file	h_0 (g water/ g protein)	h_0 (H_2O/protein) molar ratio	protein surface area (Å^2)	area per water binding site (Å^2)
lysozime	14.331	2LYZ	0.080	64	5672	88.6
β-lactoglobulin	18.387	2Q2M	0.059	60	7881	131
α-chemotripsin	25.000	3NK8	0.069	96	8102	84.4
ovalbumin	172.438	1OVA	0.058	556	57877	104.1

the RC protein, the average area A_{bd} per binding site on the detergent belt can be evaluated from the relation:

$$\frac{1}{A_b} = \frac{1}{A_{bp}}\left(\frac{A_p}{A_T}\right) + \frac{1}{A_{bd}}\left(\frac{A_d}{A_T}\right) \qquad \text{(eq.6.9)}$$

where A_p and A_d are the surface areas of the water exposed RC protein and of the detergent ring, respectively, and $A_T = A_p + A_d$. From eq.6.9 we obtain A_{bd} =15 A^2 and A_{bd} =19 A^2 for LDAO and OG, respectively. These values, when considering the area per detergent head group evaluated from our geometrical model, would correspond to a number of water molecules tightly bound to each detergent head group ranging from ~9 to ~5 for LDAO and of ~2.5 for OG. The larger hydration of LDAO is in qualitative agreement with molecular dynamics simulations performed in LDAO (Lorenz, 2011) and OG (Konidala, 2006) micelles, which resulted in an average hydration number ~8 and ~5 respectively.

According to the Hailwood and Horrobin fit, the activity K_1 of the strong water binding sites is about 5 times larger in the RC-LDAO as compared to the RC-OG complex (Table 6.1). Since the area of the exposed protein surface represents a comparable fraction of the total area in the RC-LDAO and RC-OG complex, the observed difference in K_1 values implies that the water activity of the tight binding sites is even more than 5-times larger for the LDAO than for the OG molecules of the detergent ring which surrounds the RC. This observation is consistent with the H bonding properties of the polar head of the two detergents, emerging from simulative

studies. Amine oxides are highly hydrophilic despite having only one polar atom (oxygen) able to interact with water. A recent *ab intio* study of the LDAO interaction with water (Kocherbitov, 2007) features a maximum of 3 water molecules H bonded to the amine oxide group. The mean energies of the H bonds (55 kJ/mol, 52 kJ/mol, and 49 kJ/mol for 1, 2 and 3 water molecules) are much larger than the H bond energy of the water dimer (~13 kJ/mol) (Curtiss, 1979; Feyereisen, 1996). As to the strength of the H bonds between the OG hydroxyl groups and water, *ab initio* molecular dynamics simulations of a glucose-water system indicate that hydroxyl groups form weak acceptor and stronger donor H bonds (Suzuki, 2008). The strength of the latter was found comparable to that of the water dimer.

Finally we notice that a description of water sorption to soluble proteins (lysozime, β-lactoglobulin, ovalbumin, keratin) according to the Hailwood and Horrobin isotherm (Lüscher-Mattli, 1982) yielded K_1 values between ~9 and ~15 which are comparable to the K_1 value determined for the RC-LDAO complex (Table 6.1). This suggests a similar affinity of the binding sites localized on the exposed RC protein and on the LDAO ring.

Equilibrium sorption isotherms characterize thermodynamically two main populations of water molecules adsorbed to the RC-detergent complex: those tightly bound at primary hydration sites, and those, less tightly bound, presumably condensing at the surface of the partially hydrated complex when the relative humidity increases. This basic picture is confirmed by the spectral analysis of the intramolecular ($\nu_2+\nu_3$) combination band of water, which has been decomposed into three Gaussian sub-bands attributed to sub-populations of water molecules differing in H bonding organization. Detailed models have been proposed, in which the resolved sub-bands have been ascribed to water molecules forming a different number of H bonds with their immediate neighbors (Fornés, 1978; Malsam, 2009; Takeuchi, 2005) and/or involved in symmetrical or unsymmetrical H bonds of different strength (Bonner, 1974b) or characterized by a different H bond connectivity on a larger scale (Brubach, 2005). Despite differences in the structural interpretations, often reflecting different views on the structure/dynamics of liquid water, the lowest frequency sub-band (band 1) can be reasonably attributed to water molecules highly connected through an extended H bond organization, in which each water molecules forms a few H bonds (3-4) with its neighbors, typical of pure, bulk water. The breaking of this structure, leading to the distortion of H bonding and weakening of connectivity, typical of small water

aggregates and dimers, appears to originate band 2, of intermediate frequency, and the highest frequency band 3, associated with highly disconnected water molecules, possibly involved in a single H bond (Malsam, 2009; Takeuchi, 2005).

In highly hydrated RC-detergent systems the three sub-bands are centered at the same wavenumbers observed in pure water. As in pure water, the bandwidth decreases monotonically from band 1 (centered at the lowest frequency) to band 3 (highest frequency). Such a coincidence is not surprising: under these conditions, as indicated by the Hailwood and Horrobin isotherm, water sorption is largely dominated by weakly bound water molecules, forming a multilayer structure in which the H bonding organization and energetics are not expected to be significantly perturbed as compared to liquid water. When, according to the Hailwood and Horrobin isotherm, the population of the weakly bound water molecules is decreased, the relative contribution of band 1 (attributed to highly H bond connected water structures, typical of bulk water) is also decreased and disappears at relatively low hydration levels ($r < 40\%$), suggesting that a significant fraction of the residual water interacts directly with the RC-detergent complex and that the interaction with the surfactant head groups causes a disruption of the H bond network present in bulk water. The disappearance of band 1 is in line with the results of a Gaussian analysis of the OH stretching band of water in reverse micelles (Onori, 1993). This study showed that the contribution of the lowest frequency sub-band decreases from ~50% to ~15% when the [H_2O]/[detergent] molar ratio (W) is decreased from 12 to 0.4. The lowest frequency Gaussian component prevailing in pure water is closely related to band 1 of the water combination band, and is also attributed to water molecules organized in regular structures with unstrained H bonds (Brubach, 2005; Onori, 1993). The vanishing of band 1 observed in RC-detergent films upon dehydration appears therefore to reflect the disappearance of bulk-like water molecules. Interestingly, the decrease of band 2 and increase of band 3 fractional areas observed in RC-detergent films when reducing further the relative humidity to about 10% also resembles the evolution of the corresponding OH stretching sub-bands in reverse micelles characterized by a progressively lower water content (Onori, 1993). The qualitatively similar behavior observed in RC-detergent films and in reverse surfactant micelles at low hydration levels suggests a progressive reduction of H bond connected domains of water molecules adsorbed at the surface of the RC detergent belt. During this evolution of the ($\nu_2+\nu_3$) combination band, the peak of both band 2 and 3 shifts to lower wavenumbers, indicating that the H bonds involving the residual populations of

adsorbed water become stronger. At $r \leq 6$ % the contribution of band 2 increases at the expenses of band 3 and the peak wavenumber of band 3 undergoes an additional, steep downward shift (Fig.6.4A,B and A',B'), suggesting further rearrangements of the H bonding organization at extreme draught. The different structural and dynamical properties of these residual water molecules are also inferred from the impressive narrowing of band 2 and 3 (Fig.6.4C and C'), pointing to a dramatic reduction in the number of accessible configurations and H bond angles for the water molecules most tightly bound to the RC-detergent complex. At such low hydration levels the absolute number of water molecules per complex evaluated from the area of the ($\nu_2+\nu_3$) band (<100 at r=3%) is certainly a very rough estimate, implying the crude assumption that the average oscillator strength weighted over the band is still unaffected by the hydration state of the system. It is however tempting to speculate that under this extreme dryness the inner hydration shell of the complex has been strongly depleted, and that even some molecules belonging to highly structured water clusters bound within RC cavities (Koepke, 2007) have been possibly removed.

The changes detected at $r < 10\%$ in the ($\nu_2+\nu_3$) intramolecular water combination band correlate with the strong alterations of the association band at low hydration (Fig.6.5). Previous studies performed in lipid liquid-crystalline phases (Nilsson, 1991), in saccharide-coated liposomes (Chiantia, 2005), as well as in sugar/water and protein/sugar/water amorphous matrices (Giuffrida, 2006), indicate that the intermolecular association band is a sensitive structural probe of the interactions experienced by the water molecules. In particular, Cordone and coworkers (Giuffrida, 2003; Giuffrida, 2006) proposed that the structuring of the association band and the value of the ratio r_A between the area of the association band and that of the ($\nu_2+\nu_3$) band give a rough estimate of the relevance of the interaction between water molecules and non-water H bond forming groups. The evolution of the association band observed by us in response to dehydration of RC-detergent films is fully consistent with this notion. Both in RC-LDAO and in RC-OG films the association band undergoes an impressive narrowing upon dehydration, but only at $r < 10\%$ a clear structuring of the profile takes place, paralleled by a steep increase of r_A (Table 6.2). It is noteworthy that the increase of r_A occurs only when, according to the Hailwood and Horrobin analysis of the hydration isotherms, most of the weakly bound water molecules have been removed. Under these conditions, the different structure of the band in the presence of LDAO and OG indicates that even in the most dried samples (r =3%) a significant

fraction of the residual water is tightly bound to the detergent ring and reflects a different organizations of H bonding between residual water molecules and the polar head groups of LDAO and OG.

6.2.2 The hydration of the RC-detergent complex modulates the RC dynamics and the stability of the primary charge separated state.

Dehydration of RC-detergent films results in accelerated and broadly distributed kinetics of $P^+Q_A^-$ recombination, in qualitative agreement with previous results (Francia, 2009). In our previous observations (Palazzo, 2002; Francia, 2009) we reported effects somewhat variable and weaker than shown in the present paper. In these works the kinetic effects were not correlated with the content of residual water, which could not be determined in extensively dried films due to the low sensitivity of the NIR dispersive spectrometer used to record the combination band of water. In the present study a systematic analysis of $P^+Q_A^-$ recombination kinetics as a function of the hydration level was made possible by: (a) the use of FTIR spectroscopy to determine the water content of the films; (b) the strict control of the hydration level of the RC-detergent films reached by equilibrating them with an atmosphere of defined relative humidity. This approach has shown indeed that large effects on the kinetics of $P^+Q_A^-$ are observed only at very low hydration levels.

The dependence of the average rate constant <k> and of the width of the rate distribution σ upon the relative humidity *r* (Fig.6.9) shows that both parameters do not change significantly for $0.43 < r < 0.94$, i.e. when the water content is reduced from ~3.5 $\cdot 10^4$ to ~$2 \cdot 10^3$ water molecules per RC-LDAO complex and from ~10^4 to ~10^3 water molecules per RC-OG complex. Upon further dehydration <k> and σ increase steeply following a sigmoidal dependence. It is noteworthy that <k> and σ follow the same dependence upon *r* in RC-LDAO and RC-OG complexes (see below).

As outlined in the Introduction, these kinetic effects, previously detected upon dehydration of amorphous RC/water/trehalose matrices at room temperature (Palazzo, 2002; Francia, 2004b; Francia, 2008; Francia, 2009; Savitsky, 2010) and upon freezing RCs in water/glycerol to cryogenic temperatures (McMahon, 1998; Kleinfeld, 1984; Ortega, 1996; Kriegl, 2004) can be taken to reflect a strong inhibition of the RC conformational dynamics on the time scale probed by $P^+Q_A^-$ recombination. The increase of the average rate constant <k> is taken to indicate an impairment of the RC relaxation from the *dark-adapted* to the *light-adapted* conformation, resulting in

destabilization of the $P^+Q_A^-$ charge separated state. The increase in σ is considered to reflect the "freezing" of the interconversion among RC conformational substates, which makes observable the structural and kinetic heterogeneity of the RC population over the time scale of charge recombination (McMahon, 1998; Kriegl, 2004). The maximal values reached by <k> and σ at low hydration levels of the RC-detergent films (corresponding to a few hundreds of water molecules per RC-detergent complex) are quantitatively comparable with those measured in extensively dried RC/water/trehalose matrices at room temperature (Francia, 2009). Dehydration mimics the effects of freezing the RC complexes in water/glycerol systems (Kriegl, 2004) at T<50K. In the hydrated system, upon decreasing the temperature from 200 K to 150 K, and to 50 K, <k> increases from ~10 s^{-1} to ~30 s^{-1}, and to ~45 s^{-1}, respectively (Kriegl, 2004). We infer that an extensive dehydration of the RC-detergent complex brings about a drastic reduction of the RC conformational dynamics, simulating the effects of cryogenic temperatures.

The critical role of hydration water in determining the internal motions, and hence the function, of globular proteins has been deeply investigated during the last decades (see e.g. Mattos, 2002, and references therein), and it is now well-ascertained that a threshold level of hydration is required to fully activate protein dynamics (and functionality) (Rupley, 1991). The interplay between solvent and protein dynamics has been rationalized in a "unified model of protein dynamics" (Frauenfelder, 2009) which systematizes a large body of experimental and theoretical investigations in myoglobin (Fenimore, 2004). Three classes of protein dynamical processes are identified: (a) class I processes, including typically large-scale motions of the protein, driven by thermal fluctuations of the bulk solvent, and found to obey dielectric α relaxations; (b) class II processes, e.g. ligand migration inside myoglobin, powered and controlled by the solvent fluctuations of the hydration shell which surrounds the protein, and following dielectric β relaxations; (c) class III processes, such as molecular vibrations in the force-field potential of atom-atom interactions, not controlled by external fluctuations. In the high-field EPR study presented in chapter 5 (Savitsky, 2010) we have applied these concepts to clarify the control exerted on electron transfer kinetics by the protein/solvent environment when RC complexes are embedded into trehalose glasses and poly (vinyl alcohol) matrices. We have proposed to ascribe the relaxation of the RC from the *dark-* to the *light-adapted* conformation, as well as the thermal interconversion between lower tier conformational substates of the RC, to Class II processes, slaved to

the fluctuations of the hydration shell. As outlined in the introduction to the present chapter, the main reason to study RC-detergent films in the absence of sugars was to verify this attribution. Our results strongly support this view: in the absence of any saccharide or polymeric matrix, in fact, the relaxation from the *dark-* to the *light-adapted* conformation is progressively hampered upon removal of water molecules bound to the RC-detergent complex. At very low hydration levels the degree of inhibition of the conformational relaxation is comparable to the one attained at cryogenic temperature in water/glycerol media, as predicted for Class II dynamical processes driven by the β-fluctuations of the hydration shell (Frauenfelder, 2009). It is noteworthy that, as shown by the similar dependence of <k> and σ upon the relative humidity, the interconversion among lower tier substates and the relaxation from the *dark-* to the *light-adapted* conformation are inhibited in parallel when the hydration of the protein complex is reduced. This suggests that the protein conformational fluctuations and the relaxation processes which stabilize the $P^+Q_A^-$ charge separated state are dynamically coupled, both being driven by the fluctuations of the hydration shell. Interestingly, it has been shown recently that IR bands attributed to water molecules weakly H bonded to the RC are perturbed upon light-induced reduction of Q_A (Iwata, 2009). The dielectric relaxation of these water molecules has been proposed to play an important role in stabilizing the primary charge separated state (Iwata, 2009).

As already observed, the same unique dependence is obtained when <k> and σ are plotted as a function of the relative humidity *r* at which the RC-LDAO and RC-OG films are equilibrated (Fig.6.9 A and B), in spite of the fact that, at any given *r* value, the amount of water bound to the RC-detergent complex is considerably larger in the presence of LDAO as compared to OG (see the adsorption isotherms in Fig.6.2). This observation strongly suggests that the hydration state of the detergent belt has no real impact on the RC dynamics which govern the kinetics of $P^+Q_A^-$ recombination. Since at any fixed *r* value the exposed protein will have the same level of hydration, independent of the detergent, we suggest therefore that the RC dynamics probed by the recombination kinetics is essentially determined by the hydration state of the exposed protein surface, i.e. of the globular domain of the H subunit and of the hydrophilic portions of the LM complex which *in vivo* face the periplasmic space. We also notice that according to the geometrical model developed to interpret the water sorption results (Fig.6.11) the area of the exposed protein surface is comparable in the RC-LDAO ($7.65 \cdot 10^3$ Å^2) and in the RC-OG complex ($6.55 \cdot 10^3$ Å^2).

The Hailwood and Horrobin isotherms determined for the RC-LDAO and the RC-OG complex (Fig.6.2) provide overall thermodynamic parameters for water sorption averaged over the detergent belt and the exposed portion of the RC. However, the hydration state of the exposed protein at a given relative humidity can be roughly estimated by assuming that the affinity K_1 for tight water binding of the exposed RC surfaces is reasonably approximated by values determined from a Hailwood and Horrobin analysis of water sorption in soluble proteins. Using the set of proteins already considered in Table 6.4, the data of Lüscher-Mattli and colleagues (Lüscher-Mattli, 1982) yield an average affinity K_1= 13.8 with a standard deviation equal to 2.9. By replacing this value in the first term of the Hailwood and Horrobin equation (eq.6.2) we can easily evaluate the fraction of occupied tight binding sites of the exposed RC surface as a function of the relative humidity. As mentioned above, inhibition of the RC conformational dynamics, as probed by an increase of <k> and σ values, starts at *r* ~0.4 (Fig.6.9). At this relative humidity more than 80% of the tight water binding sites of the exposed surface of the RC complex are still occupied. The maximum inhibition of the RC conformational dynamics is found at *r* between 6% and 3% (Fig.6.9). At these values of relative humidity, 55% and more than 70%, respectively, of the tight water binding sites are empty. This behavior indicates that removal of a large part of the hydration shell of the exposed RC protein is needed to arrest the β-slaved RC dynamical processes on the time scale probed by $P^+Q_A^-$ recombination.

The kinetic analysis summarized in Fig.6.6,.6.7 and.6.8 and Table 6.3 shows that a limited decrease of the amount of residual water (when *r* decreases from 11% to 9%) leads to the appearance of a second, well resolved and much faster phase of charge recombination ($\tau \sim 3 \cdot 10^2$ μs), suggesting that a sharp structural/dynamical transition has occurred in a large fraction (~50%) of the RC population. Consistently, this strong alteration of the kinetics is paralleled by drastic spectral changes of the residual water, which, as discussed in section 6.2.1, reflect a strong reduction in the accessible H bonding configurations of the inner hydration shell. The fast phase is also distributed in rate (Fig. 6.8C and Table 6.3) indicating that the corresponding RC subpopulation is also frozen over a large ensemble of conformational substates. To our knowledge, such a fast phase of $P^+Q_A^-$ recombination has not been observed previously as a result of environmental alterations, or genetic mutations or even in RC complexes frozen at 10 K (McMahon, 1998; Kriegl, 2004). We therefore ascribe this fast recombination to a new conformation produced by the removal of specific, tightly bound water molecules,

which play a specific structural and/or energetic role in stabilizing the primary light-induced charge separated state.

In the frame of the semi-classical Marcus model of electron transfer, which is supposed to hold at room temperature, the rate constant of the process is given by (Marcus, 1985):

$$k = \frac{4\pi^2}{h} V^2 \frac{1}{\sqrt{4\pi\lambda k_B T}} exp\left[-\frac{(\epsilon-\lambda)^2}{4\lambda k_B T}\right] \qquad \text{(eq.6.10)}$$

where ε is the difference in free energy between $P^+Q_A^-$ and PQ_A states, λ the reorganization energy, *V* the electronic interaction matrix element describing the weak coupling between the initial and final electronic states, k_B and *h* the Boltzmann and Planck constants, and *T* the absolute temperature. It is generally assumed that, to a reasonable approximation, V^2 falls off exponentially (Moser, 1992) with the distance *R*, i.e.:

$$V^2 = V_0^2 exp(-\beta R) \qquad \text{(eq.6.11)}$$

where β=1.4 $Å^{-1}$. In terms of eqs.6.10 and 6.11 an increase in *k* can be accounted for by a decrease of *R*, an increase in the free energy difference ε, or a decrease of the reorganization energy λ. It may be instructive to evaluate to which extent a variation in each of these parameters could individually account for the difference between the average rate constant of the slow phase (~50 s^{-1} in LDAO, ~40 s^{-1} in OG) and that of the fast phase (~3500 s^{-1} in LDAO, ~1800 s^{-1} in OG) detected at extreme draught. Eq.6.11 immediately shows that such an acceleration of the electron transfer process could be caused by a decrease in *R* equal to 3.0 Å (in RC-LDAO) and to 2.7 Å (in RC-OG complexes). This corresponds to a contraction of about 10% of the distance (28.5 Å) measured between the Q_A ring and the center of a line connecting the Mg atoms of the P dimer (pdb 2J8C; Koepke, 2007). As to the change required in ε or in λ to obtain the same kinetic effect, it depends significantly on the values assumed for these two parameters when the reaction proceeds with the rate constant of the slow phase. Estimates of the free energy change associated with the reaction range between 500 and 600 meV (Gopher, 1985). Different approaches yielded the following estimates of the reorganization energy λ (meV): 640 (Feher, 1988), (600±100) (Gunner, 1989), 1250

(Franzen, 1993), 900 (Ortega, 1996; Lin, 1994), (820±30) (Allen, 1998), 667 (McMahon, 1998). By assuming a value of ε between 500 and 600 meV (see above) eq.6.10 shows that even the largest decrease in the reorganization energy allowed without entering the inverted Marcus region is unable to account for the rate constant of the fast phase, unless the largest estimate (1250 meV) is used for the unperturbed λ. In this case the required decrease in the reorganization energy is ~500 meV. A similar situation holds when the effect of a variation in ε is considered. Again the effect can be accounted for only by assuming an unperturbed λ=1250 meV and a large variation of ε (about 500 meV). It should be considered, however, that an increase of ε, i.e. an increase of the energy level of the $P^+Q_A^-$ state, implies a decrease of the energy difference (ΔG^0_I) between $P^+Q_A^-$ and the intermediate charge separated state involving the bacteriopheophytin cofactor, P^+BPhe^-. It has been shown (Gopher, 1985) that such a decrease allows the thermal repopulation of the intermediate P^+BPhe^- state, activating an indirect pathway of $P^+Q_A^-$ charge recombination, in addition to the direct one (see the scheme in Figure 6.12). When considering this possibility, the observed rate constant k_{obs} of $P^+Q_A^-$ recombination is given by the rate constant of the direct (tunneling) process, k_{PA} (given by eq.6.10), plus the contribution of the thermally activated, indirect route (Gopher, 1985), i.e.:

$$k_{obs} = k_{PA} + k_{PI}\, exp(-\Delta G_I^0 / k_B T) \qquad \text{(eq.6.12)}$$

where k_{PI}=$8 \cdot 10^7$ s^{-1} is the rate constant for P^+BPhe^- recombination, and $\Delta G^0_I \cong 550$ meV in native RCs (Moser, 1992). By combining eq.6.10 and eq.6.12 we can estimate that, assuming intermediate unperturbed values for ε and λ (i.e. 500 meV and 800 meV, respectively), an increase in ε of about 300 meV (implying $\Delta G^0_I \cong 250$ meV) results in $k_{obs} \cong 3.7 \cdot 10^3$ s^{-1}, a value comparable to that measured for the fast phase of $P^+Q_A^-$ recombination in dehydrated RC-LDAO complexes. In other words, a limited destabilization of the $P^+Q_A^-$ state can result in a strong acceleration of charge recombination, due to the activation of the indirect route through the P^+BPhe^- state.

The three different effects considered could cooperate in determining the fast recombination kinetics observed under extreme dehydration. In fact, it is plausible that the removal of water molecules bound at specific sites and orientations inside the RC complex can affect the electrostatics of the P and Q_A cofactors environment, increasing

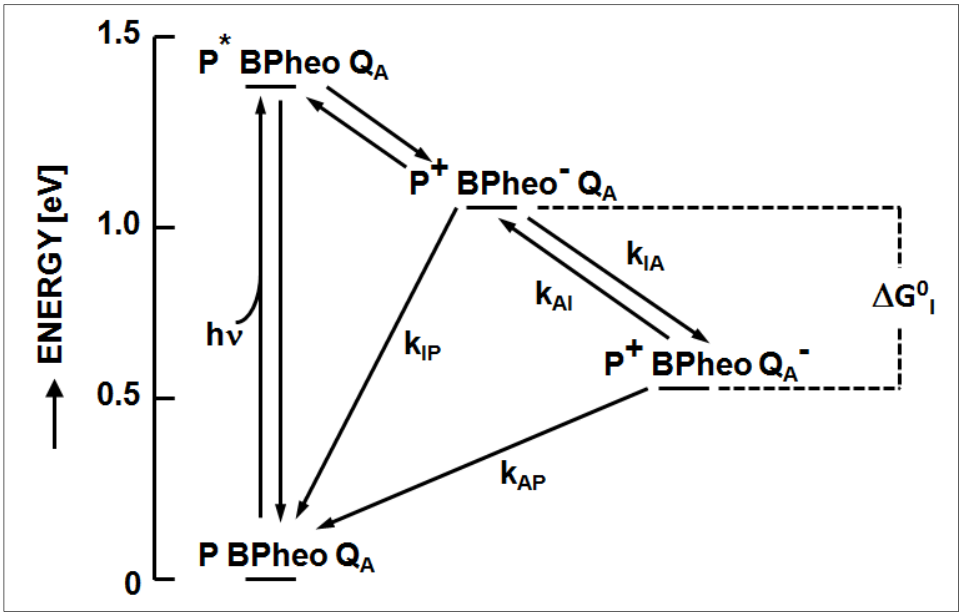

Figure 6.12
Simplified energy level scheme showing the direct (k_{PA}) and indirect route (regulated by ΔG^0_I and k_{PI}), which involves the thermal repopulation of the intermediate P^+BPhe^- state. Adapted from Gopher, 1985.

the value of ε and decreasing the value of the reorganization energy for the direct recombination, due to a decrease in the number (and mobility) of interacting solvent dipoles. At the same time it is not unreasonable that the RC, upon partial depletion of water molecules in its cavities and clefts, respond with a structural shrinking which might affect the distance between P^+ and Q_A^-. Remarkably this strong destabilization of the charge separated state, possibly involving significant structural rearrangements, is fully reverted upon rehydration of the RC-detergent films.

Finally the effects of dehydration observed in RC-detergent films *as compared* to the ones previously reported for RC-water-trehalose glassy matrices (Palazzo, 2002; Francia, 2004b; Francia, 2008; Francia, 2009; Savitsky, 2010) deserve some comments. Except for the presence of an additional, much faster kinetic phase of $P^+Q_A^-$ recombination, which was not detected in RC-trehalose glasses, dehydration leads in both systems to a comparable increase of <k> and σ of $P^+Q_A^-$ recombination, which indicates a restriction of the associated conformational dynamics. This similarity might cast some doubts on the effective role of trehalose and of the glassy state of the RC-water-sugar matrix in controlling the RC internal dynamics, which might be suspected to simply arise from dehydration of the RC-detergent complex also in the presence of trehalose. We have at variance proposed that trehalose takes an active and peculiar role

in conditioning the protein dynamics through the formation of a network of H bonds interconnecting sugar molecules of the rigid glassy matrix with water molecules of the hydration shell which are in turn H bonded to surface groups at the protein (Francia, 2004b; Cordone, 2005; Francia, 2008; Francia, 2009; Savitsky, 2010). This results in a strong slaving of the protein dynamics to that of the glassy matrix. A comparison of the water contents of the samples at which the kinetic effects on $P^+Q_A^-$ recombination become observable in the absence and in the presence of trehalose does not provide relevant information, because the trehalose matrix itself (formed by approximately 10^4 sugar molecules per RC) binds a considerable amount of water, even under extremely dehydrating conditions; consistently the discussed kinetic effects are observed in the presence of trehalose at higher (H_2O/RC) molar ratios (~10^4) (Palazzo, 2002; Francia, 2008; Francia, 2009) as compared to RC films without sugar (H_2O/RC~10^3). The following two observations, however, mark important structural and dynamical differences in the two systems: (a) as previously reported (Francia, 2008), and verified in this work under controlled, extreme dehydration, in RC-detergent films the primary photochemistry is irreversibly suppressed and the RC bacteriochlorin cofactors lose their native coordination after about three days of incubation at 37°C; the thermal stability of the RC is tremendously enhanced in the trehalose matrix, where on the contrary no degradation occurs even after several days of incubation at 37°C (Francia, 2008); (b) in extensively dehydrated RC-trehalose glassy matrices $P^+Q_A^-$ recombination after a few seconds of continuous, intense photoexcitation is only slightly decelerated as compared to the one recorded after a laser flash, indicating that a prolonged permanence of the system in the charged separated state can remove only partially the matrix-induced inhibition of the conformational relaxation (Francia, 2004b). At variance, as will be shown in chapter 8, in extensively dried RC films a comparable period of continuous illumination leads to a total recovery of the kinetics observed in the fully hydrated system, indicating that the impairment of the conformational protein dynamics induced by dehydration is less severe than in the glassy matrix and can be totally removed upon continuous photoexcitation. The latter behavior (see chapter 8) and the dramatically different resistance to thermal denaturation observed in RC-films and in RC-trehalose glasses (investigated in detail in chapter 7) suggest that the inhibition mechanism of the RC dynamics, although involving in both systems the hydration shell of the RC-detergent complex, is different in RC-films and in RC-trehalose glasses, and

that in the presence of trehalose the protein dynamics is inhibited because it is tightly slaved to that of the embedding glassy matrix.

6.3 Appendix.

A formula is derived for calculation of the surface area of an ellipsoidal ring, formed by revolution of an ellipse of semiaxes *a* and *b* around a cylindrical core of radius *R*, with axis along *x*. The area element *dA* of the surface of revolution obtained by rotating the arc segment *ds* of curve *f(x)* about the *x* axis is:

$$dA = 2\pi f(x)ds = 2\pi f(x)\sqrt{1 + [f'(x)]^2}dx$$

so that the surface area *A* obtained by rotating the arc between $x=-a$ and $x=+a$ will be:

$$A = 2\pi \int_{-a}^{+a} f(x)\sqrt{1 + [f'(x)]^2}dx \qquad \text{(eq.A6.1)}$$

For the described ellipsoidal ring, the function to be evaluated is

$$f(x) = R + y$$

where *y* obeys the equation of the ellipse

$$\frac{x^2}{a^2} + \frac{y^2}{b^2} = 1$$

so that

$$f(x) = R + \frac{b}{a}(a^2 - x^2)^{1/2} \qquad \text{(eq.A6.2)}$$

After taking the derivative of eq.A6.2, replacing in eq.A6.1, and rearranging, we obtain:

$$A = \frac{2\pi b}{a} \int_{-a}^{+a} \left[a^2 - \frac{x^2}{a^2}(a^2 - b^2) \right]^{1/2} dx$$

$$+ 2\pi R \int_{-a}^{+a} \left[1 + \frac{b^2 x^2}{a^2(a^2 - x^2)} \right]^{1/2} dx \qquad \text{(eq. A6.3)}$$

7. THE EFFECT OF THE TREHALOSE/PROTEIN MOLAR RATIO ON THE INHIBITION OF THE RC DYNAMICS

In the previous chapter (see section 6.2.2) it has been shown that an extensive dehydration of RC films in the absence of trehalose results in a strong acceleration of the $P^+Q_A^-$ kinetics, indicating that the depletion of the hydration shell leads to inhibition of the RC dynamics which stabilizes the charge separated state. In RC-films equilibrated at a relative humidity ~ 10%, the observed $P^+Q_A^-$ recombination kinetics are comparable to those measured in dehydrated trehalose glasses, revealing that the extent of inhibition of the RC dynamics coupled to this electron transfer process is also comparable in the two systems. As already discussed in section 6.2.2, this observation poses the problem of the effective role of the trehalose matrix and prompts for additional investigations addressed to shed light on the differences and on the analogies of the mechanisms which determine the inhibition of RC dynamics in dehydrated RC-detergent films as compared to RC embedded in α,α-trehalose glassy matrices.

In the first part of this chapter we have used the isopiestic method previously applied to RC-detergent films (chapter 6; Malferrari, 2011) to control the hydration state of RC-trehalose glassy matrices characterized by a sugar/protein molar ratio equal to 5 x 10^3 and 10^4. Analysis of $P^+Q_A^-$ recombination shows that the dependence of the kinetic parameters upon the hydration level of the matrix is significantly affected by the sugar/protein molar ratio. In the second part of the chapter we have studied the kinetics of thermal denaturation at 44°C in RC-LDAO films and in trehalose-RC glassy matrices characterized by a series of sugar/protein molar ratios ranging between 5 x 10^3 and 25. We found that the resistance of dehydrated LDAO-RC films to thermal denaturation was dramatically lower as compared to that of RCs embedded into trehalose matrices at a sufficiently high sugar/protein ratio.

These finding emphasizes the specific role played by trehalose in inhibiting the protein dynamics coupled to electron transfer as well as the internal RC dynamics which leads to thermal denaturation. They also support the different molecular mechanisms proposed in section 6.2.2 to explain the inhibition of the RC dynamics in dehydrated RC films and in RC-trehalose glasses.

7.1 Results.

7.1.1 Room temperature dehydration kinetics of trehalose-RC glassy matrices incubated at different values of relative humidity.

In previous studies (Palazzo, 2002; Francia, 2004b; Francia, 2008; Francia, 2009; Savitsky, 2010) RCs were always embedded in α,α-trehalose glassy matrices characterized by a disaccharide-protein molar ratio of 10000; the protein was purified in most cases from the carotenoid-less strain R26 (Palazzo, 2002; Francia, 2004b; Francia, 2008; Savitsky, 2010), but also the carotenoid-containing wild type strain 2.4.1 was used (Francia, 2009 and chapter 4 of the present thesis). In all cases, the progressive and extensive dehydration of the glassy samples was obtained by alternating cycles of dry nitrogen flow and prolonged incubation under nitrogen atmosphere at room temperature or at 30°C (for more details see par.3.2).

With the aim to extend the isopiestic method described in chapter 6 (Malferrari, 2011) to RC-trehalose glassy samples and to compare the behaviour of matrices dehydrated following this new method with the previously published results, the isopiestic method was first applied to α,α-trehalose-RC wt 2.4.1 amorphous glassy matrices characterized by a disaccharide-protein molar ratio of 10^4.

The results obtained by exposing the RC-trehalose sample to relative humidities equal to 11%, 6% and 3% are reported in Figure 7.1. Panel A shows the progressive removal of residual water molecules following incubation at these relative humidity values. The residual water content was evaluated with a NIR dispersive spectrometer, as illustrated in par.3.2. At r = 11% approximatively 5 days were needed to lower the water content of the matrix from 1.4 to 1.2 H_2O/trehalose; at r =6% a further comparable decrease (from 1.2 to 0.95 H_2O/trehalose) requires incubation for approximatively 12 days; finally at r =3% a hydration level of ≈ 0.65 H_2O/trehalose could be reached in about 2 days. During the described dehydration process of the matrix, we have measured in parallel the kinetics of $P^+Q_A^-$ recombination after a laser pulse. As described previously for RC embedded at room temperature in α,α-trehalose glassy matrices (see chapter 4), the kinetics accelerate and become progressively distributed in rate upon dehydration of the glass. $P^+Q_A^-$ decays can be fitted by a single power law (eq.1.2; see par.1.6) and yield the values of the average rate constant, <k> , and of the rate distribution width, σ, shown in panels B and C, respectively, of Figure 7.1. During incubation at r 11%, an appreciable acceleration and increase in the rate

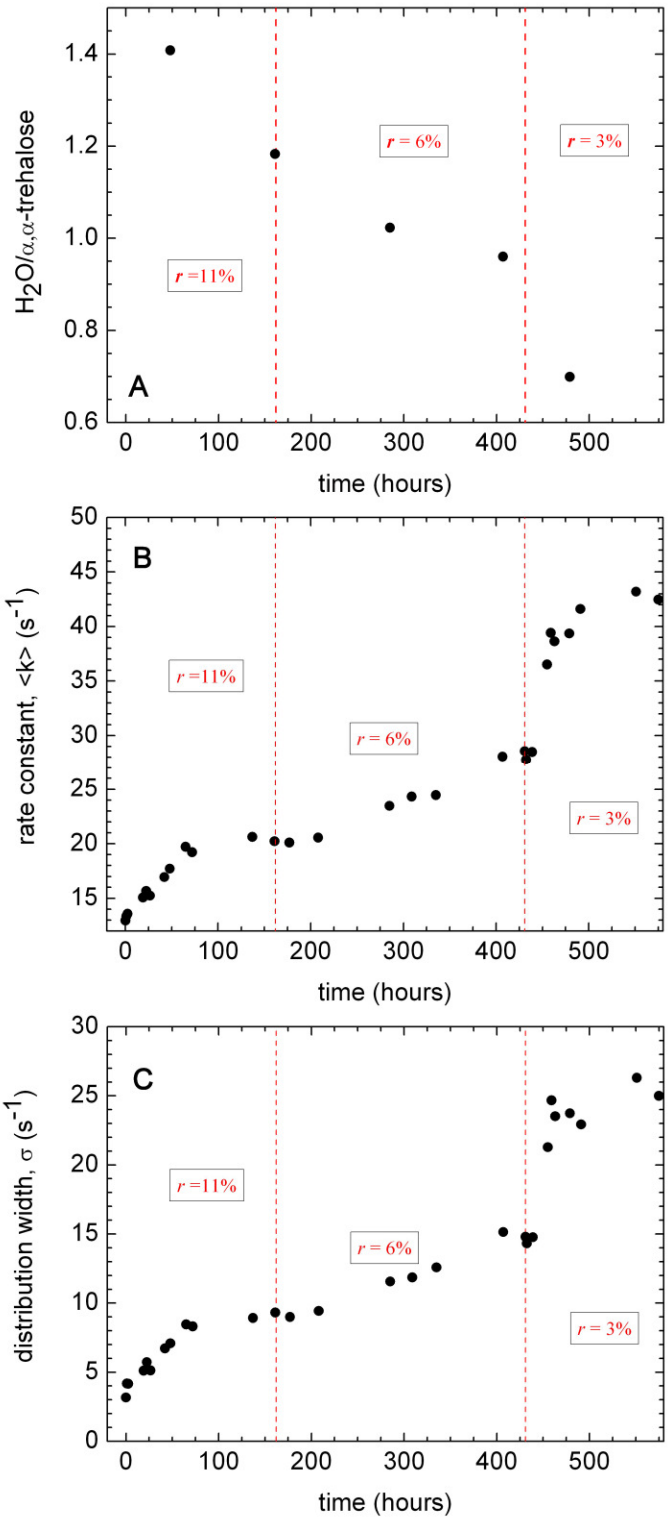

Figure 7.1
Dehydration kinetics (A) of an α,α-trehalose/RC wt 2.4.1 glassy sample incubated in sequence at a relative humidity equal to 11%, 6% and 3%. The vertical dashed lines define the time intervals during which the sample was incubated at the relative humidity indicated by the label. The time dependence of the kinetic parameters of charge recombination, i.e. the average rate constant, <k>, and the rate distribution width, σ, are shown in panel B and C, respectively. The parameter values were obtained by fitting to a single power law (eq.1.2) the $P^+Q_A^-$ kinetics measured during the slow dehydration of the matrix.

distribution width of the recombination process is observed as a consequence of partial dehydration of the sample: <k> and σ increase from values close to those measured in solution (<k>≈13 s^{-1}, σ ≈ 4 s^{-1}) to about 20 s^{-1} and 9 s^{-1} respectively. At *r* =6% a further acceleration is attained (<k> ≈ 28 s^{-1} and σ ≈ 14 s^{-1}); finally incubation at *r* =3% causes a steep increase in the values of the kinetic parameters: kinetic analysis of the traces acquired after about two days of incubation yielded <k> ≈ 40 s^{-1} and σ ≈ 25 s^{-1}; these values approach the maximal ones reported previously (Francia, 2009 and chapter 4 of the present thesis). However, the results of measurements performed during the subsequent 4 days of incubation at *r* =3% show a very limited additional increase of the kinetic parameters (see Fig.7.1, panel B and C) indicating that a kind of stationary condition is reached, and suggesting that a higher dehydration, and therefore a higher inhibition of the RC dynamics cannot be obtained with reasonable, not too long, periods of incubation even at this very low relative humidity (*r* =3%).

The dependencies of the kinetics parameters, evaluated from the best fit of $P^+Q_A^-$ kinetics to a single power law, upon the residual water content of the amorphous glassy matrix are plotted in Figure 7.2 (red circles). For the sake of comparison the figure also shows data obtained previously in similar samples (black circles), which had been dehydrated progressively using a flow of dry nitrogen (chapter 4; Francia, 2009), rather than the isopiestic method. The same dependence is obtained within the experimental error, independently of the dehydration method used, indicating additionally a very good reproducibility of the measurements when different matrices are tested.

The results presented above show that the isopiestic method can be profitable employed to control the hydration state of a RC-trehalose matrix, reaching dehydration levels which produce a considerable inhibition of the RC dynamics. We notice however that the dehydration process is very slow for trehalose containing matrices, as compared to RC films (i.e. in the absence of saccharides). When using the isopiestic method with RC-LDAO films, we could estimate that, at all the relative humidity values tested between 3 and 94%, the hydration equilibrium was reached after about 3 hours of incubation (see par.3.2). The data of Fig.7.1 indicate that dehydration occurs over a much longer timescale (weeks) in RC-trehalose glasses; panel A of Fig.7.1 shows, in particular, that equilibrium is never attained even on the long time scale tested. As a consequence the maximal inhibition of RC dynamics, i.e. values of <k> ≈ 50-60 s^{-1} and σ ≈ 35-45 s^{-1}, cannot be reached even following several days of incubation at the lowest relative humidity (*r* =3%). The extremely slow dehydration observed in the saccharide

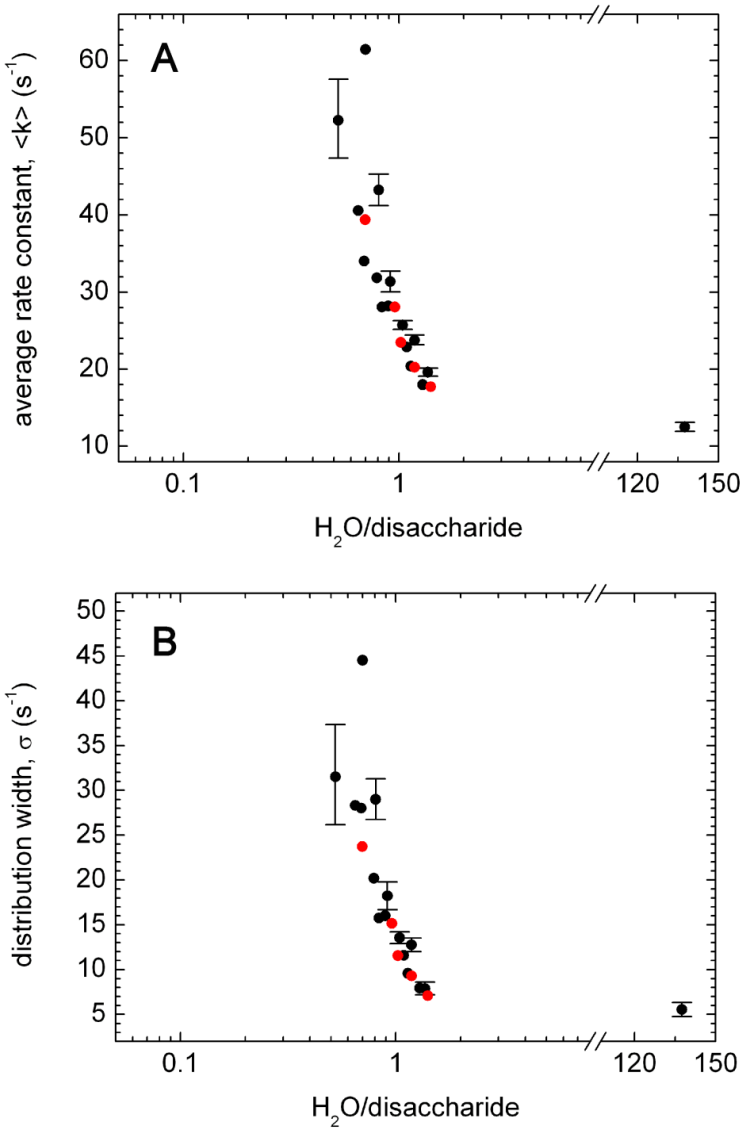

Figure 7.2
The dependence of the average rate constant, <k>, and of the distribution width, σ, upon the residual water content of trehalose-RC wt 2.4.1 glassy samples, characterized by a sugar/protein molar ratio of 10^4. Filled black circles represent the same data shown in Figure 4.2 (see chapter 4 and Francia, 2009), obtained in samples dehydrated by N_2 flow or by prolonged incubation under a nitrogen atmosphere at room temperature; red filled circles represent data obtained in samples characterized by the same sugar/protein molar ratio, but dehydrated using the isopiestic method (see Fig.7.1).

matrices is fully consistent with the high affinity of saccharides, and especially of trehalose, for water molecules (Heyden, 2008).

7.1.2 The effect of the trehalose/RC molar ratio on the time course of dehydration and on the kinetics of charge recombination.

In view of the limitation discussed above, and since the slowness of the dehydration processes is clearly due to the slow exchange of water molecules between the vapour phase and trehalose in the matrix, we decided to test the efficacy and reproducibility of the isopiestic method in RC-trehalose matrices characterized by a halved trehalose/RC molar ratio (i.e. 5 x 10^3 instead of 10^4) while keeping constant the RC mass in the sample. We expected that such a decrease in the absolute mass of trehalose could speed up the dehydration of the matrix, eventually allowing the attainment of equilibrium following a reasonable incubation time. This choice implied the development of a new protocol to produce homogenous amorphous protein-sugar matrices (see par.3.1.2 for details). In fact, as discussed in par.3.1.2, the decrease of the trehalose concentration in the liquid sample used to obtain the amorphous matrices, significantly decreases its viscosity. This causes, upon dehydration, a capillary flow of the RC towards the perimeter of the RC-trehalose liquid drop during dehydration. At low viscosity (low trehalose concentrations) this migration results in a strong inhomogeneity of the RC-trehalose matrix, with most of the RC confined to a narrow ring at the perimeter of the glass (see par.3.1.2).

The dehydration kinetics measured in α,α-trehalose/RC wt 2.4.1 glassy matrices characterized by a trehalose/RC ratio equal to 5 x 10^3 are shown in Figure 7.3 at a relative humidity r =11% and 3%. The time course of water removal is shown at r =11% for two independent RC-sugar glassy samples (see open and closed symbols in Fig.7.3): data are fairly reproducible, as a stable residual water content is reached in both cases roughly after 200 hours (≈ 8 days) with values of H_2O/trehalose ≈ 0.48 (0.43 and 0.54 H_2O/trehalose in the two independent experiments).

The dehydration kinetics are reasonably fitted to an exponential decay function, i.e.:

$$w(t) = [w(0) - w(e)] * e^{-kt} + w(e) \qquad \text{(eq.7.1)}$$

where *w(t)*, *w(0)* and *w(e)* are respectively the water content at time t, at time 0 and at the equilibrium; *k* is the rate constant of the dehydration process. Time 0 is taken as the time at which the incubation at a given value of the relative humidity starts. The best fit to the exponential decay (see Fig.7.3, red dashed line) returns a half-time, $t_{1/2} \approx 25$

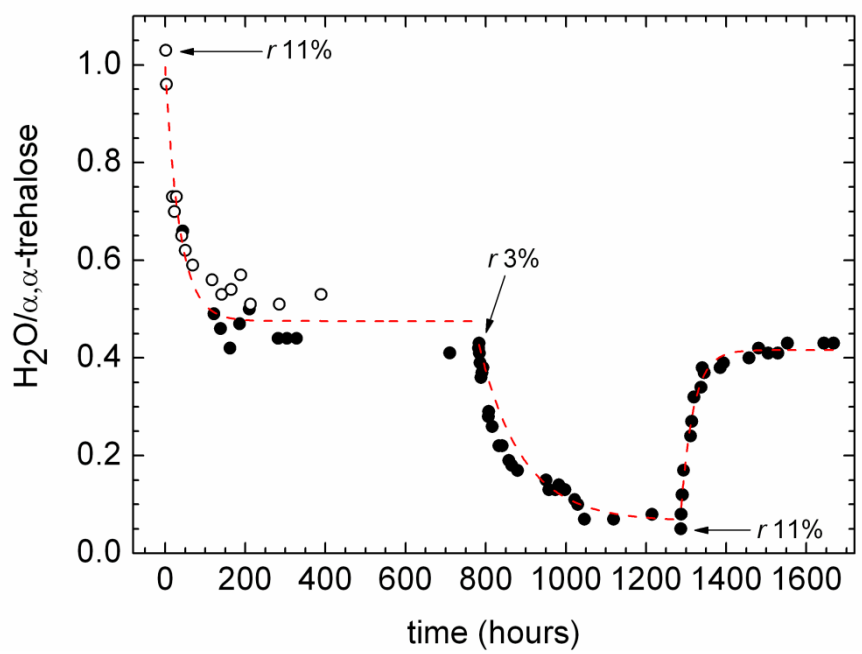

Figure 7.3
The dehydration kinetics measured at room temperature in α,α-trehalose-RC wt 2.4.1 amorphous glassy matrices characterized by a sugar/protein molar ratio equal to 5 x 10^3, incubated at r =11% and r =3%. The water content was evaluated by FT-NIR spectroscopy (see par.3.2). The black filled symbols represent data obtained on the same sample; the results shown as open black circles have been obtained in an independent trehalose-RC glassy matrix characterized by the same sugar/protein ratio. For each relative humidity, the red dashed lines represent the best fit of the dehydration (or rehydration) process to an exponential function; the values of the half times ($t_{1/2}$) derived from the best fit of the dehydration or rehydration kinetics are reported in the text.

hours. When the sample is subsequently incubated at r =3%, additional dehydration takes place, resulting in a very low residual water content at equilibrium, i.e. approximately of 0.07 H_2O/trehalose. The dehydration process is slower at r =3% as compared to r =11% and the best fit to eq.7.1 *(exponential decay)* yields at the lower humidity $t_{1/2} \approx 72$ hours (red dashed line in Fig.7.3).

To test the reversibility of our isopiestic method during desorption/sorption cycles, we have studied the rehydration at r =11% of a glass previously equilibrated at r =3%. As shown in Figure 7.3, the rehydration at r =11% demonstrates, within the error of our estimations of the hydration contents, the full reversibility of the desorption/sorption processes in α,α-trehalose/RC amorphous glassy samples characterized by a sugar/RC molar ratio equal to 5 x 10^3. A residual water content ≈

0.43 H_2O/trehalose, at equilibrium, was reached in about 250 hours (i.e. ≈ 10 days). The rehydration kinetics have been fitted to an exponentially growing function, i.e.:

$$w(t) = w(0) + [w(e) - w(0)][1 - e^{-kt}] \quad \text{(eq.7.2)}$$

where *w(t)*, *w(0)*, *w(e)* and *k* are defined as for eq.7.1). The best fit returns $t_{1/2} \approx 21$ hours for the rehydration process; it appears that the rehydration from *r* =3% to *r* =11% (during the last time interval of Fig.7.3) and the initial dehydration of the wet sample at *r*=11% exhibit essentially the same kinetics. Most importantly it appears that hydration/dehydration cycles in the range of relative humidity between 11% and 3% are fully reversible.

The dehydration behavior of the RC-trehalose matrices characterized by a sugar/protein molar ratio of 10^4 and 5 x 10^3 shows that, as expected, at the lower sugar content a faster and more extended control of the hydration state of the matrix is obtained by the isopiestic method (cf. Fig.7.1 and Fig.7.3).

In view of this, we have performed a detailed analysis of $P^+Q_A^-$ charge recombination kinetics after a laser excitation during the dehydration of α,α-trehalose/RC matrices characterized by 5 x 10^3 trehalose molecules per RC. The results obtained are shown in Fig.7.4, and compared with those obtained in α,α-trehalose/RC glassy samples characterized by 10^4 trehalose molecules per RC (i.e. the data already reported in Figure 7.2). Quite interestingly, the dependence of both <k> and σ upon the hydration state of the matrix (H_2O/trehalose molar ratio) is significantly affected by the sugar/protein molar ratio of the glassy matrix. As the data of Fig.7.4 show clearly, at a (H_2O/trehalose) ratio ≈ 0.5, for which <k> and σ reach the maximum values in the matrix characterized by 10^4 trehalose molecules per RC, the average rate constant and the rate distribution width are considerably lower in the matrix where the trehalose/RC ratio is 5 x 10^3. It appears therefore that a lower hindering of the RC dynamics involving lower tier conformational substates, as well as a lower inhibition of the RC relaxation from the *dark-* to the *light-adapted* conformation takes place in the matrix in which the trehalose molar fraction is lower, at the same hydration level. Furthermore, the same maximal values of <k> and σ observed at a (trehalose/RC) molar ratio equal to 10^4 (i.e. <k> ≈ 60 s^{-1} and σ ≈ 50 s^{-1}) are attained also in the matrix characterized by a halved (trehalose/RC) molar ratio, but only at much lower hydration levels (i.e. at about 0.1 H_2O molecules per trehalose molecule). In other words, the dependence upon

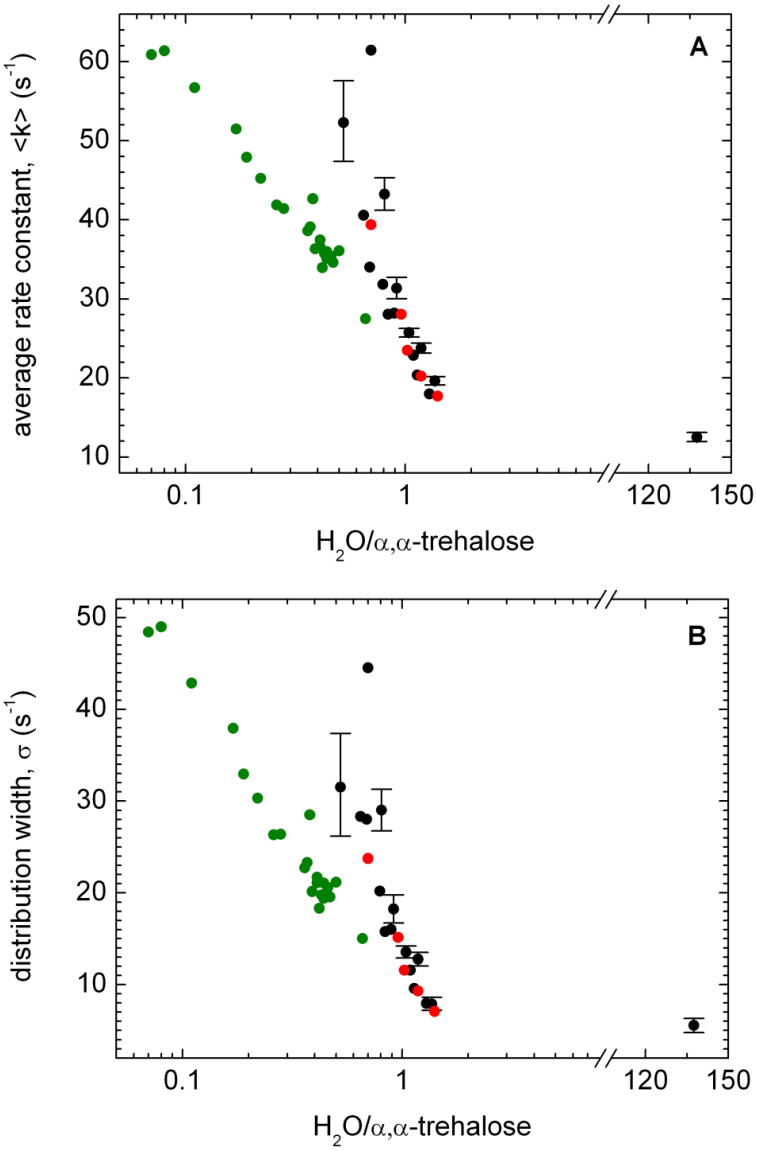

Figure 7.4
Dependencies of the average rate constant, <k> (panel A) and of the distribution width, σ (panel B) upon the residual water content of the matrix in α,α-trehalose/RC glassy samples characterized by a disaccharide/protein molar ratio equal to 10^4 (red and black circles) and $5 \cdot 10^3$ (green circles). Kinetic parameters have been obtained by fitting the $P^+Q_A^-$ recombination kinetics to a single power law (eq.1.2).

dehydration diverges significantly when <k> and σ start to increase in the two systems. These differences are not related to the dehydration method employed (as we have shown that the dehydration procedure has no effect (see Fig.7.2). Therefore we strongly suggest that the halving of the (sugar/RC) molar ratio from 10^4 to 5 x 10^3 soften significantly the protein-sugar glassy matrix. Indeed, to obtain the same level of inhibition in the RC dynamics (i.e. comparable values of <k> and σ) the residual water

content has to be decreased by almost one order of magnitude at the lower sugar/protein molar ratio.

7.1.3 The efficiency of the trehalose glassy matrix in protecting the RC from thermal denaturation at 44°C: a comparison between denaturation kinetics in RC-films and in RC-trehalose matrices characterized by $5 \cdot 10^3$ trehalose molecules per RC.

Previous studies, showing the peculiar efficacy of α,α-trehalose glasses in protecting the RC protein against thermal denaturation, as compared to RC-LDAO films and sucrose glassy matrices, were all performed at 37°C and in matrices characterized by 10^4 trehalose molecules per RC (Francia, 2008). In order to further characterize the dynamical behavior of trehalose/RC glasses at a sugar/protein ration equal to $5 \cdot 10^3$ and to compare them with dehydrated RC-film at controlled relative humidity we report in this section on thermal denaturation assays performed on both systems at 44°C. We have chosen this temperature, instead of 37°C (Francia, 2008), to compare our data with the results of thermal denaturation experiments of RC performed at 44°C in solution samples (Palazzo, 2010).

As described previously (Hughes, 2006), the thermal denaturation of the RC can be studied by following the evolution of the NIR spectrum of the RC bacteriochlorin cofactors during the incubation at high temperature. The relative area of the three Gaussian bands into which the spectrum can be decomposed probes in fact the loss of the native structure of the individual cofactors (i.e. the bacteriochlorophyll dimer, P, the two monomeric bacteriochlorophyll and bacteriopheophytin molecules), since the Gaussian contribution of each cofactor is sufficiently separated in the NIR spectrum between 700 nm and 950 nm. The details of the analysis (Hughes, 2006; Francia, 2008) are given in par.3.4. In Figure 7.5A-B representative NIR spectra, measured at different times during incubation at 44 °C, are shown for RC-LDAO films (panel A) and RCs embedded in α,α-trehalose amorphous matrices (panel B). The evolution of the NIR spectra in Fig.7.5A puts in evidence the progressive loosening of the native structure of bacteriochlorin pigment binding sites in RC-LDAO films as a consequence of its exposure to high temperature. After 1 hour of incubation at 50°C a conspicuous increase of the band centered around 750 nm, due to the absorption of the bacteriopheophytin molecules, at the expense of the bands attributed to the monomeric bacteriochlorophylls and to the P special pair, centered respectively around 800 nm and 860 nm, is observed.

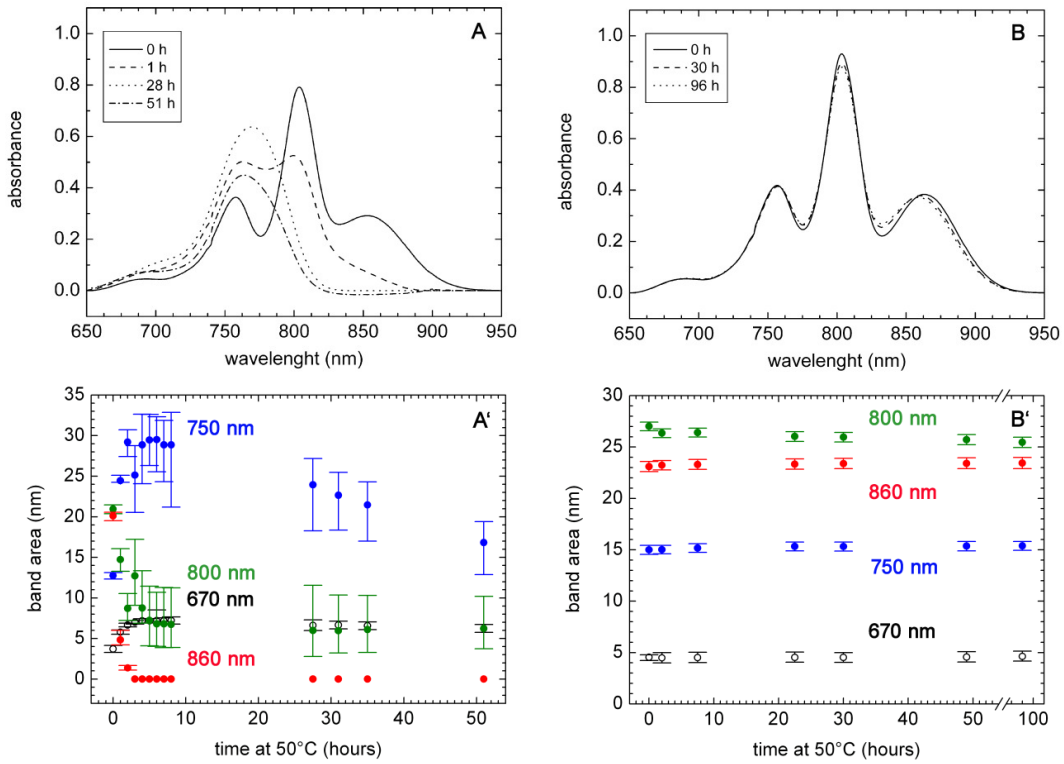

Figure 7.5
Thermal denaturation assays at 44°C of RC-LDAO films, equilibrated at r =11% (950 H_2O/RC), and of a dehydrated α,α-trehalose/RC amorphous matrix characterized by 5 · 10^3 trehalose molecules per RC and by a residual water content corresponding to 2400 H_2O/RC. The NIR spectra of RC-LDAO films (A) and of the RC-trehalose glassy matrix (B) are shown for representative incubation times. Panel A: before incubation (continuous line), after 1 h (dashed line), after 28 h (dotted line), and after 51 h of incubation (dashed-dotted line). Panel B: before incubation (continuous line), after 30 h (dashed line), and after 96 h (dotted line) of incubation. Panels A' and B' show the relative area of the Gaussian components of the spectra for the RC films and for the RC-trehalose matrix, respectively. Spectra were decomposed into four bands, centered at 670 nm (black empty symbols), 750 nm (blue filled symbols), 800 nm (green filled symbols) and 860 nm (red filled symbols). The vertical bars give the confidence intervals within two standard deviations (for details see par.3.4).

This suggests that, in a significant fraction of the RC population, the bacteriochlorophyll molecules have lost their native structure, i.e. they have lost the magnesium atom coordinated by the porphyrin ring or the native protein structure that form the pigment binding pocket has been altered, eventually causing a complete release of the pigment from the protein binding site. In the spectra of the RC-LDAO film taken after 28 h and 51 h of incubation at 44°C the P pair band at 860 nm has disappeared and only a broad band around 765 nm is observed, which includes contributions from both the monomeric bacteriochlorophylls and the bacteriopheophytins, significantly decreasing during the thermal treatment. The

alterations in the spectra of the RC-LDAO film at 28 h and 51 h additionally indicate at least a partial loosening of the tertiary structure of the RC: it has been reported in fact that, when the NIR spectra of the RC shows the disappearance of the bacteriochlorophylls bands and the concomitant appearance of broad band centered around 750 nm, the fluorescence of the tryptophan residues of the RC, which is usually quenched by the bacteriochlorin cofactors bound to the protein, dramatically increases (Palazzo, 2010). This behavior is attributed to a dramatic increase in the distances between the bacteriochlorin molecules and the tryptophan residues, due to strong alterations in the tertiary structure of the RC. On the contrary, as shown in panel B of Fig.7.5, the spectrum of RCs embedded in α,α-trehalose glassy matrices is essentially unaffected even after 96 hours of incubation at 44°C, demonstrating that the sugar matrix completely preserves the native structure of the pigment binding sites.

The dependence of the band area of the bacteriopheophytins (750 nm), of the monomeric bacteriochlorophylls (800 nm) and of the P special pair (860 nm) on the incubation time at 44°C is reported in panel A' and B' of Fig.7.5 for the RC-LDAO film (at r =11%) and for the trehalose-RC glassy matrix, respectively. The origin of the fourth Gaussian band (centered at 670 nm), which had to be included to accurately fit the spectrum is not known (see Fig.1.7). This precludes any interpretation of the small changes which occur during incubation in the area of this minor band, only in RC-films. As far as the RC-trehalose glass is concerned, the areas of the three main bands remain constant within the experimental errors during the 96 hours of incubation at 44°C. On the contrary, the big changes produced by the thermal treatment in the spectrum of RC-LDAO films result in significant alterations of the relative contributions of the different bands. The area of the band attributed to the monomeric bacteriochlorophylls (at 800 nm) decreases during the first hours of incubation to 38% of its initial value before incubation, and the area of the band attributed to the P special pair (at 860 nm) essentially vanished in approximately 3 hours. The higher sensitivity of the bacteriochlorophyll molecules forming the P pair is consistent with the fact that they are closer to the surface of the complex as compared to the monomeric bacteriochlorophylls, which should be more protected also by the detergent micelle surrounding the protein complex. This behaviour is also in line with the higher sensitivity of the P absorption band to other perturbing agents, such as pH changes and ionic strength, reported previously (Palazzo, 2004). Consistently with the decrease of both bacteriochlorophyll bands, a strong increase in the contribution of the

bacteriopheophytin is observed during the first 10 hours of incubation, suggesting that the bacteriochlorophylls have lost the magnesium atom or came out of their protein binding site (Tandori, 2005). In agreement with what observed (following much shorter incubation times) in denaturation assays at 44°C of RC solution (Palazzo, 2010), when the dehydrated RC-LDAO films are incubated at 50°C for more than 10 hours the Gaussian contribution at ≈ 750 nm slowly decreased, probably as a consequence of the chemical denaturation of the pigment (Palazzo, 2010).

Summarizing, we can conclude that when the RC is embedded in α,α-trehalose glassy matrices, in the presence of $5 \cdot 10^3$ trehalose molecules per RC, the native structure of the pigment binding sites of the RC is completely preserved at variance with what occurs in dehydrated RC-LDAO films, where the protein experiences over the same time scale an almost complete thermal denaturation, as revealed by the spectral alteration of its bacteriochlorin pigments.

7.1.4 The kinetics of RC thermal denaturation at 44°C in α,α-trehalose glassy matrices at different disaccharide/protein molar ratios.

This section reports on the kinetics of thermal denaturation studied at 44 °C in RC embedded in α,α-trehalose glassy matrices characterized by a variable disaccharide/protein molar ratio; the molar ratios explored were 0 (i.e. RC-LDAO film, in the absence of trehalose), 25, 100, 200, 500, 10^3 and 10^4. The measurements were performed before the development of the isopiestic method to control the hydration state of films and sugar matrices: RC-films and trehalose-RC glasses were therefore extensively dehydrated under N_2 flow before incubation at 44 °C. Except for this difference in the method of dehydration, the extent of thermal denaturation during incubation was determined by decomposing into Gaussian bands the NIR spectrum of the RC, essentially as described by Hughes and colleagues (Hughes, 2006). Fig.7.6 shows the relative area of the bands attributed to the bacteriopheophytin cofactors (750 nm, panel A), to the monomeric bacteriochlorophylls (800 nm, panel B) and to the bacteriochlorophylls of the P pair (860 nm, panel C) as a function of the incubation time at 44 °C. For each spectral contribution, the area of the bands have been normalized for each time at the initial area before incubation at high temperature. This procedure allowed to compare data acquired in different RC-trehalose glassy matrices, which due to a variability in their thickness gave rise to different absolute absorbance values in the considered NIR spectral region.

A correlation between the disaccharide/protein molar ratio and the efficacy of the trehalose matrix to protect against thermal denaturation can be qualitatively inferred at a first sight from the data of Fig.7.6. First of all, in qualitative agreement with the results of the previous section (see Fig.7A' and B'), essentially no spectral alteration is observed even after 100 hours of incubation at 44°C in matrices characterized by a sugar/RC ratio larger than 10^3, while an essentially complete thermal denaturation occurs over this time scale in the absence of trehalose (RC-films). A closer inspection of the data, at intermediate saccharide/RC molar ratio, reveals additional features, which yield information on the effect of the sugar/protein ratio on the overall dynamics of the system involved in thermal denaturation.

When considering the time evolution of the bacteriochlorophyll contribution (panels B and C of Fig.7.6), as already observed in the case of RC-LDAO films at *r* =11% (Fig.7.5A, A'), it appears that the bacteriochlorophyll molecules belonging to the P special pair are more sensitive to thermal denaturation as compared to the monomeric bacteriochlorophylls. In the case of the monomeric ones, in fact, a loosening of the native structure is evident only at a very low (sugar/RC) molar ratio, equal to 25, and in the absence of sugar (RC-LDAO film). In the latter system, loss of the native structure is complete, while in the presence of 25 trehalose molecules per RC it occurs only in a fraction of the RC population, since about 50% of the initial area of the band at 800 nm survives even after a 120 h incubation (Fig.7.6 B). At molar ratios higher than 25 no significant decrease is observed upon incubation at high temperature in the area of the band centered at 800 nm. On the other hand, the area of the band at 860 nm undergoes a substantial decay during exposure to the high temperature for trehalose/protein molar ratios lower or equal to 200 (Fig.7.6C), showing that in a large fraction of the RC population the P bacteriochlorophyll is losing its native structure. Interestingly, upon decreasing the sugar/RC molar ratio the decay becomes progressively faster, and the fraction of the bacteriochlorophyll P special pair pigments withstanding exposition to high temperatures also decreases, as can be estimated from the residual normalized area of the band at 860 nm for incubation times longer than 120 h.

The kinetics of the spectral changes related to the band at 750 nm, attributed to bacteriopheophytin or to bacteriochlorophyll molecules released from their binding sites, are consistent with the variations of the bands at 800 nm and 860 nm described above. The normalized area of the 750 nm band, in fact, increases for sugar/protein ratios lower or equal to 200; moreover the kinetics becomes progressively faster and the

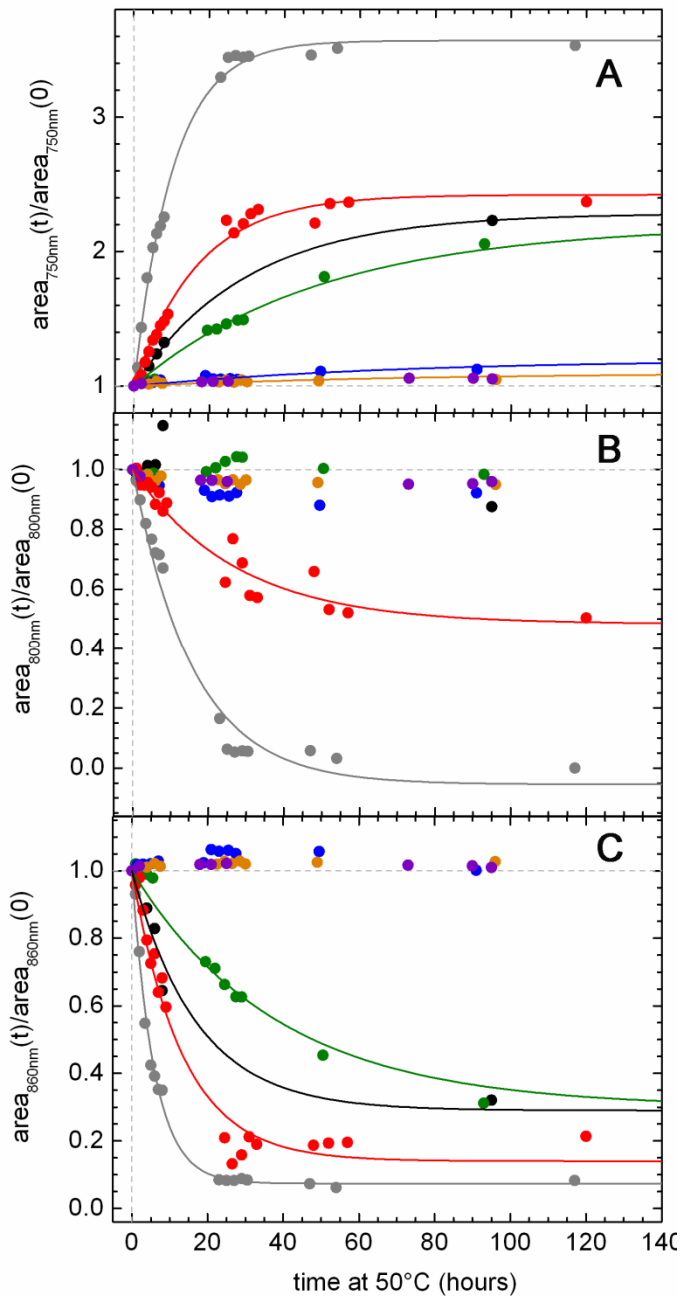

Figure 7.6
Thermal denaturation assays at 44°C of α,α-trehalose/RC wt 2.4.1 glassy matrices characterized by a disaccharide/RC molar ratio equal to 0 (RC-LDAO film, dark grey), 25 (red), 100 (black), 200 (green), 500 (blue), 10^3 (orange) and 10^4 (violet). The time evolution of the relative area of the Gaussian bands centered at approximately 750 nm, 800 nm and 860 nm are shown in panel A, B and C, respectively. For each band, the relative area evaluated at each time during incubation has been normalized to the area of the band before incubation (t=0). Continuous lines represent best fits to eq.7.3 for the data in panel B and C, and best fits to eq.7.4 for panel A. The values of the fitting parameters *A* and *k* (see eqs.7.3 and 7.4) are plotted in Figure 7.7.

maximal variation recorded after 100 h incubation increases progressively upon decreasing the sugar/protein ratio (see Fig.7.6A).

The kinetics of Fig.7.6 are reasonably described by exponential decaying (or growing) functions. Best fits are shown in Figure 7.6 with continuous lines only in the case of sugar/RC molar ratios for which a significant change of the band area is detected. For the area of the band centered around 800 and 860 nm, which decreases during the thermal denaturation assays, an exponentially decaying function has been considered:

$$\frac{area_i(t)}{area_i(0)} = A \cdot e^{-kt} + (1 - A) \quad \text{(eq.7.3)}$$

where $area_i(t)$ and $area(0)$ are the area of the i-th band at time t and before incubation respectively, k is the rate constant of the denaturation process, and A is the maximum variation of $area_i$ throughout the denaturation assay. Similarly, to describe the increase of the band area centered approximately at 750 nm, the following exponentially growing function has been used:

$$\frac{area_i(t)}{area_i(0)} = 1 + A \cdot (1 - e^{-kt}) \quad \text{(eq.7.4)}$$

where $area_i(t)$, $area_i(0)$, A and k have the same meaning as in eq.7.3.

The dependences of the kinetic parameter k and A upon the disaccharide/RC molar ratio are plotted in Figure 7.7. As shown in panel A, a monotonic decrease of the rate constants which describe the time evolution of the bands at 750, 800 and 860 nm is observed in response to the increase of the sugar/RC ratio. Values of k significantly differing from zero are observed only at molar ratios larger than or equal to 200. At all the molar ratios, k values which describe the variation of the 860 nm and of the 750 nm bands seem to exceed systematically those which govern changes of the 800 nm band. Also the maximal variation of the normalized area, A, decreases monotonically upon increasing the trehalose/RC molar ratio (Fig.7.7B). In the case of the 800 and 860 nm, A can vary by definition between 0 and 1. The small A values obtained for these two bands at disaccharide/RC molar ratios higher than 200 show that the vast majority of the RCs are protected against thermal denaturation under these conditions. The A values for

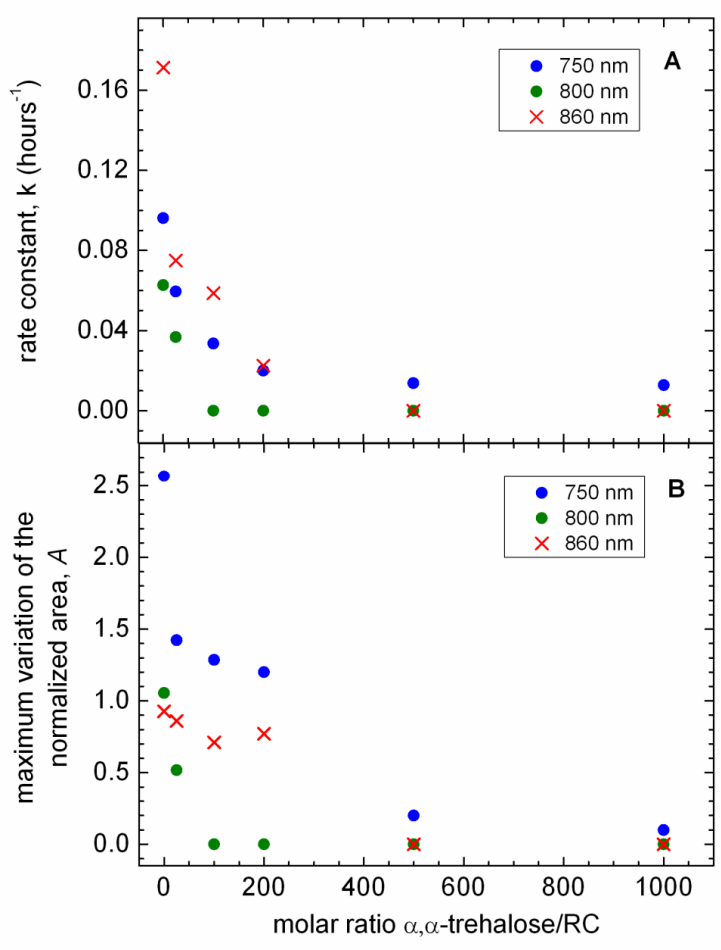

Figure 7.7
The dependence of the fitting parameters *k* (panel A) and *A* (panel B) upon the trehalose/RC molar ratio, obtained by fitting the data in Figure 7.6 to eqs.7.3 and 7.4. The data corresponding to the contribution of the bacteriopheophytin, of the accessory bacteriochlorophylls and of the P pair are plotted with blue filled circles, green filled circles and red crosses, respectively.

the 750 nm band, are systematically larger than the corresponding ones obtained for the 800 nm and 860 nm bands. This agrees with the notion that the decrease of the bands at 800 nm and 860 nm, reflecting the formation of bacteriopheophytin from bacteriochlorophyll or severe structural alterations in the binding pocket of the bacteriochlorophyll molecules, has to be paralleled by an increase of the band at 750 nm, to which both bacteriopheophytin and unbound bacteriochlorophyll molecules contribute (Tandori, 2005).

The data of Fig.7.7 support the conclusion that, when the disaccharide/protein molar ratio is decreased from 200 to 0, a progressively higher fraction of the RC population becomes involved in the denaturation process. We suggest that above a threshold of about 200 trehalose molecules per reaction center the RC-trehalose glassy

matrix essentially blocks the RC dynamics which leads to thermal denaturation. When the sugar/protein ratio is decreased below this threshold the mechanical constraints which hampers the RC dynamics coupled to denaturation are progressively released in parallel with an overall softening of the RC-water-trehalose system.

7.2 Discussion.

The first aim of the studies presented in this chapter has been to test the efficacy of the isopiestic method previously applied to RC-films (see chapter 6) in controlling the hydration level of RC-trehalose glassy matrices. The attempt to apply the method, at relative humidity values between 11% and 3%, to RC-trehalose glassy matrices characterized by a relatively high sugar/protein molar ratio (equal to 10^4) showed that the hydration level of the system could be finely modulated. It also turned out that the dependence of the kinetics of $P^+Q_A^-$ recombination upon the content of residual water of the matrix was pretty reproducible, irrespective of the method used to dehydrate the system: the same dependence was in fact obtained when the RC-trehalose matrix was dehydrated under N_2 flow or by incubated at controlled relative humidity values, defined by the appropriate saturated salt solutions present inside the sample holder (Fig.7.2). In view of this results, the isopiestic method offers obvious advantages in measurements that require a subtle tuning of the hydration level and stable hydration levels of the matrix. On the other hand, dehydration of the matrix was extremely slow, as compared to that observable in the absence of the saccharide (i.e. in RC films). Furthermore the dehydration kinetics and the kinetics of $P^+Q_A^-$ recombination, measure in parallel after a laser flash, have shown that even after 20 days of incubation at low values of the relative humidity (in the range 11% - 3%) a true hydration equilibrium could not be attained. This precluded to obtain, after a reasonable incubation time, the dehydration levels which cause the maximal inhibition of the RC dynamics, as probed by $P^+Q_A^-$ recombination kinetics.

These limitation of the isopiestic method have been fully removed by decreasing the trehalose/RC molar ratio, as shown by the dehydration/rehydration kinetics measured in RC-trehalose matrices characterized by $5 \cdot 10^3$ trehalose molecules per RC (Fig.7.3). We have demonstrated that under these conditions the matrix equilibrates fully with the water vapour at relative humidity values equal to 11% and 3% and that stable, reproducible hydration levels can be obtained reversibly (i.e. following dehydration or rehydration). In matrices characterized by $5 \cdot 10^3$ trehalose molecules per

RC, the use of the isopiestic method allowed therefore to study carefully the dependence of the recombination kinetics of $P^+Q_A^-$ upon the hydration level, testing, in particular, the effect of the sugar/molar ration on the inhibition of the RC protein dynamics. As described in section 7.1.2 (see Fig. 7.4) it appears that at the lower trehalose/RC ratio ($5 \cdot 10^3$ as compared to 10^4) a much more extensive dehydration of the matrix is necessary to reach the maximal inhibition of the RC dynamics probed by the electron transfer process. In other words, for a given content of residual water per saccharide molecule, both the relaxation of the RC from the dark- to the light-adapted state, and the RC fluctuations among lower-tier conformational substates, are significantly less inhibited in the matrix characterized by a lower trehalose/protein ratio.

These results, besides emphasizing the role of trehalose in determining the dynamics of the RC embedded in the matrix, suggest that a limited decrease (form 10^4 to $5 \cdot 10^3$) in the molar fraction of the sugar within the glassy matrix has relevant effects on the mechanical properties of the matrix and/or on the coupling between the protein and matrix dynamics. In order to evaluate the plausibility of such effects, it is instructive to attempt an estimate of some geometrical properties of the protein-sugar matrix. Although a realistic structural molecular model of the glassy matrix would be desirable, even very rough estimates, based on crude assumptions, can provide valuable information on the effect of changes of the trehalose molar fraction on parameters such as the average thickness of the trehalose protein coating and the average distance between individual RCs embedded into the matrix. An extremely crude representation of the RC coating by trehalose molecules in the matrix can be obtained by considering a spherical cell consisting of a spherical RC-detergent complex coated by a spherical trehalose shell. The volume of the RC –detergent complex can be estimated on the basis of the structural model introduced previously to interpret the water sorption isotherms in RC-detergent films (see chapter 6: Fig.6.11 and par.6.2.1, and ref. Malferrari, 2011): in the presence of the detergent LDAO a total volume, $V_{RC\text{-}LDAO}$, $\approx 142 \bullet 10^3$ Å^3 has been calculated. The volume of a single α,α-trehalose molecule, $V_{trehalose}$, has been evaluated by using the Swiss-PDBViewer software (Guex, 1997) and by averaging five conformers of the α,α-trehalose molecule, obtained rotating the two glucosidic moieties around the glicosidic bond. Following this approach we have obtained $V_{trehalose}$ = (278±7) Å^3. By varying the number of trehalose molecules per RC a very rough estimate of the thickness of the spherical trehalose shell which coats the RC-LDAO complex, as a function of the trehalose molar fraction, can be calculated.

Table 7.1
The effect of varying the trehalose/RC molar ratio on the geometrical parameters for the coating of the RC-LDAO complex by the glassy matrix. Volumes of 278 Å^3 and 142•10^3 Å^3 have been estimated for the α,α-trehalose molecule ($V_{trehalose}$), and for the RC-LDAO complex ($V_{RC\text{-}LDAO}$), respectively (for more details see par.7.2).

trehalose/RC	10000	5000	1000	500	200	100	25
Cell volume (Å^3)	2.9x10^6	1.5x10^6	4.2x10^5	2.8x10^5	1.97x10^5	1.7x10^5	1.5x10^5
$\frac{V_{trehalose}}{V_{RC-LDAO}}$	19.6	9.8	1.96	0.99	0.39	0.20	0.05
Cell radius (Å)	88	71	46	40	36	34	33
Trehalose matrix thickness (Å)	56	39	14	8	4	2	1

These simple geometrical parameters of the system are summarized in Table 7.1 for several representative values of trehalose/RC molar ratio. When molar ratio is decreased from 10000 to 5000 the ratio between the volume of the RC-LDAO and the trehalose moieties, ($V_{trehalose}$ / $V_{RC\text{-}LDAO}$), and the thickness of the trehalose coating are approximately halved, the latter parameter being reduced from 56 Å to 39 Å. Although this geometrical representation is extremely crude, and in particular the model suffers from the fact that the considered spherical cells cannot obviously be packed to form a continuous RC-trehalose glass, the obtained values provide a useful insight into the order of magnitude of the average distance between adjacent RC-LDAO complexes hosted by the matrix. In fact, when considering that the sphere representing the RC with its micelle has a diameter of ≈ 64 Å, at a sugar/protein ratio of 10^4 the average separation between two adjacent RC-detergent complexes is roughly comparable to the dimension of the RC-LDAO complex. This simple observation suggests that the presence of the (soft) protein moiety cannot be neglected when considering the overall mechanical (structural and dynamical) properties of the RC-trehalose matrix. The hardness of a dehydrated trehalose matrix is likely to be significantly decreased when the matrix incorporates RC-protein complexes at such relatively high "densities". Since upon decreasing the sugar/protein ratio to 5 · 10^3 the thickness of the trehalose coating becomes even smaller than the diameter of the RC-LDAO complex, it is conceivable that the overall RC-trehalose matrix is considerably "softened" and that, in particular, the dynamics of the incorporated RC is less hampered for a given hydration of the

matrix, as compared to the system characterized by 10^4 trehalose molecules per RC complex. These considerations provide a reasonable explanation for the effect of the trehalose/RC molar ration on the kinetics of $P^+Q_A^-$ recombination (Fig.7.4). We expect, for instance, that in the "softened" matrix (molar ratio equal to $5 \cdot 10^3$) a larger dehydration, hardening the less extended trehalose matrix interposed between RCs, is necessary to attain the maximal hampering of the RC dynamics, reached already under more hydrated conditions in matrices characterized by a lower "density" of the incorporated protein complexes (i.e. at a molar ratio equal to 10^4).

The much slower (and incomplete) equilibration observed when using the isopiestic method to dehydrate RC-trehalose matrices with a molar ratio equal to 10^4, as compared to $5 \cdot 10^3$, can also be qualitatively understood in the light of the above arguments; we expect, in fact, that in the softer matrix (lower sugar/protein), diffusion of water from the less exposed regions of the matrix, and particularly from the protein-matrix interface, will be favoured by the less inhibited overall dynamics of the trehalose-RC matrix. In the "harder" system, moreover, the water molecules segregated at the surface of the RC complex, will have to cross a thicker (and "harder") trehalose matrix in order to leave the system during the dehydration process.

The values calculated for the geometrical parameters of the RC-trehalose matrix, as a function of the sugar/protein molar ratio can also help to rationalize the results of thermal denaturation assays performed at 44 °C, for different molar ratios (Fig.7.6 and 7.7). The main conclusion of these measurements was that for values of the trehalose/RC ratios larger than 200 no significant thermal denaturation takes place even over the long time-scale explored (about 5 days). Upon decreasing the sugar/protein ratio below this threshold, thermal denaturation involves a progressively larger fraction of the RC population and a progressively faster denaturation kinetics is observed. As already mentioned in section 7.1.3 we ascribe the extraordinary ability of the trehalose matrices to protect the RC against thermal denaturation to the extremely tight coupling between the dynamics of the embedded RC and the dynamics of the solid trehalose matrix. This tight dynamical "slaving" (Frauenfelder, 2009) results in a strong inhibition of the RC conformational dynamics which governs the loss of the protein-cofactor native structure, thus preventing for long time thermal denaturation even at high temperatures.

This scenario appears to be consistent with the observation of a threshold in the sugar/protein ratio, below which the protective effect of the trehalose matrix becomes

ineffective. We expect, in fact, that the inhibition of the RC protein dynamics involved in thermal denaturation is a collective effect, which requires a minimum coating of the RC complex surface by trehalose molecules. According to the *anchorage hypothesis* (see par.1.5) inhibition of the RC dynamics will require in particular the development, upon dehydration, of a sufficiently extended network of multiple H bonds, involving simultaneously surface residues of the protein, water molecules at the water matrix interface, and trehalose molecules of the matrix. Below a critical number of trehalose molecules per RC this matrix effect will clearly vanish, since the H bond network will collapse. In spite of the crude assumptions made, the geometric parameters of Table 7.1 are consistent with this model, and provide some additional insight into the mechanism of inhibition of the RC dynamics. We expect that a discontinuity will occur in the H bond network which locks the surface of the RC complex when the trehalose coating of the surface starts to be incomplete. In terms of the geometrical representation of Table 7.1, this threshold is determined very roughly by a trehalose matrix thickness comparable to the dimension of a single trehalose molecule. From the volume calculated for the trehalose molecule, used in Table 7.1, $V_{trehalose} \approx 278$ Å^3 a diameter of the trehalose molecule of approximately 8 Å is easily calculated in the spherical approximation. It can be suggested, therefore that, this is the approximate thickness of a continuous monolayer of trehalose molecules coating the the RC-LDAO complex. From the data of Table 7.1, we see that the continuity of such a minimum trehalose coating is lost for disaccharide/protein molar ratios lower than 500 (which corresponds to a trehalose matrix thickness equal to 8 Å). This conclusion agrees very well with the experimental results presented in Figure 7.6 and 7.7, showing that below this threshold the bacteriochlorin cofactors of the RC start to lose their native structure upon prolonged incubation at 44 °C.

The systematically lower sensitivity of the 800 nm band (i.e. the lower propensity of the monomeric bacteriochlorophyll cofactors to undergo thermally induced denaturation) is probably due to the localization of their binding pockets, which are deeply buried inside the RC-detergent complex. We tentatively propose that the alteration of the local environment of these buried cofactors requires a more complete unfolding of the RC protein, as compared to the more exposed bacteriochlorophyll dimer P.

Finally, the comparison of the thermal denaturation assays performed at controlled relative humidity on a RC-LDAO film and on a RC-trehalose glassy sample

characterized by $5 \cdot 10^3$ trehalose molecules per RC (see Fig.7.5) deserves some comments. Both systems have been equilibrated in the presence of a saturated LiCl solution, i.e. at a relative humidity r =11%. As discussed in the last part of section 6.2.2 the kinetic analysis of $P^+Q_A^-$ recombination after a laser pulse showed that the extensive dehydration of RC-LDAO films and RC-trehalose glasses results in a comparable inhibition of RC dynamics over the time scale (0.1 s) of this electron transfer process (see Fig.7.4, Fig.6.9 and Table 6.3). The results of thermal denaturation assays reveal however a quite different behaviour in these two systems: while in the dehydrated trehalose glassy matrix, the RC preserves its structural and functional integrity even following several days of incubation at 44 °C, in the dehydrated RC-LDAO film the protein-pigment complex undergoes an essentially complete denaturation after about 5 hours of incubation at the same temperature.

This observation leads to the conclusion that the dynamical constraints which limit the RC dynamics in the two dehydrated systems are different and affect differently dynamics which involve different time- and space- scales. Thermal denaturation, in particular, is expected to be governed by large-scale dynamics, while the stabilization of the primary charge separated state $P^+Q_A^-$ is supposed to be coupled to a faster, small scale dynamics, although is structural basis is still debated (see par.1.4). We have already discussed at length in section 6.2.2 the different molecular mechanisms which, according to our view, lead to a comparable inhibition of the RC dynamics coupled to charge recombination in dehydrated trehalose glasses and RC-films. In the frame of the unified model of protein dynamics recently proposed by Frauenfelder (Frauenfelder, 2009) we have assigned the conformational relaxation which stabilizes the primary charge separated state, as well as the fast RC fluctuations among lower-tier conformational substates, to the so-called β-slaved processes, which are dynamically coupled to the fluctuations of the hydration shell of the protein complex. On this basis, we have proposed that in the two systems inhibition of these RC dynamics are caused respectively by a substantial depletion of the protein hydration shell (RC films) and by a dramatic reduction in the dynamics of the residual water molecules belonging to the protein hydration shell (trehalose-RC glasses).

According to the Frauenfelder unified model we should expect that dehydration of the RC complex, even in the absence of the trehalose matrix, inhibit the protein dynamics responsible for thermal denaturation, since large scale conformational changes are predicted to be blocked in extensively dehydrated systems. Indeed, our

thermal denaturation assays in dehydrated RC-LDAO films show that loss of the native structure occur over a time scale of hours. It appears therefore that the denaturation process is tremendously slowed down in dehydrated RC films as compared to solution, where a complete loss of the RC tertiary structure occurs over the time scale of minutes (Palazzo, 2010). The fact that in dehydrated trehalose glasses, under the same conditions, RC denaturation is totally prevented, at least over a time scale of a few days, shows that embedding the RC into the trehalose glasses totally suppresses the residual degree of motional freedom which in RC films allow at 44 °C a slow denaturation process. This observation further supports the notion that at low water content an extremely tight structural and dynamical coupling is set up between the protein and the trehalose glassy matrix, which impairs severely specific protein dynamics occurring over time-scales which differ by orders of magnitude.

8. THE KINETICS OF $P^+Q_A^-$ RECOMBINATION FOLLOWING CONTINUOUS ILLUMINATION IN DEHYDRATED RC FILMS AND RC-TREHALOSE GLASSES

In the previous chapter it has been shown that the isopiestic method allows an efficient control of the hydration level not only in RC-LDAO films (see chapter 6 and Malferrari, 2011), but also in α,α-trehalose/RC sugar glassy matrices characterized by a sugar/RC molar ratio equal to $5 \cdot 10^3$ (see par.7.1.1 and 7.1.2). Although a comparable inhibition of the RC dynamics probed by the kinetics of $P^+Q_A^-$ recombination after a laser pulse is observed in the two system under appropriate dehydration levels, the results discussed in the previous chapter, and in particular the effects of the sugar/protein ratio on the kinetics of $P^+Q_A^-$ recombination as a function of hydration, indicate that in RC-trehalose matrices protein-water-trehalose interactions play a critical role in the inhibition of the RC dynamics, as postulated by the *anchorage model* (see par.1.5). At variance, in dehydrated RC films, the inhibition of the RC dynamics which stabilizes the $P^+Q_A^-$ state is drawn back to the depletion of the hydration shell of the protein complex (see par.6.2.2). In both systems the RC dynamics coupled to the electron transfer process is "slaved" to the dynamics of the hydration shell, which is however regulated by different mechanisms and interactions in RC films and RC-trehalose glasses. The results of the previous chapter have also shown that the RC dynamics associated to thermal denaturation of the protein complex differ significantly in dehydrated RC-trehalose matrices and in RC films. In the latter system loss of the native structure occurs on the time scale of hours, while in the former one no thermal denaturation is seen for at least several days at 44 °C. This observation suggests that the presence of trehalose in the amorphous matrix gives rise to stronger structural constraints which impair more effectively the RC dynamics.

In order to obtain further insights into the different dynamical behaviour of dehydrated RC films and RC-trehalose glasses, we examine in this chapter the kinetics of $P^+Q_A^-$ recombination following periods of intense, continuous illuminations. Previous studies (Francia, 2004b; Cordone, 2005) have in fact demonstrated that when dehydrated RC-trehalose glassy matrix characterized by a strong RC dynamics inhibition are subjected to continuous, bright excitation of progressively longer duration, the kinetics of $P^+Q_A^-$ recombination following the photoexcitation becomes

progressively slower and less distributed, i.e. more similar to the one measured in solution. This partial recovery has been taken to indicate that following a sufficiently long photoexcitation of the system, the inhibition of the RC dynamics stabilizing the primary charge separated state is partially (and temporarily) removed (Francia, 2004b; Cordone, 2005). As outlined in par.1.6, similar effects, induced by prolonged, continuous photoexcitation in RC-trehalose matrices, have been observed also in relation with the conformational gating mechanism governing the electron transfer from Q_A^- to Q_B (Francia, 2003). These continuous illumination effects were interpreted by proposing that the persistence of the electric field produced by the $P^+Q_A^-$ charge separated state causes the continuous attempts of the protein to undergo dielectric conformational relaxation, most likely resulting in a temporary and partial disruption of the H bond network which, in the *dark-adapted* system, strongly inhibits any RC dynamics. As a consequence, following a sufficiently long photoexcitation, the relaxation from the *dark-adapted* to the *light-adapted* conformation can take place in a fraction of the RC population. By comparing the kinetics of $P^+Q_A^-$ recombination in dehydrated RC films and in RC-trehalose matrices after continuous illumination we have found that only in the former system a complete recovery of the kinetics observed in solution can be observed. This finding further supports the conclusion that in the dehydrated RC film residual degrees of motional freedom are present, which, at variance, are completely suppressed in the RC-trehalose matrix.

8.1 Results.

Figure 8.1 shows $P^+Q_A^-$ charge recombination kinetics following a 7 ns laser pulse, measured in a RC-trehalose glassy matrix characterized by a trehalose/RC ratio equal to $5 \cdot 10^3$ (Fig.8.1 A, black trace) and in RCs embedded in RC-LDAO films (Fig.8.1B, black trace), both equilibrated at a relative humidity r =11%. Kinetic traces have been fitted to a single power law (eq.1.2), except for the trace acquired in the RC film, following a laser pulse, which showed the presence of a second, additional much faster kinetic phase (see section 6.1.3), and was fitted to the sum of two power laws (eq.6.4). The amplitude of the fast phase accounted for 40% of the total decay. As discussed in section 6.2.2 the faster decay phase already observed in extensively dried RC films can be attributed to RCs in which the geometry of the $P^+Q_A^-$ radical pair and/or the energetics of charge recombination have been substantially altered,

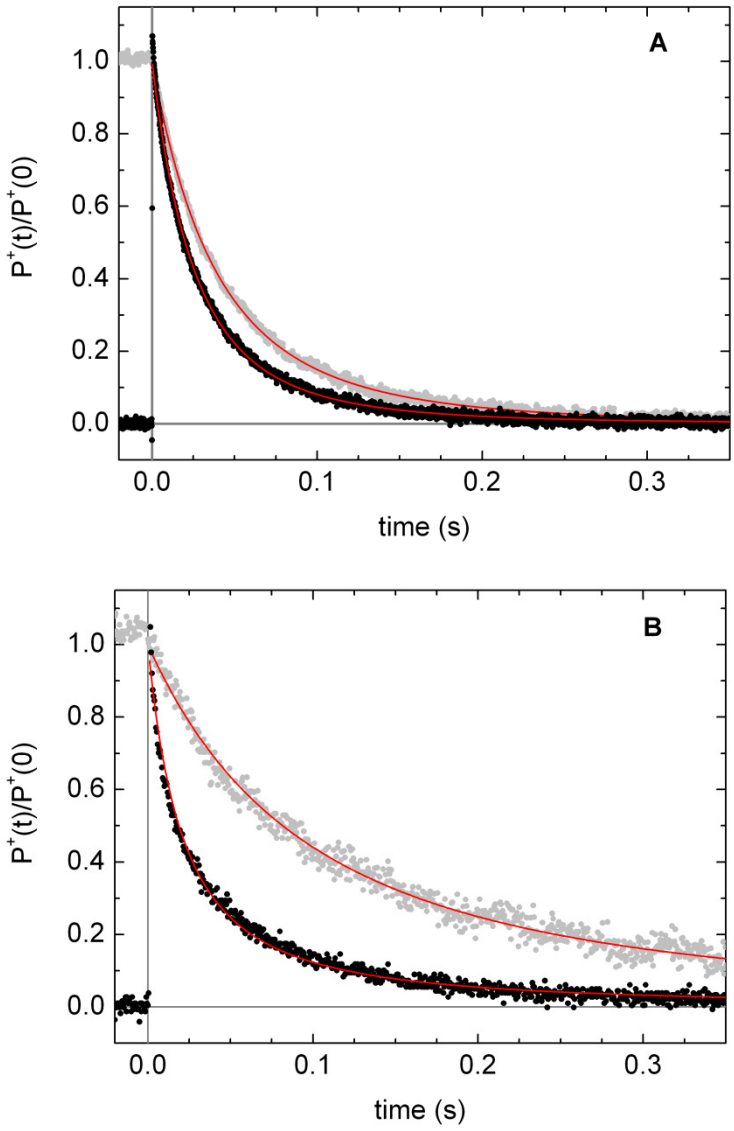

Figure 8.1
$P^+Q_A^-$ charge recombination kinetics following a laser pulse (black traces) and 20 s of continuous photoexcitation (grey traces) in a RC-trehalose glassy matrix characterized by a trehalose/RC molar ratio equal to $5 \cdot 10^3$ (A) and a RC-LDAO film (B), both equilibrated at *r* =11%. The residual water content of the RC-trehalose matrix and of the RC films was 2400 H_2O/RC and 950 H_2O/RC, respectively. Continuous red lines represent the best fit of the $P^+Q_A^-$ decay to the sum of two power laws (eq.6.4) in the case of the RC-LDAO film photoexcited by a laser pulse and to a single power law (eq.1.2) for all the other traces. Values of the obtained kinetic parameters are listed in the following (the corresponding confidence intervals within two standard deviations are given in brackets). For the RC-trehalose glassy sample (panel A): laser pulse, <k> = 38.5 (38.20, 38.90) s^{-1}, σ = 21.65 (21.24, 22.02) s^{-1}; 20 s continuous illumination, <k> = 25.40 (25.23, 25.61) s^{-1}, σ = 13.74 (13.51, 13.97) s^{-1}. For the RC-LDAO film (panel B): laser pulse,<k_F> = 1569 (568, 3964) s^{-1}, σ_F = 1505 (398, 5458) s^{-1}, <k_S> = 38.75 (35.62, 42.15) s^{-1}, σ_S = 29.84 (24.19, 35.21) s^{-1}; 20 s continuous illumination, <k> = 10.22 (9.97, 10.43) s^{-1}, σ = 7.39 (7.00, 7.78) s^{-1}.

presumably due to the removal of water molecules bound inside the RC protein. This phase, therefore, will not be further considered in the present analysis.

In RCs embedded in the trehalose matrix, best fitting of the kinetics recorded after the laser pulse yields <k> ≈ 39 s^{-1} and σ ≈ 22 s^{-1} (Fig.8.1, panel A); the same values, within the experimental error) have been obtained for the slow kinetic component in the RC-LDAO film, i.e. <k> ≈ 38 s^{-1} and σ ≈ 26 s^{-1} (Fig.8.1, panel B). From the essentially coincident values of the kinetic parameters, we infer that when the two systems are dehydrated by equilibrating them with an ambient relative humidity *r* =11% the RC experiences, over the time scale of the charge recombination process, a comparable protein dynamics inhibition.

As shown in Figure 8.1 (grey traces) when the $P^+Q_A^-$ decay is recorded after 20 s of continuous photoexcitation (for details on the illumination source see par.3.3) in both the RC-LDAO film and the RC-trehalose glassy matrix the recombination kinetics is considerably slowed down, as compared to the one following the laser pulse excitation. In the case of the RC-trehalose matrix the average rate constant <k> and the distribution width σ decrease to 25 s^{-1} and 14 s^{-1} respectively. Quite remarkably a much bigger effect is observed in the RC films, where <k> and σ, following continuous illumination, decrease to 10 s^{-1} and 7 s^{-1} respectively. We notice that the value of <k> obtained after continuous illumination coincides with that of $P^+Q_A^-$ recombination in solution (see figure caption of Fig.4.1 and par.4.1.1). It appears therefore that, in the RC film, continuous photoexcitation fully restores the ability of the RC to undergo the conformational relaxation which stabilizes the primary charge separated scale, as probed on the time scale of this electron transfer process.

Fig.8.2 shows the dependence of <k> (panel A) and of σ (panel B), determined from the measured $P^+Q_A^-$ recombination kinetics (see Fig.8.1), upon the duration of photoexcitation over a time range which extends from that of the laser pulse ($7 \cdot 10^{-9}$ s) to 100 s. In the RC-trehalose matrix equilibrated at *r* =11% (purple symbols) both kinetic parameters decrease progressively upon increasing the photoexcitation time period. The effect saturates at a photoexcitation time of about 100 ms. As observed above, even for the longer continuous illumination times the <k> and σ values are markedly larger than the one measured in solution (see figure caption of Fig.4.1 and par.4.1.1). At variance, in the RC-LDAO film equilibrated at the same relative humidity *r* =11%, <k> and σ values decrease more steeply than in the RC-trehalose matrix, and

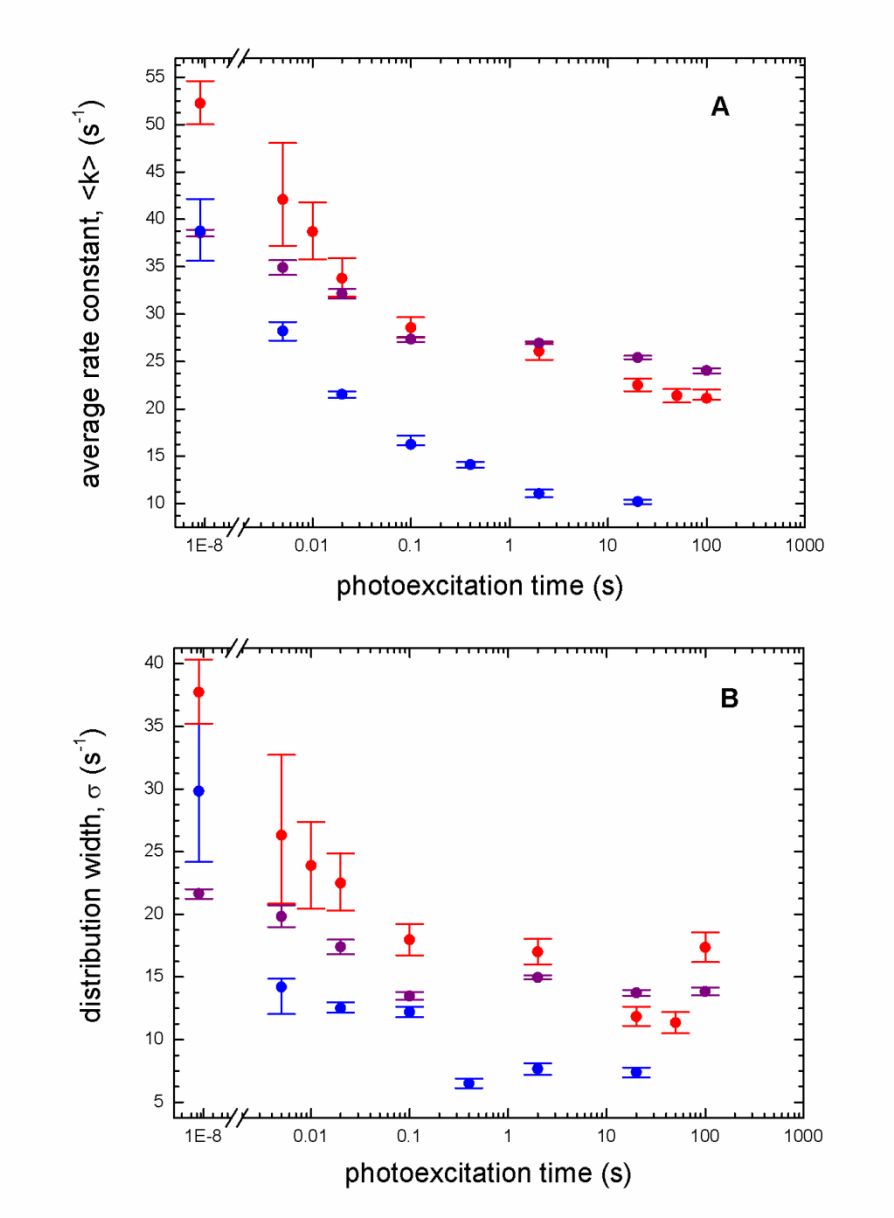

Figure 8.2
The dependence of the average rate constant, <k> (panel A), and of the distribution width, σ (panel B) upon the duration of photoexcitation in the RC-LDAO film at *r* =11% (blue circles) and in the α,α-trehalose/RC wt 2.4.1 glassy matrix, equilibrated at *r* =11% (purple circles) and at *r* =3% (red circles). Kinetic analysis was performed as illustrated in Fig.8.1. The parameters shown in the case of the RC film photoexcited by the laser pulse refer to the dominating slow kinetic phase. Vertical bars represent the calculated confidence intervals within two standard deviations.

significant changes are observed at longer illumination times, i.e. up to 2 s. Furthermore, for such durations of photoexcitation, the average rate constant, <k>, has decreased to values of about 10 s^{-1}, i.e. to the value measured in solution samples (see Fig.4.1 and Fig.4.2 for kinetic data in solution wt 2.4.1 RCs). The different response to continuous illumination of RC-trehalose glasses and of RC films indicates that in the former system the permanence of the charged separated state for about 100 ms only partially restores the ability of the RC to relax from the dark-adapted to the light-adapted conformation. On the contrary, in the absence of trehalose, i.e. in RC films, a prolonged (1 s) exposure of the RC to the electric field generated by the $P^+Q_A^-$ state allows a complete stabilization of the primary charge separated state. Interestingly, under these condition, the exponential character of the charge recombination process is not fully restored, also in RC films: the rate distribution width, σ, in fact, is significantly decreased upon increasing to 1 s the duration of continuous illumination, but, even at the longest photoexcitation times, level at about 7 s^{-1}, i.e. well above the values measured in solution. This suggests that the interconversion among lower tier conformational substates remains slower than in solution even when photoexcitation is attained continuously for several seconds.

The kinetics of $P^+Q_A^-$ recombination in the RC-trehalose glass has been studied as a function of the photoexcitation also under more dehydrating conditions, i.e. following equilibration at r =3%. The results are shown in Fig, 8.2 with red symbols. The residual water content of the RC-trehalose glass, when equilibrated at r =11% and at r =3% was 0.48 and 0.07 water per trehalose molecule, respectively. In the matrix equilibrated at r =3%, the analysis of $P^+Q_A^-$ recombination kinetics following a laser pulse yields <k> = 52 s^{-1}, σ = 38 s^{-1} (as compared to <k> = 39 s^{-1}, σ = 22 s^{-1} in the same matrix equilibrated at r =11%), indicating a stronger inhibition of RC dynamics at r =3% as compared to r =11%. In spite of this, the effect of continuous illumination is quite similar to that observed in the less dehydrated matrix; in particular <k> and σ values decrease progressively upon increasing the photoexcitation time, and the same minimum values are attained. As observed in the matrix equilibrated at r =11%, also in the more dehydrated matrix, the maximal recovery is observed already following a 100 ms photoexcitation. The data obtained in the matrix equilibrated at r =3% confirm that in RC-trehalose matrix, at variance with dehydrated RC films, continuous illumination only partially reverts the inhibition of RC dynamics.

8.2 Discussion.

The results illustrated above show that the effects of the prolonged illumination on RC purified from the wt 2.4.1 strain, embedded in dehydrated trehalose glassy samples, are consistent with what already published for RC purified from the carotenoid-less strain R26 (Francia, 2003; Francia, 2004b). Although the values of <k> and σ estimated from the $P^+Q_A^-$ recombination kinetics following a laser pulse are systematically larger in the carotenoid-containing RC as compared to the carotenoid-less one (see chapter 4, Fig.4.1 and 4.2), upon continuous photoexcitation a comparable fractional decrease in these kinetic parameters is observed. Most importantly in both RC types the slowing down of the kinetics occurs over the same range of photoexcitation duration (i.e. between 7 ns and 100 s), and the minimum values of <k> and σ reached are still consiberably higher than the ones observed in solution RCs. These minimum values coincide in the RC-trehalose matrix equilibrated at a relative humidity equal to 11% or 3%, indicating that in both cases the inhibition of the RC relaxation which stabilizes the charge separated state is only partially removed following prolonged continuous illumination.

In the frame of the *anchorage model* (par.1.5) the simplest interpretation of the continuous photoexcitation effects is that, during the continuous illumination period, the RC protein is continuously exposed to the electric field generated by charge separation and, in its continuous attempts to relax to the *light-adapted* conformation, perturbs the hydrogen bond network which connects protein surface residues to the trehalose matrix through residual water molecule at the protein-matrix interface. This perturbation seems to be able to disrupt partially the H-bond network which inhibits the RC dynamics. Following the partial collapse of the H bond network which tightly locks the surface of the RC complex to the sugar matrix, the RC protein regains some degrees of motional freedom and, during the continuous illumination period, undergoes a partial relaxation towards the *light-adapted* state. The $P^+Q_A^-$ kinetics recorded after a sufficiently long photoexcitation is therefore slower than that observed after a ns laser pulse, as a consequence of the partial energetic stabilization of the charge separated state. Interestingly, the partial disruption of the H bond network appears to be fully reversible in the dark. In fact, when a continuous photoexcitation kinetic measurement is followed by a laser-flash kinetic measurement, after a short (about 1 minute) dark adaptation, a fast $P^+Q_A^-$ decay is observed, characterized by the maximal <k> and σ values which are normally recorded following the laser pulse in dark adapted samples. We have not

studied systematically the kinetics of the dark adaptation after continuous illumination periods, but it is clear from the timing of our measurements that no hysteresis is observed in the effects of prolonged illumination (at least up to 100 s) when dark adaptation of about 1 minute is allowed between successive measurements. We infer that after the continuous photoexcitation and the decay of the $P^+Q_A^-$ state, the tight network of H bonds is re-constructed during a short dark adaptation.

The interpretation of continuous illumination effects described above is consistent with the finding that, following continuous photoexcitation, the $P^+Q_A^-$ recombination kinetics is not only slowed down, but also becomes less distributed in rate (i.e. also the value of σ decreases. This suggests that the partial disruption of the H bond network which limits the RC relaxation also allows, on the time scale of charge recombination, thermal fluctuations among some of the low tier conformational substates of the protein, thus producing a partial averaging of the kinetic heterogeneity observable after a laser flash.

The proposed interpretation is in line with the results of flash-photolysis experiments performed in dried trehalose-coated carboxy-myoglobin (MbCO) samples (Abbruzzetti, 2005). In this system, preillumination with continuous light increases the diffusion of CO from the distal to the proximal heme side. In analogy with what previously observed in RCs (Francia, 2004a; Francia, 2003), this effect has been taken as reflecting a decoupling of the protein internal degrees of freedom from those of the external water-sugar matrix (Abbruzzetti, 2005). Evidence of a conformational relaxation induced by continuous illumination at temperatures lower than 160 K had been previously reported in myoglobin (Chu, 1995).

The results shown in Figure 8.2 depict a very different scenario for the effects of prolonged illumination on dehydrated RC-LDAO films equilibrated at r =11% (blue symbols). In this system, in fact, following a 2 s period of continuous photoexcitation the value of <k> decreases to the one (<k> $\approx$ 10 s^{-1}) observed in solution RC samples, indicating that the inhibition of the RC relaxation which stabilizes the $P^+Q_A^-$ state (*light-adapted* conformation) is *completely* removed. In section 6.2.2 we have discussed the inhibition of RC dynamics caused by extensive dehydration (RC films) in the frame of the unified model of protein dynamics proposed by Frauenfelder (Frauenfelder, 2009). The results of our high-field EPR studies (chapter 5) are consistent with the notion that the RC dielectric relaxation, as well as fluctuations among lower tier conformational substates, are β-slaved processes (section.5.2, see also section.6.2.2), dynamically

coupled to the thermal fluctuations of the water molecules which form the hydration shell of the protein, strongly interacting with its surface groups (see par.1.2). If this is the case, we expect that, as indeed probed by the kinetics of $P^+Q_A^-$ recombination, a progressive removal of the hydration shell of the RC-detergent complex leads to a drastic slowing of the considered RC dynamics. This dynamics will appear essentially "frozen" during the time scale of charge recombination (0.1 s), giving rise to fast and strongly distributed recombination kinetics after a laser-flash excitation. The fact that the inhibition of the RC relaxation from the *dark-adapted* to the *light-adapted* conformation appears to be *totally* removed after a sufficiently long (2 s) period of continuous photoexcitation, suggests that, in dehydrated RC films, this conformational dynamics is not totally suppressed, i.e. completely blocked, but only slowed by orders of magnitude, as compared to RC solutions. When the system is photoexcited by a laser pulse (10^{-9} s) the slowed conformational relaxation to the *light-adapted* state cannot occur, and a fast recombination is observed from the *dark-adapted*, unstabilized conformation. When however the RC is kept in the charge separated state for a much longer time (from 10^{-2} s to 1s) the slowed relaxation can occur to a progressively higher extent for increasing photoexcitation times. For sufficiently long photoexcitation times (2 s) the RC can completely relax to the light-adapted state, and, correspondingly, $P^+Q_A^-$ recombination can proceeds for the completely-stabilized, light-adapted conformation, exhibiting the slow kinetics measurable in solution samples. We do not exclude that also in the RC film an extensive dehydration leads to significant interactions between RC-detergent complexes, due to their close packing upon removal of the hydration layer, possibly mediated by the detergent micelle which surrounds the hydrophobic portion of the RC. These interactions may contribute to reduce the RC dynamics probed by the charge recombination kinetics, hampering in particular the interconversion between conformational substates. If this is the case, it is conceivable that the RC-detergent matrix formed upon dehydration is also perturbed during a prolonged illumination period, resulting in a higher internal mobility of the RC. This would explain why, following continuous photoexcitation, the kinetics becomes progressively less distributed in rate: the rate distribution width, σ, decreases from 30 s^{-1} for the kinetics measured after the laser pulse to about 8 s^{-1} following a 2 s period of continuous photoexcitation (Fig. 8.2, panel B). The latter value is still significantly larger than the one (about 2 s^{-1}) measured in solution, suggesting that the structural

heterogeneity of the RC population is not completely averaged over the time scale of charge recombination.

The different effects of continuous illumination on the charge recombination kinetics observed in RC films and in RC-trehalose matrices are in line with the results of thermal denaturation studies described in the previous chapter (section 7.1.3). They show in fact that also the large scale dynamics, though to be associated with loss of the RC native structure, are much less impaired in dehydrated RC films, as compared to RC-trehalose matrices. As a whole the data suggest that the different dynamical processes considered, i.e. thermal fluctuations among conformational substates, relaxation to the *light-adapted* state, and rearrangements of large protein domains at high temperature, are correlated. The results indicate that in general the RC retains a significantly higher internal mobility when dehydrated in the absence of sugar, being the different dynamics probed by electron transfer and by propensity to thermal denaturation more strongly inhibited when the RC complex is incorporated into trehalose glasses.

9. LIGHT-MINUS-DARK FTIR DIFFERENCE SPECTROSCOPY STUDIES ON HYDRATED AND DEHYDRATED RC FILMS

In chapter 4 it has been shown that the stabilization of the primary charged separated state, as probed by the kinetics of $P^+Q_A^-$ recombination after a laser pulse, is strongly affected by the hydration state of the RC. These results (see in particular par.6.1.3 and par.6.2.2) indicated that the conformational relaxation which stabilizes the $P^+Q_A^-$ state was dramatically hindered when removing water molecules from the protein hydration shell (Malferrari, 2011). On this basis, in order to better understand the molecular basis of this conformational relaxation, we have measured light-induced $P^+Q_A^-/PQ_A$ difference FTIR spectra of RC-LDAO films characterized by two well defined hydration levels, i.e. in samples equilibrated at a relative humidity r =76% and r =11% (see par.3.6 for more details on FTIR difference spectroscopy).

As already outlined in par.1.4, the molecular mechanism of the relaxation from the *light-* to the *dark-adapted* conformation is still debated and several different hypothesis have been proposed during the last decades. Recently, Iwata and colleagues (Iwata, 2009), on the basis of light induced FTIR Q_A^-/Q_A difference spectra of RC-LDAO films at r =98%, have suggested that water molecules, weakly hydrogen bonded to the RC, play a critical role in relaxation process. We thought to extend the analysis of Iwata and colleagues by comparing directly FTIR light-minus-dark difference spectra in hydrated and significantly dehydrated RC-LDAO films. We also aimed to investigate the correlation between RC and water FTIR bands affected by the hydration level and the extent of protein dynamics inhibition inferred from $P^+Q_A^-$ recombination kinetics.

At variance with the study by Iwata and co-workers (Iwata, 2009) who studied Q_A^-/Q_A difference spectra, we have examined $P^+Q_A^-/PQ_A$ difference spectra, because under our more dehydrated condition the photoxidized primary donor P^+ cannot be rapidly reduced by exogenously added redox agents, due to the impairment of diffusional processes. We notice that, although $P^+Q_A^-/PQ_A$ difference spectra with good signal-to-noise ratio are not easily obtained (due to the strongly absorbing contributions of P^+), these spectra provide in principle a more relevant information as compared to Q_A^-/Q_A difference spectra. In fact, the RC state which undergoes the dielectric relaxation under study is characterized by the $P^+Q_A^-$ radical pair, and the electric charge

on P^+ can induce specific conformational changes, probed by difference FTIR spectroscopy, which do not take place when only the semiquinone anion (Q_A^-) is present.

The light induced FTIR difference spectra presented in this chapter have been obtained during a stage in the laboratory of the *Institut de Biologie et Technologies de Saclay IBITeC-S-CEA*, in collaboration with Dr. Alberto Mezzetti and Dr. Winfried Leibl of the Group of Photocatalysis and Biohydrogen.

9.1 Results.

Previous studies (Mäntele, 1988; Bauscher, 1990; Nabedryk, 1990a; Breton, 1992) have shown that $P^+Q_A^-$ light-minus-dark difference spectra in the 5000-1000 cm^{-1} range contain a large number of vibrational bands, attributed to the bacteriochlorophylls of the P special pair, to the quinone in the Q_A site, to the peptide and to water molecules interacting with the RC. Dehydration of the RC films (from r =76% to r =11%) induces a number of changes in the differential $P^+Q_A^-/PQ_A$ spectra, which can be conveniently grouped according to their spectral region and are examined in detail in the following paragraphs.

9.1.1 The electronic band of P^+ around 2600 cm^{-1} and the continuum bands in the 2900-2200 cm^{-1} region.

Over the 5000-1000 cm^{-1} spectral range the biggest contribution to the differential light-dark spectrum is given by a broad band centred around 2600 cm^{-1} which is due to an electronic transition of P^+ (Breton, 1992; Iwaki, 2002). In RC-LDAO films equilibrated at r =76% the amplitude of the electronic band of P^+ is systematically larger than in films equilibrated at r =11% (not shown). From the amplitude of this light-induced band, in view of the comparable RC concentration and optical path of the samples (as evaluated from the area of the amide II band of the RC, measured in the dark) it appears that the extent of primary electron donor P steadily photo-oxidized under continuous photo-excitation is systematically lowered upon decreasing the hydration level of the system. This observation was confirmed by optical spectroscopy performed in parallel to the FTIR measurements (see below, par.9.1.5) which also indicated a much lower P photoxidation level under continuous illumination (cf. Fig.9.5A). This behaviour is consistent with the strong acceleration of flash induced $P^+Q_A^-$ charge recombination kinetics observed in RC-LDAO films upon dehydration

(see par. 9.1.5 and Fig.9.5B). In fact, since the steady level of photo-oxidized P is determined by the competition between light-induced primary charge separation and $P^+Q_A^-$ recombination, we expect that the faster charge recombination in the dehydrated system will result in a decreased amplitude of the electronic band of P.

As a consequence, to better compare the differential $P^+Q_A^-/PQ_A$ spectra measured at the two hydration levels, we have normalized them to the extent of photo-induced P^+, estimated from the amplitude of the differential bands at 1749/1739 cm^{-1} attributed to the 10a-ester C=O mode of the bacteriochlorophylls of the P special pair (Leonhard, 1993; Nabedryk, 1993) (see also par. 9.1.3); as a control of the consistency of this procedure, following normalization also the amplitude of the electronic band of P at the two values of *r* coincided within the experimental error.

On the top and on the lower wavenumber ridge of the electronic band, in the 2900-2200 cm^{-1} interval, a series of four smaller differential broad bands can be identified (Fig.9.1). Although over this wavenumber range the electronic P^+/P band accounts for about 90% of the total differential signal, three positive peaks (at 2818, 2709 and 2611 cm^{-1}) and a positive shoulder (2756 cm^{-1}) can be resolved, which appear to be in relation (also for their structure) with the bands detected in Q_A^-/Q_A spectra, characterized by peaks at 2818, 2756, 2709, and 2611 cm^{-1} (Iwata et al., 2009). The bands detected in the Q_A^-/Q_A spectrum were tentatively assigned to the electrostatic response, upon quinone photoreduction, of highly polarisable H-bonds located in the surroundings of the quinone acceptor molecules. This extended H-bond network has been proposed to involve aminoacidic residues and ordered water chains (Breton, 1998). A subsequent study has provided evidence that an unusually strong hydrogen bond between the N_π-H group of the His-M219 and the carbonyl of Q_A contributes substantially to this spectral region (Breton, 2007), accounting specifically for the peak at 2709 cm^{-1}. The possible contribution of protonated water molecules to the bands between 2820 and 2550 cm^{-1} has been recently questioned since this region of Q^-/Q spectra did not show any shift by ^{18}O water replacement (Iwata, 2009). These authors have suggested that the bands more likely originate from N-H stretches which form strong H-bonds, as His-M219. In line with this notion, in our $P^+Q_A^-/PQ_A$ spectra equilibrated at *r* =76% D_2O substitution causes a strong decrease or elimination of the bands, except for the one at 2818 cm^{-1} (Fig.9.1B), while H_2O^{18} replacement does not appear to cause any shift in the band peaks (Fig.9.1C). Also, the position and the

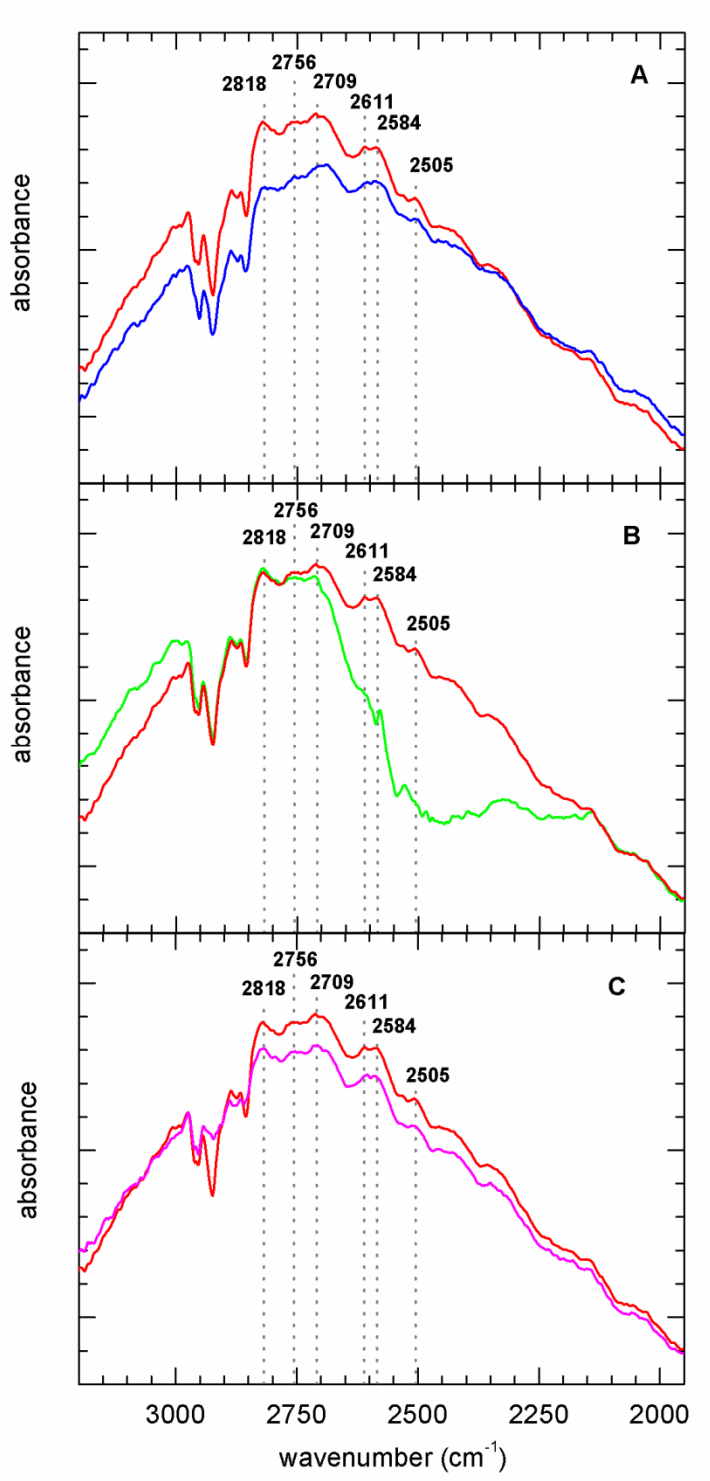

Figure 9.1
Light-induced $P^+Q_A^-/PQ_A$ difference FTIR spectra of RC-LDAO films in the 3200-2000 cm^{-1} region. Panel A compares the spectra recorded in films hydrated with H_2O at r =76% (red line) and r =11% (blue line). The effects of D_2O and H_2O^{18} substitution at r =76% are shown in panel B (green line) and C (magenta line), respectively. As a reference, the main peaks identified in the H_2O spectrum at r =76% are marked by grey dotted vertical lines (the interval in the ordinate axis between two major divisions corresponds to 0.5 absorbance unit).

amplitude of these broad bands do not change significantly when the films are equilibrated at a lower relative humidity, *r* =14% (Fig.9.1A).

Dehydration of the RC films (from *r* =76% to *r* =11%) induces a number of changes in the differential $P^+Q_A^-/PQ_A$ spectra, which can be conveniently grouped according to their spectral region and are examined in detail in the following paragraphs.

9.1.2 $P^+Q_A^-$ light-minus-dark difference spectra in the 3750-3550 cm^{-1} range.

The $P^+Q_A^-/PQ_A$ spectrum of RC-LDAO films hydrated at *r* =76% with H_2O is reported in Fig.9.2 (red line) in the spectral range where O-H vibrations due to weakly hydrogen bonded water molecules are expected to contribute (Iwata, 2009; Lórentz-Fonfria, 2008; Noguchi, 2002; Maréchal, 2011). In spite of the weakness of the differential signals in this region, two positive and one negative peaks can be identified: the two positive bands are centered at 3664 and 3628 cm^{-1} and the broader negative band peaks around 3587 cm^{-1}. Even if this region should be quite free of spectral contribution other than those mentioned above, in order to safely assign these bands to weakly hydrogen bonded water molecules, $P^+Q_A^-/PQ_A$ spectra were measured in RC-LDAO films hydrated at *r* =76% alternatively in D_2O and H_2O^{18}. Following substitution of water with D_2O and H_2O^{18} the peaks of the bands due to water molecules are expected to undergo a red-shift of about 900 cm^{-1} (Lappi, 2004) and ≈ 6-18 cm^{-1}, respectively (Lappi, 2004; Marechal, 2011). In principle the substitution of H_2O with H_2O^{18} provides by itself a definitive test for the assignment of these bands to water molecules. The D_2O substitution, causing a much larger bandshift, allows additionally a better estimate of the efficiency of the isotopic replacement procedure.

$P^+Q_A^-/PQ_A$ spectra of RC-LDAO films hydrated with D_2O and H_2O^{18}, compared to the one obtained in RC-LDAO films equilibrated at the same relative humidity (*r* =76%) in H_2O, are presented respectively in Figure 9.2A (green line) and 9.2B (magenta line). As a consequence of D_2O substitution the three peaks identified above completely disappear. In the H_2O^{18} substituted sample the peaks detected at 3664 and 3628 cm^{-1} in the H_2O hydrated sample shifts to 3652 and 3617 cm^{-1}, whereas the negative peak observed in H_2O at 3587 cm^{-1} disappears. The complete removal of the bands from the 3750-3550 cm^{-1} spectral range after D_2O substitution and the 12 and 11 cm^{-1} shifts of the peaks at 3664 and 3628 cm^{-1} observed upon H_2O^{18} substitution are fully consistent with the attribution of these two latter differential peaks to weakly

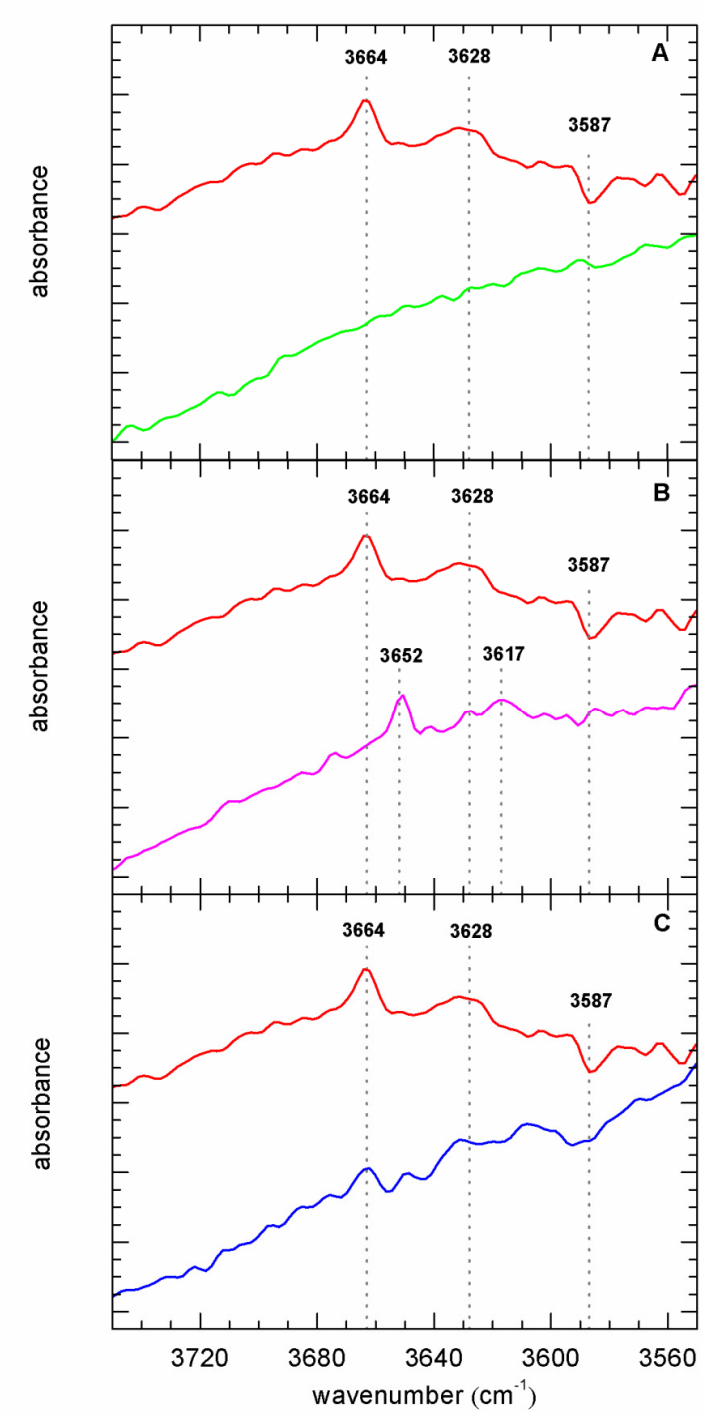

Figure 9.2
Light induced $P^+Q_A^-/PQ_A$ FTIR difference spectra of RC-LDAO films in the 3750-3550 cm^{-1} range. The spectrum recorded in films hydrated with H_2O at r =76% (red line) is compared with those measured following D_2O (panel A, green line) and H_2O^{18} substitution (panel B, magenta line). Panel C compares the spectrum of RC-LDAO films equilibrated with H_2O vapour at r =76% (red line) and r =11% (blue line). As a reference, the main peaks identified in the H_2O spectrum at r =76% are marked by grey dotted line. The interval between two major divisions of the y-axis corresponds to $1 \cdot 10^{-5}$ absorbance unit; spectra have been offset for visual clarity.

hydrogen bonded water molecules. In the H_2O^{18} hydrated samples, a small peak seems to be still present at 3628 cm^{-1}, but we are reluctant to interpret it as a residual of the band observed at this wavenumber in H_2O hydrated samples, being its amplitude in the range of the signal noise. Although the expected shift of the negative peak at 3587 cm^{-1} was not observed in the H_2O^{18} hydrated samples, the disappearance of the band from both the D_2O and H_2O^{18} substituted samples suggests a tentative assignment to weakly hydrogen bonded water molecules also for this negative band.

The disappearance of the peaks following D_2O substitution indicates that the replacement of the water molecules giving rise to the light-induced bands is very high (see. par.3.6; Malferrari, 2012 submitted).

Figure 9.2C compares the spectrum of the hydrated RC-LDAO film, equilibrated with water vapour at r =76% (red curve), with that of the partially dehydrated sample, equilibrated at r =11% in H_2O (blue curve). Due to the smaller extent of photoxidized RC in the dehydrated sample (see above) the signal to noise ratio is worst for the film equilibrated at r=11%. In spite of this it is clear that the three bands observed at 3664, 3628 and 3587 cm^{-1} in the hydrated sample are strongly reduced upon dehydration at r =11%. If residual bands are still present, their amplitude is comparable to the noise level. It appears therefore that, upon reducing the hydration of the RC-LDAO complex, the water molecules weakly hydrogen bonded to the RC which respond to the light-induced charge separation are either removed or unable to undergo the structural relaxations which give rise to the spectral changes observed in the hydrated samples.

9.1.3 $P^+Q_A^-$ light-minus-dark difference spectra in the 1800-1200 cm^{-1} range.

The $P^+Q_A^-/PQ_A$ difference spectrum in the 1800-1200 cm^{-1} range is shown in Figure 9.3A for RC-LDAO hydrated films, equilibrated with H_2O vapour at r =76%. This light induced spectrum has been extensively studied in hydrated RC films at temperatures around 250 K (Mäntele, 1988; Nabedryk, 1990a), and at 100 K (Nabedryk, 1990a). By comparing these differential spectra with the redox-induced infrared spectrum of bacteriochlorophyll-a cation formation (BChl-a^+/BChl-a) (Mäntele, 1988) and with the electrochemically-induced spectra of ubiquinone anion formation ($Q^{\bullet -}/Q$) (Bauscher, 1990) and of P^+/P (Leonhard, 1993), the assignment of many of the differential bands of this spectral interval was achieved. It is also clear from the literature cited above, and from Q_A^-/Q_A and Q_B^-/Q_B difference spectra (Breton, 1991a; Breton, 1991b), that in the $P^+Q_A^-/PQ_A$ differential spectrum over the 1800-1200 cm^{-1}

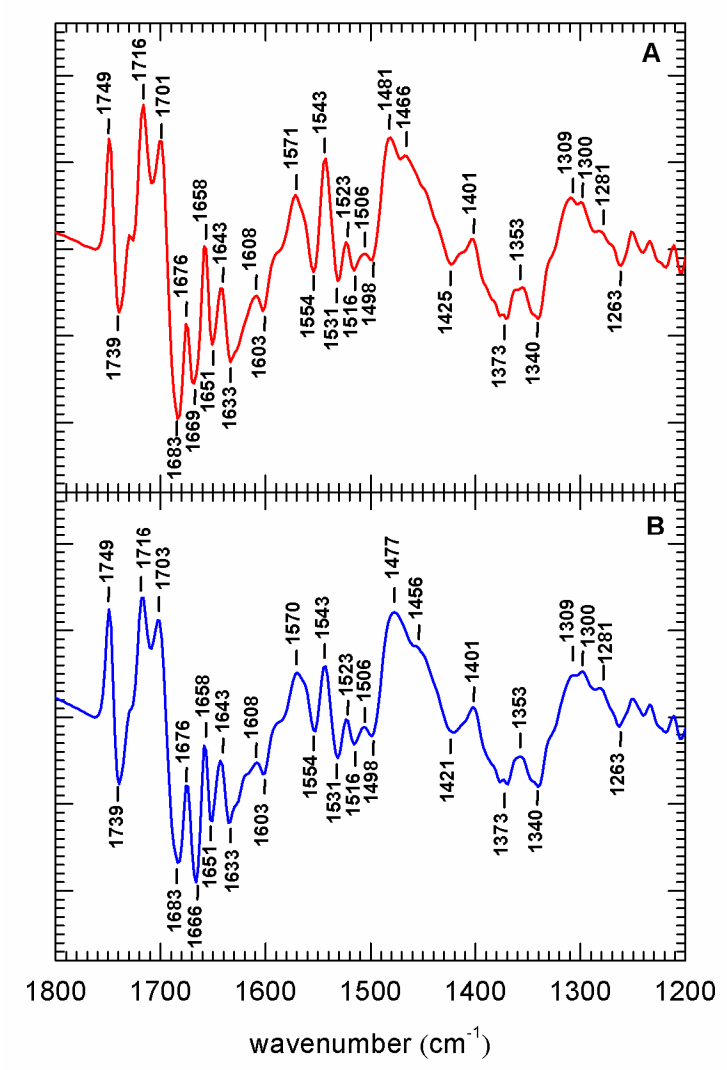

Figure 9.3
Light induced $P^+Q_A^-/PQ_A$ FTIR difference spectra in the 1800-1200 cm^{-1} range of RC-LDAO films equilibrated at a relative humidity r =76% (A) and r =11% (B) in the presence of H_2O vapour. The interval between two major divisions of the ordinate axis corresponds to $1 \cdot 10^{-5}$ absorbance units.

range the amplitudes of the light-induced bands associated with the primary donor P are much bigger than those related to the quinone.

Some of the differential bands in the 1760-1620 cm^{-1} carbonyl region have been assigned to C=O modes of the bacteriochlorophyll molecules of the P special pair. The bands at 1749/1739 cm^{-1} are associated to the 10a-ester C=O mode (Nabedryk, 1993), while the positive and negative peaks at 1716-1701/1683 cm^{-1} are considered to originate from the overlapping of the 9-keto C=O modes of the two bacteriochlophylls molecules P_L and P_M (Mäntele, 1988; Nabedryk, 1993). It was suggested that also the negative band at 1665 cm^{-1} (1669 cm^{-1} in our spectrum) arises from one keto C=O of P

and that the positive band at 1658 cm^{-1} originates from the acetyl C=O mode of P^+, although possible contributions of the quinone and of the protein to both bands were not excluded (Mäntele, 1988). On the basis of subsequent studies it was concluded that the negative peak at 1665 cm^{-1} is more probably due to a peptide C=O from a transmembrane helix in the environment of P (Nabedryk, 1992) or near the photoreduced bacteriopheophytin or Q_A^- (Maiti, 1993).

Although the negative peak at 1651 cm^{-1} lies in the spectral range where C=O modes of ubiquinone are expected (Bauscher, 1990), several independent observations (Bagley, 1990; Nabedryk, 1990a) have led to tentatively assign it to the peptide component of the RC, and the AlaM260 or the ThrM222 residues have been proposed as possible candidates (Nabedryk, 1990a).

The peak at 1603 cm^{-1} is the only peak in light-induced $P^+Q_A^-/PQ_A$ differential spectra that is assigned to Q_A. This peak (reported at 1604 cm^{-1} in the $P^+Q_A^-/PQ_A$ spectrum recorded in hydrated RCs at 100K (Breton, 1994a)) appears to be related to the 1601 cm^{-1} band observed in the Q_A^-/Q_A spectra, which has been associated to the 4-C=O of Q_A (Breton, 1994a; Brudler, 1994).

The presence in the light-induced spectrum of RC-LDAO films equilibrated with H_2O vapour at r =76% of four negative peaks, at 1669, 1651, 1633 and 1603 cm^{-1} (Figure 9.3A), is fully consistent with the assumption that, due to the presence of o-phenanthroline, we are observing the differential $P^+Q_A^-/PQ_A$ spectrum. As reported by Nabedryk et al. (Nabedryk, 1990a), in fact, these four peaks are a signature of the $P^+Q_A^-/PQ_A$ spectrum, being the $P^+Q_B^-/PQ_B$ spectrum characterized by only three peaks, at 1664, 1638 and 1618 cm^{-1} in this spectral interval. We conclude therefore that, even following continuous 20-s photoexcitation of the samples, electron transfer from Q_A^- to Q_B is fully inhibited in our samples. This is consistent with spectra recorded in the O-H vibration of weakly hydrogen bonded water, 3750-3550 cm^{-1} (Fig.9.2), which are also very similar to the Q_A^-/Q_A and quite distinct from the Q_B^-/Q_B difference spectra (Iwata, 2009). This point will be relevant when examining the kinetics of charge recombination after a 20-s period of continuous illumination, i.e. under the same photoexcitation conditions used in the acquisition of differential FTIR spectra (see par. 9.1.5 and 9.2).

In the spectral ranges from 1570 to 1498 cm^{-1} and from 1387 to 1340 cm^{-1}, positive and negative peaks have been assigned generally to the bacteriochlophylls of the P special pair (Mantel, 1988): the peaks at 1571, 1543, 1523, 1516 and 1498 cm^{-1}

were assigned to C=C and C-C modes, those at 1353 and 1340 cm^{-1} to C-N and C-H modes respectively.

The assignment of the two peaks at 1481 and 1466 cm^{-1}, on the broad positive band ranging from 1498 to 1425 cm^{-1}, seems not so straightforward, due to the presence in this spectral interval of both P and ubiquinone contributions. At first, on the basis of infrared differential redox-induced BChl-a^{+}/BChl-a spectra (Mäntele, 1988) and electrochemically-induced infrared $Q^{\bullet -}$/Q spectra (Bauscher, 1990), signals in this spectral interval were tentatively assigned to ubiquinone modes. Soon after, however, Leonhard and colleagues (Leonhard, 1993) showed that in the electrochemically-induced P^{+}/P differential infrared spectrum a big broad band ranging from 1496 to 1418 cm^{-1} with two peaks at 1474 and 1456 cm^{-1} was present. When considering the small amplitude of the differential bands due to Q_A^{-} and Q_B^{-} formation in light-induced Q_A^{-} /Q_A and Q_B^{-}/Q_B difference spectra (Breton, 1991a; Breton, 1991b), it seems reasonable to conclude that this interval includes contributions from both P and quinone modes, with the former prevailing on the latter. The attribution of the three large, structured bands in the 1580-1530, 1500-1430, and around 1290, mainly to the BChl dimer is also supported by the observation that these bands are absent (or very small) in the $P^{+}Q^{-}$/PQ spectra of heterodimer mutants from *Rb. capsulatus*, where the charge is located on a single BChl (Nabedryk, 1992). However, especially the 1480 cm^{-1} band contains also small contributions from the quinone anion C-O and C-C modes. In particular the positive 1466 cm^{-1} peak (in our spectrum) corresponds to the one of the main band of Q_A^{-}/Q_A spectra (Breton, 1994b), which comes predominantly from a C-O stretch semiquinone (Breton, 1994b; Brudler, 1994).

In order to examine the effects of dehydration, Figure 9.3B presents the correspondent $P^{+}Q_A^{-}$/PQ_A difference spectrum measured in RC-LDAO films, equilibrated with H_2O vapour at r =11%. A comparison with the spectrum of Figure 9.3A shows that the only changes occurring upon dehydration are: (i) a shift of the positive peak at 1701 cm^{-1} and of the negative one at 1669 cm^{-1} in the hydrated film to 1703 cm^{-1} and 1666 cm^{-1}, respectively; interestingly both peaks are attributed to the keto C=O mode of the P bacteriochlorophyll (Mäntele, 1988), and in particular to P_M (Nabedryk, 1993); (ii) a shift of the peaks at 1481 cm^{-1} and 1466 cm^{-1} at r =76% to 1477 cm^{-1} and 1456 cm^{-1}, respectively, at r =11%.

9.1.4 $P^+Q_A^-$ light-minus-dark difference spectra in the 3550-3150 cm^{-1} range.

In the spectral range between 3550 and 3150 cm^{-1} the spectra of protein films contain contributions arising from the stretching of OH groups of strongly hydrogen bonded water molecules or of lateral groups of amino acids residues, as serine, tyrosine and protonated carboxylic acids (Kandori, 2000; Lórenz-Fonfría, 2008), and from the stretching of hydrogen bonded NH groups of the protein (Hecht, 1956). Although studies of this spectral region have been performed in bacteriorhodopsin (Lórenz-Fonfría, 2008) and in the photoactive yellow protein from *Ectothiorhodospira halophyla* (Kandori, 2000), as far as we know, a systematic analysis of this interval in differential light-induced FTIR spectra of RC samples is still lacking.

In Figure 9.4A we show the differential light-induced spectrum measured in this spectral range on hydrated RC-LDAO films, equilibrated with H_2O at r =76%. We also report the light-induced $P^+Q_A^-/PQ_A$ difference spectra recorded in RC-LDAO samples hydrated with D_2O (Figure 9.4C) or H_2O^{18} (Figure 9.4D) at r =76%. The comparison between the spectrum obtained in the H_2O hydrated film and the ones after D_2O and H_2O^{18} substitution indicates that none of the numerous positive and negative bands detected in this spectral interval can be assigned to water molecules. In fact, none of the differential bands disappears after D_2O substitution (Figure 9.4C), with the only exception of the band peaking at 3483 cm^{-1} in the H_2O hydrated sample; however, after H_2O^{18} substitution, no clear shift of this peak is observed. This behaviour suggests that the peak at 3483 cm^{-1} is due to a NH or OH group of the peptide which undergoes deuterium exchange in D_2O. This agrees with the attribution suggested by Iwata and colleagues (Iwata, 2009) for the positive peak detected at 3487 cm^{-1} in the Q_A^-/Q_A differential spectrum of fully hydrated RC films. Interestingly this peak, observed at 3487 cm^{-1} in films equilibrated at r =98% (Iwata, 2009), shifts to 1483 cm^{-1} at r =76% and to 1481 cm^{-1} at r =11% (Fig.9.4B); similarly the negative peak detected at 3501 cm^{-1} in the Q_A^-/Q_A spectrum at r =98% (Iwata, 2009) moves to 3498 cm^{-1} at r =76% and to 3496 cm^{-1} in our $P^+Q_A^-/PQ_A$ spectra. This behaviour suggests a systematic shift of the negative and positive bands to lower wavenumbers upon dehydration of the RC complex. The NH or OH groups of the residues which originate presumably these bands are likely to be close to the Q_A cofactor, since the positive and negative peaks observed in $P^+Q_A^-/PQ_A$ are even more clearly detected in Q_A^-/Q_A spectra (Iwata, 2009).

The broad band peaking at 3417 cm^{-1} in the H_2O hydrated film moves to 3425 cm^{-1} in the D_2O hydrated samples. No shift of this band is observed after H_2O^{18}

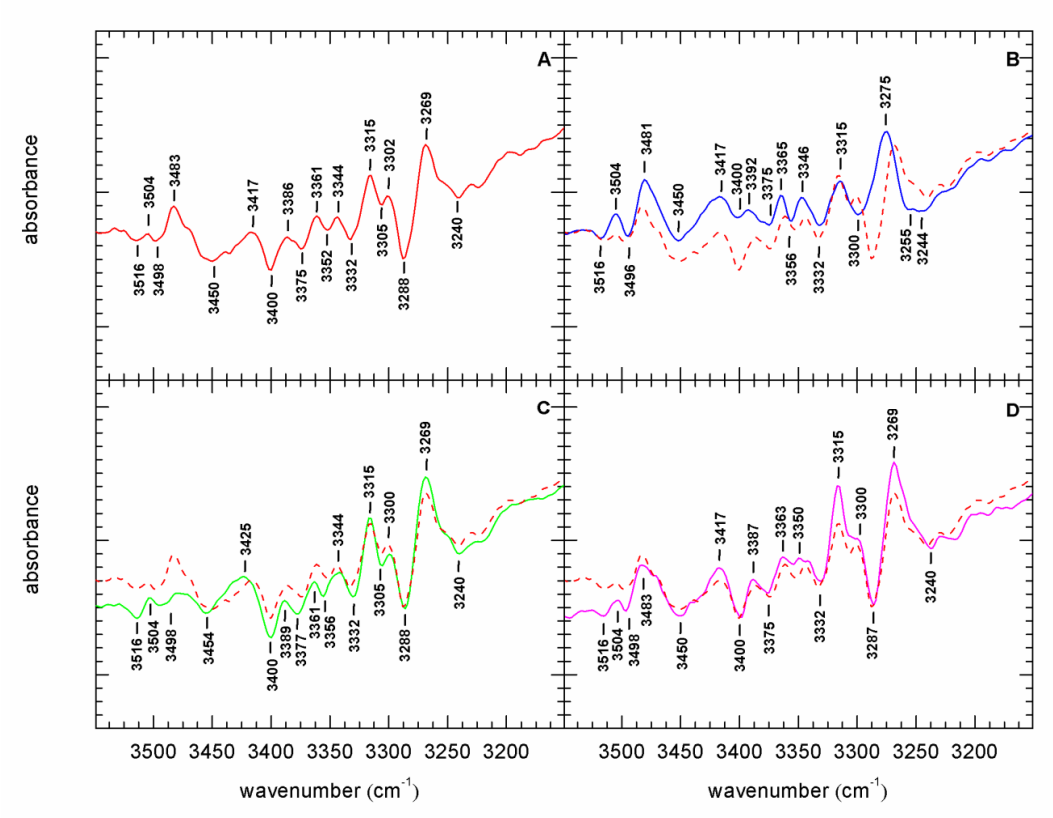

Figure 9.4
Light induced $P^+Q_A^-/PQ_A$ FTIR difference spectra measured in the 3550-3150 cm^{-1} range on RC-LDAO films hydrated with H_2O at a relative humidity *r* =76% (panel A, red line) and *r* =11% (panel B, blue line). The corresponding spectra recorded at *r* =76% after D_2O or H_2O^{18} substitution are shown in panel C (green line) and panel D (magenta line), respectively. For the sake of comparison the spectrum in panel A, measured at *r* =76% in H_2O, is also shown in panel B, C, and D with a dashed red line. The interval between two major divisions of the ordinate axis corresponds to $1 \cdot 10^{-5}$ absorbance units.

substitution. The same behaviour characterizes the peaks at 3386, 3375 and 3352 cm^{-1} in the H_2O hydrated sample, which also do not seem to change following H_2O^{18} substitution, and undergo small shift of 2-4 cm^{-1} to higher wavenumbers upon D_2O replacement. These observations preclude to ascribe the above bands to hydrogen bonded water.

The comparison between the hydrated (*r* =76%) and dehydrated (*r* =11%) RC-LDAO films (Figure 9.4B) evidences, besides the shift of the 3498 cm^{-1} band described above, additional significant alterations in the light-induced spectrum. Small (2-4 cm^{-1}), can be noticed for the peak at 3483 cm^{-1} and for the three peaks in the 3392-3342 cm^{-1} range. Much more prominent differences can be observed between 3300 and 3240 cm^{-1}. Over this spectral interval, while in the hydrated sample negative peaks appear at 3305, 3288 and 3240 cm^{-1} and positive ones at 3302 and 3269 cm^{-1}, in the dehydrated films a

large positive peak is detected at 3275 cm^{-1}, delimited by two negative peaks at 3300 and 3255 cm^{-1}. As no significant shift can be observed in this spectral region following D_2O and H_2O^{18} substitution (see above), these bands should originate from NH or OH stretching modes of RC amino acid residues which respond differently to photoexcitation in the hydrated (r =76%) and in the dehydrated (r =11%) RC-detergent complex.

In line with structural information (Katona, 2005) the latter observations point to the involvement of protein groups of the RC in conformational changes induced by a prolonged illumination of the RC. These conformational dynamics appear to be markedly affected by the hydration level of the RC-detergent complex, thus suggesting a tight dynamical coupling between the protein and its hydration shell (see Discussion, par. 9.2). Since, as outlined previously (see par.1.4), the kinetics of recombination of the light-induced $P^+Q_A^-$ state provides a sensitive probe of the RC internal dynamics and of the conformational relaxations which follow charge separation, we report in the following on the kinetics of this electron transfer process, analyzed under the same photoexcitation and hydration conditions employed in the FTIR measurements described above.

9.1.5 $P^+Q_A^-$ recombination kinetics in hydrated and dehydrated RC-LDAO films.

Figure 9.5A shows the absorbance changes at 422 nm induced by a 20 s photoexcitation of RC-LDAO films equilibrated with water vapour at relative humidity r =76% (red trace) and r =11% (blue trace). Absorbance changes at this wavelength are due to the redox changes of the P^+/P couple, and, to a minor extent, to those of Q^-/Q (Sloten, 1972). The signals monitor therefore the kinetics of $P^+Q_A^-$ formation upon photoexcitation and recombination in the dark. The amplitude of the light-induced signal (i.e. the fraction of the RC population which upon continuous illumination is maintained steadily in the $P^+Q_A^-$ charge separated state) is more than three times larger in the hydrated sample (r =76%) as compared to the dehydrated sample (r =11%). This behaviour is qualitatively consistent with the observation (Malferrari, 2011) that, following a laser pulse, the $P^+Q_A^-$ recombination process is strongly accelerated in dehydrated RC-detergent complexes. Since the steady level of charge separation under continuous photoexcitation is considered to be determined by the kinetic competition between the processes of charge separation and recombination (Gouscha, 2000; Andréasson, 2003), an acceleration of the latter is expected to result in a decreased

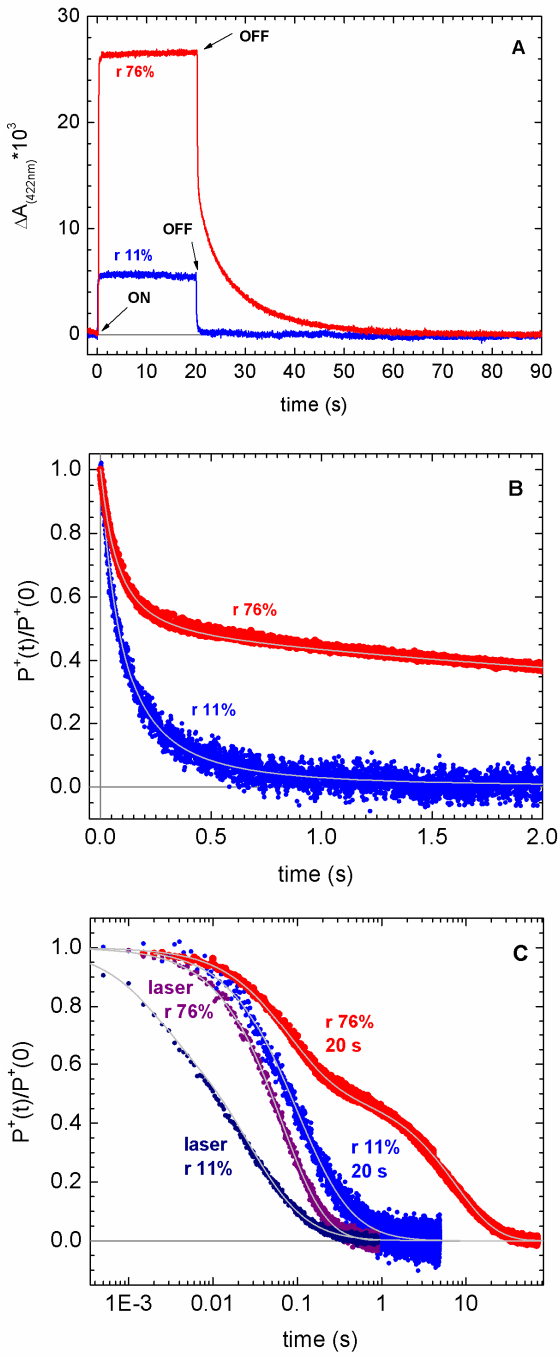

Figure 9.5
$P^+Q_A^-$ charge recombination kinetics in RC-LDAO films characterized by two different hydration levels, i.e. equilibrated with water vapour at relative humidity *r* =76% and *r*=11%. A. Time course of the absorbance change induced at 422 nm by a 20 s period of continuous illumination in the hydrated (*r* =76%, red trace) and dehydrated (*r* =11%, blue trace) RC film. B. Normalized kinetics of $P^+Q_A^-$ recombination obtained from the traces shown in panel A by expanding the time scale. The grey lines represent best fit to a single power law (eq.1.2) for the decay at *r* =11%, and to the sum of two power laws (eq.6.4) for the decay at *r* =76%. Values of the best fitting parameters are: at *r* =76% , $A_F = 0.51$, $\langle k_F \rangle = 13.0\ s^{-1}$, $\sigma_F = 8.4\ s^{-1}$, $\langle k_S \rangle = 0.13\ s^{-1}$, $\sigma_S = 4.9 \cdot 10^{-2}\ s^{-1}$; at *r* 11% , $\langle k \rangle = 10.2\ s^{-1}$, $\sigma = 7.4\ s^{-1}$. C. The normalized kinetics of $P^+Q_A^-$ recombination after a 20 s period of continuous photoexcitation (from panels A and B) are compared with the kinetics recorded after a 7 ns laser pulse in RC-LDAO films equilibrated at *r* =76% (purple trace) and *r* =11% (cyan trace). Best fit to a single power law of the decays after the laser pulse are plotted in grey and correspond to the following values of parameters: at *r* =76%, $\langle k \rangle = 15.2\ s^{-1}$, $\sigma = 7.0\ s^{-1}$; at *r* =11%, $\langle k \rangle = 38.8\ s^{-1}$, $\sigma = 29.8\ s^{-1}$.

steady $P^+Q_A^-$ signal observable in continuous light. The levels of $P^+Q_A^-$ optically detected in the hydrated and dehydrated films agree with those estimated from the FTIR electronic band of P (see par. 9.1.1).

From Figure 9.5A it also appears that, following a 20-s period of continuous illumination, the overall decay of the light-induced $P^+Q_A^-$ signal is dramatically slower in the hydrated RC film (r =76%) as compared to the dehydrated one (r =11%). In the latter sample the decay is unresolved over the time scale of seconds, while, at r =76%, about 10% of the photoxidized RCs are still in the charge separated state after a dark time of about 12 s. The charge separated state is therefore strongly stabilized in the hydrated RC-LDAO film as compared to the dehydrated sample.

A closer inspection of the decay kinetics (which are shown expanded in time and normalized to the maximal amplitude in Figure 9.5B) evidences that in the dehydrated sample the decay is essentially monophasic, with an half time of approximately 80 ms; at variance in the hydrated condition (r =76%) the recombination process is distinctly biphasic, including a fast phase comparable in rate to the decay observed in the dehydrated sample (r =11%) and an extremely slow kinetic phase, that accounts for at least half of the total amplitude, characterized by an half time of approximately 5 s.

Figure 9.5C compares, over a logarithmic time scale, the kinetics shown in panels A and B, recorded after prolonged, continuous illuminations, with $P^+Q_A^-$ recombination kinetics measured in the same RC films following a short (7 ns) laser pulse. As previously reported (see chapter 4; Malferrari, 2011) $P^+Q_A^-$ recombination after a laser pulse is significantly accelerated upon dehydration of the RC-detergent film. Furthermore, the non exponential character of the decay becomes more evident in the dehydrated film (at r =11%), which exhibits a recombination kinetics strongly distributed in rate (see Figure 9.5C).

In agreement with our previous results (see section 6.1.3 and 8.1.1) the trace recorded in the hydrated film fits accurately a single power law (eq.1.2), while a minor faster component (which requires an additional, second power law) is present in the dehydrated (r =11%) kinetics. The latter fast phase will not be further considered, since, as already discussed it reflects recombination in a minor fraction of the RC population which has undergone severe structural and/or energetic alterations. Best fits to $P^+Q_A^-$ recombination after a laser pulse are shown in Figure 9.5 C with grey continuous lines. In the case of the kinetics recorded at low hydration (r =11%) the kinetics parameters refer to the slow phase (see above). Upon dehydration the average rate constant

increases from <k>=15.2 s^{-1} (at *r* =76%) to <k>=38.8 s^{-1} (at *r* =11%); in parallel the width of the rate distribution also increases from σ = 7.0 s^{-1} (at *r* =76%) to σ = 29.8 s^{-1} (at *r* =11%). As summarized in the Introduction (par.1.4), these effects, which mimic at room temperature similar effects observed in water-glycerol RC solutions upon freezing the system at cryogenic temperatures (Kleinfeld, 1984; McMahon, 1998), can be taken to reflect a strong inhibition of the RC relaxation from the *dark-* to the *light-adapted* conformation as well as a dramatic hindering of the interconversion between RC conformational substates (McMahon, 1998; Palazzo, 2002; Francia, 2009).

Interestingly, the kinetics of $P^+Q_A^-$ recombination following prolonged, continuous illumination, differ substantially at both hydration levels from the corresponding ones measured after a short laser photoexcitation. The kinetics measured after continuous illumination in the RC film equilibrated at *r* =11% fit a single power law (eq.1.2), with <k>=10.2 s^{-1} and σ = 7.4 s^{-1}. It appears that, in agreement with what already observed (see section 8.1) and discussed (see section 8.2), the kinetic effects of dehydration observable after a laser flash have totally reverted following a long continuous photoexcitation, since the kinetics are even slower and less distributed in rate than the ones recorded after a laser pulse in the hydrated film, at *r* =76% (see Figure 9.5C). The kinetics observed after continuous light in the dehydrated film are comparable to those observed in a RC solution at room temperature (Fig. 4.1 and Fig. 4.3; Francia, 2009). In the hydrated film (*r* =76%) the recombination kinetics following continuous photoexcitation is also slowed down as a whole as compared to the one recorded at the same hydration after a laser pulse (see Figure 9.5 C). Furthermore, the $P^+Q_A^-$ kinetics after 20 s photoexcitation at *r* =76% is clearly biphasic, and has been fitted to the sum of two power laws (see eq.6.4).

The values of the obtained kinetic parameters (reported in the caption of Figure 9.5B) show that the kinetics of the fast phase, accounting for about 50% of the total decay, are comparable to those of the monophasic recombination measured at *r* =11% after 20 s photoexcitation. This result suggests that continuous illumination totally removes over the time scale of charge recombination the hindering of the RC conformational dynamics caused by dehydration, which is probed by $P^+Q_A^-$ decay kinetics after a short photoexcitation (see Discussion in par. 9.2, below). In addition, the appearance as a consequence of 20 s continuous illumination of a very slow kinetic phase, characterized by $<k_S>$= 0.13 s^{-1} and σ_S= $4.9 \cdot 10^{-2}$ s^{-1}, in RC-LDAO films at *r* =76%, indicates that in a significant fraction (about 50%) of the RC population the

primary charge separated state has undergone a dramatic stabilization as a result of the prolonged photoexcitation. In order to safely attribute the slow phase of the decay measured at 422 nm to a genuine $P^+Q_A^-$ recombination, excluding for instance side reactions which could re-oxidize the photo-reduced Q_A^-, leaving the photoxidized P^+ without a recombination partner, we have measured in parallel the kinetics of absorbance change at 450 nm. As outlined previously (see par.3.3 and par.6.1.3), at 450 nm and 422 nm both P^+ and Q_A^- contribute to the light-induced absorbance change. However, at 422 nm the relative contribution of P^+ dominates, with the spectral contribution of the semiquinone accounting for about 14% of the total. At 450 nm the relative contribution of Q^- increases to about 40% at the expense of that due to P^+ (Sloten, 1972). Since the same decay kinetics, also after a prolonged continuous illumination, have been observed at the two wavelengths in the hydrated RC film (data not shown), we attribute both kinetic phases, including the extremely slow one observed in the hydrated RC film, to $P^+Q_A^-$ recombination.

We recall that comparably slow kinetic phases of $P^+Q_A^-$ recombination have been observed in RC solution samples at room temperature following continuous photoexcitation periods longer than 5 minutes (Andréasson, 2003). Such a stabilization of the primary charge separated state, which resembles the one observed by us in the hydrated RC film, has been proposed to originate from slow structural changes of the RC protein which occur during continuous illumination (Andréasson, 2003; Katona, 2005).

In conclusion the kinetic analysis of $P^+Q_A^-$ recombination after prolonged continuous photoexcitation suggests a correlation between the light-induced FTIR spectral changes sensitive to the hydration state (par. 9.1.2-9.1.5) and the strong stabilization of the primary charge separated state which is observed after continuous illumination only in the hydrated RC film (see the next section).

9.2 Discussion.

The different role of water molecules, belonging to the protein hydration shell, to the bulk solvent or placed in the interior of the protein, in governing specific functions and dynamics of proteins is receiving an increasing interest (Mattos, 2002; Frauenfelder, 2009; Grossman, 2011). Several FTIR difference studies have contributed to clarify the function of internal water molecules in different membrane proteins, as bacteriorhodopsin (Lórentz-Fonfria, 2008), cytochrome c oxydase (Maréchal, 2011),

photosystem II (Noguchi, 2002), and the bacterial reaction center (Garczarek, 2006). Recently, light-induced Q_A^-/Q_A FTIR difference spectra in the 3700-3450 cm^{-1} range have been measured in hydrated RC films equilibrated at r =98% (Iwata, 2009) and vibrational changes attributed to weakly hydrogen bonded water molecules have been observed as a consequence of Q_A^- formation; on these basis, the reorientation of water dipoles near Q_A has been tentatively proposed as the main conformational (dielectric) relaxation stabilizing the $P^+Q_A^-$ state in the RC.

We have extended the study by Iwata and co-workers (Iwata, 2009) in different directions: i) we examined $P^+Q_A^-/PQ_A$ FTIR difference spectra rather than Q_A^-/Q_A spectra, in order to detect events which are induced in the presence of the electric field, generated *in vivo* by the light-induced radical pair ($P^+Q_A^-$), thus including processes which might be coupled to the formation of P^+; ii) two hydration states of the RC film have been considered to study the effect of the protein hydration level on the water differential bands observed by Iwata and colleagues (Iwata, 2009) as well as on other light-minus-dark IR bands; iii) a large IR spectral range has been explored to reveal the possible contribution of other chemical groups to the stabilization of the charged separated state; iv) we have analyzed the charge recombination kinetics of the $P^+Q_A^-$ state following the same continuous illumination regime used in the FTIR measurements, in order to probe the stability of the charge separated state and correlate it with the light-induced IR spectral changes observed in parallel. We aimed at linking the information on RC dynamics and relaxation provided by charge recombination kinetics to the structural information eventually emerging from FTIR light-minus-dark difference measurements.

At the two hydration levels studied, in fact, the kinetics of $P^+Q_A^-$ recombination after the 20 s continuous illumination period used to record light-induced FTIR difference spectra, was markedly different, indicating a more stabilized charge separation in the hydrated RC-LDAO film as compared to the dehydrated one (Fig.9.5).

Three differential bands are resolved in the light-minus-dark FTIR difference spectrum of hydrated RC-LDAO films in the 3750-3550 cm^{-1} range (red trace in Fig.9.2), which, in view of the effects of water substitution with D_2O and H_20^{18}, have been attributed to weakly hydrogen bonded water molecules (par.9.1.2). From the high efficiency of isotope substitution (discussed in detail in par.3.6) it can be concluded that they are located in sites accessible to the solvent. Among these three bands, the positive one at 3664 cm^{-1} and the negative one at 3587 cm^{-1} peak at the same wavenumbers of

two of the difference bands detected by Iwata and colleagues (Iwata, 2009) in Q_A^-/Q_A spectra. We identify therefore these bands with the ones observed by Iwata and colleagues in the presence of the only semiquinone anion, attributed to weakly hydrogen bonded water molecules which respond with a vibrational rearrangement to the light-induced formation of Q_A^-. In the spectral interval between these two bands, our $P^+Q_A^-/PQ_A$ difference spectrum is somewhat different from the Q_A^-/Q_A spectrum reported by Iwata and colleagues. They have identified a small negative bands at 3622 cm^{-1}, also attributed to weakly hydrogen bonded water molecules in the vicinity of Q_A^-; at variance we have observed a rather broad, more intense positive band at approximately 3628 cm^{-1}, which (as reported in par. 9.1.2) undergoes the expected 10 nm shift upon water substitution with H_20^{18}, thus indicating that it originates from water molecules weakly bound to the RC. Although we cannot exclude that these difference are due, at least in part, to spectral interference with the intense and large electronic band of P^+, it is possible that the band detected by us at 3628 cm^{-1} originates from water molecules interacting predominantly with the primary donor P, rather than with the Q_A acceptor. We notice, in this respect, that the crystallographic structure of the *Rb. sphaeroides* RC (Koepke, 2007) shows several water molecules in the immediate surroundings of the P special pair.

When the water content of hydrated RC films (equilibrated at r =76%) was markedly reduced (at r =11%) we have observed a drastic reduction in the amplitude (or possibly the disappearance) of the three differential bands discussed above and attributed to RC bound water molecules. The most direct and simple interpretation is that the majority of the weakly bound water molecules which originate the light-induced bands have been removed upon dehydration. However, since the depletion of the RC hydration shell obtained by decreasing the relative humidity to 11% causes a strong inhibition of the RC/solvent dynamics (see chaper 6), it is also possible that the water molecules responsible for the bands at 3664, 3628 and 3587 cm^{-1} at r =76% are still present, but sufficiently "immobilized" to be unable to reorient and/or undergo vibrational rearrangements in response to light-induced charge separation. Also in this case a substantial decrease of the difference bands is expected.

The strong reduction of the difference water bands observed upon dehydration occurs in parallel with a strong destabilization of the primary charge separated state, as inferred from the $P^+Q_A^-$ recombination kinetics recorded after a 20 s period of continuous photoexcitation (Fig.9.5), i.e. following the same illumination regime under

which the difference FTIR spectra have been acquired. This suggest a correlation between the dynamics of the weakly hydrogen bonded water molecules contributing to the difference bands in the 3750-3550 cm^{-1} range and the conformational processes which stabilize the $P^+Q_A^-$ state.

Our results (see par.9.1.5) indicate that the stabilization of the charge separated state, depends not only upon the hydration state of the RC complex, but also upon the duration of the photoexcitation. Fig.9.5 C shows in fact that, at both hydration levels, a prolonged (20 s) illumination, as compared to a 7 ns (laser) photoexcitation, leads to a considerably more stable $P^+Q_A^-$ state (i.e. to a substantial overall slowing of $P^+Q_A^-$ recombination). The effects observed in the RC film equilibrated at r =11% are in excellent agreement with those previously observed at the same hydration (see par. 8.1.1) and already discussed in par. 8.2: they indicate that the inhibition of the RC relaxation probed by the charge recombination kinetics after the laser flash is essentially reverted following a prolonged illumination. In the hydrated RC film, however, an additional relaxation process appears to place upon continuous illumination. At r =76%, in fact, the continuous 20 s photoexcitation results in a clearly biphasic decay of the $P^+Q_A^-$ state. The fast distributed phase exhibits kinetic parameters similar to those observed in solution, again showing a reversion of the inhibition of the RC dynamics observed after a laser flash. The second kinetic phase, accounting for half of the kinetics, decays in the tens-of-seconds time scale, with an average rate constant ($<k_S>$=0.13 s^{-1}) smaller by one order of magnitude. The presence of this dramatically slow recombination phase strongly suggests that different, additional relaxation processes have occurred during the prolonged illumination at this hydration level: these processes increase by one order of magnitude the stability of the primary charge separated state in about half of the RC population. Extremely slow components in the $P^+Q_A^-$ decay, comparable in rate to the one described above, have been observed in RC solution samples at room temperature as a consequence of continuous illumination for time periods ranging from 5 to 10 minutes (Andréasson, 2003); this extra-stabilization of the charge separated state has been attributed to an additional conformational relaxation, promoted by the prolonged illumination regime and occurring over a much longer time scale, as compared to the relaxation from the *dark-* to the *light-adapted* conformation probed by the $P^+Q_A^-$ recombination kinetics recorded after a single laser pulse (Kleinfeld, 1984; McMahon, 1998). We propose therefore that, following a long (20 s) photoexcitation, a similar, additional conformational relaxation, occurs in

hydrated (r =75%) RC films, which is inhibited by dehydration in RC films equilibrated at r =11%.

To summarize the behaviour described above, it appears that, following long periods of continuous photoexcitation, the difference in the RC dynamics between the hydrated and the dehydrated system concerns mainly the slow conformational relaxation leading to extra-stabilization of the charge separated state: this process takes place in the hydrated system, but is absent (inhibited) in the dehydrated RC. The light-induced difference bands in the 3750-3550 cm^{-1} range (Fig.9.2), which are strongly reduced upon dehydration, are observed during such a long (20 s) photoexcitation of the system. We suggest therefore that the spectral response of the weakly bound water molecules which originate these bands is more likely related to the slow (lifetime τ~10 s), extra-stabilizing RC conformational relaxation, rather than to the fast ($\tau<10^{-2}$ s) conformational change evidenced by laser-flash experiments, as it was previously proposed by Iwata and colleagues (Iwata, 2009).

Besides the difference bands ascribed to water molecules weakly bound to the RC, other features of the light-minus-dark difference spectrum are affected by the hydration level of the RC, including, in the 1750-1650 cm^{1} region, spectral contributions attributed to the 9-keto groups of the special pair bacteriochlorophyll molecules (Fig.9.3), and a few bands in the 3550-3150 cm^{-1} range (Fig.9.4). In this spectral region, which, in our knowledge, has not been analyzed before in *Rb. sphaeroides* RCs, no band could be attributed to water molecules, since we have not observed any shift upon isotopic substitution with D_2O and H_20^{18}. Interestingly, several changes were observed as a consequence of water depletion: shifts of few cm^{-1} for difference bands between 3375 and 3300 cm^{-1}, and strong alterations in the spectral features between 3300 and 3240 cm^{-1}. Although no attribution to specific amino acidic residues is available for these differential bands, we can conclude that several OH or NH groups of amino acidic residues undergo relevant vibrational changes in parallel with dehydration, and therefore with the inhibition of the RC conformational relaxation inferred from the kinetic analysis of $P^+Q_A^-$ recombination (Fig.9.5). This observation is in line with X-ray diffraction data collected at low temperature in *Rb. sphaeroides* RC crystals during continuous illumination with bright light (Katona, 2003). The comparison with data acquired in crystals that were not illuminated showed significant movements (up to 0.7 Å) in a large number of amino acidic residues of the H subunit between ProH121 and ThrH226.

As mentioned above, upon dehydration we observed also shifts in bands (peaking at 1701 and 1669 cm^{-1} in RC films at r =76% (Fig.9.3)) which have been attributed to the 9-keto groups of the P bacteriochlorophyll special pair. Therefore, not only amino acidic residues and bound water molecules localized on the cytoplasmic acceptor side of the RC might be involved in the light-induced conformational relaxation, but also groups on the opposite periplasmic donor side. This notion is consistent with recent X-ray diffraction and functional studies aimed to elucidate the structural basis of RC relaxations induced by photoexcitation. By applying time-resolved Laue diffraction to catch light-induced structural changes in the RC of *Blastochloris viridis*, Wöhri and co-workers (Wöhri, 2010) found that the side chain of TyrL162, a residue strictly conserved in purple bacterial RCs which lies next to P special pair, moves 1.3 Å closer to P after photoactivation. Furthermore, by studying the effect of prolonged illumination (1-2 min) on $P^+Q_A^-$ kinetics in 11 mutants of *Rb. sphaeroides* RC characterized by different hydrogen bonding patterns of the primary electron donor P it was concluded that the relaxation event which stabilizes the $P^+Q_A^-$ state in the seconds time scale could be the deprotonation of one or more amino acidic residues in the vicinity of the special pair P (Deshmuckh, 2011); interestingly TyrM210, which is in the close proximity of the 9-keto group of the bacteriochlorophyll P_M, has been proposed as the most probable candidate for the deprotonation.

As a whole our results indicate that several different pigment-protein groups, both on the acceptor and donor side of the RC, as well as water molecules weakly bound to the RC, undergo structural/dynamic changes in parallel with the stabilization of the $P^+Q_A^-$ state on a second time scale. Although it is tempting to speculate that all these groups contribute, possibly over different time-scales and to a different extent, to stabilize the primary charge separated state of the RC in a collective process, our results do not allow to disentangle conformational changes which actively and primarily stabilize the $P^+Q_A^-$ state by dielectric screening from structural (vibrational) alterations which are a consequence of the primary conformational changes. Time-resolved FTIR difference measurements, aimed to better clarify the nature and the sequence of the relaxation processes, are underway in our laboratories.

10. CONCLUSIONS AND OUTLOOK

The work reported was meant to investigate at the molecular level protein/solvent interactions and their relevance in protein function through the use of amorphous matrices at room temperature. As a model protein, we used the bacterial photosynthetic reaction center, a pigment protein membrane complex which catalyzes well defined light-induced electron transfer processes. The close coupling between electron transfer and internal protein dynamics has been proved in this system by structural and functional studies performed at cryogenic temperatures (par.1.4). The results obtained in the present thesis have shown that the incorporation of this large membrane protein into amorphous matrices of controlled hydration represents a powerful tool when examining the function/dynamics coupling: this approach allows in fact to modulate *at room temperature* the internal protein dynamics to an extent comparable to that attained at cryogenic temperatures, providing complementary and more specific information on the dynamical coupling between the internal protein motions which regulate electron transfer and the dynamics of the protein environment. As an embedding amorphous matrix we have used primarily reaction center-sugar glasses formed by trehalose, a disaccharide which exhibits an extraordinary ability in protecting biostructures under extreme dehydration and high temperature.

The studies performed on this system by exploiting different spectroscopic tools (i.e. flash spectrophotometry, FTIR and EPR spectroscopy) have provided information in two directions. On one side they have contributed to better understand the mechanisms by which the incorporation of the protein into a dehydrated trehalose matrix inhibits dramatically specific protein dynamics, both on short ($< 10^{-3}$ s) and long (hours) time scales. These dynamics govern, respectively, the protein dielectric relaxation which stabilizes the primary light-induced charge separated state and the thermal denaturation of the pigment-protein complex. On the other side, the reported observations, based on the use of dehydrated matrices, have shed some light on the structural basis of the RC dynamics coupled to stabilization of the charge separated state, a topic which is still lively debated (see par.1.4).

Concerning the tight structural and dynamical coupling between the trehalose glassy matrix and the incorporated protein, we have adopted as a working model the *anchorage hypothesis* (see par.1.5). According to this model the inhibition of protein

dynamics in dehydrated trehalose glasses is caused by the locking of the protein surface to the solid sugar matrix: the *anchorage* is mediated mainly by the residual hydration shell of the protein, which, upon progressive dehydration, becomes more and more involved in multiple hydrogen bonds with surface groups of the protein and with sugar molecules of the embedding matrix.

The results obtained, as a whole, are fully consistent with the *anchorage hypothesis* and have allowed to better define the mechanisms of the protein/matrix dynamical coupling in the frame of the model. In particular:

(a) The spatial constraints introduced at the RC surface by extensively dehydrated trehalose matrices can inhibit internal motions which involve deeply buried residues; the extent and specificity of this internal motional hindrance appears to be determined by the local mechanical properties of the protein. This has been inferred from a combined experimental and computational analysis, i.e. by comparing the kinetics of charge recombination in two RC structures (a carotenoid-containing wt and a carotenoid-less mutant) incorporated into trehalose matrices, and by analyzing the protein flexibility of the two structures by means of coarse-grained Brownian dynamics simulations (chapter 4). The RC dynamics simulations showed additionally that limited structural changes can have long range effects on the protein flexibility: removal of the carotenoid molecule from the RC appears to induce a protein rearrangement which affects substantially the RC dynamics, altering the rigidity of residues located at more than 20 Å from the carotenoid. In this respect, we think particularly relevant that coarse-grained Brownian dynamics simulations give a picture of the RC mechanical properties at the residue level, which is consistent with the effects experimentally observed in dehydrated trehalose matrices on a specific electron transfer process.

(b) The incorporation of the RC into a dehydrated, glassy trehalose matrix does neither affect the electronic and structural properties of the radical ions, P^+ and Q_A^-, and their radical pairs, $P^+Q_A^-$, nor the local dynamics of Q_A^- in its binding pocket, as indicated by the high-field EPR characterization (chapter 5). This finding is considered to be of particular relevance because it implies that the strongly accelerated and distributed $P^+Q_A^-$ recombination kinetics observable in such trehalose matrices are not related to structural distortions affecting the cofactor geometry nor to alterations in the local cofactor dynamics. These kinetic effects are rather a genuine probe of the protein/solvent conformational dynamics which govern the stabilization of the

primary RC charge-separated state, as we had previously proposed (Palazzo, 2002; Francia, 2009). It is argued that trehalose glasses provide in general a suitable tool to modulate the RC dynamics at room temperature.

(c) The central role postulated by the *anchorage hypothesis* for the dynamics of residual water molecules at the protein matrix interface is fully supported by the thermodynamic, spectral and kinetic data obtained in dehydrated RCs in the absence of sugar (chapter 6). In fact, as revealed by FTIR analysis, dehydration of the RC-detergent films below a critical threshold leads to dramatic structural and dynamical alterations of the residual hydration shell which are paralleled by a drastic inhibition of the RC relaxation from the *dark-adapted* to the *light-adapted* conformations, as well as of the interconversion among lower tier substates.

(d) At the same time, a close comparison between the kinetics of $P^+Q_A^-$ recombination after a laser pulse (7 ns) and following a prolonged, continuous illumination (up to a few seconds) in dehydrated trehalose-RC matrices and in RC films, indicates that the water-RC-sugar structures formed in the presence of trehalose hinder more severely the RC protein dynamics, as compared to a mere dehydration of the protein-detergent complex (chapter 8).

(e) Even more significant is the superior efficacy of trehalose glasses in blocking larger scale RC dynamics which are supposed to be involved in its thermal denaturation. In fact, at variance with dehydrated RC films, in which a slow loss of the native pigment-protein structure occurred at 44 °C on the time scale of hours, incorporation into a dehydrated trehalose matrix totally prevented thermal denaturation even after several days of incubation at the same temperature.

(f) The protection of the trehalose matrix against thermal denaturation exhibits a clear threshold effect when studied as a function of the sugar/protein molar ratio. As expected from the *anchorage model*, the minimum number of trehalose molecules needed to totally suppress the RC dynamics involved in thermal denaturation (~ 200 trehalose molecules per RC complex) corresponds roughly to the coating of the RC-detergent complex with a single layer of trehalose molecules (chapter 7).

(g) Also the much faster RC dynamics which stabilizes the primary charge separated state is quite sensitive to the sugar/protein molar ratio (chapter 7), suggesting that the degree of protein dynamics inhibition for a given hydration level is determined by the overall dynamics of the RC-water-trehalose structure, as assumed by the *anchorage model*.

To further test the *anchorage hypothesis*, future experiments will need to focus on the structural and dynamic properties of the residual water at the RC surface, and on the coupled fluctuations of surface residues of the protein as a function of the hydration level of the embedding trehalose matrix. We expect that direct information on the dynamics of the RC protein surface and on the possible involvement of exposed RC residues in water-mediated hydrogen bonding with the matrix can be obtained by combining site-specific $NO^{\cdot}$ spin labelling of the RC H-subunit (e.g., labelling of the native cysteine at position 156 (Poluektov, 2003; Borovykh, 2006) with high-field EPR spectroscopy (Möbius, 2009), and incorporating the labelled RC complex into trehalose matrices at different hydration levels. Experiments along these lines, in collaboration with Prof. Klaus Möbius, Prof. Wolfgang Lubitz, and Dr. Anton Savitsky, are in progress at the Max-Planck-Institut für Bioanorganische Chemie.

In view of the points summarized above, defining several aspects of protein-matrix interactions, we believe that room temperature trehalose glassy matrices represent in general an appropriate, valuable tool when examining function/dynamics relationships in proteins. The experimental efficacy of this approach has been significantly enhanced by introducing the isopiestic method (par.3.2) to achieve a reproducible control and a fine tuning of the hydration levels of amorphous protein matrices, both in the absence (chapter 6) and in the presence of trehalose (chapter 7,8,9).

On these bases, the following conclusions can also be drawn, which concern the relaxation of the RC stabilizing the light-induced primary charge separated state:

(h) The transition from the *dark-adapted* to the *light-adapted* conformation following a short (ns) photoexcitation does not seem to involve alterations of the relative geometry of the $P^+Q_A^-$ radical pair, or in the local structure and dynamics of the Q_A^- binding site, as probed by high-field EPR results, both in cw and pulse modes (chapter 5).

(i) Within the frame of the unified model of protein dynamics recently proposed by Frauenfelder (Frauenfelder, 2009), we ascribe the conformational relaxations which stabilize the charge-separated state, as well as lower tier thermal fluctuations of the RC, probed by the kinetics of $P^+Q_A^-$ recombination to Class II (β-slaved) processes, driven and governed by the dynamics of the protein hydration shell. This is consistent with the EPR data, strongly supported by the study of dehydrated RC films (chapter 6), and fully in line with the *anchorage model*.

(j) The structural rearrangement stabilizing $P^+Q_A^-$ (*dark-* to *light-adapted* conformational transition) is likely to involve protein residues localized on the quinone acceptor side of the RC. This is suggested by the comparison of the rigidity profiles of the wt and carotenoid-less mutant, which show that most of the residues undergoing the largest differences in the calculated force constant cluster around the iron atom (chapter 4).

(k) Interestingly the comparative analysis of light-induced FTIR difference spectra performed in hydrated and dehydrated RC films (chapter 9) indicates that the conformational rearrangements in response to charge separation might also involve residues located in the vicinity of the primary donor P as well as water molecules, weakly hydrogen bonded to the RC, proximal to the primary quinone acceptor, Q_A. It has to be noticed, however, that the difference FTIR results, provide information on putative relaxation events occurring over a long (10 s) time scale. This conformational adaptation leads, in the hydrated RCs, to an additional, ten-times larger stabilization of the charge-separated state, as compared to the one occurring after a laser pulse.

We tend to propose that the dielectric relaxation of the RC/solvent system induced by the primary charge separation is a collective process, possibly involving protein groups and bound water molecules localized in different regions of the complex. Furthermore, different relaxation processes are likely to take place over different time scales (covering at least the 10^{-3}-10^2 s time range), depending on the duration of photoexcitation. Time-resolved FTIR measurements are in progress, which could help to better define the structural basis of the conformational relaxations occurring over different time scales.

11. REFERENCES

Abbruzzetti, S., Giuffrida S., Sottini, S., Viappiani, C., Cordone, L.. **2005**. *Cell Biochem. Biophys.* 43: 431.

Abramowitz, M., Stegun, I.A.. **1965**. *Handbook of Mathematical Functions*; Dover Publications: New York.

Albertorio, F., Chapa, V.A., Chen, X., Diaz, A.J., Cremer, P.S.. **2007**. *J.Am.Chem.Soc.* 129: 10567.

Allen, J.P., Feher, G., Yeates, T.O., Rees, D.C., Deisenhofer, J., Michel, H.. **1986**. *Proc. Natl. Acad. Sci. USA* 83: 8589.

Allen, J.P.; Williams, J.C.; Graige, M.S.; Paddock, M.L.; Labahn, A.; Feher, G.; Okamura, M.Y.. **1998**. *Photosynth. Res.* 55, 227.

Andréasson, U., Andréasson, L.E.. **2003**. *Photosynth. Res.* 75: 223.

Austin, R.H., Beeson, K.W., Eisenstein, L., Frauenfelder, H.. **1975**. *Biochemistry* 14(24): 5355.

Baccarini-melandri, A., Melandri, B.A.. **1971**. *Methods Enzymol.* 23: 556.

Baciou, L., Michel, H.. **1995**. *Biochemistry* 34: 7967.

Bagley, K.A., Abresch, E., Okamura, M.Y., Feher, G., Bauscher, M., Mäntele, W.G., Nabedryk, E., Breton, J.. **1990**. *Current Research in Photosynthesis* 1, pp.77, (Baltscheffsky, M. ed.) Kluwer, Dordrecht.

Barth, A.. **2007**. *Biochim. Biophys. Acta* 1767: 1073.

Bauscher, M., Nabedryk, E., Bagley, K., Mäntele, W.G.. **1990**. *FEBS* 261(1): 191.

Beechem, J.M**.. 1992**. *Methods Enzymol.* 20: 37.

Belton, P.S., Gil, A.M.. **1994**. *Biopolymers* 34: 957.

Bevington, P.R.. **1969**. *Data Reduction and Error Analysis for the Physical Sciences*; McGraw-Hill: New York.

Bonner, O.D., Choi, Y.S.. **1974a**. *J. Phys. Chem.* 78: 1723.

Bonner, O.D., Choi, Y.S.. **1974b**. *J. Phys. Chem.* 78: 1727.

Borovykh, I. V., Ceola, S., Gajula, P., Gast, P., Steinhoff, H. J., Huber, M.. **2006**. *J. Magn. Reson.* 180: 178 .

Bowyer, J.R., Meinhardt, S.W., Tierney, G.V., Crofts, A.R.. **1981**. *Biochim. Biophys. Acta* 635: 167.

Breton, J., Thibodeau, D.L., Berthomieu, C., Mäntele, W., Verméglio, A., and Nabedryk, E.. **1991a**. *FEBS* 278 (2): 257.

Breton, J., Berthomieu, C., Thibodeau, D.L., Nabedryk, E.. **1991b**. *FEBS* 288 (1,2): 109.

Breton, J., Nabedryk, E., Parson, W.W.. **1992**. *Biochemistry* 31: 7503.

Breton, J., Boullais, C., Burie, J.-R., Nabedryk, E., Mioskowski, C.. **1994a**. *Biochemistry* 33: 14378.

Breton, J., Burie, J.-R., Barthomieu, C., Berger, G., Nabedryk, E.. **1994b**. *Biochemistry* 33: 4953.

Breton, J., Nabedryk, E.. **1998**. *Photosynth. Res.* 55: 301.

Breton, J.. **2004**. *Biochemistry* 43: 3318.

Breton, J., Lavergne, J., Wakeham, M.C., Nabedryk, E., Jones, M.R.. **2007**. *Biochemistry* 46: 6468.

Brubach, J.-B., Mermet, A., Filabozzi, A., Gerschel, A., Roy, P.. **2005**. *J. Chem. Phys.* 122: 184509.

Brudler, R., de Groot, H.J.M., van Liemt, W.B.S., Steggerda, W.F., Esmeijerl, R., Gast, P., Hoff, A.J., Lugtenburg, J., Gerwert, K.. **1994**. *EMBO J.* 13: 5523.

Brunauer, S.; Emmet, P.H.,; Teller, E.. **1938**. *J. Am. Chem. Soc.* 60: 309.

Burghaus, O., Plato, M., Rohrer, M., Möbius, K., MacMillan, F., Lubitz, W.. **1993**. *J. Phys. Chem.* 1993(97): 7639.

Careri, G.; Giansanti, A.; Gratton, E.. **1979**. *Biopolymers* 18: 1187.

Carpenter, J.F., Crowe, J.H.. **1989**. *Biochemistry* 28: 3916.

Chiantia, S.; Giannola, L.I.; Cordone, L.. **2005**. *Langmuir* 21: 4108.

Cho, H.S., Dashdorj, N., Schotte, F., Graber, T., Henning, R., Anfinrud, P.. **2010**. *Proc. Natl. Acad. Sci. USA* 107(16): 7281.

Chu, K., Ernst, R.M., Frauenfelder, H., Mourant, J.R., Nienhaus, G.U., Philipp R.. **1995**. *Phys. Rev. Lett.* 74: 2607.

Cordone, L., Cottone, G., Giuffrida, S. , Palazzo, G., Venturoli, G. , and Viappiani, C.. **2005**. *Biochim. Biophys. Acta* 1749:252.

Cramer W.A., Knaff D.B.. **1990**. *Energy Transduction in Biological Membranes*, Springer-Verlag, New York.

Crowe, J.R., Carpenter, J.F., Crowe, L.M.. **1998**. *Annu. Rev. Physiol.* 60: 73.

Curtiss, L.A.; Frurip, D.J.; Blander, M.. **1979**. *J. Chem. Phys.* 71: 2703.

Czarnik-Matusewicz, B.; Pilorz, S.. **2006**. *Vib. Spectrosc.* 40: 235.

D'Arcy, R.L.; Watt, I.C.. **1970.** *Trans. Faraday Soc.* 66: 1236.

Debus, R. J., Feher, G., Okamura, M. Y.. **1986**. *Biochemistry* 25: 2276.

Deegan, R.D., Bakajin, O., Dupont, T.F., Huber, G., Nagel, S.R., Witten, T.A.. **1997**. *Nature* 389: 827.

Deisenhofer, J., Epp., O., Miki, K., Huber, R., Michel, H.. **1985**. *Nature* 318: 618.

Deshmuck, S.S., Williams, J.C., Allen, J.P., Kalman, L.. **2011**. *Biochemistry* 50: 3321-3331.

Dickens, B.; Dickens, S.H.. **1999**. *J. Res. Natl. Inst. Stan.* 104, 173-183.

Doster, W., Cusack, S., Petry, W.. **1989**. *Nature* 337: 754-756.

Doster, W.. **2010**. *Biochimica et Biophysica Acta* 1804: 3-14.

Eaton, G.R. & Eaton, S.S.. **2000**. Relaxation times of organic radicals and transition metal ions. in Distance Measurements in Biological Systems by EPR Vol. 19 (eds. Berliner, L.J., Eaton, G.R. & Eaton, S.S.) 29–154 (Kluwer Academic/Plenum Publishers, New York).

Ebbinghaus, S., Kim, S.J., Heyden, M., Yu, X., Heugen, U., Gruebele, M., Leitner, D.M., Havenith, M.. **2007**. *Proc. Natl. Acad. Sci. USA* 104(52): 20749.

Eisenberg, D.; Kauzmann, W.. **1969**. *The Structure and Properties of Water*, Oxford University Press: London.

Eisenmesser, E.Z., Bosco, D.A., Akke, M., Kern, D.. **2002**. *Science* 295: 1520-1523.

Ermak, D.L., McCammon, J.A.. **1978**. *J. Chem. Phys.* 69: 1352.

Ermler, U., Fritzsch, G., Buchanan, S. K., Michel, H.. **1994**. *Structure* 2, 925.

Farias-Rodriguez, R., Mellor, R.B., Arias, C., Peňa-Cabriales, J.J.. **1998**. *Physiol. Plantarum* 102: 353.

Feher, G., Isaacson, R. A., Okamura, M. Y., Lubitz, W.. **1985**. In *Antennas and Reaction Centers of Photosynthetic Bacteria*; Michel-Beyerle, M. E., Ed.; Springer: Berlin; pp 174–189.

Feher, G.; Arno, T.R.; Okamura, M.Y.. **1988**. In *The Photosynthetic Bacterial Reaction Center*; Breton, J., Vermeglio, A., Eds.; Plenum Press: New York, pp.271-287.

Fenimore, P. W., Frauenfelder, H., McMahon, B. H., Young, R. D.. **2004**. *Proc. Natl. Acad. Sci. USA* 101, 14408.

Ferrand, M., Dianoux, A.J., Petry, W., Zaccai, G.. **1993**. *Proc. Natl. Acad. Sci. USA* 90: 9668.

Feyereisen, M.W., Feller, D., Dixon, D.A.. **1996**. *J. Phys. Chem.* 100: 2993.

Flores, M., Savitsky, A., Abresch, E. C., Lubitz, W., Möbius, K.. **2008**. In *Photosynthesis. Energy from the Sun*; Allen, J. F., Osmond, B., Golbeck, J. H., Gantt, E., Eds.; Springer: Heidelberg; pp 59.

Flores, M., Savitsky, A., Paddock, M.L., Abresch, E.C., Dubinskii, A.A., Okamura, M.Y., Lubitz, W., Möbius, K.. **2010**. *J. Phys. Chem. B* 114: 16894.

Fornés, V.; Chaussidon, J.. **1978**. *J. Chem. Phys.* 68: 4667.

Francia, F., Palazzo, G., Mallardi, A., Cordone, L., Venturoli, G.. **2003**. *Biophys. J.* 85: 2760.

Francia, F., Giachini, L., Palazzo, G., Mallardi, A., Boscherini, F., Venturoli, G.. **2004a**. *Bioelectrochemistry* 63: 73.

Francia, F., Palazzo, G., Mallardi, A., Cordone, L., Venturoli, G.. **2004b**. *Biochim. Biophys. Acta* 1658: 50.

Francia, F., Dezi, M., Mallardi, A., Palazzo, G., Cordone, L., Venturoli, G.. **2008**. *J. Am. Chem. Soc.*130: 10240.

Francia, F., Malferrari, M., Sacquin-Mora, S., Venturoli, G.. **2009**. *J. Phys. Chem. B* 113: 10389.

Frank, G. A.. **2007**. *J. Phys. Chem.* Ref. Data 36: 1279.

Franzen, S.; Boxer, S.G.. **1993**. *J. Phys. Chem.* 97: 6304.

Frauenfelder, H., Leeson, D.T.. **1998**. *Nature Struct. Biol.* 5(9): 757.

Frauenfelder, H., McMahon, B.H.. **2000**. *Ann. Phys.* 9: 655.

Frauenfelder, H., MacMahon, B.H., Austin, R.H., Chu, K., Groves, J.T.. **2001**. *Proc. Natl. Acad. Sci. USA* 98(5): 2370.

Frauenfelder, H., Chen, G., Berendzen, J., Fenimore, P. W., Jansson, H., McMahon, B. H., Stroe, I. R., Swenson, J., Young, R. D.. **2009**. *Proc. Natl. Acad. Sci. USA* 106: 5129.

Frauenfelder, H.. **2010**. *The Physics of Proteins. An Introduction to Biological Physics and Molecular Biophysics*. S.S. Chan and W.S. Chans, Eds.. Springer.

Fritzsch, G., Koepke, J., Diem, R., Kuglstatter, A., Baciou, L.. **2002**. *Acta Cryst. D* 58: 1660.

Gafert, J., Pschierer, H., Friederich, J.. **1995**. *Phys. Rev. Lett.* 74(18): 3704.

Gall, A., Ellervee, A., Bellisent-Funel, M.C., Robert, B., Freiberg, A.. **2001**. *Biophys. J.* 80:1487.

Gall, A., Ellervee, A., Robert, B., Freiberg, A.. **2004**. *FEBS Lett.* 560: 221.

Garczarek, F., Gerwert, K.. **2006**. *Nature* 439(5): 109.

Gast, P., Hemelrijk, P.W., van Gorkom, H.J., Hoff, A.J.. **1996**. *Eur. J. Biochem.* 239: 805.

Giachini, L., Francia, F., Cordone, L., Boscherini, F., Venturoli, G.. **2007**. *Biophys. J.* 92: 1350.

Giguère, P.A.; Chin, D.. **1961**. *Can. J. Chem.* 39: 1214.

Ginet, N., Lavergne, J.. **2001**. *Biochemistry* 40 : 1812.

Giuffrida, S., Cottone, G., Librizzi, F., Cordone, L.. **2003**. *J. Phys. Chem. B* 107: 13211.

Giuffrida, S., Cottone, G., Cordone, L.. **2006**. *Biophys. J.* 91: 968.

Giustini, M., Palazzo, G., Colafemmina, G., Della Monica, M., Giomini, M., Ceglie, A.. **1996**. *J. Phys. Chem.* 100: 3190.

Graige, M. S., Feher, G., Okamura, M.Y.. **1998**. *Proc. Natl. Acad. Sci. USA* 95: 11679.

Gray, K.A., Farchaus, J.W., Wachtveitl, J., Breton, J., Oesterhelt, D.. **1990**. *EMBO J.* 9: 2061.

Greenspan, L.. **1977**. *J. Res. Natl. Bur. Stand. A* 814: 89.

Grossman, M., Born, B., Heyden, M., Tworowski, D., Fields, G.B., Sagi, I., Havenith, M.. **2011**. *Nature Struct. Mol. Biol.* 18(10): 1102.

Gopher, A., Blatt, Y., Schönfeld, M., Okamura, M.Y., Feher, G., Montal, M.. **1985**. *Biophys. J.* 48: 311.

Gouscha, A.O., Kharkyanen, V.N., Holzwarth, A.R.. **1997**. *J. Phys. Chem. B* 101: 259.

Gouscha, A.O., Kharkyanen, V.N., Scott, G.W., Holzwarth, A.R.. **2000**. *Biophys. J.* 79: 1237.

Gouscha, A.O., Manzo, A.J., Scott, G.W., Christophorov, L.N., Knox, P.P., Barabash, Y.M., Kapoustina, M.T., Berezetska, N.M., Kharkyanen, V.N.. **2003**. *Biophys. J.* 84: 1146.

Guex, N., Peitsch, M.C.. **1997**. *Electrophoresis* 18: 2714.

Gunner, M.R., Dutton, P.L.. **1989**. *J. Am. Chem. Soc.* 111: 3400.

Hailwood, A.J., Horrobin, S.. **1946**. *Trans. Faraday Soc.* 42B: 84.

Hales, B. J., Case, E. E.. **1981.** *Biochim. Biophys. Acta* 637: 291.

Hecht, K.T., Wood, D.L.. **1956**. *Proc. Roy. Soc. London Ser. A* 235: 174.

Henzler-Wildman, K., Kern, D.. **2007**. *Nature* 450: 964.

Heyden, M., Bründermann, E., Heugen, U., Niehues, G., Leitner, D.M., Havenith, M.. **2008**. *J. Am. Chem. Soc.* 130: 5773.

Hochkoeppler, A., Zannoni, D., Venturoli, G.. **1995**. *Biochim. Biophys. Acta* 1229: 81.

Hoeckstra, F.A., Golovina, E.A., Buitink, J.. **2001**. *Trends Plant Sci.* 6(9): 431.

Holzwarth, A.R.. **1996**. In *Biophysical Techniques in Photosynthesis.* pp. 75. Amesz, J., Hoff, A.J.. Eds; Kluwer Academic Publishers, Dordrecht, The Netherland.

Hore, P. J.. **1989**. In *Advanced EPR, Applications in Biology and Biochemistry*; Hoff, A. J., Ed.; Elsevier: Amsterdam; pp 405.

Hughes, A.V., Rees, P., Heathcote, P. and Jones, M.R.. **2006**. *Biophys. J.* 90: 4155.

Iben, I.E.T., Brauenstein, D., Doster, W., Frauenfelder, H., Hong, M.K., Johnson, J.B., Luck, S., Ormos, P., Schulte, A., Steinbach, P.J., Xie, A.H., Youmg, R.D.. **1989**. *Phys. Rev. Lett.* 62(16): 1916.

Isaacson, R. A., Lendzian, F., Abresch, E. C., Lubitz, W., Feher, G. **1995**. *Biophys. J.*, 69: 311.

Iwaki, M., Andrianambinintsoa, S., Rich, P., Breton, J.. **2002**. *Spectrochim. Acta A* 58: 1523.

Iwata, T., Paddock, M. L., Okamura, M.Y., Kandori, H.. **2009**. *Biochemistry* 48: 1220.

Kalman, L., Maroti, P.. **1994**. *Biochemistry* 33: 9237.

Kandori, H.. **2000**. *Biochim. Biophys. Acta* 1460: 177.

Katona, G., Snijder, A., Gourdon, P., Andréasson, U., Hansson, O., Adréasson, L.E., Neutze, R.. **2005**. *Nature Struct. Mol. Biol.* 12 (7): 630.

Kawai, T., Umemura, J., Takenaka, T., Kodama, M., Seki, S.J.. **1985**. *J. Colloid. Interface Sci.* 103: 56.

Kim, S. S., Weissman, S. I.. **1979**. *J. Am. Chem. Soc.* 101: 5863.

Kleinfeld, D., Okamura, M. Y., Feher, G.. **1984**. *Biochemistry* 23: 5780.

Kocherbitov, V., Veryazov, V., Söderman, O.. **2007**. *J. Mol. Struc-Theochem* 808: 111.

Koder, R.L., Anderson, J.L.R., Solomon, L.A., Reddy, K.S., Moser, C.C., Dutton, P.L.. **2009**. *Nature* 458: 305.

Koepke, J., Krammer, E.M., Klingen, A.R., Sebban, P., Ullmann, G.M., Fritzsch, G.. **2007**. *J. Mol. Biol.* 371: 396.

Konidala, P., He, L., Niemeyer, B.. **2006**. *J. Mol. Graphics Modell.* 25: 77.

Kriegl, J.M., Forster, F.K., Nienhaus, G.U.. **2003**. *Biophys. J.* 85: 1851.

Kriegl, J. M., Nienhaus, G. U.. **2004**. *Proc. Natl. Acad. Sci. USA* 101: 123.

Kuglstatter, A., Emler, U., Michel, H., Baciou, L., Fritzsch, G.. **2001**. *Biochemistry* 40: 4253.

Kuntz, I.D., Kauzmann, W.. **1974**. *Adv. Protein Chem.* 28: 239.

Labahn, A., Bruce, J.M., Okamura, M.Y., Feher, G.. **1995**. *Chem. Phys.* 197(3): 355.

Lappi, S.E., Smith, B., Franzen, F.. **2004**. *Spectrochim. Acta A* 60: 2611.

Lavery, R., Sacquin-Mora, S.. **2007**. *J. Biosci.* 32: 891.

Lee, G.M., Craik, C.S.. **2009**. *Science* 324: 213.

Leonhard, M., Mäntele, W.G.. **1993**. *Biochemistry* 32: 4532.

Lin, X., Murchison, H.A., Nagarajan, V., Parson, W.W., Allen, J.P., Williams, J.C.. **1994**. *Proc. Natl. Acad. Sci. USA* 91: 10265.

Lins, R. D., Pereira, C. S., Hunenberger, P. H.. **2004**. *Proteins* 55: 177.

Lorenz, C.D., Hsieh, C.-M., Dreiss, C.A., Lawrence, M.J.. **2011**. *Langmuir* 27: 546.

Lórenz-Fonfria, V.A., Furutani, Y., Kandori, H.. **2008**. *Biochemistry* 47: 4071.

Lubitz, W., Abresch, E. C., Debus, R. J., Isaacson, R. A., Okamura, M. Y., Feher, G.. **1985**. *Biochim. Biophys. Acta* 808: 464.

Lunkenheimer, P., Schneider, U., Brand, R., Loidl, A.. **2000**. *Contemp. Phys.* 41(1): 15.

Lüscher-Mattli, M., Rüegg, M.. **1982**. *Biopolymers* 21: 403.

Maiti, S., Cowen, B.R., Diller, R., Iannone, M., Moser, C.C., Dutton, P.L., Hochstrasser, R.M.. **1993**. *Proc. Natl. Acad. Sci. USA* 90: 5247.

Malferrari, M., Francia, F., Venturoli, G.. **2011a**. *J. Phys. Chem. B* 115 (49):14732.

Malferrari, M., Venturoli, G., Francia, F., Mezzetti, A.. **2011b**. *Spectroscopy - Biomedical Applications*, submitted.

Malsam, J.; Aksan, A.. **2009**. *J. Phys. Chem. B* 113: 6792.

Mäntele, W.G., Wollenweber, A.M., Nabedryk, E., Breton, J.. **1988**. *Proc. Natl. Acad. Sci. USA* 85: 8468.

Manzo, A.J., Gouscha, A.O., Berezetska, N.M., Kharkyanen, V.N., Scott, G.W.. **2011**. *J. Phys. Chem. B* 115: 8534.

Marcus, R.A., Sutin, N.. **1985**. *Biochim. Biophys. Acta* 811: 265.

Maréchal, A., Rich, P.R.. **2011**. *Proc. Natl. Acad. Sci. USA* 108 (21): 8634.

Maroti, P., Wraight, C. A.. **1997**. *Biophys. J.* 73: 367.

Mattos, C.. **2002**. *Trends Biochem. Sci.* 27: 203.

Max, J.J., Chapados, C.. **2002**. *J. Chem. Phys.* 116: 4626.

McMahon, B. H., Müller, J. D., Wraight, C. A., Nienhaus, G. U.. **1998**. *Biophys. J.* 74: 2567.

McPherson, P.H., Okamura, M.Y., Feher, G.. **1990**. *Biochim. Biophys. Acta* 1016: 289.

Möbius, K., Savitsky, A.. **2009**. *High-Field EPR Spectroscopy on Proteins and their Model Systems*; RSC Publishing: Cambridge UK.

Møller, J.V., le Maire, M.. **1993**. *J. Biol. Chem.* 268: 18659.

Moser, C.C., Keske, J.M., Warncke, K., Farid, R.S., Dutton, P.L.. **1992**. *Nature* 355: 796.

Nabedryk, E., Tiede, D.M., Dutton, P.L., Breton, J.. **1982**. *Biochim. Biophys. Acta* 682: 273.

Nabedryk, E., Bagley, K.A., Thibodeau, D.L., Bausher, M., Mäntele, W., Breton, J.. **1990a**. *FEBS Lett.* 266: 59.

Nabedryk, E., Bagley, K. A., Thibodeau, D. L., Bauscher, M., Mäntele, W., Breton, J.. **1990b**. *FEBS Lett.* 266: 59.

Nabedryk, E., Robles, S.J., Goldman, E., Youvan, D.C., Breton, J.. **1992**. *Biochemistry* 31: 10852.

Nabedryk, E., Allen, J.P., Tagichi, A.K.W., Williams, J.C., Woodbury, N.W., Breton, J.. **1993**. *Biochemistry* 32: 13879.

Nilsson, A., Holmgren, A., Lindblom, G.. **1991**. *Biochemistry* 30: 2126.

Noguchi, T., Sugiura, M.. **2002**. *Biochemistry* 41: 2322.

Onori, G., Santucci, A.. **1993**. *J. Phys. Chem.* 97: 5430.

Onuchic, J.N., Luthey-Schulten, Z., Wolynes, PG.. **1997**. *Annu. Rev. Phys. Chem.* 48: 454.

O'Reilly, JE.. **1973**. *Biochim. Biophys. Acta* 292: 509.

Ortega, J.M., Mathis, P., Williams, J.C., Allen, J.P.. **1996**. *Biochemistry* 35: 3354.

Pal, S.K., Peon, J., Bagchi, B., Zewail, A.H.. **2002**. *J. Phys Chem. B* 106: 12376.

Palazzo, G., Mallardi, A., Hochkoeppler, A., Cordone, L., Venturoli, G.. **2002**. *Biophys. J.* 82: 558.

Palazzo, G., Mallardi, A., Francia, F., Dezi, M., Venturoli, G., Pierno, E., Vignati, E., Piazza, R.. **2004**. *Phys. Chem. Chem. Phys.* 6: 1439.

Palazzo G., Francia, F., Mallardi, A., Giustini, M., Lopez, F., Venturoli, G.. **2008**. *J. Am. Chem. Soc.* 130: 9353.

Palazzo, G., Lopez, F., Mallardi, A.. **2010**. *Biochim. Biophys. Acta* 1804: 137.

Poluektov, O. G., Utschig, L. M., Dalosto, S., Thurnauer, M. C.. **2003**. *J. Phys. Chem. B* 107: 6239.

Parak, F., Frolov, E. N., Kononenko, A. A., Mössbauer, R. L., Goldanskii, V. I., Rubin, A. B.. **1980**. *FEBS Lett.* 117: 368.

Parak, F., Knapp, E.W., Kucheida, D.. **1982**. *J. Mol. Biol.* 161 : 177.

Pereira, C., Lins, R.D., Chandrasekhar, I., Freitas, L.C.G., Hunenberger, P.H.. **2004**. *Biophys. J.* 86: 2273.

Pereira, C., Hunenberger, P.H.. **2006**. *J. Phys. Chem. B* 110 : 15572.

Rahaman, A., Wheeler, R.A.. **2004**. *ChemPhysChem* 5: 249.

Rivas, E., Reiss-Husson, F., Le Maire, M.. **1980**. *Biochemistry* 19: 2943.

Rojas, O.J., Neuman, R.D., Claesson, P.M.. **2005**. *J. Phys. Chem. B* 109: 22440.

Roszak, A.W., McKendrick, K., Gardiner, A.T., Mitchell, I.A., Isaacs, N.W., Codgell, R.J., Hashimoto, H., Frank, H.A.. **2004**. *Structure* 12: 765.

Roth, M., Lewit-Bentley, A., Michel, H., Deisenhofer, J., Huber, R., Oesterhelt, D.. **1989**. *Nature* 340: 659.

Roth, M., Arnoux, B., Ducruix, A., Reiss-Husson, F.. **1991**. *Biochemistry* 30: 9403.

Rozenberg, M., Loewenschuss, A., Marcus, Y.. **2002**. *Phys. Chem. Chem. Phys.* 2: 2699.

Rupley, J.A., Careri, G.. **1991**. *Adv. Protein Chem.* 41: 37.

Schnegg, A., Fuhs, M., Rohrer, M., Lubitz, W., Prisner, T. F., Möbius, K.. **2002**. *J. Phys. Chem. B* 106: 9454.

Sacquin-Mora, S., Lavery, R.. **2006**. *Biophys. J.* 90: 2706.

Sacquin-Mora, S., Sebban, P., Derrien, V., Frick, B., Lavery, R., Alba-Simionesco, C.. **2007a**. *Biochemistry* 46: 14960.

Sacquin-Mora, S., Laforet, E., Lavery, R.. **2007b**. *Proteins* 67: 350.

Sales, K., Brandt, W., Rumbak, E., Lindsey, G.. **2000**. *BBA-Biomembranes* 1463: 267.

Sampedro, J.G., Uribe, S.. **2004**. *Mol. Cell. Biochem.* 256/257: 319.

Savitsky, A., Dubinskii, A. A., Flores, M., Lubitz, W., Möbius, K.. **2007**. *J. Phys. Chem. B* 111: 6245.

Savitsky, A., Malferrari, M., Francia, F., Venturoli, G., Möbius, K.. **2010**. *J. Phys. Chem. B* 114: 12729.

Schotte, F., Soman, J., Olson, J.S., Wulff, M., Anfinrud, P.A.. **2004**. *J Struct. Biol.* 147: 235.

Simperler, A., Kornherr, A., Chopra, R., Jones, W., Motherwell, W. D., Zifferer, G.. **2007**. *Carbohyd. Res.* 342: 1470.

Sistrom, W.R.. **1960**. *J. Gen. Microbiol.* 22: 778.

Sloten, L.. **1972**. *Biochim. Biophys. Acta* 275: 208.

Smock, R.G., Gierasch, L.M.. **2009**. *Science* 324: 198.

Steinbach, P. J., Chu, K., Frauenfelder, H., Johnson, J. B., Lamb, D. C., Nienhaus, G. U., Sauke, T. B., Young, R. D.. **1992**. *Biophys. J.* 61: 235.

Stehlik, D., Bock, C. H., Petersen, J.. **1989**. *J. Phys. Chem.* 93: 1612.

Stoll, S., Schweiger, A.. **2006**. *J. Magn. Reson.* 178: 42.

Stoll, S., Schweiger, A.. **2007**. In *ESR Spectroscopy in Membrane Biophysics*; Hemminga, M. A., Berliner, L. J., Eds.; Springer: New York, Vol. 27; pp 299.

Stowell, M.H.B., McPhillips, T.M., Rees, D.C., Soltis, S.M., Abresch, E., Feher, G.. **1997**. *Science* 276: 812.

Straley, S.C.; Parson, W.W.; Mauzerall, D.C.; Clayton, R.K.. **1973**. *Biochim. Biophys. Acta* 305: 597.

Sum, A.K., Faller, R., de Pablo, J.J.. 2003. *Biophys. J.* 85: 2830.

Sussich, F., Skopec, C., Brady, J., Cesáro, A.. **2001**. *Carbohydr. Res*. 334: 165.

Suzuki, T.. **2008**. *Phys. Chem. Chem. Phys.* 10: 96.

Takeuchi, M., Martra, G., Coluccia, S., Anpo, M.. **2005**. *J. Phys. Chem. B* 109: 7387.

Tandori, J., Tokaji, Z., Misurda, K., Maroti, P.. **2005**. *Photochem. Photobiol.* 81: 1518.

Tanford, C.. **1978**. *Science* 200: 1012.

Tang, J., Utschig, L. M., Poluektov, O., Thurnauer, M. C.. **1999**. *J. Phys. Chem. B 103*: 5145.

Thiyagarajan, P.; Tiede, D.M.. **1994**. *J. Phys. Chem.* 98: 10343.

Thorn-Leeson, D., Wiersma, D.A.. **1995**. *Nature Struct. Biol.* 2: 849.

Tilton, R.F., Kuntz, I.D. Jr., Petsko, G.A.. **1984**. *Biochemistry* 23: 2849.

Timmins, P.A., Hauk, J., Wacker, T., Welte, W.. **1991**. *FEBS Lett.* 280: 115.

Tozzini, V. **2005**. *Curr. Opin. Struct. Biol.* 15: 144.

Tsai, A.M., Neumann, D.A., Bell, L.N.. **2000**. *Biophys. J.* 79: 2728.

Umena, Y., Kawakami, K., Ren-Shien, J., Kamiya, N.. **2011**. *Nature* 473(7345): 55.

Utschig, L. M., Greenfield, S. R., Tang, J., Laible, P. D., Thurnauer, M. C.. **1997**. *Biochemistry 36*: 8548.

Vandermeulen, D.L., Ressler, N.. **1980**. *Arch. Biochem. Biophys.* 199: 197.

Vinson, V.J.. **2009**. *Science* 324: 197.

Vojtechovsky, J., Chu, K., Berendzen, J., Sweet, R.M., Schlichting, I.. **1999**. *Biophys. J.* 77: 2153.

Walden, S.E., Wheeler , R.A.. **2002**. *J. Phys. Chem. B* 106: 3001.

Williams, J.C., Alden, R.G., Murchison, H.A., Peloquin, J.M., Woodbury, N.W., Allen, J.P.. **1992**. *Biochemistry* 31:11029.

Wöhri, A.B., Katona, G., Johansson, L.C., Fritz, E., Malmberg, E., Andersson, M., Vincent, J., Eklund, M., Cammarata, M., Wulff, M., Davidsson, J., Neutze, R.. **2010**. *Science* 328: 630.

Wolfram, S.. **1999**. *The Mathematica book*, Wolfram Media/Cambridge University Press.

Wraight, C.A., Cogdell, R.J., Clayton, R.K.. **1975**. *Biochim. Biophys. Acta* 396: 242.

Xu, Q., Baciou, L., Sebban, P., Gunner, M.R.. **2002a**. *Biochemistry* 41: 10021.

Xu, Q., Gunner, M.R.. **2002b**. *Biochemistry* 41: 2694.

Yeates, T.O., Komiya, H., Rees, D.C., Allen, J.P., Feher, G.. **1987**. *Proc. Natl. Acad. Sci. U.S.A.* 84: 6438.

Young, R.D., Frauenfelder, H., Johnson, J.B., Lamb, D.C., Nienhaus, G.U., Philipp, R., Scholl, R.. **1991**. *Chem. Phys.* 158: 315.

Zacharias, M. **2003**. *Protein Sci.* 12: 1271.

Zelent, B., Nucci, N.V., Vanderkooi, J.M.. **2004**. *J. Phys. Chem. A* 108: 11141.

Zhou, H.X., Rivas, G., Minton, A.P.. **2008**. *Annu. Rev. Biophys.* 37: 375.

12. ABBREVIATIONS AND ACRONYMS

Amino acids abbreviations:

Alanine: Ala, A. Arginine: Arg, R. Asparagine: Asn, N. Aspartate: Asp, D. Cysteine: Cys, C. Glutamate: Glu, E. Glutamine: Gln, Q. Glycine: Gly, G. Histidine: His, H. Isoleucine: Ile, I. Leucine: Leu, L. Lysine: Lys, K. Methionine: Met, M. Phenylalanine: Phe, F. Proline: Pro, P. Serine: Ser, S. Threonine: Thr, T. Tryptophan: Trp, W. Tyrosine: Tyr, Y. Valine: Val, V.

A_i : area of the i-th gaussian band.

A_W : area of the ($\nu_2+\nu_3$) combination band of water.

Å : angstrom.

A_{II} : area of the amide II band of the RC.

A_d : surface area of the detergent ring.

A_p : surface area of the RC protein.

A_T : sum of the areas of the RC protein and of the detergent ring.

a_W : proportionality constant (absorptivity) between the concentration of water and the area of the ($\nu_2+\nu_3$) combination band of water.

a_{II} : proportionality constant (absorptivity) between the concentration of the RC and the area of its amide II band.

BChl : bacteriochlorophyll.

BPheo : bacteriopheophytin.

$BPheo^-$: anion radical state of bacteriopheophytin.

CaF_2 : calcium fluoride.

CH_3COOK : potassium acetate.

°C : celsius degree.

Cα : alpha carbon atom.

Cβ : beta carbon atom.

Cγ : gamma carbon atom.

CO : carbon monoxide.

CPK : Corey-Pauling-Koltun color convention for atoms.

CS : conformational substate.

cw : continuous wavelength.

DAD : 2,3,5,6-tetramethyl-p-phenylene diamine.

DLATGS : duetereted L-alanine dopedtriglycine sulfate detector.

D_2O : deutereted water.

ΔA_{542} : absorption changes at 542 nm.

ΔA_{542}^{max} : maximal absorption changes at 542 nm.

ΔG^0_I : Gibbs free energy difference in standard conditions between the $P^+BPheo^-Q_A$ and the $P^+BPheoQ_A^-$ state.

EDTA : ethylenediaminetetraacetic acid.

E_h : ambient redox potential relative to an hydrogen electrode.

E_m : midpoint reduction potential.

EPR : Electron Paramagnetic Resonance.

ESE : Electron Spin Envelope.

exp(x) : *e* elevated to x.

F : Faraday constant, 96485.3365 C/mol.

Fe : iron atom.

FTIR : Fourier Transform Infrared.

Ge/KBr : germanium/potassium Bromide.

h : grams of water/grams of protein.

H-bonds : hydrogen bonds.

h_0 : constant in the Hailwood-Horrobin model, proportional to the number of the hydration sites.

H_2O : water.

H_2O^{18} : water with oxygen-18.

ID : inner diameter.

k_{AP} : rate constant for the electron transfer reaction from Q_A to P.

k_{AI} : rate constant for the electron transfer reaction from Q_A to BPheo.

k_B : Boltzmann constant, $1.3806488 \cdot 10^{-23}$ J K^{-1}.

k_{BP} : rate constant for the electron transfer reaction from Q_B to P.

KCl : potassium chloride.

k_i : effective force constant.

k_{IP} : rate constant for the electron transfer reaction from BPheo to P.

k_{obs} : observed rate constant.

k_{PA} : rate constant for the electron transfer reaction from P to Q_A.

<k> : average rate constant.

KNO_3 : potassium nitrate.

$KOH \cdot 2H_2O$: di-hydrated potassium hydroxide.

KRS-5 : Thallium Bromoiodide.

KWW: Kohlrausch-Williams-Watts function.

K_1 : constant in the Hailwood-Horrobin model, proportional to the activity of the hydration sites.

K_2 : constant in the Hailwood-Horrobin model, related to the water activity of the solid solution formed by water condensing at the surface of the RC-detergent complex.

K_2CO_3 : potassium carbonate.

IR : infrared.

LDAO : N,N-dimethyldodecylamine-N-oxide.

$LiCl_2$: lithium chloride.

LiSCN : lithium thyocianate.

MCT : Mecury Cadmium Tellurite detector.

$MgCl_2$: magnesium chloride.

$Mg(NO_3)_2$: magnesium nitrate.

mL : milliliter.

mw : microwave.

M_w : molecular weight.

µL : microliter.

μ_2 : the second moment in the cumulant expansion function.

μ_3 : the third moment in the cumulant expansion function.

NaCl : sodium chloride.

$NaOH \cdot H_2O$: mono-hydrated sodium hydroxide.

Nd:YAG : neodymium-doped yttrium aluminium garnet crystal.

NH : NH group.

NH_4NO_3 : ammonium nitrate.

NIR : near infrared.

$\tilde{\nu}$: wavenumber.

$(\nu_2+\nu_3)$: asymmetrical stretching and bending combination band.

OG : octyl-glucoside.

OH : hydroxil group.

P : bacteriochlorophylls P special pair.

pQB : p-benzoquinone.

PVA : polyvinyl alcohol.

$P_{865}^{\bullet+}$, P^+ : cation radical of the P special pair.

P_20_5 : phosphorous pentoxyde.

Q_A : Q_A binding site *or* quinone of the Q_A binding site.

Q_B : Q_B binding site *or* quinone of the Q_B binding site.

QH_2 : quinol.

Q_U : quality factor Q_U (empty).

$Q_A^{\bullet-}$, Q_A^- : anion radical of the quinone Q_A.

Q_B^- : anion radical of the quinone Q_B.

r : relative humidity.

R : gas constant, 8.3144621 J^{-1} K^{-1} mol.

Rb. sphaeroides : Rhodobacter sphaeroides.

RC : reaction center.

S : electronic spin.

SANS : small angle neutron scattering.

SDS-PAGE : sodium dodecylsulfate – polyacrylammide gel electrophoresis.

Si/CaF_2 : silicium/calcium fluoride.

σ : standard deviation.

T : absolute temperature.

T_d : denaturation temperature.

TE_{011} : TE_{011} optical transmission microwave cavity.

TREPR : Time Resolved EPR.

UQ_{10} : ubiquinone-10.

v/v : volume/volume.

w/v : weight/volume.

w/w : weight/weight.

$ZnSO_4$: zinc sulfate.

13. LIST OF PUBLICATIONS

Below we list the papers in which part of the work presented in the present thesis has been published.

Peer reviewed **publications:**

Francia, F., Malferrari, M., Sacquin-Mora, S., and Venturoli, G.. **2009**. *Charge recombination kinetics and protein dynamics in wild type and carotenoid-less bacterial reaction centers: studies in trehalose glasses.* The Journal of Physical Chemistry B, 113: 10389-10398.

Savitsky, A., Malferrari, M., Francia, F., Venturoli, G., and Möbius, K.. **2010**. *Bacterial photosynthetic reaction centers in trehalose glasses: coupling between protein conformational dynamics and electron-transfer kinetics as studied by laser-flash and high-field EPR spectroscopies.* The Journal of Physical Chemistry B, 114: 12729-12743.

Malferrari, M., Francia, F., Venturoli, G.. **2011**. *Coupling between Electron Transfer and Protein-Solvent Dynamics: FTIR and Laser-Flash Spectroscopy Studies in Photosynthetic Reaction Center Films at Different Hydration Levels.* The Journal of Physical Chemistry B, 115(49):14732-14750.

Malferrari, M., Venturoli, G., Francia, F., Mezzetti, A.. **2012**. *A new method for D_2O/H_2O exchange in infrared spectroscopy of proteins.* Spectroscopy - Biomedical Applications, submitted.

Proceedings:

Venturoli, G., and Malferrari, M.. **2009**. *La strategia dei viventi per la sopravvivenza in assenza di acqua.* L'energia e i vegetali, atti del convegno del 16 maggio 2009, pag. 277. Società Torricelliana di Scienze e Lettere, Faenza.

14. ACKNOWLEDGEMENTS

I wish to thank Prof. Giovanni Venturoli for supervising my PhD work, for encouraging me and for all his precious teachings.

Thanks to Dr. Francesco Francia for his help in the laboratory and his invaluable teachings in biochemistry; thanks also to Dr. Paola Turina for helpful suggestions and discussions.

Prof. Vincenzo Scarlato is acknowledged in his role of PhD Coordinator.

I wish to thank Elisa and my parents for encouraging me in doing PhD and all their support during these years.

I'd like to thank Dr. Winfried Leibl and Dr. Alberto Mezzetti for hosting me at the *Institut de Biologie et Technologies de Saclay IBITeC-S-CEA*, France.

I'm grateful to Prof. Wolfgang Lubitz, Prof. Klaus Möbius and Dr. Anton Savitsky for hosting me during my visits at the *Max-Plank-Institut für Bioanorganische Chemie* at Mülheim an der Ruhr, Germany.